MASSEY UNIVERSITY
COLLEGE OF SCIENCES

Switched Reluctance Electronic Drive:

Reverse Engineering To Improve The Quality And Manufacturability Of A Commercial Application

A thesis presented in partial fulfilment of the requirements for the degree of

Masters Of Engineering

In

Electronics and Computer Systems Engineering

At Massey University, Palmerston North

New Zealand

Michael John Lusby

2012

Abstract

This thesis presents a new prototype for a low maintenance and high quality switched reluctance electronic drive. Switched reluctance machine technology describes a modern brushless electric motor topology that is perhaps the most simple of all rotating electric machines. However, a switched reluctance machine requires power electronic switching and sophisticated digital control to be a viable competitor against alternative electronic machine topologies.

Commercial switched reluctance machine systems are normally designed and built by pairing the motor and the electronic drive together. This pairing increases the difficulty and cost of quality improvement. The motivation for this research is to improve the quality within a commercial switched reluctance machine electronic drive.

This particular electronic drive suffers from repeated common modes of failure. To achieve this, an accurate understanding of the interactions between functional components of the drive is crucial to reducing this complexity. This reduction in complexity can be achieved through appropriate separation of these functional components. Reverse engineering the electronic drive provides the detailed information required to design a component separated prototype solution.

The complexity of the electronic drive has been reduced by separation into power and control functional components; these components are present on separate circuit boards. This has reduced the complexity of investigating each circuit in detail and for isolating the cause of failures within each circuit. This has also standardised the necessary connections required between the power and control components should one of the circuits need to be redesigned.

Acknowledgements

I would like to thank Dr. Ibrahim Al-Bahadly for his guidance and instruction. He consistently went above and beyond his commitments as a supervisor and for that I am grateful. I also want to thank Ibrahim for maintaining a strong conviction that I would find the necessary answers, even when I believed I could not.

I received a great deal of knowledge and understanding in the subjects of analysis, reverse engineering, design, control, and critical thinking through his supervision. I would like to extend my appreciation for his mastery of the Switched Reluctance Machine.

I would also like to thank Roger Latimer, Brian Latimer, and Nathan Stantiall of Teknatool International Limited for their continued support and patience with this project. They provided me with the challenge to prove myself, and the opportunity to work co-operatively with them on this challenging and interesting project.

To my family I extend my gratitude for their endless support, and for the countless hours they provided an ear to relieve the stress of the work effort. I would like to especially thank them for continuing to believe in me.

I extend my sincere thank you to my friends, colleagues, and staff members of the School of Engineering and Advanced Technology for their continued support and inspiring words.

Thank you to everyone, without your contributions this work would not have been possible.

Michael J. Lusby
January 11, 2012

Table of Contents

List of Figures

List of Tables

Chapter 1

Introduction

"The first step towards getting somewhere is to decide that you are not going to stay where you are"

- John Pierpont Morgan

This chapter introduces and provides definition to the title of this thesis. The problem domain, motivations, and outcome objectives for this research are discussed. Finally, the structure of the information is outlined.

1.1 What is a "Switched Reluctance Machine"

The term Switched Reluctance Machine describes a specific electric machine technology usually pertaining to a rotating electric motor; however, linear actuators based on this technology do exist [1-4]. **S**witched **R**eluctance **M**achines (SRM) are utilised commercially in various applications and are characterised by simple motor construction but complex electronic drive and control topologies [5-8]. This complexity results in the motor and electronic components being designed and paired together; this pairing increases the difficulty and cost of quality improvement in commercial systems.

1.2 Definition of Quality

The definition of *Quality* used in this thesis is not a definition of quality utilised within the reliability engineering discipline specifically**.** Rather, quality is considered to be not only the reliability of the system as a whole, but also the ability to maintain, repair, and develop the system. This capability requires the availability of intimate product design knowledge which helps to improve the quality of service provided by the manufacturer; these quality aspects are investigated and improved within this thesis.

1.3 Description of Problem Domain

The motivation for this research was to improve the quality within a commercial SRM electronic drive. This commercial electronic drive suffers from repeated common modes of failure; this data can be seen in Table A-2: Fault Mode in Appendix A*, DVR Technical Information*, on page 186 of this document. The failure modes presented are the result of categorising the supplied failure and repair data; this data can be seen in Table A-1: Fault Repair Information, also in Appendix A on page 186 of this document. The frequency of the failure modes is shown in Figure 1-1:

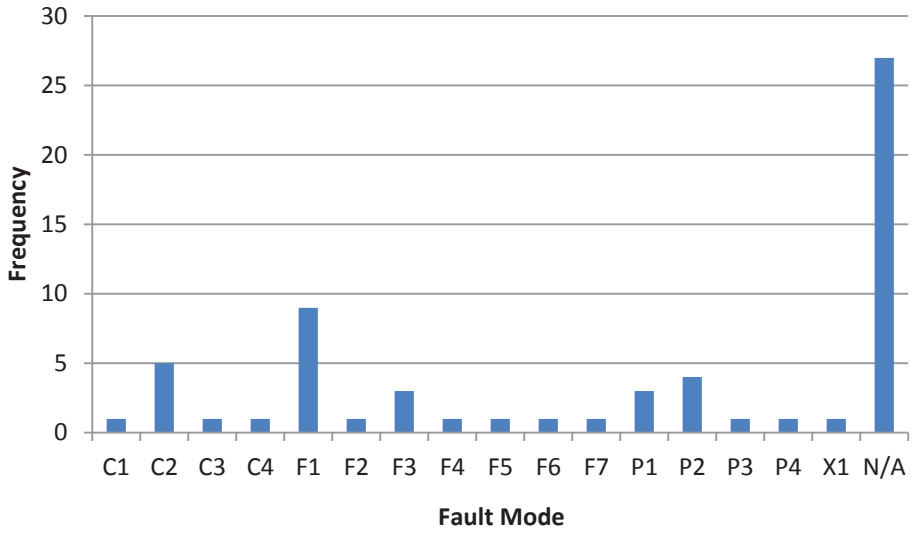

Figure 1-1: Histogram Of Fault Mode Frequency

It is shown that certain fault modes appear significantly more frequently. It is noted that N/A is the fault code category for fault events that did not contain information about the type of failure. It is also noted that no information regarding the failure mode was recorded in almost half of the cases; this is indicative of the lack of drive failure information provided.

This highlights a problem-solution framework to quality management. This quality approach results in quick fixes and recurring failures, regardless if it is intentional or not. A superior framework for quality management is **F**ailure **M**odes and **E**ffects **A**nalysis (FMEA) which highlights the need to identify the root causes of failures. This framework results in permanent solutions to quality problems, and the ability to quantify quality and improve it.

Failure of the electronic drive is undesirable due to the cost involved in replacing, or repairing the faulty drive. Identification of the underlying cause(s) of these failure modes is of critical importance.

The repeated common mode failures illustrate insufficient quality within the design, components, or manufacturing of the electronic drive. However, the complexity of the electronic drive prevents identification of the underlying cause(s) of these failures.

Therefore the problem domain can be expressed as the inability to identify the cause(s) responsible for the lack of quality within the electronic drive. This inability arises from the complexity of the electronic drive architecture. This complexity must be reduced to allow the cause(s) for the lack of quality to be discovered and corrected.

1.4 Aim and Scope of Research

The aim of this research is to resolve the quality issues associated with the electronic drive. To achieve this aim, the scope of the research is outlined as follows:

Develop an understanding of general SRM knowledge including: operating principles, construction, machine configuration, electronic drive topologies, power converter topologies, and control algorithms. This allows the identification of the specific implementations within the commercial system.

Utilise the knowledge gained via researching to identify the specific component implementations present in the commercial system, and comment on the suitability of these implementations. This development of intimate system knowledge will allow in-depth analysis of the commercial system as a whole.

Understanding how the system operates allows detailed analysis of the electronic drive, and its functional components. An accurate understanding of the interactions between these functional components is crucial to reducing complexity; this reduction in complexity can be achieved through appropriate separation of these functional components. Reverse engineering the electronic drive provides the detailed technical information required to design a component separated prototype solution.

Knowledge gained from the reverse engineering process facilitates separation at the appropriate points as dictated by: safety, component function, and suitability. The identification of these points allows the design and construction of a prototype circuit. The prototype is to be designed to a standard that is manufacturable and a direct replacement for the original electronic drive; the size and placement of the prototype circuit boards must be considered to achieve this.

Comparative evaluation testing will ensure that the performance of the prototype meets, at minimum, the performance of the original electronic drive.

Identifying areas within the design that can be investigated for quality improvement will allow the discussion of plausible solutions and facilitates the development of a quality improvement roadmap.

1.5 Research objectives

This research aims to achieve the following objectives at completion:

1. Provide intimate knowledge about the Teknatool machine configuration
2. Measurement of major signals present on the electronic drive
3. Justified separation points for the electronic drive that do not compromise safety or performance
4. A separated prototype electronic drive of manufacturable quality that is a direct replacement for the Teknatool electronic solution
5. Demonstrate that the prototype drive meets the performance of the Teknatool electronic drive via comparative analysis
6. Identification of areas for investigation of quality improvement
7. Completed documentation for the electronic drive, including complete component and signal listing, connector information, and revised schematics

These objectives will be used to determine a successful outcome of the research.

1.6 Organisation of the thesis

This thesis is organised as follows. Chapters 2 through 5 discuss the general knowledge of SRMs, while chapters 6 through 10 concentrate on the specific implementations present in the commercial machine, and achievement of the research objectives. Chapter 11 concludes and discusses the research outcomes.

Chapter 1, *Introduction*, presents the research topic, problem domain, scope, and objectives. The purpose of this chapter is to introduce the reader to the topic of discussion, and to provide a detailed structure for the content such that the information contained within this thesis is easily navigated.

Chapter 2, *Operating Principles*, discusses the operation of SRMs as a basic overview. It covers the inception of the SRM, simple control schema, torque and power generation, and comparison with competing technologies. This chapter highlights the various major components present in an SRM.

Chapter 3, *Motor Construction*, contains information concerning the stator and rotor components of an SRM. It discusses these components in various configurations, and their respective effects on performance. It draws attention to the known problems of starting ability, torque ripple, and acoustic noise generation.

Chapter 4, *Power Supply and Electronic Converter*, investigates the power supply component of an SRM in detail, notably the architecture and sub-components. *Power Factor*, a quantification of how efficiently power is drawn from the supply, is a major topic as it is of critical significance in the design of an SRM power supply.

The electronic power converter is discussed separately because of its critical importance to the efficiency and performance of an SRM. Various electronic power converter designs are demonstrated, explained, and critiqued.

Chapter 5, *Control Algorithms*, is concerned with the various methods of controlling an SRM. Schemas for both low and high speed operation are introduced. The critical system variables for successful control are identified, and their integration with the control algorithm is demonstrated. Lastly, position sensor-less operation of an SRM is discussed.

Chapter 6, *DVR SRM Implementation*, utilises the broad information presented in the previous chapters to identify and comment on the specific implementations present in the **D**igital **V**ariable **R**eluctance (DVR) SRM. This chapter provides the necessary background to understand the technical challenges in achieving the objectives of the research.

Chapter 7, *Separation Process*, describes the identification of appropriate separation points by analysis and the reverse engineering approach to achieve this. An iterative process is demonstrated to highlight the migration of the separation points as the depth of analysis and intimate system knowledge increases.

Chapter 8, *Prototype design and manufacture*, illustrates the design process of the prototype circuit boards. This prototype is intended to replace the original electronic drive. The need for further migration of the separation points is highlighted as the design of the separated prototype is attempted.

It also demonstrates the need for additional information beyond the reverse engineering process to successfully carry the prototype through to a manufacturable solution.

Chapter 9, *Instrumentation and Testing*, demonstrates the need for isolated instrumentation to successfully, and safely, take measurements from the electronic drive.

Appropriate isolation circuitry is presented to alleviate the requirement of an isolated oscilloscope for basic measurements. This chapter provides justification for the use of an isolated oscilloscope, which became necessary as the depth of analysis increased.

This chapter also compares the operation and performance of the prototype against the original electronic drive highlighting any significant difference. These differences are explained in context and prove the validity of the prototype solution.

Chapter 10, *Quality Improvement*, presents and categorises the quality observations recorded throughout the research. These improvements are discussed on their respective merits, and plausible implementations are suggested for their realisation.

Chapter 11, *Discussions and Conclusion*, discusses the research outcomes and the achievement of the objectives. The successful outcome of the research is considered, and concluding remarks and justifications are provided.

Appendix A, *DVR Technical Information*, contains information from the SRM manufacturer including fault information, motor parameters, and schematics.

Appendix B, *Measurement Data,* contains information not present in the main text obtained through experimentation on the SRM.

Appendix C, *Research Outputs,* contains additional information not present in the main text regarding the outputs from this research. Oscilloscope captures and printed circuit board designs are contained in this appendix.

Appendix D, *Datasheets*, contains the datasheets for the major components utilised in the electronic drive, and proposed component replacements.

Appendix E, *Photos*, contains a collection of photographs from the project.

Chapter 2

Operating Principles

"All knowledge has its origins in our perceptions"

- Leonardo da Vinci

This chapter presents the basic operating principles of SRM technology. Specifically: the basic machine overview, control schema, and the development of torque. The aim of this chapter is to provide sufficient background information to allow detailed discussion of specific component areas in the later chapters.

2.1 Switched Reluctance Machine Overview

SRM technology describes a modern brushless electric motor technology that is perhaps the most simple of all rotating electric machines. However, an SRM requires power electronic switching and sophisticated digital control to be a viable competitor against alternative electric machine topologies [7, 9, 10].

The heritage of the SRM can be found in the work of W.H Taylor who received a patent for an electromagnetic machine in the United States of America in 1838 [9]. The SRM has experienced strong development since the 1960's therefore it is still a relatively young technology [7]**.** It has found industrial application, in small quantities, ranging from general-purpose electric drives to appliances [11]**.** The commercial success enjoyed is due to the motor's low cost, flexibility and excellent reliability [9, 10].

A typical SRM consists of the stator housing, rotor, electronic power converter, controller, position and current sensors [7, 8, 11]. The electronic power converter delivers the current required for the motor to generate torque, while the controller and sensors provide closed-loop control to the system. It is standard practice to design and package the converter, controller, and motor together [9, 12, 13]**;** this is the result of the strong relationship between these components.

Figure 2-1 illustrates the relationship of components in an SRM topology:

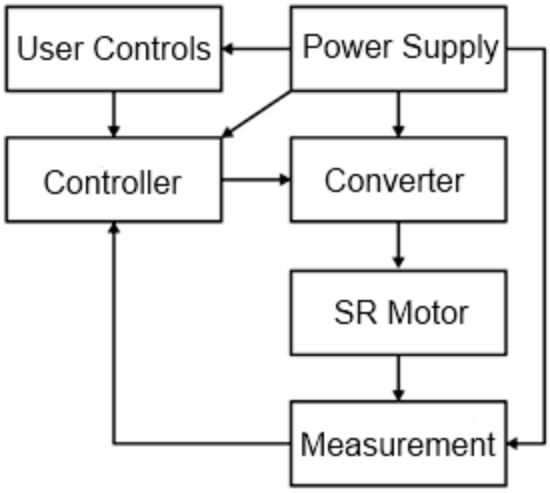

Figure 2-1: SRM Drive Architecture

Until recent advancements in microcontroller performance and features, it was standard practice to implement the control aspect of the SRM drive using analogue electronics; these advancements in microcontroller technology have seen a shift towards researching and implementing digital control algorithms [7].

2.2 Basic Principles

The SRM is a brushless design in which both the stator and the rotor contain *salient* poles; conversely there is a class of SRMs which are singly salient, known as *SSRMs*, which are not covered in this thesis. Further reading of SSRMs can be found in [14].

The doubly salient arrangement, as shown in Figure 2-2, allows the SRM its high efficiency, although not as high as competing technologies [10], as little energy is lost during electromagnetic energy conversion [7, 9]. However, a study in 1997 highlighted the cost-effectiveness and higher efficiency of the SRM against the induction motor [15].

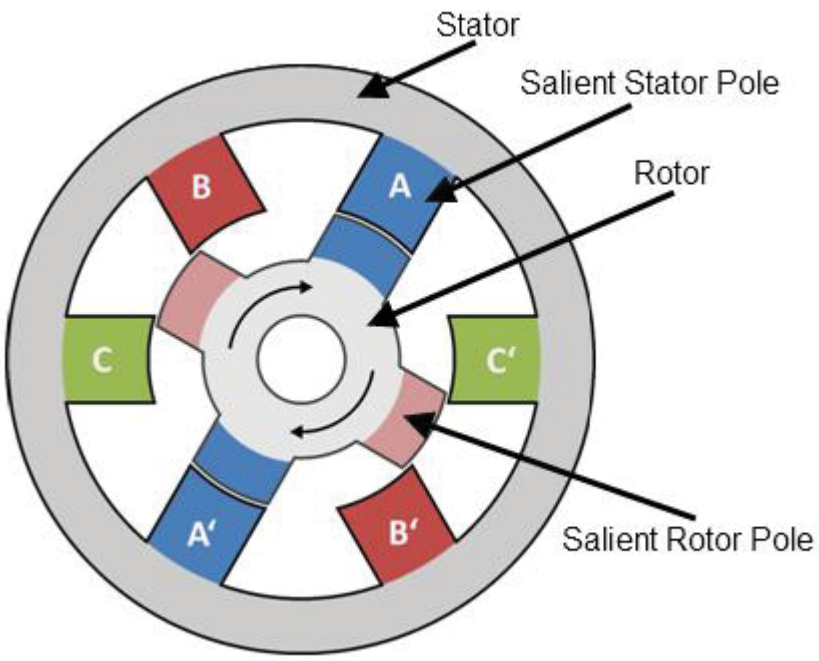

Figure 2-2: Cross-section Of A Typical SRM

Figure 2.2 illustrates the simplified cross-section of a three phase SRM containing six stator poles arranged into three phases: A, B, C, and four rotor poles; this configuration is known

as 6/4. The motor is shown at rest with *complete alignment* and *minimum reluctance* of Phase A with respect to the rotor poles.

Rotation requires excitation of phases in the correct sequence. Generation of clockwise rotation from the illustrated position requires Phase B to be excited. This causes the motor to rotate until the rotor poles are completely aligned with Phase B. Continuous rotation is caused by extension of this sequence to a repeating pattern; Phase C is next in this particular sequence. Counter-clockwise rotation is achieved by reversing the sequence.

The basic pattern for exciting rotor poles to cause a continuous clockwise rotation is shown in Figure 2-3:

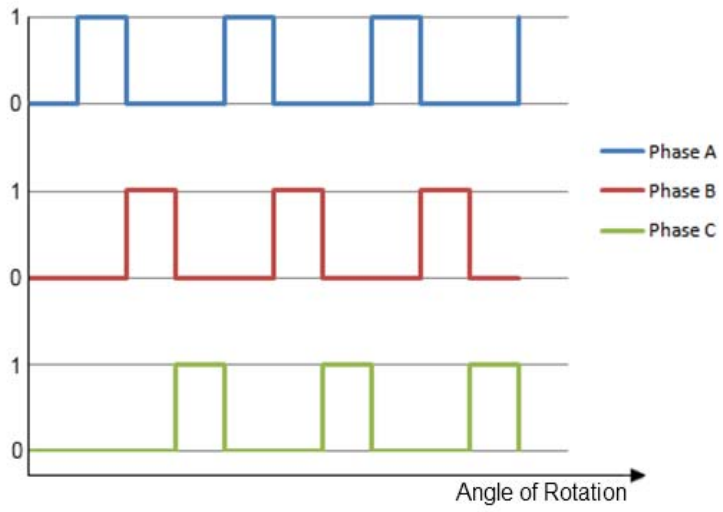

Figure 2-3: Simple Clockwise Rotation Excitation Sequence

The sequence shown illustrates excitation of the phases with mutual exclusivity; this is not plausible as the windings present an inductive load to the converter circuit. The phases need to be switched prematurely to allow sufficient time for the current to rise and decay.

The phases must be excited in this manner to ensure *positive torque generation*; thus preventing drag placed against the rotor by *negative torque generation,* which occurs when the rotor pole passes a phase which is still energised.

This behaviour results in the phase excitations overlapping, and is shown in Figure 2-4:

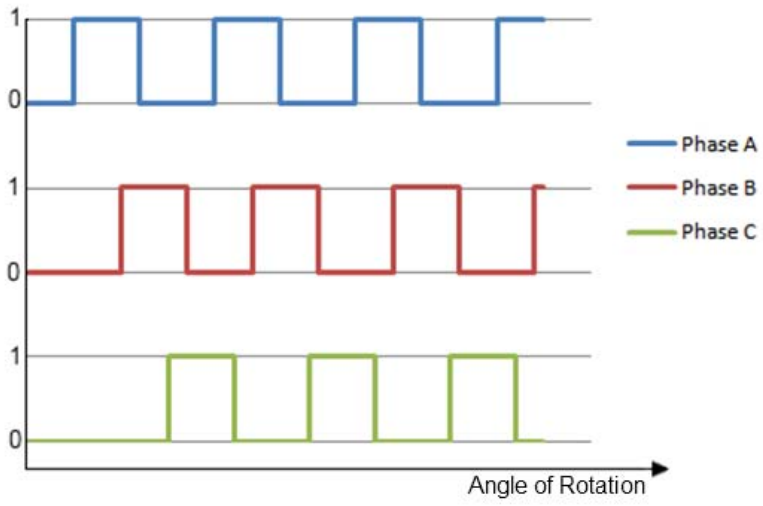

Figure 2-4: Plausible Clockwise Rotation Excitation Sequence

2.3 Motoring operation

Figure 2-5 illustrates a partial cross-section of a typical SRM; note one of the rotor poles is in *complete alignment* with a stator pole, whilst the other rotor pole illustrates *complete misalignment*.

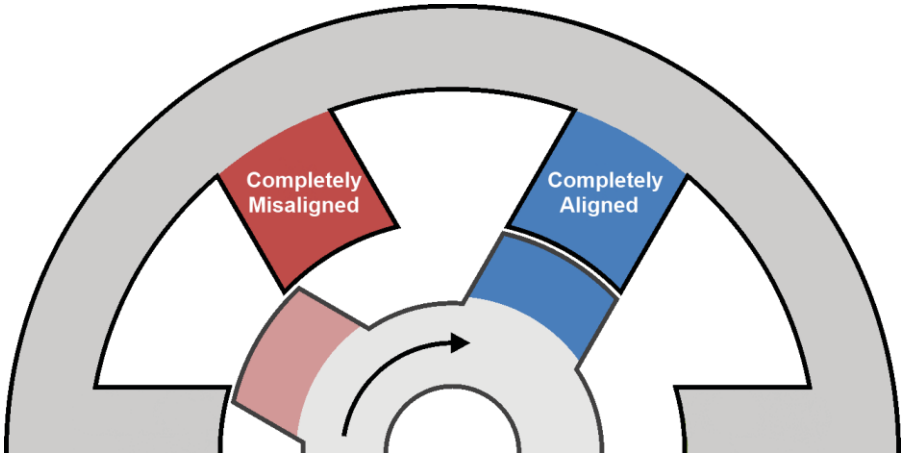

Figure 2-5: Pole Alignment Overview

Clockwise rotation of the rotor causes the completely misaligned rotor pole to rotate towards its closest stator pole; this angular region, used for motoring operation, is known as the *positive torque generation region*. This rotation also causes the completely misaligned rotor pole to rotate away from its closest stator pole; this angular region, used for generating operation, is known as the *negative torque generation region*.

Various electrical and magnetic properties for the given pole-pair change magnitude as the rotor advances from complete misalignment to complete alignment. The most significant of these properties are: the *winding inductance, flux-linkage*, *phase current*, *and instantaneous electromagnetic torque*. The typical waveforms of these properties are graphed with respect to alignment angle in the following sections.

2.3.1 Inductance

Inductance can be rudimentarily described as the capacity to store energy in the magnetic field surrounding a conductor, which is relative to the current flowing in the conductor; inductance is measured in *Henrys, H.* The inductance is said to have *saturated* when the maximum capacity of the magnetic field has been achieved [8].

The inductance is dependent upon the material of the magnetic conductor itself, the alignment angle of the rotor, and the current flowing through the phase windings [16, 17].

Reluctance is the mathematical inverse of inductance and the rotor of an SRM aligns at minimum reluctance; a plot showing inductance developed in the winding, at a fixed current, as a result of rotor angle is presented in Figure 2-6:

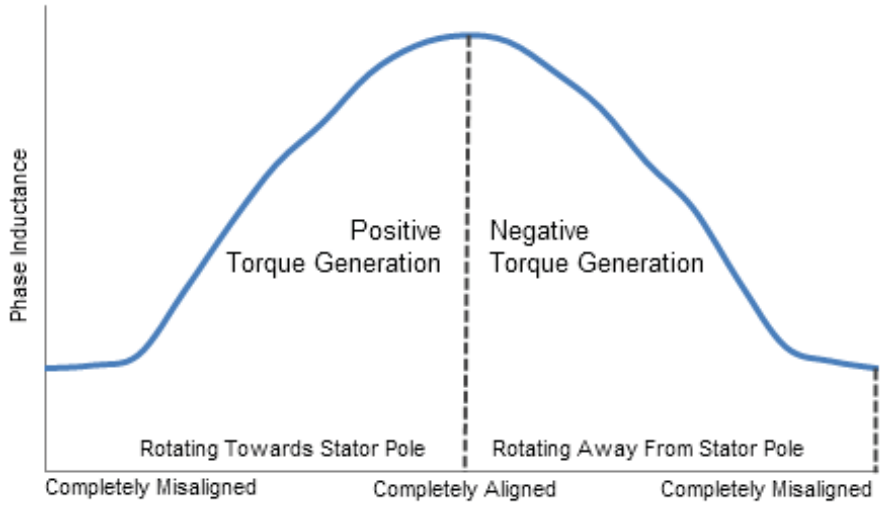

Figure 2-6: Inductance As A Function Of Rotor Angle

This shows the change in inductance with respect to the alignment. The inductance reaches the minimum value at complete misalignment, and the maximum value at complete alignment. The rate of change of the inductance determines the rate of change of the

current waveform when a voltage is applied across the windings; the maximum current that can flow is determined by the saturation of the magnetic field. This is commonly plotted comparing the resulting inductance profiles from a varying phase current magnitude, against a known rotor angle. A plot showing this behaviour is shown in Figure 2-7:

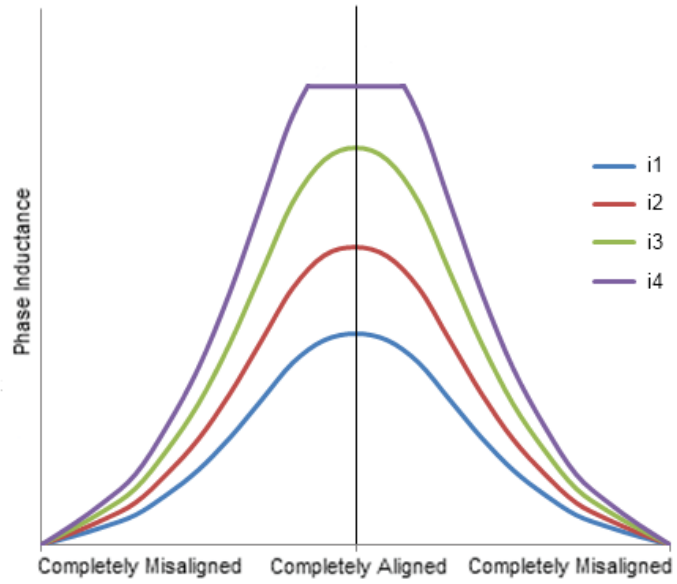

Figure 2-7: Inductance As A Function Of Rotor Angle And Current

The inductance increases with increased allowable current until saturation is achieved. At saturation the value of the inductance peaks and losses increase.

It was mentioned previously that the inductance of the winding determines the rate of change of the current flowing through it. Should the winding saturate then the current flowing will be determined by only the DC resistance of the winding; this results in high currents and high losses, therefore operation in saturation should be avoided.

The losses present in the winding as a result of the DC resistance are described by the following formula:

$$DC\ Winding\ Loss\ = i^2R \qquad \textbf{(2.1)}$$

2.3.2 Flux-linkage

Flux-linkage can be described as the total flux flowing perpendicularly through a surface, and is measured in *volt-seconds*. Flux-linkage ψ is described by the following equation:

$$\psi = N \int_S \vec{B}.dS \qquad \textbf{(2.2)}$$

Where N is the number of turns in the coil and $\vec{B}$ is the magnetic field strength vector.

Faraday discovered that the rate of change of flux-linkage passing through a magnetic loop is proportional to the **E**lectro**M**otive **F**orce (EMF) generated by the conductor, known as *Faraday's law*, and therefore we can define flux-linkage as the integral of applied voltage with respect to time:

$$\psi = \int v.dt \qquad \textbf{(2.3)}$$

Therefore the instantaneous flux-linkage, for a linear case, can be expressed in terms of instantaneous inductance L and instantaneous current i:

$$\psi = Li \qquad \textbf{(2.4)}$$

Knowing that the flux-linkage ψ is relative to both the inductance and current, we can hold the current to a known value and investigate how the flux-linkage varies with misalignment angle. This behaviour is shown in Figure 2-8:

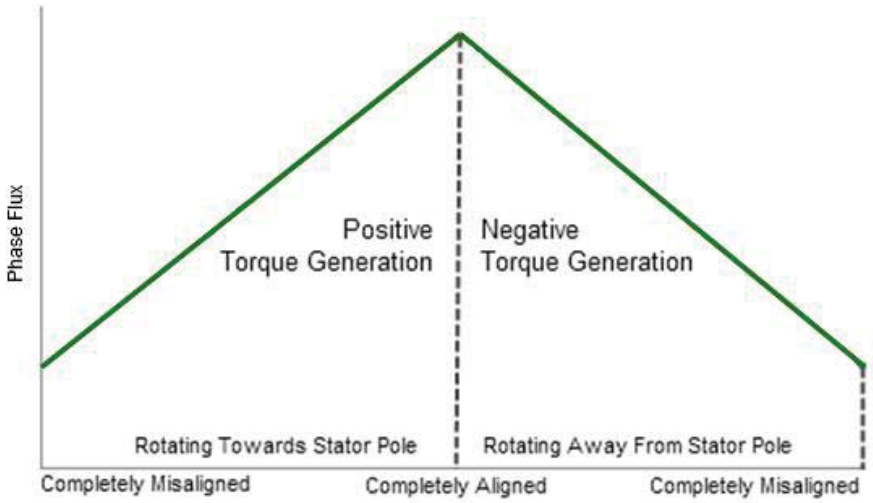

Figure 2-8: Flux-Linkage As A Function Of Rotor Angle

At complete misalignment the magnitude of the flux-linkage is at minimum which results in maximum reluctance, low likelihood of inductive saturation, and creates zero torque generation in unstable equilibrium due to the lack of pole affinity; this means that the direction of rotation is uncertain should a phase be energised [11].

Conversely, at complete alignment the flux-linkage achieves its maximum magnitude. Therefore, minimum reluctance is also achieved resulting in the high likelihood of inductive saturation, and zero torque generation in stable equilibrium due to strong pole affinity. The flux-linkage must be completely extinguished before the rotor achieves complete alignment [11].

As mentioned previously, the inductance of the SRM can saturate at higher current flows, and flux-linkage is strongly related to inductance. Therefore saturation of the inductance will also saturate the flux-linkage [8]. This behaviour is shown in Figure 2-9:

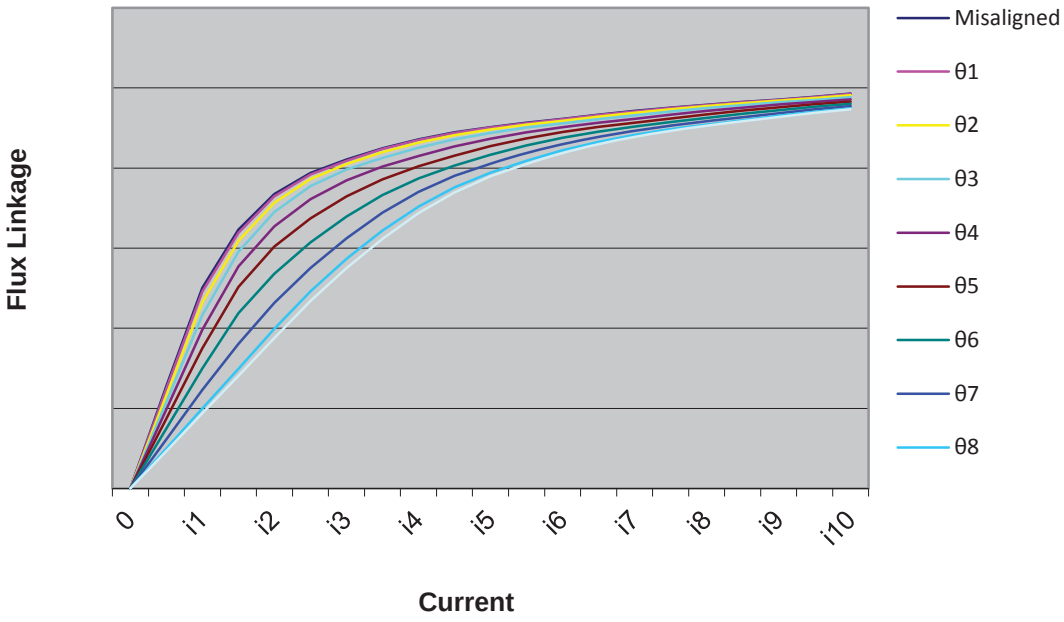

Figure 2-9: Flux-linkage As A Function Of Rotor Angle And Current

It is shown that with sufficient current the flux-linkage will saturate for any rotor angle with the difference being the time taken to saturate; this is caused by saturation of the phase inductance. Saturation of the flux-linkage should be avoided when operating in motoring because of the increase in losses.

2.3.3 Phase Current

An unconstrained phase current flow is illustrated in Figure 2-10:

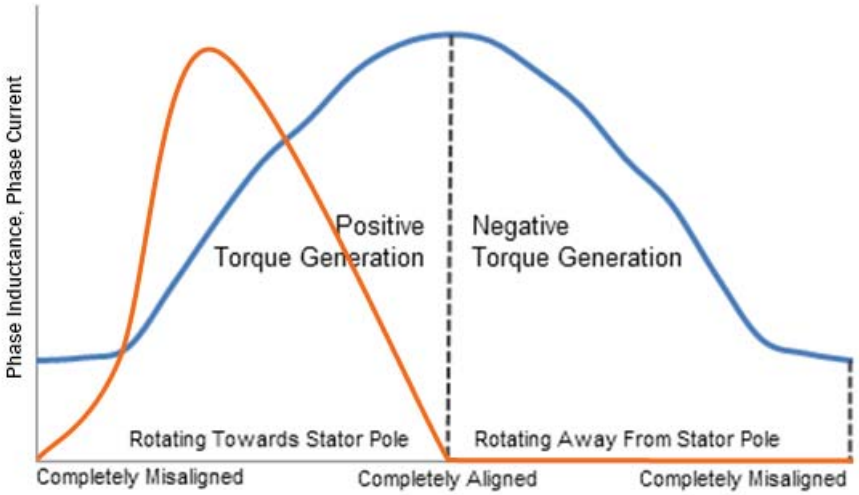

Figure 2-10: Unconstrained Phase Current As A Function Of Rotor Angle

This illustrates a typical current flow, measured in *amperes*, A, in the phase winding with respect to the alignment. This waveform assumes that the voltage is applied across the winding at complete misalignment, and is removed at the appropriate time to prevent residual current flow in the windings at complete alignment. The peak current is shown to be unconstrained for illustrative purposes; the peak value may be very high and damage the winding. The current can be effectively constrained by chopping [7-9, 11] which is shown in Figure 2-11:

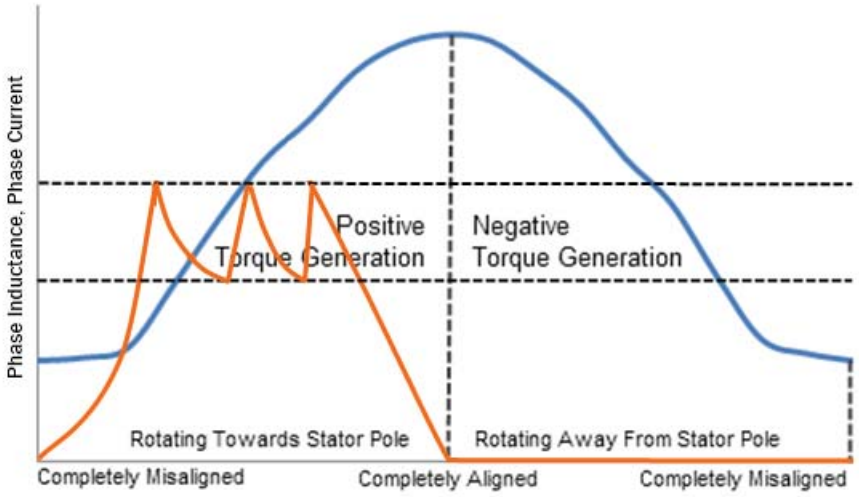

Figure 2-11: Chopped Phase Current As A Function Of Rotor Angle

This shows the phase current limited by chopping; which forms the basis of the current control within a SRM [11]. Formulae 2.5 - 2.7 are provided courtesy of [7]. The formula describing the relationship between the voltage, flux-linkage and current is:

$$v = Ri + \frac{d\psi}{dt} = Ri + \omega_m \frac{d\psi}{d\theta} \quad \textbf{(2.5)}$$

Where v is the terminal voltage, ψ is the flux-linkage in volt-seconds, i is the current flowing, R is the resistance of the phase in ohms, t is time in seconds, and ω_m is the angular velocity in radians per second. Phase inductance can be substituted for flux-linkage giving rise to the following equation, courtesy of [7]:

$$v = Ri + w_m \frac{d(Li)}{d\theta} = Ri + L\frac{di}{dt} + \omega_m i \frac{dL}{d\theta} \quad \textbf{(2.6)}$$

Where L is the inductance of the stator winding, in henrys, and θ is the angular position of the rotor, in radians. The last term is considered to be the back-EMF and can be expressed as:

$$e = \omega_m i \frac{dL}{d\theta} \quad \textbf{(2.7)}$$

2.3.4 Power and Torque

The instantaneous electrical power vi delivered to the winding can be expressed by its major constituents: the resistive voltage drop, the inductive voltage drop, and back-EMF voltage drop by the following equation, Formula 2.8 – 2.12 are provided courtesy of [7]:

$$vi = Ri^2 + Li\frac{di}{dt} + \omega_m i^2 \frac{dL}{d\theta} \quad \textbf{(2.8)}$$

The rate of change of the magnetic energy stored at any given instant is defined as:

$$\frac{d}{dt}\left(\frac{1}{2}Li^2\right) = \frac{1}{2}i^2\frac{dL}{dt} + Li\frac{di}{dt} = \frac{1}{2}i^2\omega_m\frac{dL}{d\theta} + Li\frac{di}{dt} \quad \textbf{(2.9)}$$

According to the conservation of energy principle, the mechanical power remains after the resistive losses of Ri^2 and the rate of change of magnetic energy stored are subtracted from the instantaneous electrical power vi. Mechanical power P is defined as:

$$P = \omega_m T_e \tag{2.10}$$

Where T_e is the instantaneous electromagnetic torque developed. Equation 2.7 can rearranged and substituted to obtain the equation for instantaneous electromagnetic torque developed:

$$T_e = \frac{p}{w_m} = vi - Ri^2 - \frac{d(\frac{1}{2}Li^2)}{dt} \tag{2.11}$$

$$T_e = \frac{1}{2} i^2 \frac{dL}{d\theta} \tag{2.12}$$

It should be noted that $\frac{dL}{d\theta}$ is the slope of the inductance profile, and this is negative after the angle of complete alignment allowing the generation of a negative torque. Current must be prevented from flowing during the negative inductance ramp as this places drag against the rotor.

The graph showing typical torque generation is shown in Figure 2-12:

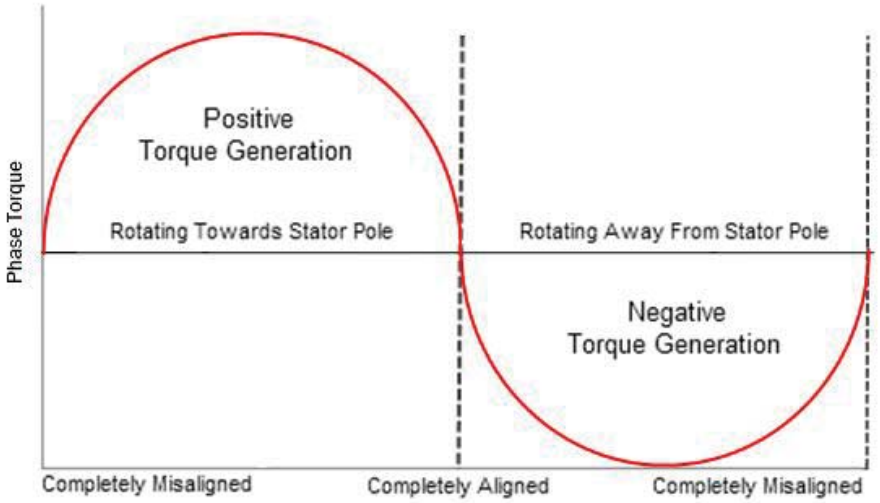

Figure 2-12: Torque Generation As A Function Of Rotor Angle

2.4 Torque-Speed and Power-Speed Relationships

The torque-speed relationship, and the power-speed, of an SRM is dependent upon the control topology [7, 9, 12], and can be modified in low-speed operation by the allowable maximum current; this is an advantage of the SRM over competing technologies.

The SRM is continuously variable between low and high torque operation depending on the average phase current. This is achieved without the requirement to dissipate energy which makes the SRM very flexible; particularly if the application requires both high and low torque operations at low speed. This highlights the machines ability to produce constant output power efficienty over a wide range of rotational speeds [10, 18].

The peak torque developed is limited by the maximum current; this is limited by the supply voltage, and the maximum temperature of the motor. The temperature rise of the stator windings is related to the magnitude of the average current flowing [11] .

Figure 2-13 illustrates the general torque-speed relationship of a SRM should maximum current flow at all rotational speeds; this plot represents the maximum achievable torque output. Figure 2-14 shows the closely related power-speed relationship.

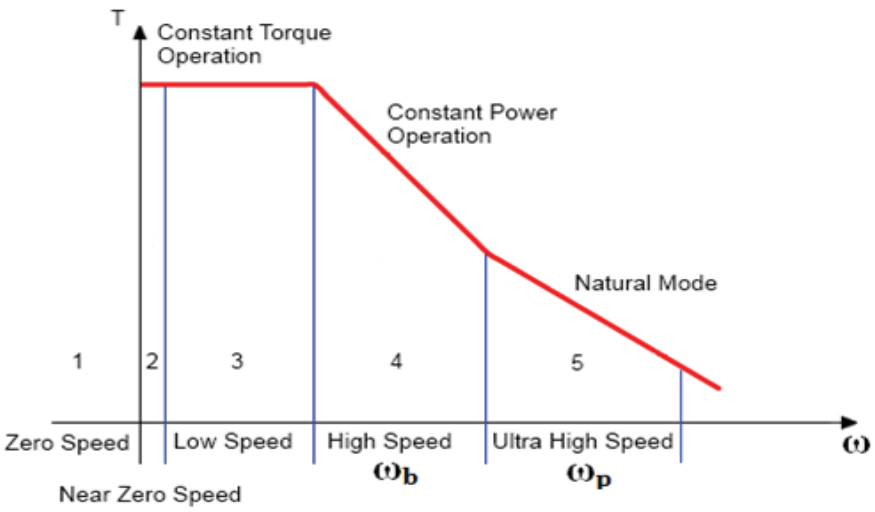

Figure 2-13: Idealised Torque Speed Relationship

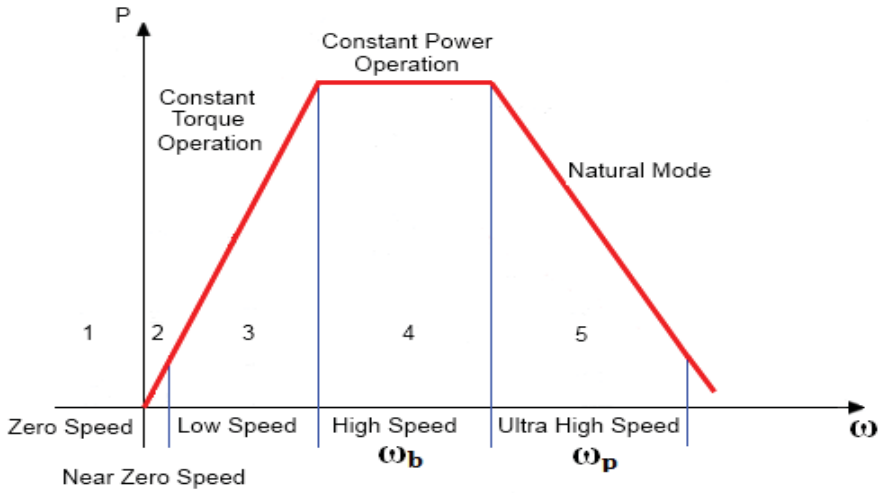

Figure 2-14: Idealised Power Speed Relationship

In explanation of Figure 2-13 and Figure 2-14 above, Region 1 represents the motor at rest, there is no excitation of the stator windings and therefore there is zero torque production.

Region 2 represents the instant at which the windings are excited with the rotor at rest. The maximum torque output is available immediately, assuming zero current rise time.

Region 3 represents the motor in low-speed operation where the maximum torque is limited by the supply voltage, or the maximum permissible current; this relationship persists with increasing rotational speed until the back-EMF begins to limit the supply voltage. The rotational speed at which this occurs is called the *base speed*, denoted by ω_b. Operation beneath the base speed is known as *constant torque operation* [7, 9].

Rotation above the base speed signifies Region 4, which is called *constant power operation*; At the base speed the maximum output power has been achieved. The motor will continue to produce its maximum output, but with increasing shaft speed torque must decrease due to the power limit being reached [9].

Further increasing rotational speed shifts the relationship into Region 5, called the *natural mode*. In this mode, increasing back-EMF causes the output power to decrease with increased rotational speed; the product of the torque and the square of the speed remain constant when in natural mode [9].

The SRM holds a strong advantage over conventional electric machines, with the difference in its maximum speed and base speed commonly being up to a factor of ten [9].

2.5 Acoustic Noise

SRMs have the potential to generate excessive levels of acoustic noise [7, 19]; the level generated is accepted to be higher than that of competing electric machine technologies [20, 21]. The acceptability of acoustic noise is dependent upon the environment the machine is operated within.

2.5.1 Sound power level

Sound power relates the volume of a noise source to the human ear, and is described by the following equation:

$$Sound\ Power\ L_w = 10\log_{10}\frac{W}{W_0} \quad \textbf{(2.13)}$$

Where L_w is the sound power level and is measured in decibels (dB), W is the power of the noise source measured in watts, and W_0 is the base power level, given to be 1pW.

The sound pressure level is defined as:

$$Sound\ Pressure\ L_P = 20\log_{10}\frac{P}{P_0} \quad \textbf{(2.14)}$$

Where L_P is the sound pressure level and is measured in decibels (dB), P is the pressure of the noise source in pascals, and P_0 is the base pressure level, given to be 20μPa (rms).

Given two separate sources, A and B, the combined sound power can be calculated by:

$$P_A + P_B = 10\log_{10}\frac{P_A}{P_0} + 10\log_{10}\frac{P_B}{P_0} = 10\log_{10}\left[10^{\frac{P_A}{10}} + 10^{\frac{P_B}{10}}\right] \quad \textbf{(2.15)}$$

$$P_A + P_B = P_A + 10\log_{10}\left[1 + 10^{\frac{P_B - P_A}{10}}\right] \quad \textbf{(2.16)}$$

This equation illustrates that the power level of two identical noise sources combined is not doubled. This is an important result for the generation of acoustic noise in noisy environments, as it indicates the acceptability of noisy environments e.g. workshops.

2.5.2 Acoustic Noise Generation

The most significant source of noise generation within a SRM is the physical distortion of the stator housing by the radial magnetic forces [7, 19, 22]; this distortion can be minimised with increased stator pole count and increased structural rigidity.

The torque generation of the SRM is discontinuous therefore the radial magnetic forces are also discontinuous; this gives rise to the potential to generate significant acoustic noise from a small current should the distortion be excited at its natural resonant frequency. However, this results in the ability to largely cancel this acoustic noise by slight modulation of the current to prevent excitation at the natural resonant frequency.

Unfortunately, such an approach assumes that there is only a single distortion frequency within the stator housing. In practice there are various vibration frequencies present which are capable of generating significant acoustic noise [7] and this suggests that cancellation by harmonic injection of the current waveform will be difficult as it requires attention to many frequencies.

Compounding the acoustic noise generation problem is the high transient switching nature of the tangential electromotive force acting on the rotor. The maximum acoustic noise generated by this factor occurs by allowing the stator windings to remain energised until the rotor pole reaches maximum alignment before exciting the next phase in sequence; this control behaviour also results in the highest torque ripple leading to a strong relationship between torque ripple and acoustic noise [23, 24].

Operating the motor in this fashion results in the rotational momentum of the motor being required to overcome the opposing electromotive force applied by the winding against the intended direction of rotation resulting in lower efficiency.

The choice of an appropriate pole configuration, electronic converter and control algorithm can greatly reduce the acoustic noise produced by the SRM [25-27]; therefore acoustic noise can be an audible indicator of control system performance.

2.5.3 Reducing Acoustic Noise

Excessive acoustic noise generation can be largely regarded as a matter of perspective. The inherent advantages of the SRM lie in low-cost manufacturing, so it is likely that they will be utilised within residential and consumer grade products; excessive noise is not acceptable within these areas [28].

It has been shown in 2.5.1, *Sound power level*, that perception of acoustic noise is strongly dependent upon other noises present in the environment. Therefore should the SRM operate in an environment which already contains significant noise pollution, the generation of acoustic noise from the SRM loses significance. The acceptability of acoustic noise generation is dependent upon the situation in which the motor is intended to be operated within.

The process of minimising the acoustic noise generated by an SRM is unique to every implementation as they vary greatly in construction and control. There are a large number of design rules which are effective at reducing the acoustic noise generated and can be applied to every SRM in the design stages. A significant few of these rules are shown below in example:

- Maximise the width of rotor and stator poles
- Increase pole configuration multiplicity; this is achieved by increasing the number of poles for a given phase.
- Increase the air-gap to the maximum permissible distance without significantly affecting the inductance profile
- Use the largest possible motor shaft diameter

An SRM was successfully designed to reduce torque ripple, acoustic noise and still retain the low-cost manufacturing benefits of the switched reluctance topology. This motor is known as the Stagger-Tooth motor [7, 29] developed by Wayne A. Pengov and received a US Patent, 5852334, on December 22 1998.

2.6 Summary

This chapter reviewed the basic topics of the SRM discipline. Specifically: the development history, comprising components, basic motor layout, simple control schema, the principles of torque and power generation for motoring operation, and acoustic noise.

The information contained in this chapter is an overview to the basic terminology and concepts required to understand the basic operation of an SRM. This information is crucial to the novice reader in understanding and placing the information presented in the following chapters.

Chapter 3

Motor Construction

"When one has finished building one's house, one suddenly realises that in the process one has learned something that one really needed to know in the worst way - before one began"

- Friedrich Nietzsche -

This chapter discusses the construction of an SRM, and why it is critical to achieving optimum performance within the intended application. Relation of performance to the construction of the machine can be separated into three major topics: materials, design of the stator and rotor to maximise flux linkage and minimise losses, and the pole and phase configuration. Material selection is outside the scope of this thesis and will not be discussed as it lies outside the scope of this work. Information regarding appropriate material selection and the effect of material on performance can be found in [17, 18, 30-33].

Optimisation of the stator and the rotor construction will be discussed in the following sections, as well as the performance impacts of differing pole and phase configurations

3.1 Stator Construction

The SRM incorporates a simple stator construction containing all of the excitation sources; therefore the total power losses are concentrated in the stator. Due to the external nature, and size of the stator, these losses are easily dissipated; especially in motors which are enclosed by a metallic frame [7, 9, 11]. Figure 3-1 shows the cross-section of an eight pole stator.

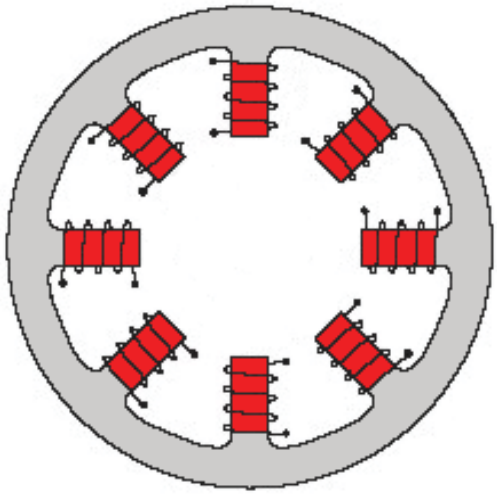

Figure 3-1: Switched Reluctance Stator And Winding Cross-section

The stator contains equidistantly spaced salient poles. These poles are encased by a concentrated single pitch winding allowing simple manufacture and repair [7, 10]**.** The windings are electrically exclusive, except windings connected in phases, and are operated in near mutual exclusivity thereby greatly reducing the insulation stresses as seen in conventional electric drives; this behaviour improves the reliability of the SRM stator by effectively eliminating the risk of phase to phase insulation failure [11].

The simplicity of the windings compared to conventional motor topologies allows them to be shorter in length, and therefore reduces the losses by minimising the end winding; which provides no beneficial torque generation when excited [11].

The stator construction allows the high efficiency, reliability, and maintainability characteristics of the SRM [7, 11]

3.2 Rotor Construction

The SRM employs a very simple rotor construction, usually constructed by stacks of laminated steel surrounding the motor shaft. The rotor contains no excitation source and this makes it extremely durable, reliable, and cost-effective to maintain [9, 11].

The cross-sectional shape of the rotor is critical to the operation of the SRM [11].The poles protrude from the rotor giving it a comparatively low rotational inertia, which is loosely described by the following equation:

$$Rotational\ Momentum\ I = MR^2 \qquad \textbf{(3.1)}$$

This improves transient behaviour of the system and reduces mechanical shock placed on the motor shaft in high gear ratio applications. Figure 3-2 details the cross-section of a basic SRM rotor.

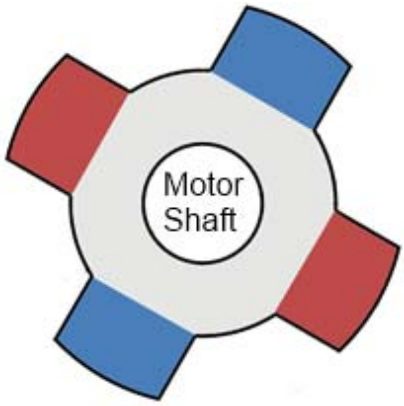

Figure 3-2: Cross-section of rotor construction

The rotor is constructed of thin laminated steel discs. It is constructed in this manner to reduce *magnetic eddy currents*, and this decreases power losses in the rotor resulting in high efficiency [9]. However, windage losses can result from poor geometry design [11, 34].

The lack of excitation sources on the rotor is advantageous; it improves the fault-tolerance such that a fault in one phase is not energised by the passing rotor, and therefore does not generate negative torque [9]. The lack of excitation sources also allows the rotor to run relatively cool, resulting in prolonged motor shaft, bearing, and lubricant life, further increasing reliability [11]. This behaviour ensures rotor power losses are very low, even at

full-load operation, and this is advantageous for high speed operation. This allows the SRM to start under full-load conditions or remain in a stalled condition with energised phases for prolonged timeframes without overheating the machine [11]

The ability to start the machine under full-load condition with exceptionally low power losses translates to an infinite number of possible full-load starts per hour and the prevention of run on losses in variable speed applications**;** such behaviours are not possible with conventional electric machines due to the comparatively high rotor losses [10].

The construction of the rotor is imperative to the performance, reliability, fault tolerance and high speed operation of the SRM. The simplistic construction allows effective in-field repairs.

3.3 Pole and Phase Configurations

The SRM can be implemented with various topologies for stator and rotor pole configurations. It is common for equidistantly spaced stator poles to be connected in phases for simultaneous excitation**;** this approach allows electromotive force to be applied tangentially to more than one face of the rotor during positive torque generation thereby improving the balance of the machine.

Pole and phase configurations impact the SRM's performance and therefore the following factors need to be considered before selecting an appropriate topology:

- Starting ability
- Direction of rotation
- High speed operation
- Cost
- Reliability
- Power density

The impact of these factors can be illustrated by investigating the behaviour of various machine configurations, and noting the capabilities of the typical machine configurations, such as single phase, two phase, three phase, and four phase are detailed in the following sections.

3.3.1 Single Phase

The simplest SRM would consist of four salient rotor poles which are all members of a single phase. The cross-section of such a machine is shown in Figure 3-3:

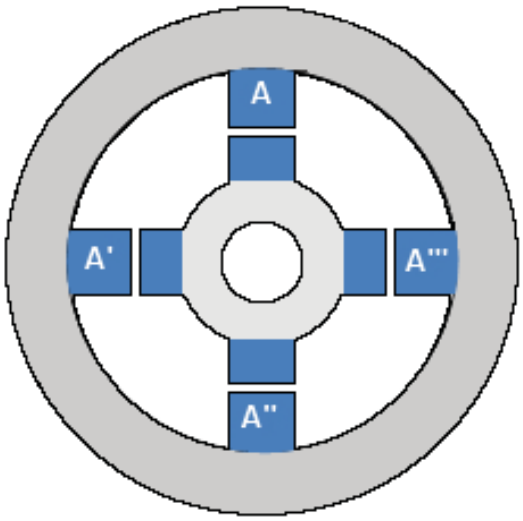

Figure 3-3: Cross-section Of A Single Phase 4/4

The motor consists of four salient stator poles grouped into a single phase, A, therefore all four poles are excited simultaneously. This is the SRM of all with respect to construction, complexity, number of electrical connections, and control.

This configuration exhibits very high torque ripple due to the binary nature of the positive torque generation. It also suffers an inability to begin rotation from rest at two separate rotational positions. If the salient poles on the rotor are resting equidistant from the salient stator poles, complete misalignment, or complete alignment, the motor will not rotate when the phase is excited due to the electromotive force being equal in magnitude in both clockwise and counter-clockwise directions. This results in zero net positive torque generation. These non-start positions can be removed by adding small permanent magnets into the stator [35].

Asymmetry in the design of the rotor poles can improve starting conditions by biasing the direction of positive torque generation; this technique is implemented in motors that are intended to rotate in a single direction [35].

This pole configuration is generally intended for use in high speed applications where the rotational momentum of the system prevents the motor from decelerating sufficiently between phase excitations to minimise torque ripple.

A simple modification to this topology allows minimisation of torque ripple and improved ease of starting at the completely misaligned rest angle. This modification is to separate the stator poles into two phases, known as a two phase SRM.

3.3.2 Two phase

The two phase motor topology is an improvement on the disadvantages of the single phase motor topology, having both reduced torque ripple and the ability to start from complete misalignment of the rotor poles. The cross-section of a two phase 4/4 is shown in Figure 3-4:

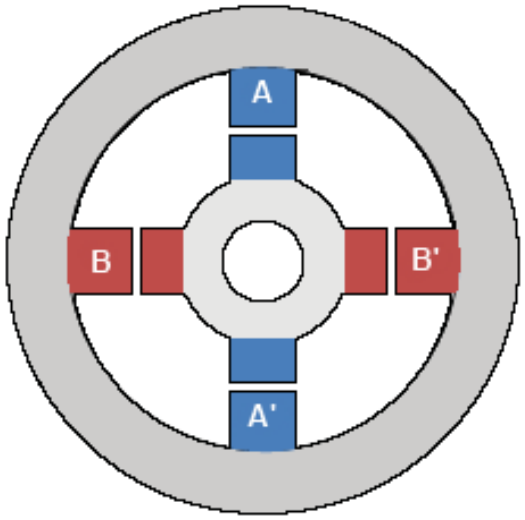

Figure 3-4: Cross-section Of A Two Phase 4/4

The two phase 4/4 SRM has almost identical construction to that of the single phase 4/4, with the major difference being the introduction of a second phase. The additional phase arises by exciting diametrically opposite salient stator poles in groups, instead of exciting all stator poles simultaneously. This change in construction results in additional complexity in the wiring, control algorithm, and converter.

The two phase SRM improves the starting problem inherent in the single phase machine by only exciting two of the stator poles at any time, therefore when the rotor poles are completely misaligned, the electromotive force is only applied in the direction of intended rotation.

If the rotor poles are aligned with the stator poles the motor will not rotate without modification to the rotor. Such modifications are shown in Figure 3-5:

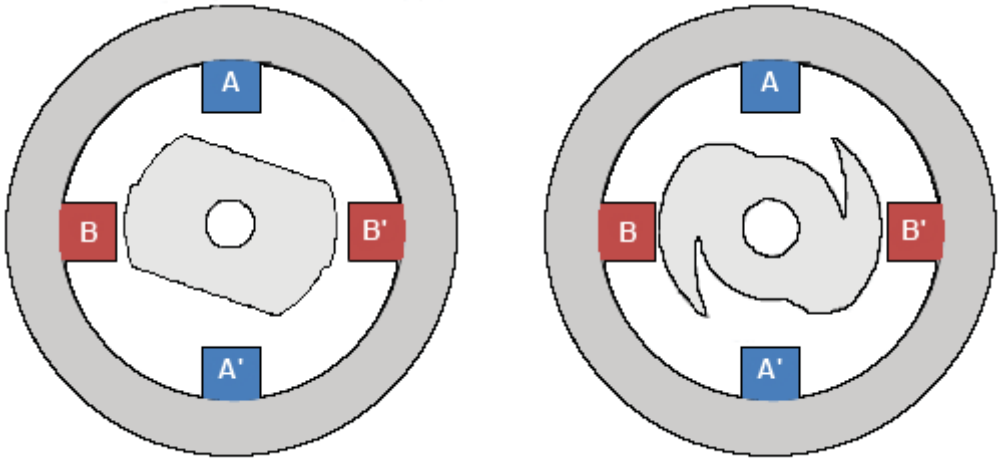

Figure 3-5: Rotor Modifications For Ease Of Starting

A stepped air gap is shown on the left, and an asymmetrical rotor is shown on the right.

The rotor requires modification to consist of fewer poles than the stator, this prevents alignment with both phases simultaneously, and either stepping the air gap or introducing asymmetry into the pole design. These designs increase the angle of complete misalignment to ninety degrees and cause the two phase 4/2 motor to become *uni-directional*. However, a technique was developed that allows bi-directional rotation based on the inherent magnetic asymmetry alleviating the need for rotor modifications [36].

The two phase machine generally exhibits a high torque ripple and fewer rotor poles than stator poles. It may employ asymmetric rotor poles, or stepped air gaps to aid in starting. It can be implemented where a mechanical or hand starting mechanism is not ideal yet the high number of phases is not justified, or high-speed operation is desired. It should be noted that the single phase and dual phase machines are not limited to four poles and an increase in both stator and rotor poles will result in smaller maximum misalignment angles and decreased torque ripple.

There has been research recently into utilising a higher number of rotor poles to stator poles to reduce the torque ripple present in two phase SRMs [37].

The most common and simple solution to the torque ripple and starting problems is the three phase SRM.

3.3.3 Three phase

The most common SRM used in industry is the three-phase [8]. The design inherently reduces the torque ripple and overcomes the starting problems associated with a lower number of phases. Therefore, the three phase motor is generally the most cost-effective motor for construction, complexity and performance [38]**.** A cross-section of a three-phase 6/4 is shown in Figure 3-6:

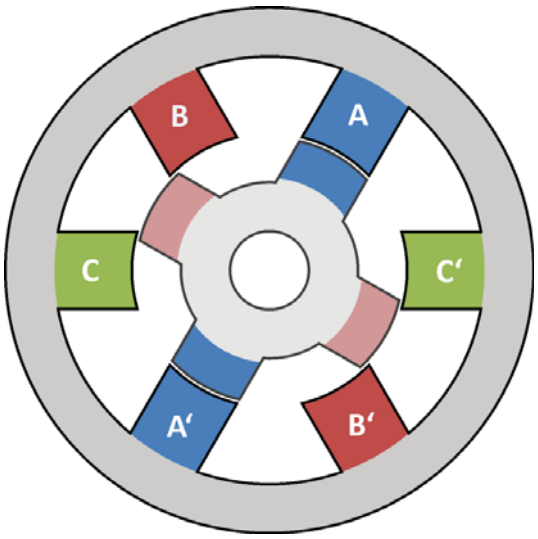

Figure 3-6: Cross-section Of A Three Phase SRM

The three phase SRM incorporates equidistantly spaced stator poles grouped to form the phases; it is not uncommon for the rotor to have less poles than the stator in this configuration. .

The uneven stator to rotor pole ratio reduces the maximum misalignment angle which allows easy starting and minimisation of torque ripple. This is because when one group of rotor poles are completely aligned, the other group are completely misaligned. However,

recent research has shown that torque ripple can be significantly decreased if the rotor contains more poles than the stator [39].

The advantage of increasing the number of poles per phase in a three-phase SRM is an improvement in the low-speed characteristics. This is achieved in three ways: the first is a reduction in the need for rotational momentum to keep the motor rotating between phase excitations thereby reducing the torque ripple. The second being that the application of the tangential electromotive force to more faces of the rotor simultaneously results in increased balance. The third benefit is significantly decreased radial forces acting upon the stator which are known to generate vibration and acoustic noise [40]. These advantages come at the cost of lower efficiency due to increased core losses [40].

Torque ripple is still measurably present in a three-phase SRM. The four phase SRM offers reduced torque ripple at the cost of increased complexity and control.

3.3.4 Four Phase

The four-phase SRM is useful when the required torque ripple cannot be met sufficiently by a three-phase machine. The cross-section of a four phase SRM is shown in Figure 3-7:

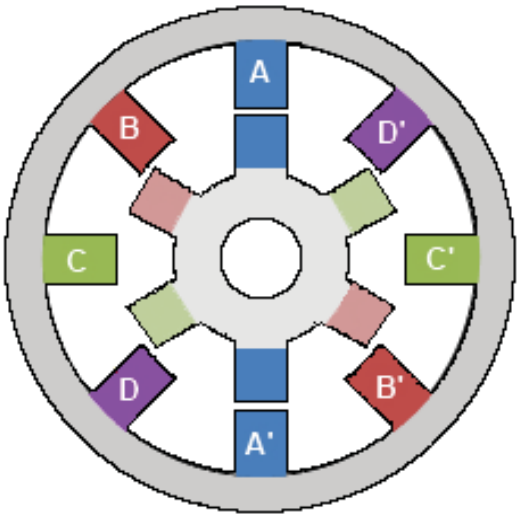

Figure 3-7: Cross-section Of A Four Phase SRM

The four phase machine offers measurable torque ripple reduction over the three phase construction [7, 38]. However, this is at the cost of complexity in both the construction and

the required control. The additional complexity in terms of electronic control and component count results in this construction not being a popular choice except in specific applications. It has generally been concluded that the three phase motor offers superior overall performance than the four phase construction due to lower switching loss and higher output capacity per volume [38].

3.3.5 Higher phase count motors

The torque ripple minimisation offered by higher phase count SRMs extends to five and six phase machines, but these implementations are very expensive and complex. Therefore they are only reserved for very specific applications.

It should be noted that as the number of phases increases so does the base switching frequency to rotate the motor at a given speed; this results in increased switching loss. A higher number of phases also limits the maximum speed the motor can reach due to the higher switching frequencies and shorter excitation times of the phases.

3.4 Summary

This chapter reviewed the basic construction principles of an SRM, concentrating equally on both the stator and rotor constructions; the advantages of the switched reluctance design over competing topologies are raised and supported.

The main area of focus is upon the configuration of poles and phases, namely the number of poles in the stator, the grouping of the stator poles into phases, and the number of poles on the rotor, and how this configuration impacts system performance.

Many of the challenges involved with SRM phase and pole configurations are raised in this chapter, particularly torque ripple and starting from all rest positions are discussed and the solutions to these problems are addressed.

Understanding the information present in this chapter is critical to understanding the design and implementation of the SRM presented in Chapter 6, *DVR SRM Implementation* on page 89 of this document.

Chapter 4

Power Supply and Electronic Converter

"Make the best use of what is in your power, and take the rest as it happens"

- Epictetus

This chapter discusses both the power supply and the electronic converter as they form integral and crucial parts of the electronic drive of an SRM. Shortcomings in either of these components will heavily affect the quality, performance, efficiency, and reliability of the final product. The following sections will discuss these components in detail, from the necessary requirements through to critiquing past and present implementations. A major factor to consider for the power supply is the power factor and this is discussed in great depth.

4.1 Power Supply Overview

The term power supply for a SRM can be used to describe the means of providing a DC voltage bus and electronic converter circuit; the phase windings only require a uni-polar current to generate rotation in either direction. The term can also be used to describe all the electrical supply rails required to operate the drive successfully, including the electronic converter circuit.

This thesis uses the term power supply broadly covering every power supply rail required to operate the drive except the electronic converter. The reason for this is the crucial role that the electronic converter circuit plays in the final characteristics of the motor. For this reason the electronic converter circuit has been covered separately to the power supply.

The power supply is required to provide a variety of outputs from a given input source; a typical power supply for a SRM would be required to provide the following power rails:

- High voltage low impedance DC Supply for the electronic converter
- Low voltage DC supply for the control electronics
- Positive and negative rails for current measurement circuitry (Negative rail dependent on current sensing implementation)
- Supply for rotor position sensors
- Supply for the control panel (if fitted)

The power supply is required to provide these rails reliably, with: minimal voltage ripple, user safety, and maximum efficiency at converting the input power source. The high power nature of electric machines means the power supply is normally required to convert a high voltage AC input source. It is common for the control and power electronics to be separated by isolation. This reduces the effect of electromagnetic interference and reduces the risk of serious electric shock for the operator.

The SRM windings present an inductive load to the output of the power supply. The phase separation of voltage and current must be corrected to ensure maximum performance; this is covered in detail in 4.3, *Power Factor*, on page 40.

4.2 Power Supply Architecture

The power supply is required to provide supply rails for various components within the switched reluctance system; these components having vastly different requirements. A block diagram is presented in Figure 4-1 to highlight the different tasks and paths present in a typical SRM drive power supply implementation.

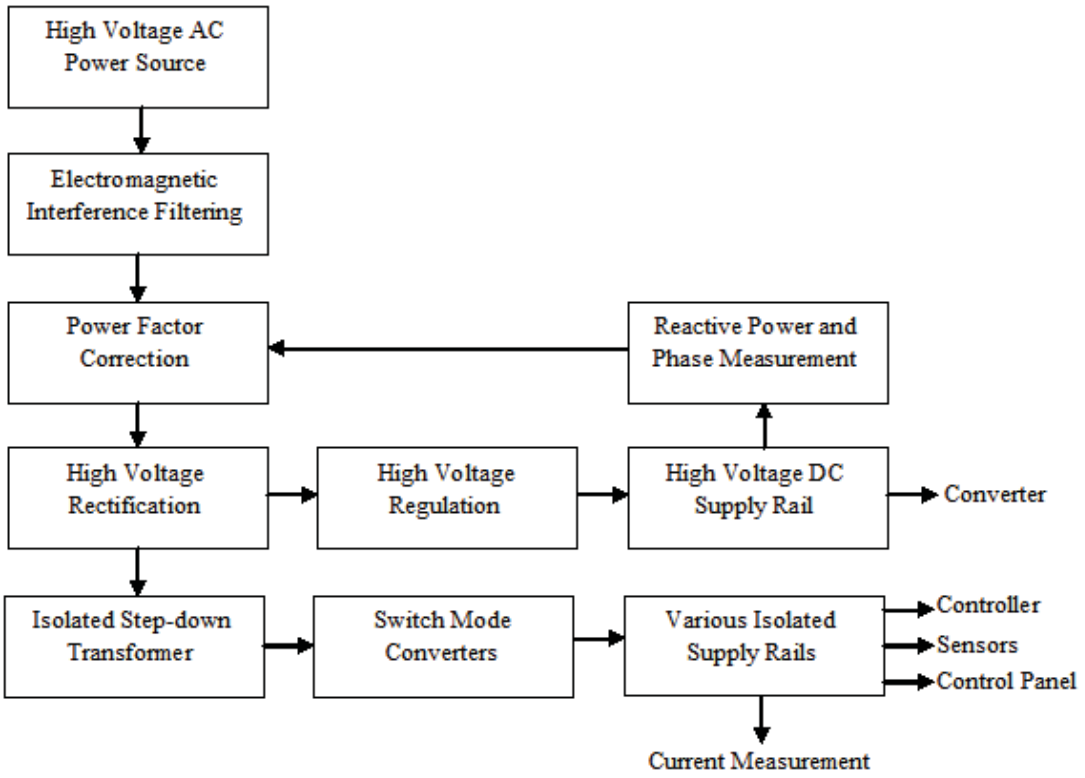

Figure 4-1: Power Supply Architecture

A point to be noted is the rectification of the high voltage AC input source before the transformer. This approach removes the requirement for handling negative voltages present in the switch mode converters that provide the isolated low voltage rails for the control circuit, user control panel, sensors and current measurement.

It should be noted that some current measurement techniques require a negative rail to operate correctly. This can be provided by a centre-tapped winding connected to the earth of the motor. This approach poses a problem for isolated control circuitry.

Isolation of low voltage electronic equipment in an electric drive is of high importance, it reduces electromagnetic interference by taking the differential of the two floating rails. Therefore any noise signal coupled to the isolated supply is largely removed by *common mode rejection*.

Isolation also has significant improvements for safety by preventing the user from being able to come into contact with any high voltage component through use of the control panel. It should be noted that the isolation barrier can pose difficulties for current measurement using sense resistors, as the control circuitry floats in relation to the motor winding. This problem can be overcome by using isolation amplifiers or by modification to the current measurement technique; these techniques can be costly.

It is not uncommon to find power supplies in commercial use that do not implement isolation between power and control components and these implementations tend to have concerns with electromagnetic interference, reliability, and safety.

An important consideration for the power supply is the implementation of **P**ower **F**actor **C**orrection (PFC). The windings of an SRM present a variable inductive load to the supply and therefore the severity of correction required is also variable. For an SRM to obtain peak line efficiency, PFC must be implemented [12, 41].

4.3 Power Factor

The perceived and measurable efficiency of any electrical device is strongly related to its **P**ower **F**actor (PF). The perceived power drawn from the supply can be labelled as the *apparent power*, while the actual power consumed is labelled *true power.* The power that is not consumed is known as *reactive power*, and this represents the power that is being returned to the supply. The relationship between true power and apparent power is known as the power factor. The power factor of a system is a unit-less ratio and is explained by the following relationship [42]:

$$Power\ Factor = \frac{Actual\ Power\ Dissipated\ (True\ Power)}{Perceived\ Power\ Drawn\ (Apparent\ Power)} \qquad \textbf{(4.1)}$$

4.3.1 Reactance Phase Shift

Power factor is affected by the presence of reactive components within a circuit. Reactive components appear to dissipate power by flowing currents and creating potential differences; this power is the result of energy being stored within the reactive component, either magnetically or electrically, to be returned to the supply at a later time. The reactive component does not dissipate this energy as heat.

A circuit which consists of only resistive components will have a power factor of one, called *unity* [43]; this is considered to be the perfect power factor because all power drawn is consumed within the circuit. The expected waveforms for a purely resistive circuit are shown in Figure 4-2:

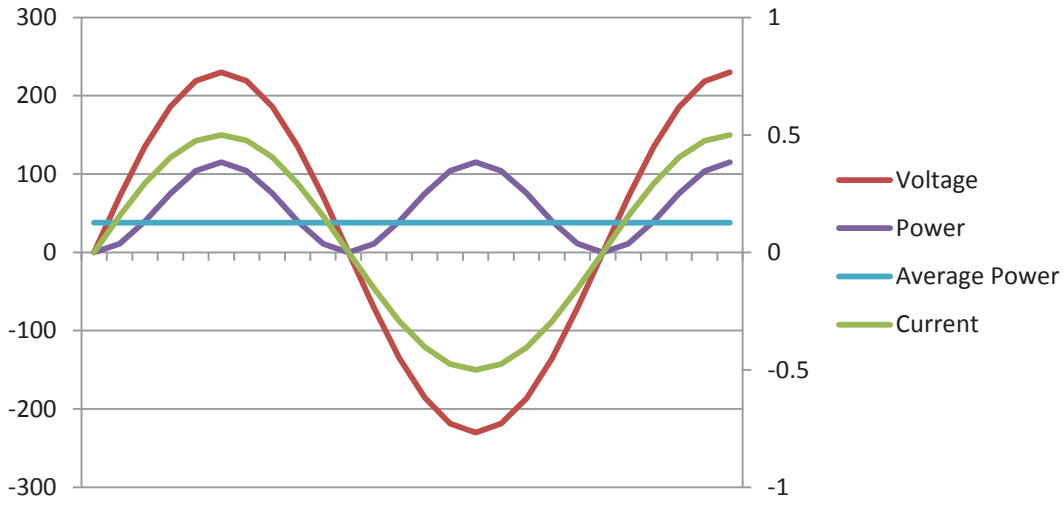

Figure 4-2: Power Waveforms Of A Unity Load

For circuits which are purely resistive, the power waveform can never be negative. This is because the voltage and current waveforms are in phase and the positive to negative transition for both waveforms occurs simultaneously [44]. Positive power represents power consumed by the device, whereas negative power represents power drawn but returned to the supply. It should also be noted that the power waveform is double the frequency of the voltage and current waveforms.

A purely reactive circuit will have a power factor of zero [43], which implies that all power drawn is returned to the supply. The expected waveforms for a purely reactive circuit, consisting only of inductance are shown in Figure 4-3:

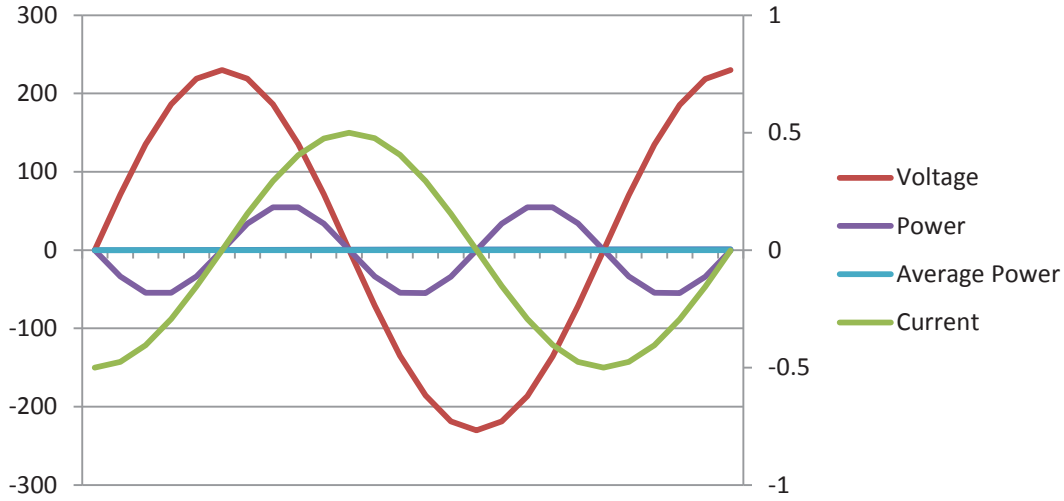

Figure 4-3: Power Waveforms Of An Inductive Load

The power waveform consists of positive and negative components. The voltage and current waveforms are ninety degrees out of phase; this causes a power factor of zero. Power is drawn from the supply during the positive cycle of the power waveform and is returned to the supply on the negative cycle [42, 44]. This power factor is called *lagging* as the current trails the voltage, and is represented as a positive.

The reactive component is not required to be purely inductive, it may be purely capacitive or a combination. For a circuit which has reactive properties stemming primarily from a capacitive reactance it is said to have a *leading* power factor, and is represented as negative and has a negative reactive power vector [43, 44]; this is because the current leads the voltage waveform.

A circuit which contains equal reactance from capacitive and inductive components has the reactive component nullified due to the opposition in sign. This would behave identically, in terms of power factor, to a purely resistive circuit; this forms the basis of power factor correction.

For a circuit containing both resistive and reactive components, the power factor will vary between zero and one. Therefore of the amount of power perceived to be drawn, a portion will be consumed within the circuit and the remaining will be returned to the supply. The expected waveforms for a 0.6 lagging power factor are shown in Figure 4-4:

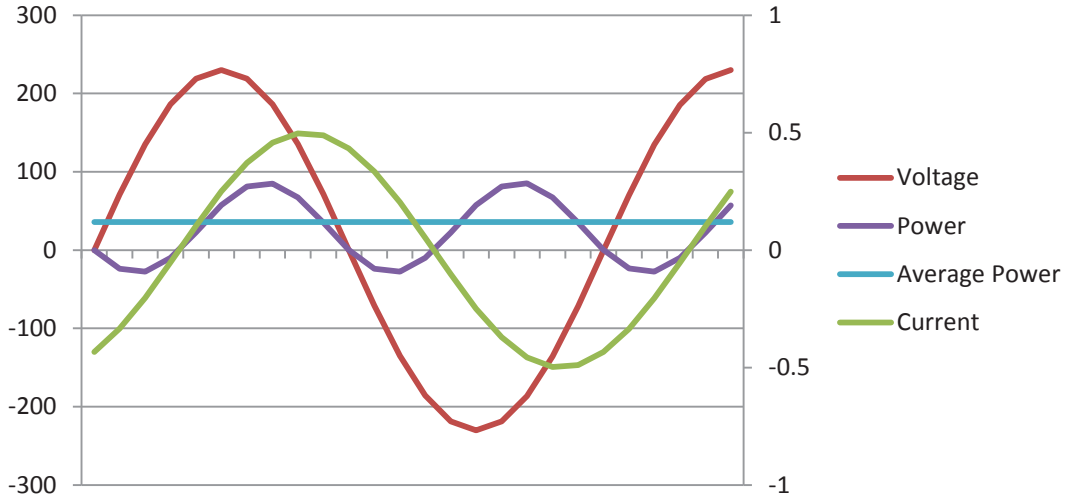

Figure 4-4: Power Waveforms Of A 0.6PF Lagging Load

The power waveform is offset vertically from the horizontal axis. This offset is affected by the presence of both reactive and resistive components. This is because the integral of the positive cycle of the power waveform exceeds the negative cycle. Due to the presence of positive power it can be said that this circuit is consuming power. This power consumption is related to the magnitude of the current drawn by the resistive components in the circuit.

4.3.2 Measurement of power quantities

AC supplies have three measurable power quantities, apparent power (**S**) which is measured in *volts-amperes* (**VA**), true power (**P**) which is measured in *watts* (**W**) and reactive power (**Q**) which is measured in *volt-amperes reactive* (**VAR**). Apparent power is related to the total circuit impedance (**Z**), true power is related to the total resistance of the circuit (**R**), and reactive power is related to the total reactance of the circuit (**X**). The equations governing these three quantities are shown below:

$$Apparent\ Power\ (S) = I^2 Z \quad \textbf{(4.2)}$$

$$Apparent\ Power\ (S) = VI \quad \textbf{(4.3)}$$

$$True\ Power\ (P) = I^2 R \quad \textbf{(4.4)}$$

$$Reactive\ Power\ (Q) = I^2 X \quad \textbf{(4.5)}$$

The formula for calculating power from voltage and current, Equation 4.3, is only applicable for calculating apparent power; this is because the formula is traditionally used to calculate power from the RMS values of voltage and current and therefore assumes total circuit impedance. This formula can be used for calculating instantaneous true or reactive power on a singular component basis only.

4.3.3 Vector relationship of power quantities

The calculation of apparent power, true power, and reactive power by relationship requires the magnitude of those quantities and the *impedance angle*. The impedance angle is the absolute angle formed by the apparent power between the true power and reactive power components; reactive power is always perpendicular with respect to true power. These quantities can therefore be treated as vector quantities, and this simplifies the relationship between the quantities to Pythagoras trigonometry as shown in Figure 4-5 [44, 45]:

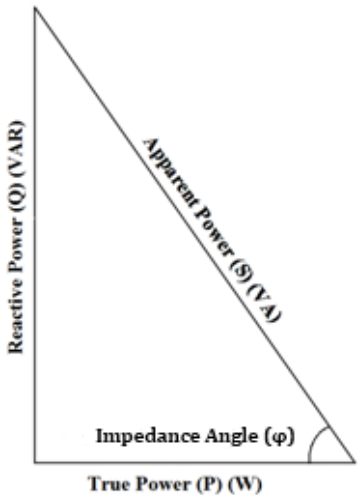

Figure 4-5: Vector representation of Power Factor quantities

Reactance can be separated into inductive reactance and capacitive reactance, which consist of **j** and **–j** phase angles respectively. Inductive and capacitive reactance are polar opposites and therefore scalar calculation can be used to calculate the overall reactance.

$$Overall\ Reactance\ (X) = jX_L - jX_c \qquad \textbf{(4.6)}$$

Figure 4-5 shows the vector relationship for a circuit which is primarily inductive, if the circuit was primarily capacitive then the reactive power would be of negative magnitude;

therefore the magnitude of the impedance angle is dependent only upon the magnitude of the reactive power. The sign of the reactive power determines if the current waveform lags or leads the voltage waveform.

The phase angle difference between the voltage and current waveforms is the same as the angle created by the various power quantities; this thesis denotes this angle *current phase angle* or ϕ, as this relates it more directly to the separation of the current and voltage waveforms.

This allows the solution of any power quantity value, given that two of the quantities are known, or the current phase angle is known. Apparent power and true power are the easily measured quantities, reactive power can be found by the following equation:

$$Q = \sqrt{(Apparent\ Power\ (S))^2 - (True\ Power\ (P))^2} \quad \textbf{(4.7)}$$

4.3.4 Calculation of power factor

Power factor is defined as the ratio between perceived power draw and actual power consumption [46], and can be expressed as:

$$PF = \frac{True\ Power\ (P)}{Apparent\ Power\ (S)} \quad \textbf{(4.8)}$$

However, since the current phase angle ϕ is equivalent to the angle between the adjacent and hypotenuse of the triangle formed by the various power quantities, the current phase angle can be used to calculate power factor by the following equation:

$$PF = |\cos(\phi)| \quad \textbf{(4.9)}$$

This equation is valid if the current waveform is purely sinusoidal. In practice, this is generally not the case as the current waveform tends to be harmonically distorted by semi-conductor devices [46]. This form of power factor distortion is covered in depth in section 4.3.6, *Harmonic Distortion*.

4.3.5 Impact of Power Factor on Circuit Performance

Power factor is an important consideration for the design of circuits operating from an alternating current supply. A low power factor results in higher peak and average currents being drawn from the supply than would be expected. The excess power is a result of the higher than expected current draw, and since it is returned to the source it can therefore not be considered real power; however it does result in real current and this current results in power loss along any conducting path in the circuit, as described by the following equation:

$$P = I^2R \tag{4.10}$$

Therefore all conductors and components must be specified to handle the excess demand. In the case of current limited supplies, power factor plays a large part in achieving the maximum output from the device. Therefore low power factor results in a low efficiency power delivery system. It is common practice for power supply companies to charge industrial customers penalties for poor power factor, generally sub 0.95 lagging [47].

4.3.6 Harmonic Distortion

The power factor disruption discussed previously is known as *displacement power factor.* When considered as a whole, *true power factor* includes harmonic distortion created by *non-linear* loads and is described by the following equation, courtesy of [46]:

$$TPF = \frac{V_{rms}I_{1,rms}|\cos\phi|}{V_{rms}I_{rms}} = \frac{I_{1,rms}|\cos\phi|}{I_{rms}} = K_p|\cos\phi| \tag{4.11}$$

Where I_{rms} is the total rms current, $I_{1,rms}$ is the fundamental rms current, and V_{rms} is the rms voltage. K_p is known as the *purity factor* of the current waveform, and is of value between 0 and 1. For a circuit which contains no harmonic distortion, then K_p is of value 1 and only the current phase angle ϕ is relevant to the power factor [46]. This is not typical for devices operating from the mains supply, as they tend to employ diode based bridge rectifiers to provide a DC supply; this introduces harmonic distortion into the current waveform reducing the value of K_p.

A non-linear load reshapes the current waveform of an AC signal by the addition of harmonics at frequencies which are multiples of the basal frequency. An example of such a component is a diode. The voltage will rise but the diode will not conduct current until the voltage is sufficiently high; this creates a high frequency step in the current. A bridge rectified low voltage alternating current supply is shown in Figure 4-6:

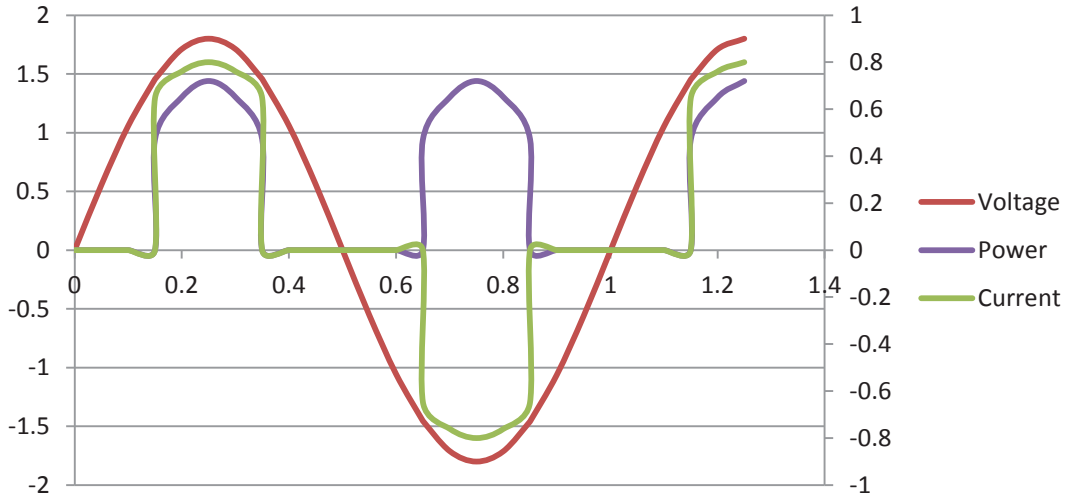

Figure 4-6: Power Waveforms For A Harmonically Distorted Load

The scenario presented is exaggerated by the small voltage waveform in relation to the forwards conductive voltage drop of the bridge rectifier. This was chosen to easily illustrate the presence of harmonic distortion as a result of non-linear loading.

It can be seen that the non-linear loading of the bridge rectifier prevents the flow of current until sufficient voltage is achieved; note that this does not affect the phase angle between the voltage and the current as the circuit presented is purely resistive; this would not be true of a reactive circuit. The non-linear load therefore introduces harmonic distortion into the current waveform which results in distortion of the same frequency to be present in the power waveform; this distortion results in a low purity factor K_p and therefore a low power factor.

While the level of harmonic distortion present in a high voltage AC circuit would be minimal in amplitude in comparison to that of the dominant frequency, it impacts the ability for the circuit to distribute power effectively and cleanly; this effect is related to the size of the non-linear load, some circuits will present large harmonic distortion due to the voltage required to cause a current flow, or the number and frequency of switching devices.

In circuits which contain a reactive component, the presence of harmonic distortion affects the total circuit impedance. Capacitive elements will offer higher admittance to harmonic currents, while inductive components will resist harmonic currents. The presence of harmonic distortion can therefore further affect the power factor by causing the total reactance of the circuit to decrease or increase.

4.4 Power Factor Correction

The root cause of low power factor is the introduction of phase difference between the voltage and current waveforms of an AC supply and generation of harmonic currents. The method of correcting low power factor is to provide the opposite reactance of the same magnitude; correction of a lagging power factor is achieved by the addition of capacitance, and a leading power factor is corrected by the addition of inductance [42].

The addition of the equal but opposite reactance means that the power that was being returned to the supply is now passed between the capacitor and the inductor. This also creates losses in the path. However, these losses are minimal in comparison to a low power factor. This is known as **P**assive **P**ower **F**actor **C**orrection (PPFC) and is used to correct the power factor of a device with the characteristics of *static reactance* and *linear loading*.

A device with static reactance has no change in reactance during operation therefore passive correction is a suitable and cost-effective solution. Should the load not be static, then the technique for correcting the power factor is **A**ctive **P**ower **F**actor **C**orrection (APFC).

The SRM is a *variable reactive load*. This results in a phase difference between the voltage and current waveforms that is dependent upon the switching frequency of the electronic converter. Active Power factor correction is important in this situation as it varies the opposing reactance presented to the AC supply to present the smallest phase angle difference; this is achieved by switching of reactive components.

4.4.1 Passive Power Factor Correction

PPFC involves the inclusion of additional passive components, without feedback control, into the circuit in an attempt to minimise the current phase angle ϕ and prevent the propagation of harmonic currents that reduce the purity factor K_p.

Passive techniques can be used to rectify displacement power factor if the reactance of the load is static; this implies that the dominant frequency of operation is fixed. It can also be used to correct harmonic distortion of the input current waveform if the harmonic behaviour is consistent; this is achieved by the addition of capacitors and inductors to create second order harmonic filters.

A harmonic filter is a frequency filter designed to prevent the propagation of the harmonic current through the load. In the case of circuit boards utilising non-rhythmic electronic switching equipment, such an approach is implausible and active power factor correction must be used.

PPFC has advantages in lower component count, higher circuit reliability, insensitivity to noise and surges, does not generate high-frequency EMI, and generally has lower power loss than active techniques due to the lack of switching components [48].

4.4.1.1 Reactance Balancing

Displacement power factor distortion is corrected passively by addition of the opposing reactance. This effectively nullifies the reactive component present in the total circuit impedance, resulting in the total circuit impedance comprising of only the resistive component [42]. This technique is only effective at correcting static reactance, and provides little benefit to prevent the propagation of harmonic currents. An example of a non-corrected inductive and resistive AC circuit is shown in Figure 4-7:

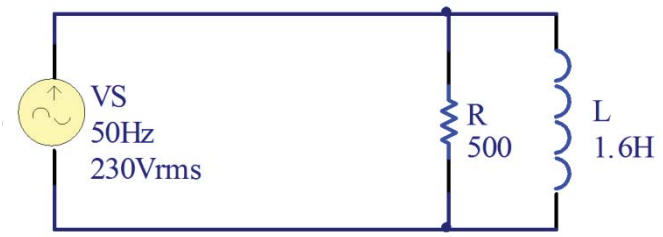

Figure 4-7: AC Circuit With Resistive And Inductive Loading

Where R is a perfect resistor of resistance 500Ω, and L is a perfect inductor of inductance 1.6H. Therefore the inductive reactance of the inductor is described by:

$$X_L = \omega L = 2\pi f L = 2\pi\ x\ 50\ x\ 1.6 = 502.4\Omega \quad \textbf{(4.12)}$$

The values of resistance, and inductive reactance can be placed directly into the power triangle shown in Figure 4-5 as they are both related by the common factor of I^2; the inductive reactance is of phase angle j. The current phase angle can be obtained by the following equation:

$$\phi = \tan^{-1}\left(\frac{X_L - X_c}{R}\right) = \tan^{-1}\left(\frac{502.4 - 0}{500}\right) = 45.13^{\circ} \quad \textbf{(4.13)}$$

Therefore the power factor of this arrangement is calculated by:

$$PF = |\cos(\phi)| = |\cos(45.13)| = 0.706 \quad \textbf{(4.14)}$$

As was mentioned previously, power factor can be corrected passively by the addition of reactance of the opposing magnitude [45]. In the circuit presented in Figure 4-7, this would be a capacitor of capacitive reactance 502.4Ω. The required capacitance can be calculated by the following equation:

$$X_C = X_L = 502.4\Omega \quad \textbf{(4.15)}$$

$$\frac{1}{\omega C} = \omega L \Rightarrow \frac{1}{2\pi f C} = 2\pi f L = 502.4 \quad \textbf{(4.16)}$$

$$C = \frac{1}{\omega X_L} = \frac{1}{2\pi f(2\pi f L)} = \frac{1}{(2\pi f)^2 L} = \frac{1}{16000\pi^2} = 6.333\mu F \quad \textbf{(4.17)}$$

Therefore a capacitor of value 6.333μF placed in parallel with the inductor L will correct the power factor passively. This addition to the circuit is shown in Figure 4-8:

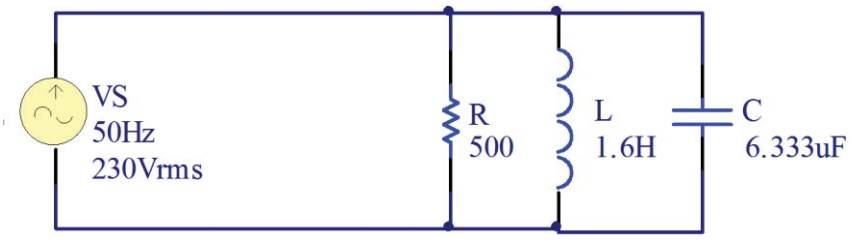

Figure 4-8: Capacitively Corrected Inductive And Resistive AC Circuit

The inductive reactance presented by the inductor L remains 502.4Ω. The resistance provided by the resistor R remains 500Ω, and the capacitive reactance provided by the capacitor is described by:

$$X_C = \frac{1}{2\pi f C} = \frac{1}{2\pi\ x\ 50\ x\ 6.333x10^{-6}} = 502.6\Omega \qquad \textbf{(4.18)}$$

Therefore the overall reactance X is described by:

$$Overall\ Reactance\ X = jX_L - jX_c = 502.4 - 502.6 = -j0.2\Omega \qquad \textbf{(4.19)}$$

The current phase angle can be solved by use of the power factor triangle resulting in a current phase angle described by:

$$\phi = \tan^{-1}\left(\frac{X_L - X_c}{R}\right) = \tan^{-1}\left(\frac{502.4 - 502.6}{500}\right) = -0.023^{\circ} \qquad \textbf{(4.20)}$$

Therefore the power factor of the passively corrected circuit is:

$$PF = |\cos(\phi)| = |\cos(-0.023)| = 0.999 \qquad \textbf{(4.21)}$$

Therefore the displacement power factor distortion of the inductive and resistive AC has been passively corrected by the addition of an appropriately sized capacitor.

4.4.2 Correction of harmonically distorted current

The technique for correction of a harmonically distorted input current waveform in passive power factor correction is the addition of passive components to create filters; these filters are tuned to sink or prevent the propagation of harmonic currents [48].

This section will outline the case of a bridge rectifier connected to the mains supply, and the various filter configurations that can be applied to correct harmonic currents. These filters will be discussed based on their strengths and weaknesses.

Figure 4-9 illustrates a rectified mains supply powering a resistive load:

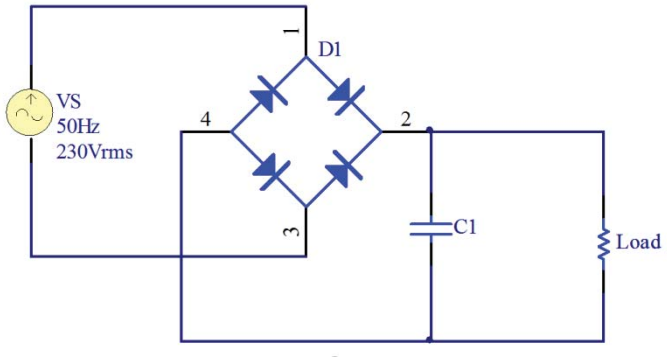

Figure 4-9: Bridge Rectified AC Supply With Smoothing Capacitor

The presence of the smoothing capacitor C1 in the bridge rectifier will cause a phase difference between the voltage and current waveforms, but this behaviour will be ignored for the purpose of illustrating harmonic correction; when a harmonic correction technique also benefits the phase angle separation it will be noted. The harmonic filtering can be used in conjunction with reactance balancing of the load to achieve minimal current phase angle and maximum purity factor.

The capacitance of the smoothing capacitor C1 will have an effect on the amplitude of the harmonic current drawn when the bridge rectifier diodes forwards conduct; the larger the value of the capacitor the greater the amplitude of the harmonic current. Reduction in the size of the capacitance will reduce the peak amplitude of the harmonic current, but significantly increase voltage ripple which is undesirable.

The harmonic filter circuits which will be discussed are:

- AC Side Series Inductance
- Series Band-pass filtering
- Harmonic trap filtering
- Capacitor-fed rectifier

4.4.2.1 AC Side Series inductance

The AC side series inductance harmonic correction is shown in Figure 4-10:

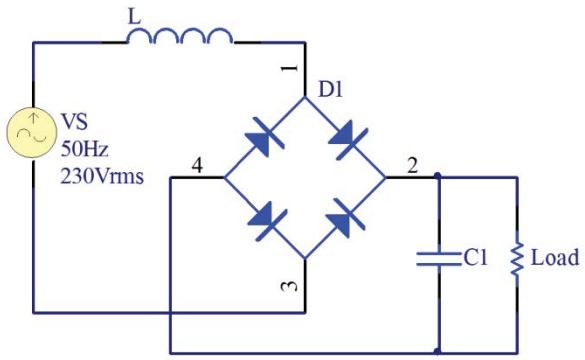

Figure 4-10: AC Side Series Harmonic Distortion Filter

The presence of the inductor between the mains supply and the rectifier smooths the current waveform and reduces the current phase angle created by the smoothing capacitor C1. The design consideration for the inductor is such that the magnitude of the current flowing is zero when the voltage waveform crosses the zero axis. The main points of comparison for this harmonic correction technique can be summarised by:

- Low-cost and high reliability due to single component
- Moderate correction to the current phase angle
- Moderate correction to the harmonic currents

4.4.2.2 Series Band-pass filtering

The series band-stop filter is shown in Figure 4-11 and is present on the AC side of the rectifier:

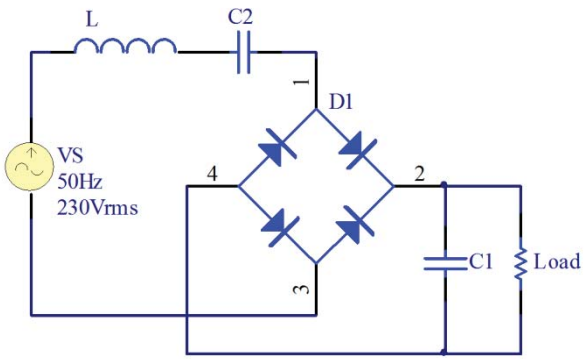

Figure 4-11: AC Side Series Band-Pass Harmonic Distortion Filter

The frequency response of the filter is described by the following equation:

$$F_c = \frac{1}{2\pi\sqrt{LC}} \qquad \textbf{(4.22)}$$

The band-pass filter consists of an Inductor L and a capacitor C2, and is tuned to allow the line frequency to pass, and to attenuate frequencies either side of the line frequency; as line frequencies are low this tends to result in large values for the band-pass components.

The band-pass harmonic filter effectively eliminates harmonic currents and provides good current phase angle correction; this phase angle change can be further corrected by reactance balancing of the load.

The main points of comparison for this technique can be summarised by:

- Moderate cost due to two high value components
- Good correction to the current phase angle
- Excellent correction of harmonic currents

4.4.2.3 Harmonic trap filtering

A modification to the series band-pass filter is the harmonic trap filter. This approach is shown in Figure 4-12 and is present on the AC side of the rectifier:

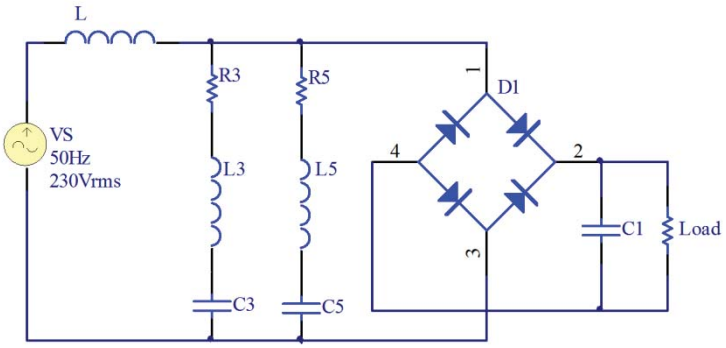

Figure 4-12: AC Side Harmonic Distortion Trap Filtering

The difference between this filter and the series band-pass filter is the series LC network is providing a very low impedance path around the bridge rectifier; this prevents the harmonic current from flowing through the load. The resistor is present in each trap filter to limit the peak value of the current flowing through the filter. The presence of this resistor reduces the efficiency of this approach.

The frequency response equation of each harmonic trap filter is same as the series band-pass. Each harmonic trap filter is tuned to a specific harmonic frequency, therefore this approach is expensive due to the high component count.

The harmonic trap filter exhibits excellent harmonic current correction, and excellent current phase angle balancing when tuned appropriately; the current phase angle can be further corrected by reactance balancing of the load.

The main points of comparison for this technique can be summarised by:

- Highest cost due to individual trap filters for each harmonic frequency
- Excellent correction of current phase angle
- Excellent correction of harmonic currents

4.4.2.4 Capacitor Fed Rectifier

The capacitor-fed rectifier is shown in Figure 4-13, and is present on the AC side of the rectifier:

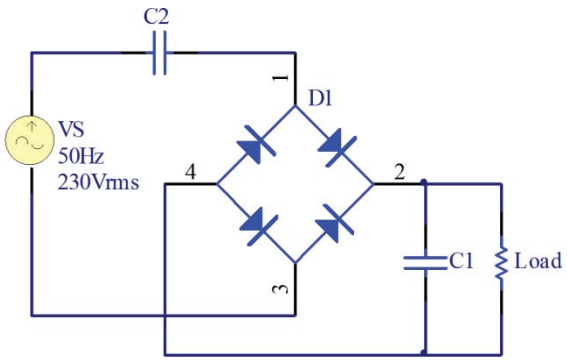

Figure 4-13: AC Side Capacitor-Fed Bridge Rectifier Harmonic Distortion Filter

The capacitor-fed rectifier is a very simple circuit which reduces harmonic current amplitudes. The harmonics are still present as steps in the sinusoidal current waveform when the rectifier switches.

The current phase angle correction of this technique is poor and will require reactance balancing of the load. There is also a significant decrease in available voltage across the load.

The main points of comparison for this technique can be summarised by:

- Very low cost due to single component
- Poor correction of current phase angle
- Poor correction of harmonic currents
- Significant reduction in output voltage

4.4.3 Active Power Factor Correction

APFC is a complete electronic system that corrects both the current phase angle ϕ and the harmonic distortions present in the current waveform by increasing K_p.

This is usually achieved by the use of a DC-DC converter following the bridge rectifier, and the switching of a reactive component into and out of the circuit. The reactive component switched is generally inductive as capacitors exhibit ringing of the voltage waveform upon switching; this requires the reactance of an inductive biased circuit to be passively overbalanced to capacitive.

One of the key drawbacks to an active power factor correction approach is the generation of high-frequency EMI; this requires passive filtering before the bridge rectifier.

Figure 4-14 shows illustrates the basic accepted topology of a power supply incorporating active power factor correction:

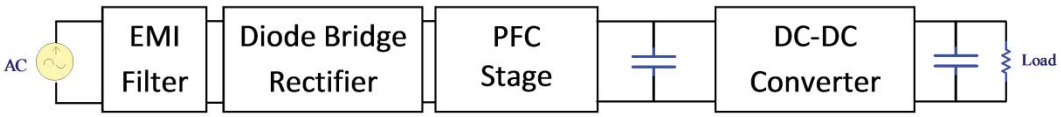

Figure 4-14: Functional Diagram Power supply Including Active Power Factor Correction

The presence of the PFC stage reduces the harmonics present in the current waveform, hence greatly improving the purity factor K_p. The switching element employed is usually an inductor, and this can be used to reduce the current phase angle ϕ if the circuit reactance has been overbalanced to capacitive resulting in excellent power factor correction.

The drawback is that the PFC stage is complex and incorporates high frequency switching which increases generation of EMI, as well as lowering overall efficiency due to increased switching losses; this lowering of efficiency results in greater heat production and therefore the PFC stage tends to consist of bulky components increasing the size, weight, and lowering the reliability of the electronics.

The DC-DC converter stage can be implemented in three various base configurations, which are as follows:

- Buck
- Boost
- Buck-Boost

4.4.3.1 Buck Converter

The buck converter, which is illustrated in Figure 4-15, is an implementation of the DC-DC Converter stage in a typical APFC:

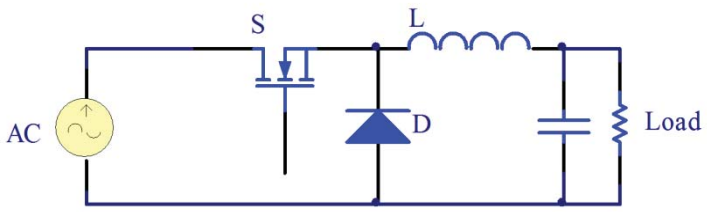

Figure 4-15: Active Power Factor Correction Buck DC-DC Converter

The buck converter has a step-down conversion, which allows an output voltage lower than that of the input voltage. However, the converter can only operate when the line voltage exceeds the output voltage; this behaviour results in discontinuous conduction of the current within the inductor which results in higher EMI generation.

The step-down conversion of the buck converter is described by the equation:

$$V_{out} = DV_{in} \quad \textbf{(4.23)}$$

Where V_{out} is the output voltage, V_{in} is the input voltage, and D is the duty cycle of the transistor; this equation ignores the semi-conductor voltage drops.

4.4.3.2 Boost Converter

The boost converter, which is illustrated in Figure 4-16, is an implementation of the DC-DC Converter stage in a typical active power factor correction circuit:

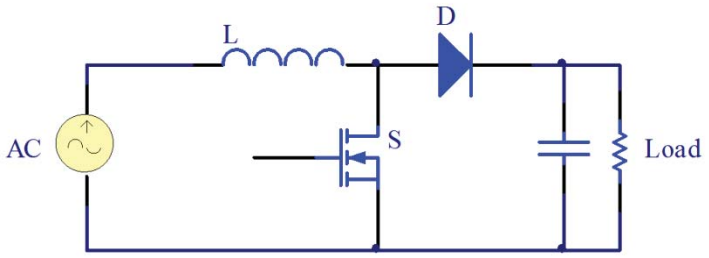

Figure 4-16: Active Power Factor Correction Boost DC-DC Converter

The boost converter has a step-up conversion relationship with the input voltage, and therefore the output voltage always exceeds the line voltage; this results in continuous current flow through the inductor as operation throughout the entire cycle of the line voltage is possible which reduces EMI generation.

As the boost converter is of a step-up relationship with the input voltage, it is a typical choice in electronics that must operate from a wide range of input voltages; typically 115Vrms or 230Vrms supplies.

The step-up conversion of the boost converter is described by the equation:

$$V_{out} = \frac{V_{in}}{1 - D} \tag{4.24}$$

Where V_{out} is the output voltage, V_{in} is the input voltage, and D is the duty cycle of the transistor; this equation ignores the semi-conductor voltage drops and assumes continuous current flow in the inductor.

4.4.3.3 Buck-Boost Converter

The buck-boost converter, which is illustrated in Figure 4-17, is an implementation of the DC-DC Converter stage in a typical APFC:

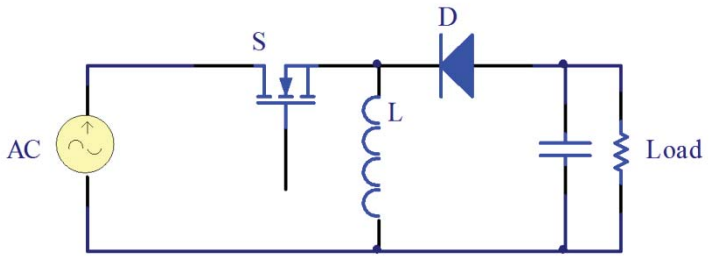

Figure 4-17: Active Power Factor Correction Buck-Boost DC-DC Converter

The buck-boost converter has both a step-up and step-down conversion relationship with the line voltage; this allows an output voltage which is higher or lower than the input voltage allowing greater freedom in design. This behaviour allows conversion throughout the entire cycle of the line voltage.

The major drawback is that the output voltage is inverted with respect to the input voltage which results in greater stress for the switching components, and the inductor current is discontinuous which results in a greater generation of EMI. The buck-boost can be implemented in a two-switch design which alleviates the stress of the inverted output voltage, at the cost of increased conduction loss and component cost [49, 50].

The voltage conversion of the buck-boost converter is described by the equation:

$$V_{out} = \frac{D}{1 - D} V_{in} \qquad \textbf{(4.25)}$$

Where V_{out} is the output voltage, V_{in} is the input voltage, and D is the duty cycle of the transistor; this equation ignores the semi-conductor voltage drops and assumes continuous current flow in the inductor.

4.5 Electronic Power Converter

There are various methods for implementing the power electronics to switch the phases, whether the phases are operated by independent or shared switching components depends on the application the motor intends to be used as. Some of the topologies introduced concentrate on lowering component count, while others allow the maximum voltage rating of the motor to be closer to that of the switch component; this is particularly useful at operating the motor to its maximum potential where the input voltage is limited

4.5.1 Split Rail Converter

The split rail converter, also known as a *Split-DC Converter,* is a high efficiency electronic power converter topology for an SRM. This efficiency is achieved through the storage of electrical energy from the DC Bus into capacitors, and free-wheeling the current when the phases are de-energising into these capacitors for energy recovery; the drawback of this approach is that the DC Bus voltage is effectively halved.

The split rail converter also boasts a lower component count than competing topologies; this is due to only one switch per phase and therefore one free-wheeling diode.

The basic schematic for a split rail converter is shown in Figure 4-18:

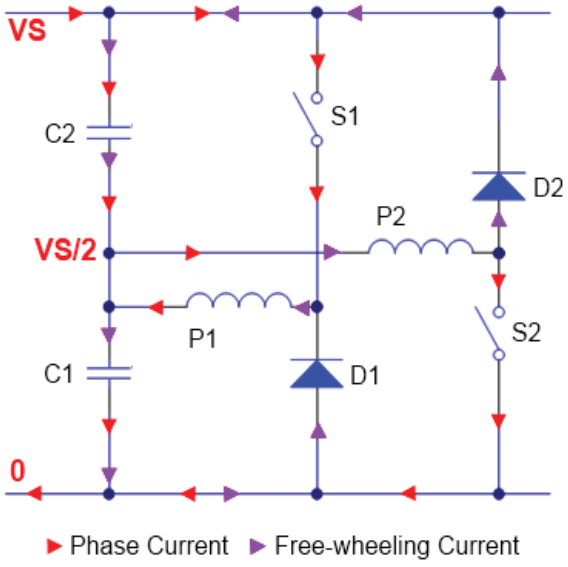

Figure 4-18: Split Rail Converter Schematic

This converter operates in two modes, phase excitation, and phase discharging.

To excite a given phase, the respective switch is closed to allow conduction of current through the winding; closing switch S1 results in a current flow through phase winding P1 and closing switch S2 results in a current flow through phase winding P2. When the current flowing through a given winding exceeds the maximum permissible current, the converter will operate in phase discharging mode

In phase discharging mode, the respective switch for the active phase winding is opened, causing the corresponding free-wheeling diode to conduct and freewheel the current through the capacitor for energy recovery. Opening switch S1 will cause diode D1 to free-wheel, while opening switch S2 will cause diode D2 to free-wheel. The winding has approximately half the DC bus voltage applied across it in reverse polarity, resulting in a rapid decay of the current, thereby increasing the chopping frequency over competing topologies.

The typical voltage and current waveforms of a split rail converter are shown in Figure 4-19:

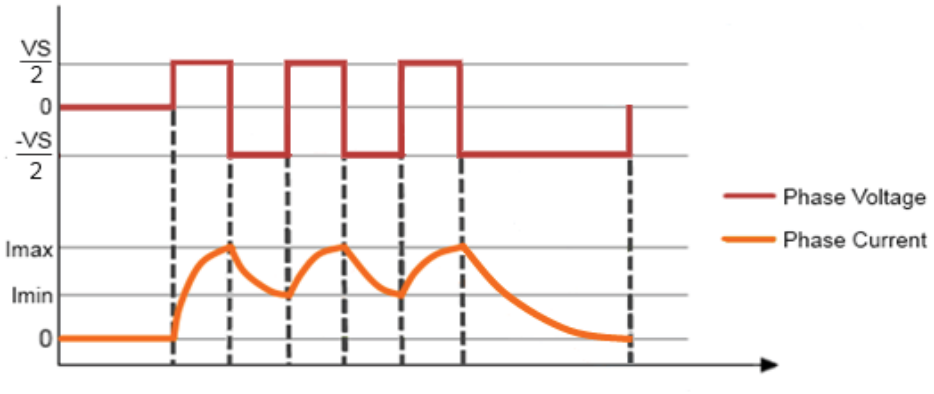

Figure 4-19: Split Rail Converter Voltage And Current Waveforms

This converter is capable of chopping to control the average current flowing; this chopping is achieved by phase excitation followed by partial phase discharging. The switching of the operation mode from phase excitation to phase discharging is determined when the current exceeds the maximum reference, or decays beneath the minimum reference. The single switch and free-wheeling diode per phase arrangement of this converter topology limit the control of current decay to bi-polar switching therefore current decay is rapid. The phases are not required to be operated in mutual exclusivity.

4.5.2 Miller converter (N+1 topology)

The Miller converter is also known as the *N+1 topology converter* as the number of switch elements is always one greater than the number of phases.

The advantage of this topology is the reduction in the number of switching elements, and providing the full DC bus voltage across the phase windings; resulting in a high inverter power rating to drive power rating ratio.

The main drawback of this converter is lack of flexible phase current control. This stems from the presence of a common mode switch; this limits the commutation period and prevents two phases from being excited simultaneously. This lack of allowable overlap results in higher torque ripple.

The basic schematic for a miller converter is shown in Figure 4-20:

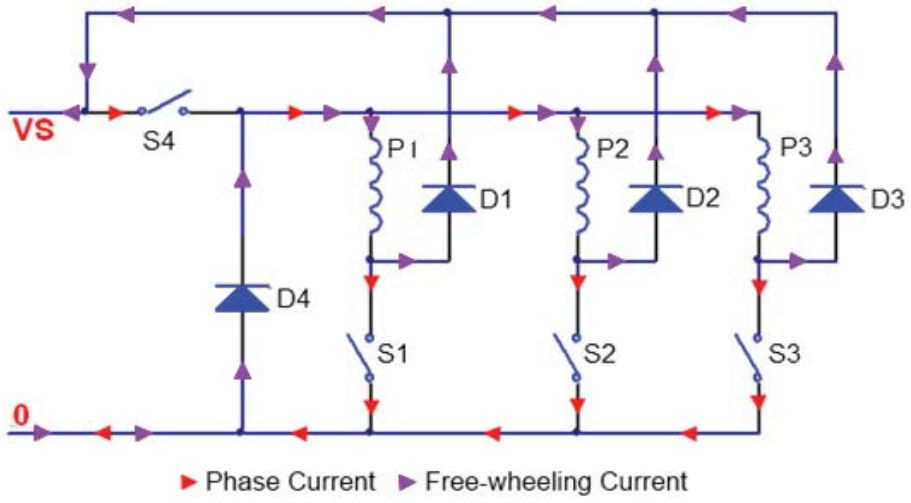

Figure 4-20: Miller Converter Schematic

The Miller converter operates in three distinct modes, phase excitation, current chopping, and phase discharging.

In phase excitation, the common mode S4 will conduct in pair with another phase winding switch. To excite phase A, switch S4 and switch S1 will be closed and the current flowing through the phase winding P1 will begin to increase; the current supplied from the source is equal to the current drawn by the motor winding.

Chopping occurs when the phase current surpasses the maximum reference and the common mode switch S4 will be opened, this will result in common mode diode D4 conducting. This results in a zero-volt-loop and the currently will decay slowly.

When the current beneath the reference, common mode switch S4 will conduct and the phase winding will have the full DC bus voltage applied across it and the current will begin to increase.

This converter operates between phase excitation and chopping modes while the rotor is moving towards the stator pole. Before the rotor reaches the stator pole, the converter will operate in phase discharging mode.

Phase discharging results in both the common mode switch S4 and all phase switches being open circuit. Continuing the example of phase A results in conduction of both diode D1 and the common mode diode D4 as the phase winding current decays and recharges the DC bus.

The typical voltage and current waveforms of a miller converter are shown in Figure 4-21:

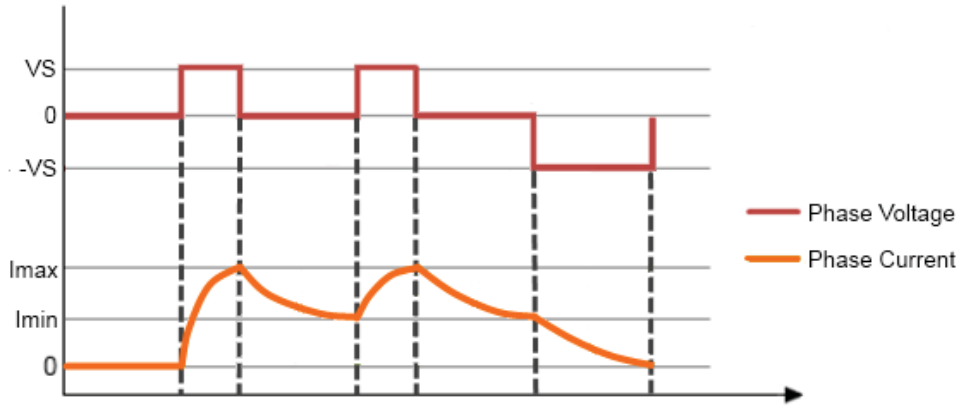

Figure 4-21: Miller Converter Voltage And Current Waveforms

4.5.3 Resistor-dump Converter

The resistor dump converter is a low cost topology. This is due to the presence of a single switching component per phase without the need for a common mode switch; this further reduces component count over the Miller converter presented in 4.5.2.

The drawback is the presence of a resistive dump component. This results in low efficiency as the energy that is removed from the phase during discharging is lost as heat.

The schematic of a resistor-dump converter in shown in Figure 4-22:

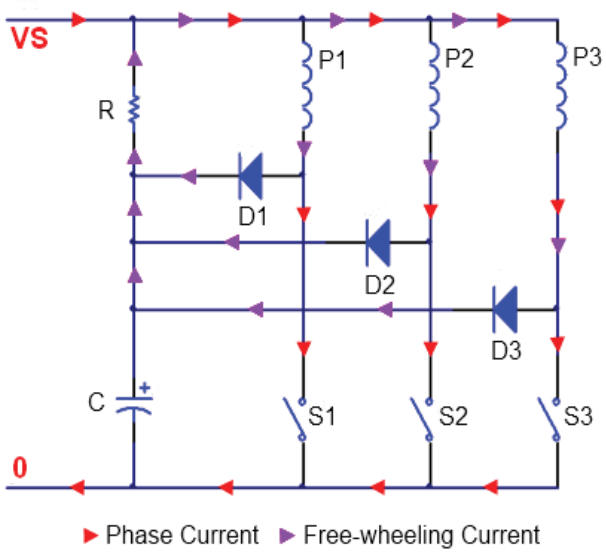

Figure 4-22: Resistor-dump Converter Schematic

The resistor-dump converter has two modes of operation, phase excitation and phase discharging.

The phases are excited by closing the respective switch to cause a current flow through the winding. For example, phase P1 will be excited by closing switch S1; this results in the DC supply voltage being applied across the phase winding P1. The current supplied by the DC bus is not always equal to that of the phase winding as this converter topology allows simultaneous excitation of phase windings.

Phase discharging occurs when the winding current increases to the maximum reference. Switch S1 is opened and diode D1 will conduct as the inductor voltage rises. The capacitor

voltage will exceed the DC supply voltage due to conduction of diode D1. The path for the current to decay is through the dump resistor R. Therefore the differential voltage applied to the phase winding P1 is negative.

The result is the decay of phase current P1 and the associated energy dissipated bled by the resistor R. The presence of the capacitor C is to snub the turn-off overvoltage condition that presents during switching; this reduces energy switching losses and extends the life of the switching components.

The typical voltage and current waveforms of a resistor-dump converter are shown in Figure 4-23:

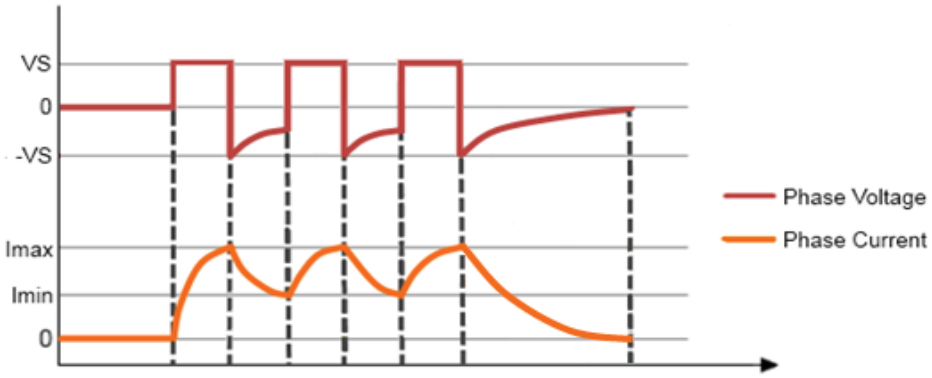

Figure 4-23: Resistor-dump Converter Voltage And Current Waveforms

This converter is capable of chopping to control the average current; this chopping is achieved by phase excitation followed by partial phase discharging. The switching of the operation mode from excitation to discharging is determined when the current exceeds the maximum reference, or decays beneath the minimum reference. The single switch and free-wheeling diode per phase arrangement of this converter topology limit the control of current decay to bi-polar switching; therefore current decay is rapid.

4.5.4 Capacitor-dump converter

Figure 4-24 illustrates the schematic of a capacitor-dump converter; it operates on a similar principle as the resistor-dump converter. However, as the dump component is reactive, the energy in phase discharging is conserved. Therefore, this converter has greater efficiency than the resistor-dump converter.

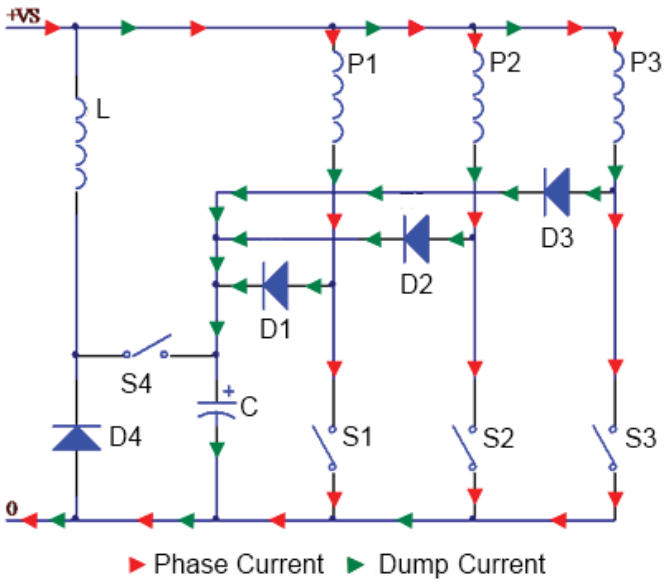

Figure 4-24: Capacitor-dump Converter Schematic

This topology is also a single switch per phase which reduces cost by reduction in component count.

The capacitor present across the DC bus reduces voltage ripple in the supply and this presents itself in reduced torque ripple.

This topology allows more precise control of the phase current increase and decay curves by providing the ability to negatively bias the phase windings. However, this converter is not capable of freewheeling. Therefore, the energy stored into the capacitor must be discharged appropriately. This converter is inflexible due to the presence of the common switch and is only capable of operating in *motoring mode*.

The capacitor-dump converter is capable of operating in seven different modes, although only four modes are generally used. These are phase excitation, current chopping, capacitor voltage regulation, current dumping.

In phase excitation mode, switch S1 will be closed and current will increase through the phase winding. When the phase current reaches the maximum reference switch S1 will be opened and diode D1 is forced to conduct; this operation mode is current chopping.

In current chopping mode the voltage applied across the winding is –Vs, phase current decreases until minimum reference is reached at which point switch S1 will be closed and the converter will operate in phase excitation mode.

The typical voltage and resulting current waveforms of a capacitor-dump converter are shown in Figure 4-25:

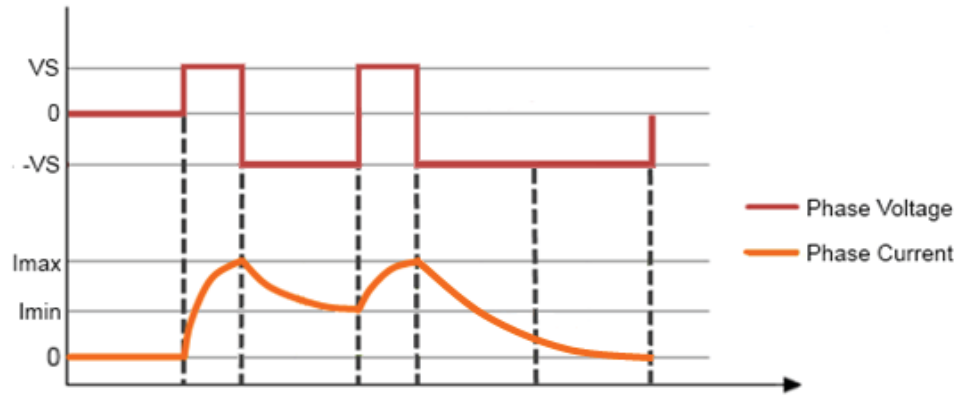

Figure 4-25: Capacitor-dump Converter Voltage And Current Waveforms

During capacitor voltage regulation mode, switch S4 is closed, and none of the phase diodes are conducting. The inductor L, diode D4, and switch S4 create a DC-DC step-down converter and this reduces the voltage of capacitor C. There is a similar mode of operation in which the phase diodes are also conducting; this mode is more complex and is not usually implemented as it provides no beneficial behaviour.

4.5.5 Freewheeling Capacitor-dump converter

Figure 4-26 illustrates the schematic of a free-wheeling capacitor-dump converter; this converter topology offers the benefits of the capacitor-dump converter. It offers strong advantages over the traditional capacitor-dump converter, primarily the ability to free-wheel current and utilise a uni-polar switching scheme.

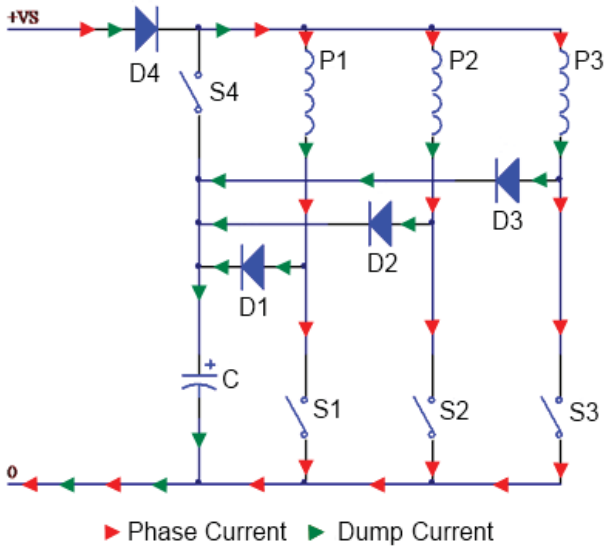

Figure 4-26: Freewheeling capacitor-dump Converter Schematic

The converter operates in five modes, phase excitation, capacitor charging, current chopping, phase-discharging, and capacitor discharging. In practice, only three of these are utilised.

In phase excitation, switch S1 is closed and current flow increases through the phase winding P1. When this current reaches the maximum reference switch S1 is opened, diode D1 will conduct, and switch S4 is closed providing a zero-volt loop across the phase winding to slowly decay the current, this is the current chopping mode of this converter.

In phase discharging mode, switch S1 is opened while switch S4 remains closed, this provides –Vs across the phase winding decreasing the current rapidly.

The typical voltage and current waveforms of a freewheeling capacitor-dump converter are shown in Figure 4-27:

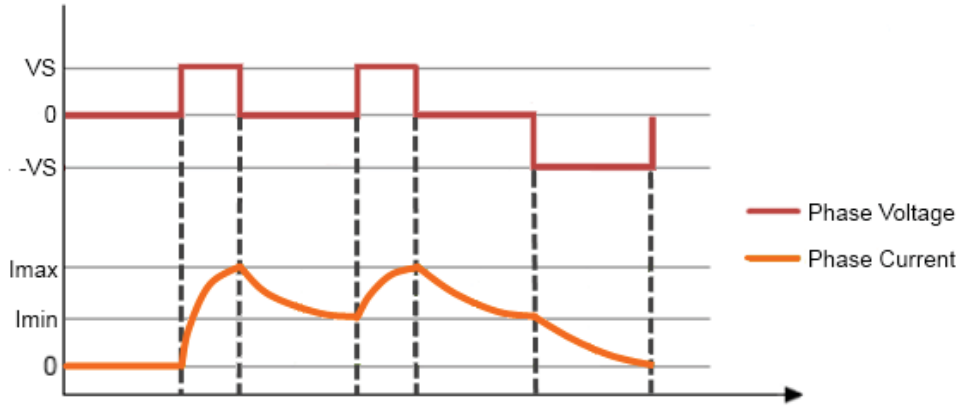

Figure 4-27: Freewheeling Capacitor-dump Converter Voltage And Current Waveforms

In capacitor charging mode, Switch S4 is opened while none of the phase diodes are conducting, this results in the capacitor C charging up to the DC bus voltage. When the capacitor voltage exceeds the DC bus voltage from current dumping of the phases, Switch S4 can be closed to reduce the capacitor voltage.

This converter is also a single switch per phase converter and therefore offers reduced component count, and reduced complexity when compared with the capacitive-dump converter.

4.5.6 Asymmetric half-bridge converter

The asymmetric half-bridge converter is a commonly implemented as the electronic converter in an SRM. The reasons for this is converter offers very flexible control as the phases are switched independently, and the presence of two switches per phase allows the choice of uni-polar or bi-polar switching; this control flexibility comes at the cost of increased component count.

This is a high efficiency converter as it recharges the DC supply when current chopping and discharging the phase winding. This converter topology allows the motor to run extremely close to the rail voltages.

The basic schematic diagram for an asymmetric half-bridge converter is shown in Figure 4-28:

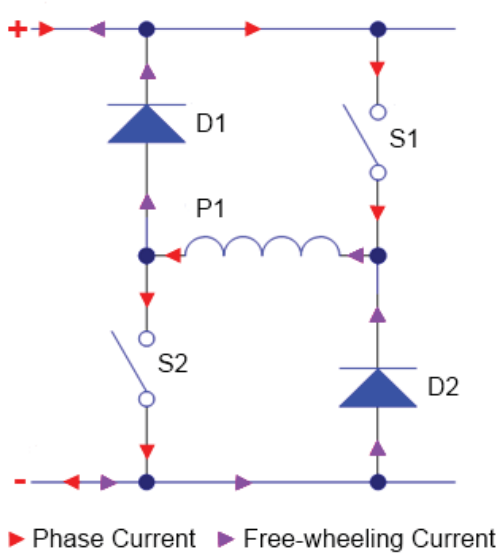

Figure 4-28: Asymmetric Half Bridge Converter

This converter operates in three modes, phase excitation, current chopping, and phase discharging.

In phase excitation, both the top and bottom switches, S1 and S2 respectively, of the converter bridge will conduct allowing a current to flow in the motor winding P1. As the current in the motor winding crosses the maximum reference, switch S1 will stop conducting and the converter will operate in current chopping mode.

In current chopping mode, switch S2 continues to conduct, while switch S1 is open circuit. Therefore the energy stored in the phase winding will create a freewheeling current flow through switch S2 and Diode D2. This provides a zero-volt-loop which allows the current in the winding to decay slowly to the minimum reference; this switching schema is known as bi-polar switching and is effective at reducing the chopping frequency.

When the phase is to be completely discharged, both switches will not conduct and the winding will rapidly discharge into the DC supply through the freewheeling diodes; this is achieved by reversing the polarity of the voltage applied to the winding.

Switch S2 is commonly named the *commutation transistor*, as it tends to be switched on at the beginning, and off at the end, of the positive torque generation region; thereby controlling commutation time of the winding. The associated free-wheeling diodes are named by the same nomenclature.

Switch S1 is commonly named the *chopping transistor*, as it tends to be switched on and off continuously through the commutation period, determined by switch S2, to control the current flowing in the winding. the associated free-wheeling diode is named by the same nomenclature.

The typical voltage and resulting current waveforms of an asymmetric half-bridge converter are shown in Figure 4-29:

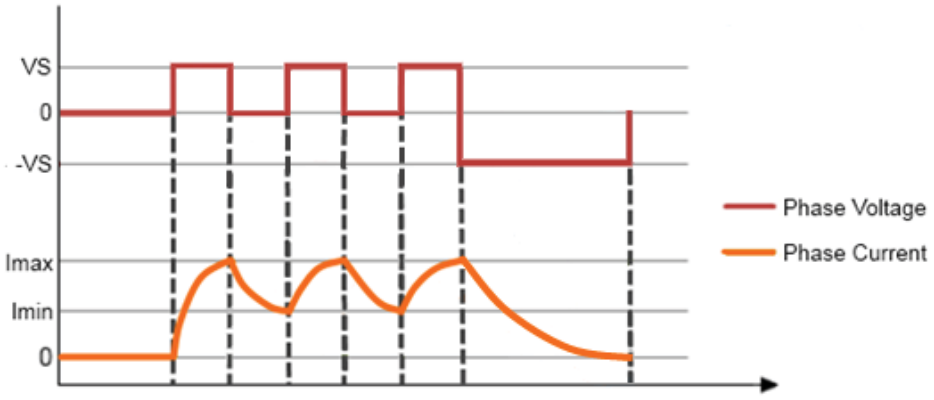

Figure 4-29: Asymmetric Half Bridge Converter Voltage And Current Waveforms

4.5.7 Shared Switch Converter

A shared switch asymmetric half-bridge converter reduces the component cost of the asymmetric half-bridge converter but with an impediment to current control flexibility as the phases are not mutually exclusive. The shared switch must be rated to at least twice the peak winding current flow.

The schematic for a shared switch asymmetric half-bridge converter is shown in Figure 4-30:

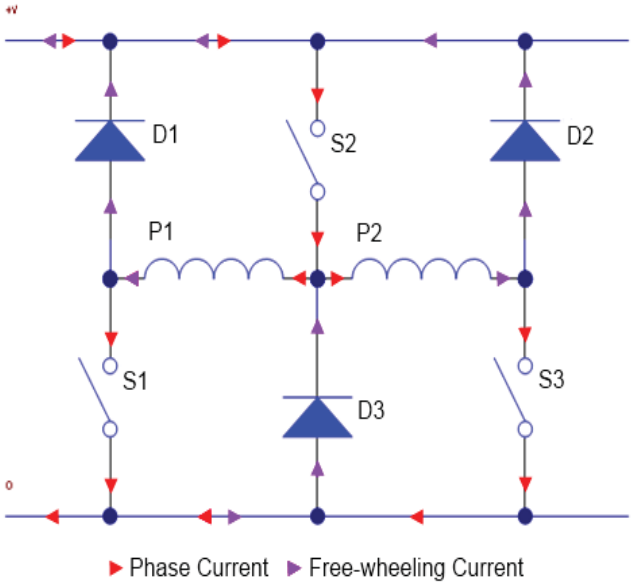

Figure 4-30: Shared Switch Converter

This converter operates in three different modes, phase excitation, current chopping, and phase discharging.

In phase excitation, the common switch S2 and switch S1 are closed, and the current through phase winding increases. When this current reaches the maximum reference switch S1 will open and a zero-volt-loop will be created through diode D3, the converter is now operating in current chopping mode.

In current chopping mode, the common switch remains closed as phase winding P2 is still in phase excitation mode, and this creates a slower current decay rate reducing chopping frequency. The phase current will decrease slowly until it reaches the minimum reference at which point switch S1 will close and phase current will increase as the converter is now operating in phase excitation mode.

In phase discharging mode, both common switch S2 and switch S1 will open, this results in both diodes D3 and D1 conducting and applying –Vs across the phase winding; this rapidly decays the current until it reaches zero.

The typical voltage and resulting current waveforms of a shared switch asymmetric half-bridge converter are shown in Figure 4-31:

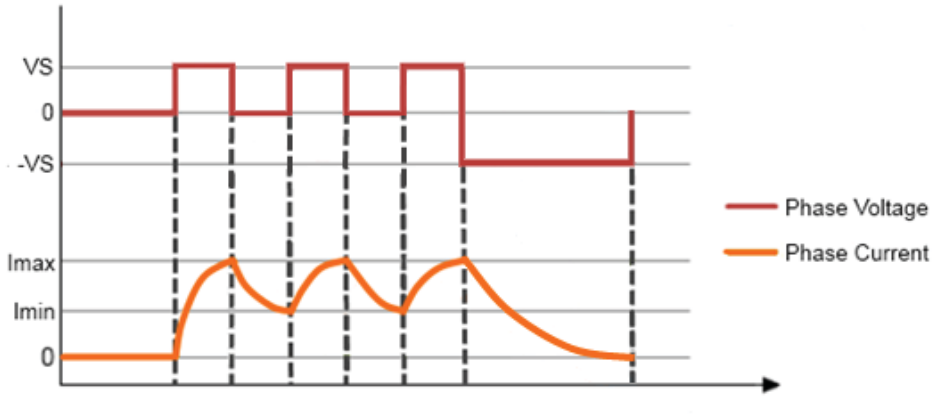

Figure 4-31: Shared Switch Converter Voltage And Current Waveforms

4.6 Summary

This chapter investigates a detailed field in SRMs, the power supply and electronic converter. These are both extremely important topics as they are crucial components in achieving the best performance and efficiency from an SRM.

Power factor, and power factor correction, are both covered in depth in this chapter as these topics largely impact the efficiency of the power supply. Power factor is a significant design consideration for the electronic drive of an SRM.

Electronic power converters are also covered in depth, as they are not only critical to the efficiency of the machine; they also provide the ability to control it appropriately.

The information contained within this chapter is critical to understanding the specific implementation of the power electronics present in the commercial system which is presented in Chapter 6, *DVR SRM Implementation*.

Chapter 5

Control Methodology and Algorithms

"The cybernetic exchange between man, computer and algorithm is like a game of musical chairs: The frantic search for balance always leaves one of the three standing ill at ease"

- Alan J. Perlis

This chapter covers the various aspects of providing appropriate control to an SRM. It covers the basic approach to control, and the various modes that the motor operates within, namely low and high speed motoring. The information in this chapter relates to information in earlier chapters which brings rise to the mentioned control methodologies presented. There is a brief mention of a control methodology which is currently being actively researched, known as sensor-less control.

5.1 Control Algorithm Overview

The choices for control algorithms are limited for an SRM; although use of the correct algorithm at the correct point in the torque-speed relationship is of critical importance [7, 9]. There are various factors to be considered when choosing the control algorithm, these are:

- Rotational Speed
- Impact on motor performance
- Efficient use of energy
- Reduction in generation of acoustic noise
- Prevention of negative torque generation
- Greater machine uptime

The maximum instantaneous torque produced is proportional to the peak current flowing in the winding, while the rotational speed of the motor is dependent upon the ability for the average torque to accelerate the load and the frequency at which the phases are excited. It should be noted that the frequency that the phases are switched at is not a causative relationship with rotational speed, but rather the phases must have increased switching frequency with increased rotational speed to prevent negative torque generation; therefore rotational speed has the causative relationship with the frequency.

As current tends to be constrained at higher rotational speeds due to the growing back-EMF, the control algorithm needs to be adaptive if it is to correctly control torque and speed.

As mentioned earlier it is important to choose the appropriate control algorithm based upon the position in the torque-speed relationship. This is because at rotational speeds beneath the base speed, $\omega_{b,}$ the peak current must be constrained by the control algorithm to prevent damage to the motor windings; this control method is known as chopping control.

Rotational speeds above the base speed result in natural current constraint and therefore peak current control is not a requirement of the control circuit at such speeds. This behaviour results in a singular rise and fall in the current in the winding, therefore this control methodology is known as *singular pulse control*.

The control algorithms can be separated into two distinct categories, *average torque control*, and *instantaneous torque control* [7]; there are various categories of control within these two major groupings generally dependent on the rotational speed of the motor. Instantaneous torque control is an advanced control theory topic and is outside the intended scope of this thesis and is therefore not discussed. Information regarding instantaneous torque control can be found in [7, 51-53]

These modes are known as *low speed operation* and *high speed operation*, depending if the rotational speed of the motor is beneath or above the base speed; this assumes the full torque of the motor is required. It is still possible to implement current chopping above the base speed if the full torque is not required.

5.2 Average Torque Control

Due to the SRM's discontinuous nature of operation, electromagnetic torque is developed in impulses; these impulses are the result of current flowing in the phase windings. Average torque is defined to be the average of the torque developed over one complete stroke. The number of strokes S, and corresponding stroke angle ε, in an SRM are defined to by:

$$S = mN_r \tag{5.1}$$

$$\varepsilon = \frac{2\pi}{S} \times 360^0 = \frac{2\pi}{mN_r} \times 360^0 \tag{5.2}$$

Where m is the number of phases, and N_r is the number of salient rotor poles.

The function of the control algorithm is to synchronise the phase currents with rotor position in order to achieve the desired operational behaviour of the motor; be it constant torque, constant speed, shaft position, or a combination. The commonly accepted control diagram an SRM is shown in Figure 5-1:

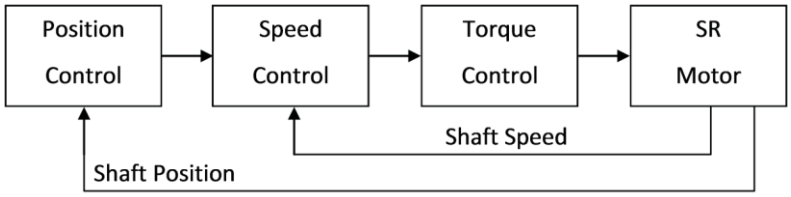

Figure 5-1: General Control diagram For An SRM

This control diagram is similar to that of other electric machines. With the exception that the torque control aspect is very specific to the SRM; this is due to the discontinuous nature of torque generation. Therefore, the required torque signal must be interpreted into individual current reference signals for each individual phase [28]. It is apparent that the torque control is open loop due to the lack of a torque sensor, therefore the torque control algorithm must utilise a motor model in order to achieve smooth torque generation; this differs from competing electric machine technologies which can be characterised by a simple torque-ampere ratio**.** The need for motor specific modelling within the torque control algorithm results in the requirement of designing, optimising and packaging the motor and controller together [7]**;** this prevents the development of a universal electronic drive for an SRM.

The torque control algorithm is required to be rotational speed dependent as rising shaft speed increases the back-EMF generation; this back-emf will rise until there is insufficient phase voltage to sufficiently regulate the current. Therefore, the techniques for average torque control can be categorised into either low-speed operation or high-speed operation, and are discussed in the following sections:

5.3 Low-speed motoring

Low speed operation refers to all operating speeds beneath the base speed ω_b; this is because at low speeds the peak current must be constrained by the controller, which in turn controls the torque output of the motor [7, 11]. This requirement arises due to the fact that the back-EMF *e* is insignificant when compared to the DC bus voltage.

There are four options for controlling average torque output during low-speed operation, these are: current hysteresis, current hysteresis delta modulation, voltage pulse width modulation, and singular pulse control [7, 54].

Voltage pulse width modulation is characterised by the use of a fixed chopping frequency and varying the duty cycle to control the average current. Current hysteresis establishes minimum and maximum references that the current is constrained within, this results in a variable chopping frequency. Singular pulse control operates on the principle of varying the *firing angle*, and the *dwell angle.*

It most common to implement current chopping techniques at low rotational speeds as they offer the greatest flexibility. The firing angle, dwell angle, average current, and current decay rate can be controlled by appropriate switching of the electronic converter. The current decay rate can be controlled by the voltage applied across the windings, which is +VS, 0, and –VS if the voltage drops of the transistors are ignored; 0V only applies to converters which are capable of uni-polar switching.

The simplest approach to average torque control in low-speed motoring is to ensure constant current supply throughout the positive torque generation region. The controller attempts to reach achieve this by varying the dwell angle, the allowable current hysteresis in variable frequency chopping, the duty cycle of the pulse in fixed frequency chopping, or a combination of these techniques.

These techniques are designed to limit the peak current and achieve an average current over the longest possible timeframe. If the motor speed is currently below the target speed the controller will allow the generation of excess torque, this leads to rotational acceleration of the motor. If the motor speed is above the target speed, the controller will only allow the generation of a small torque to cause the motor to slow in a controlled fashion.

The various low-speed operation techniques are discussed in the following sections:

5.3.1 Current Hysteresis Control

Current hysteresis control, more commonly known as bang-bang control, variable chopping or the current control method, operates on the principle of a maximum and minimum permissible current, flowing through a given winding.

This is achieved by the creation of a *hysteresis zone*, in which current is allowed to flow through the winding until the magnitude has exceeded the upper limit, at which point no further increase in current is permitted and the current is forced to decay. The decay rate of the current is dependent upon the electronic converter topology used, and if bi-polar, hard chopping, or uni-polar, soft chopping, switching is utilised. The current will then decay to the minimum permissible magnitude at which point, the maximum permissible current is allowed to flow again resulting in current rise in the windings.

If the switching scheme is bi-polar, then both switches will be turned off during chopping, resulting in both freewheeling diodes conducting. The current flow through the winding will continue in the same direction. However, the polarity of the voltage being applied across the winding will be reversed to allow forward biasing of the freewheeling diodes. This will result in rapid decay of the current flowing through the winding; this switching scheme tends to result in higher current ripple and higher switching frequencies.

The alternative switching method is uni-polar, in this method only one of the switches is turned off during chopping. This causes one of the freewheeling diodes to conduct, resulting in a zero volt loop with the phase winding and a slower current decay. This switching scheme tends to offer reduced switching frequency, and a reduction in power factor distortion.

When the motor has rotated to the end of the dwell angle period, both switches are turned off regardless of switching scheme. This allows the current to decay very quickly. This rapid decay allows a larger dwell angle and therefore a longer period of torque generation. This is because the current rapidly approaches zero magnitude before negative torque generation would occur.

The control diagram of current hysteresis control algorithm is shown in Figure 5-2:

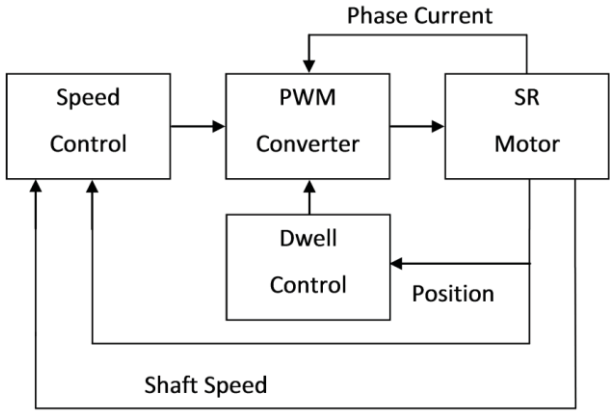

Figure 5-2: Control diagram For A Current Hysteresis Controller

This current control behaviour is only allowed to occur during the phase excitation period, known as the dwell angle. The current must be of a zero magnitude before the rotor pole aligns with the stator pole or negative torque generation will occur.

This approach controls peak torque production and thereby average torque production and is useful at providing constant rotational speed by adjusting the current hysteresis with rotational speed and phase current feedback.

Ignoring the set target speed for the controller to achieve, the controller must first ensure that the preset current has been achieved before the decision to increase or decrease the reference current can be made; the current error is directly used to control the state of the transistors. Therefore, as the current error increases so does the switching frequency. This discontinuous behaviour presents both a non-static reactive load and non-linear load to the power supply which increases the difficulty of maintaining a high power factor and filtering of electromagnetic noise.

It is standard practice to fix the dwell angle to a static setting; this helps to minimise torque ripple by increasing the commutation angle. This allows a lower peak current to obtain the average torque desired as the torque is applied for a longer period of the stroke angle. The dwell angle is normally set as to provide significant overlapping of the excited phases, yet prevent negative torque generation.

5.3.2 Current Hysteresis Control – Delta Modulation

A variant upon the current hysteresis controller is the delta modulation controller. The main difference is that the current waveform is sampled at a fixed frequency rather than continuously polled; this does not result in a fixed switching frequency, but the switching frequency cannot exceed the sampling frequency.

If the phase current has exceeded the maximum reference current then the controller establishes either a zero volt loop, or reverses the polarity of the DC bus voltage; this decision is dependent upon the magnitude of the current overshoot.

If the phase current has decayed beneath the minimum reference current, then the controller re-establishes the DC bus voltage across the winding to increase the phase current.

This converter shares the same control diagram as the current hysteresis control methodology as the sampling rate of the phase current is internal to the PWM converter.

The main advantage to this controller is that it places an effective hard upper limit on the switching frequency; this simplifies filtering of electromagnetic noise. It also simplifies programming of the control algorithm, as the current control becomes a timed event; bringing this controller topology closer to a PWM technique.

5.3.3 Voltage Pulse Width Modulation Control

It is apparent that the disadvantage of the current hysteresis control method is the variable switching frequency. The alternative is to use a fixed switching frequency; thereby simplifying the problems associated with solving distorted power factor and the increased variable reactance present with a variable switching frequency.

Voltage pulse width modulation control is categorised by varying the duty cycle of either one, known as uni-polar, or both, known as bi-polar, of the transistors present in the phase-leg of an electronic converter at a fixed frequency; this prevents the ability of instantaneous torque control. Peak current is constrained by switching off one, or both, of the transistors to cause current to free-wheel and decay.

While operating in uni-polar mode, the commutation transistor in the phase-leg will determine the firing angle, and remain on throughout the entire dwell angle. When the

chopping transistor is switched on the full DC bus voltage is applied across the phase winding and the current begins to increase. When the chopping transistor is switched off the current will free-wheel through a zero volt loop and decay slowly. When both chopping and commutation transistors are switched off the DC bus voltage is applied in reverse polarity across the phase winding and this results in rapid current decay.

In bi-polar mode, the commutation and chopping transistor are switched simultaneously resulting in inability to provide a zero volt loop across the phase winding during current chopping; this results in greater fluctuation in the current waveform, or the use of a higher switching frequency.

The control diagram of a voltage pulse width modulation controller is shown in Figure 5-3:

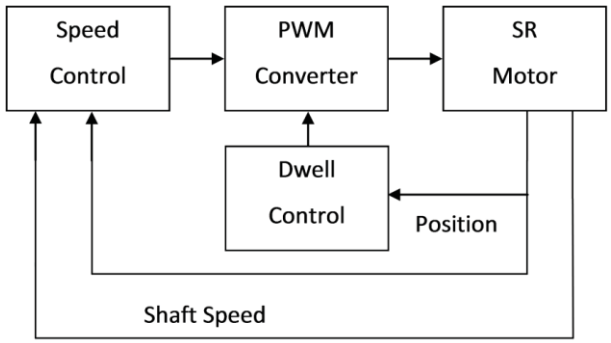

Figure 5-3: Control Diagram For A Voltage PWM Controller

It is standard practice to fix the dwell angle to a static setting while operating in chopping mode; this helps to minimise torque ripple. This is achieved by allowing a long conduction time but a low peak current to provide torque of a smaller magnitude but for a longer time. The dwell angle is normally set up to provide significant overlapping of the excited phases, yet prevent negative torque generation.

A higher duty cycle allows the current more time to increase, and less time to decay, while the opposite is true for a lower duty cycle. Therefore average current can be stabilised by varying the duty cycle over the dwell angle to result in an identical rise in and fall in current.

An over-current reference level is setup so that the controller can protect the windings. There is no need for individual phase current sensors because the peak current flowing in the windings will not occur during phase overlap; therefore only the DC bus current needs to be monitored.

5.3.4 Singular Pulse Control

As a rule varying the dwell angle as the only variable to control low-speed operation is generally not advised as this is very difficult to obtain stable torque production [7]. If the dwell angle is varied appropriately in combination with the current control methods then safer operation and greater flexibility in controlling the SRM can be achieved. This control approach generally exhibits poor system control and excessive torque ripple in low-speed operation. This control methodology is explained in depth in 5.4, *High-speed motoring* section of this thesis

5.4 High – speed motoring

High speed operation refers to all operating speeds above the base speed ω_b. Therefore the motor is operating in either constant power or natural mode. In both of these modes the back-EMF *e* results in natural current constraint due to reduction of the available DC bus voltage. Due to this behaviour and ever reducing commutation time, hysteresis control methods for regulation of the current is difficult. Therefore, they are not viable control methodologies for regulation of torque generaton at high speeds.

The only effective control methodology available for use in high speed operation, and ultra-high speed operaton, is singular pulse control. The control diagram of a singular pulse controller is shown in Figure 5-4:

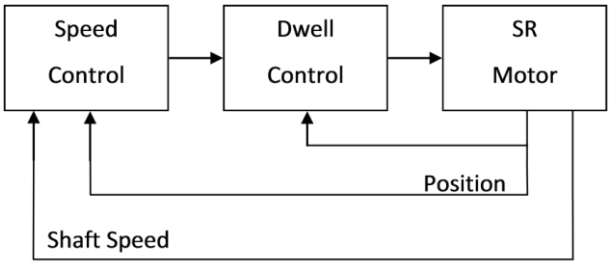

Figure 5-4: Control Diagram For A Singular Pulse Controller

This control methodology operates by adjusting the switch on and switch off angles for a given phase. This provides the ability to advance and retard the firing angle as well as dwell

angle. Adjustment of the firing angle can control the rate at which the current rises by shifting the switch on position in the inductance ramp.

The switch off angle determines the total dwell angle, which is adjusted such that the peak current can never exceed the maximum limit. This behaviour can cause large but discontinous torque production. This is because truncation of the dwell angle prevents overlapping of the phase torques creating periods of zero positive torque generation. This discontinous production of positive torque results in excessive torque ripple.

If the motor is required to accelerate, the firing angle is normally advanced to result in longer and earlier torque generaton, thereby increasing average torque. If the motor is required to decelerate the firing angle is delayed to reduce the commutation period and therefore decrease average torque.

The current is constrained by the back-EMF and is not required to be controlled, hence the terminology of singular pulse control. Unlike the current control methodologies the controller does not attempt to stabilise any current flow or system variable until a decision can be made to increase or decrease reference values.

The rotational speed error is used to directly alter the firing and dwell angles. The turn-off angle is usually only advanced as a function of increasing rotational speed to prevent negative torque generation.

5.5 Sensor-less Control

Sensor-less operation refers to the elimination of the rotor position sensors, and is a misnomer because it implies that the motor is controlled sensors; this is not true, sensor-less control has a greater reliance upon accurate current sensing. Sensor-less control does not currently offer the same level of performance as position sensed controllers, and therefore the traditional control topologies remain popular [7].

Sensor-less control is not directly related to the work of this thesis, therefore the discussion will provide a broad overview of the fundamentals and techniques.

The main motivations for sensor-less control are:

1. Cost reduction: Eliminating the rotor position sensors reduces the number of components in the electronic drive; this results in a significant cost saving.
2. Reliability: The position sensors are usually optical or magnetic, and are a common point of failure; current sensors are considered to be more robust. This increase in reliablity ensures greater machine uptime.
3. Simplification: The rotor position sensors require additional mechanical components and space in the motor cavity. Care must be taken when assembling or maintaining the motor not to damage the sensors.

The basis of many sensor-less operation techniques is the accurate estimation of the rotor position from the phase current and voltage waveforms, either energised or non-energised.

The accurate measurement of these variables facilitates the calculation of the flux-linkage and inductance; both of these magnetic properties are related to the alignment angle of the rotor. The relationship of flux-linkage to current and rotor position in shown in Figure 2-9 on page 17.

This illustrates the non-linearity in the relationship between flux-linkage, current and the alignment angle; however the alignment angle is clearly defined. It can been seen that magnetic saturation limits rotor position fidelity at higher current flows.

$$V = Ri + \frac{d\psi}{dt} = Ri + L\frac{di}{dt} + \omega_m i\frac{dL}{d\theta} \qquad \textbf{(5.3)}$$

The sensor-less control techniques can be represented in three categories based upon the fundamental idea of rotor position detection. These categories are:

- Stability Torque Control
- Energised Phase
- Non-Energised Phase

Stability torque control is an open loop control methodology; it does not provide a direct indication of rotor position. Examples of techniques that fall into this category are *dwell angle compensation*, and *commutation angle compensation*.

The energised phase methodologies rely on measurement of electrical properties, voltage and current, of an energised phase to indirectly assess rotor position; this allows the

calculation of magnetic properties, flux-linkage and inductance, which are functions of rotor position. An example of this approach is described in [55], and [56].

An early publication regarding indirect detection of rotor position was [57]. An interesting approach which utilises irregularity in the rotor and stator pole constructions for detection of the rotor position received a US Patent, 6150778, on the 21st of November 2000.

Non-energised methodolies rely on measurent of inductance ,for a given rotor angle, in an non-excited phase; this is usually achieved by the injection of a low magnitude chopping current. This approach effectively reduces the effect of back-EMF or irregular torque generation, and eliminates the issues associated with saturation. An example of this technique is shown in [58].

5.6 Summary

This chapter summarises the major challenges and categories present in controlling SRMs. The control methodologies presented are for average torque control and cover both low and high speed operation. Instantaneous torque control is mentioned, but due to the complexity of this topic being outside the scope of this thesis it is not discussed.

The methodologies discussed are voltage pulse width modulation, current hysteresis, currrent hysteresis delta modulation, and singular pulse control for high speed operation; sensor-less control is investigated and discussed.

This information provided in this chapter is important to understanding the control algorithm utilised wihtin the Teknatool DVR electronic drive which is presented in Chapter 6, *DVR SRM Implementation* of this thesis.

Chapter 6

DVR SRM Implementation

"Knowledge is a process of piling up facts; wisdom lies in their simplification"

- Martin H. Fischer

This chapter discusses the SRM topologies implemented with the Teknatool DVR motor. Specifically, the construction of the motor including phase and pole configuration, the requirements and technical aspects of the power supply, the topology of the electronic converter circuit utilised and how control of the machine is achieved. The information presented here will be related to the information presented in the literature in Chapters 2 through 5, and provide some technical insight into the real world implementation of such a machine.

6.1 Motor Construction

The SRM utilised in the Teknatool DVR products follows conventional construction methodology as presented in Chapter 2. The stator is encased in the cast metal body of the lathe, preventing the propagation of electromagnetic interference while providing sufficient heat-sinking for dissipation of heat as a result of power losses within the stator. The stator contains twelve salient poles arranged into three phases.

The rotor is also of conventional construction, being produced of thin iron laminates arranged around a motor shaft. The rotor is supported on the motor shaft by a key-way; this prevents the rotor slipping against the shaft when producing torque. The motor shaft is suspended within the cast casing of the lathe body by two bearings, one at each end of the shaft. The rotor contains eight salient poles.

The pole and phase configuration of this motor is a three-phase 12/8; this configuration satisfies the ideal rotor and pole ratio for ease of starting and minimisation of torque ripple. The maximum angle of misalignment to a specific phase is 22.5 degrees. However, the angle between maximum misalignments of sequential phases is 15 degrees resulting in significant phase overlap. The inductance profile of this motor construction is shown in Figure 6-1:

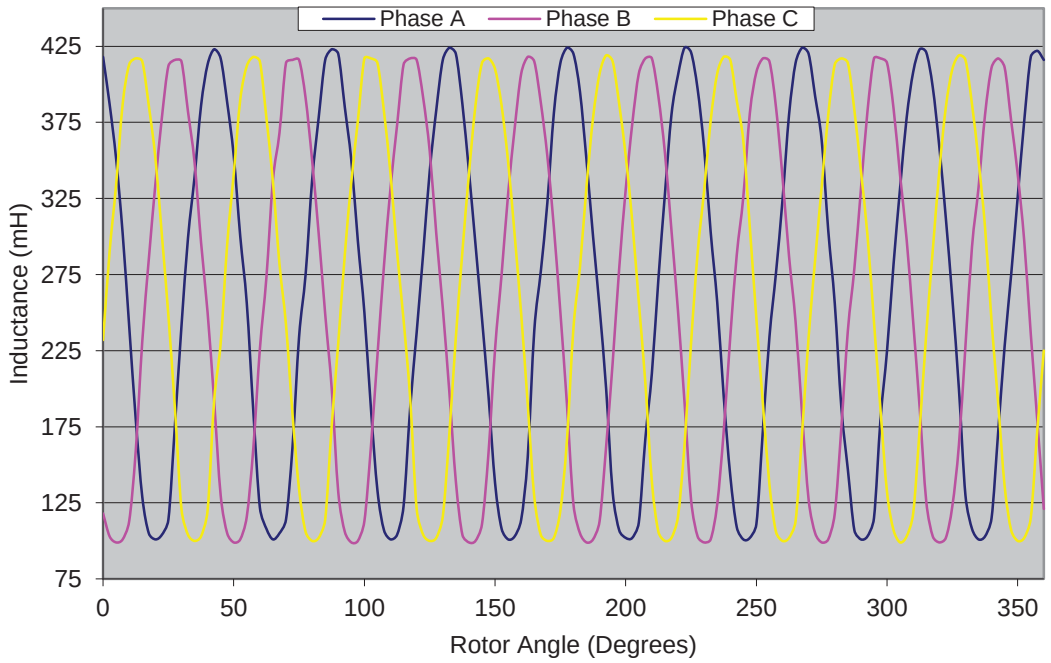

Figure 6-1: Teknatool DVR SRM Inductance Profile

The higher number of windings per phase minimise torque ripple at the expense of higher switching frequency, thereby increased losses and distorted power factor, and a lower maximum rotational speed due to increased reactance with the motor windings; however high rotational speed is not a usual requirement of woodworking lathe motors whereas minimisation of torque ripple is critical**.**

The motor has been constructed to the meet the following criteria:

- Minimisation of torque ripple due to significant phase overlap
- Sufficient commutation period due to significant misalignment angle
- Ability to produce rotation in both directions
- Ability to begin rotation from any rest angle
- Machine reliability due to high number of phases
- High peak torque across wide rotational speed range
- Ability to rotate at speeds up to 5500rpm

The achievement of these criteria by the SRM makes this motor construction a suitable choice for use as a woodworking lathe motor. The full motor dimensions can be found in Appendix B.1, *Motor Dimensions,* on page *198*.

6.2 Phase Characteristics

Measurement of the flux-linkage and inductance characteristics of the motor can be achieved by measurement of the current profile at differing rotor angles [59-61]. Accurate measurement of the phase characteristics is crucial to developing a precise motor model. The flux-linkage can be calculated by the following equation:

$$\psi = \int (v - iR).\, dt \qquad \textbf{(6.1)}$$

Where v is the applied voltage, i is the current and R is the DC resistance of the winding. The measured winding DC resistances are 9.85Ω for Phase A, 9.96Ω for Phase B, and 10.13Ω for Phase C; an imbalance of 2.84% of the smallest phase impedance. This is not a large imbalance but it is significant.

A circuit was designed and built to allow measurement of the phase characteristics; this experimental setup is shown in Figure 6-2.

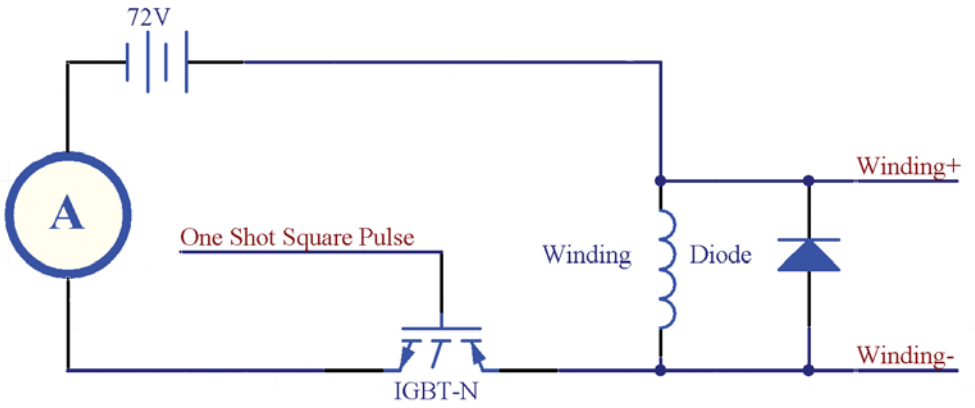

Figure 6-2: DVR Phase Characteristics Measurement Circuit

The voltage of 72V was chosen as to allow saturation of the windings due to high DC resistance. The circuit operates by biasing the IGBT for a sufficient time period as to allow the current to rise to saturation without damaging the windings. The diode is present to free-wheel the energy stored in the winding when the IGBT stops conducting. The rotor was locked to a range of angles and the voltage and current waveforms were captured. The flux-linkage was calculated and has been tabulated and is shown in Appendix B on page 199. The flux-linkage characteristics shown in Figure 6-3: DVR Phase Flux-Linkage Characteristics

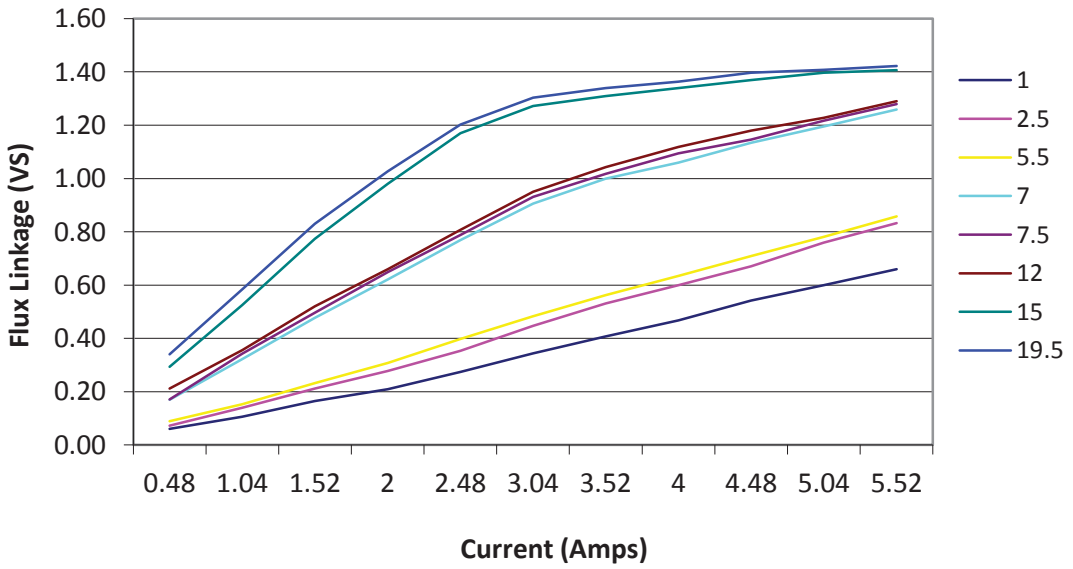

Figure 6-3: DVR Phase Flux-Linkage Characteristics

The flux-linkage can be seen to be approximately linear at lower current, however as current increases the flux-linkage begins to saturate; this is especially true as the rotor approaches alignment. The general shape of the flux-linkage graph agrees with the idealised plot shown in Chapter 2, *Operating Principles*.

The inductance profile is related to the flux-linkage by equation 2.4 in Chapter 2, *Operating Principles*.

Utilising this relationship the inductance profile was calculated and is tabulated in Appendix B on page 199. The graph of the inductance profile is shown in Figure 6-4:

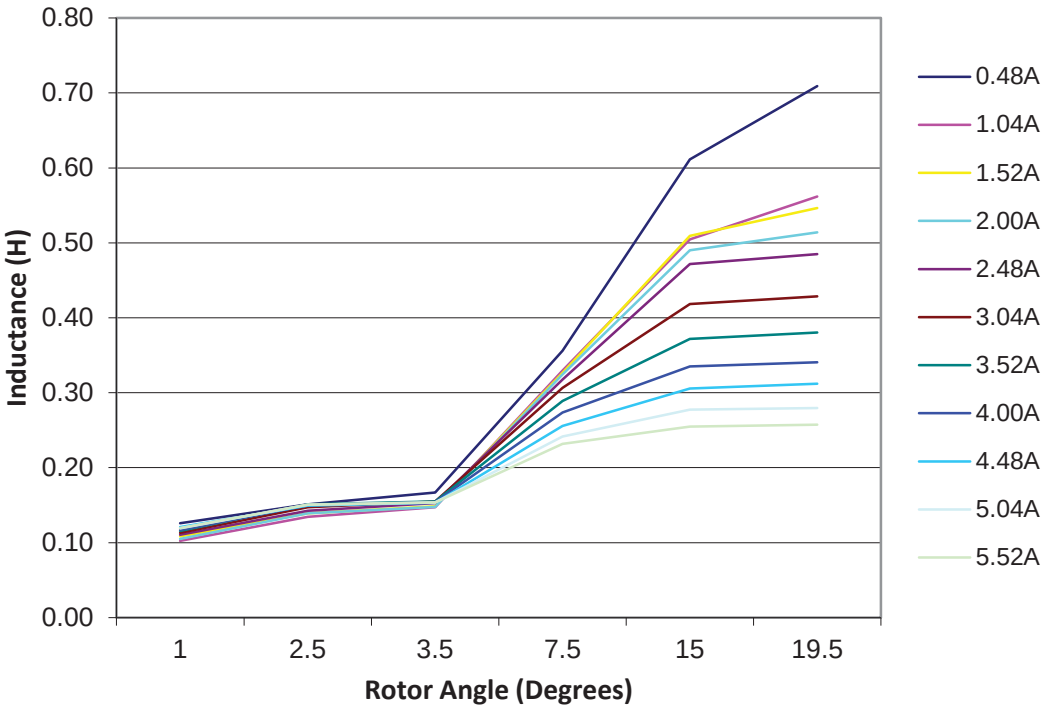

Figure 6-4: DVR Phase Inductance Characteristics

The inductance profile also begins to saturate at the same rotor angle and current combinations as the flux-linkage, which is an expected behaviour. The inductance profile shown agrees with the idealised plot in shown in Chapter 2, *Operating Principles*, on page 15.

6.3 Power Supply

The Teknatool DVR power supply is required to operate the motor from both 115V and 230V RMS alternating current supplies; this allows a single electronic drive design for all countries the product will be sold in.

The power supply forms a crucial component in the system as the SRM is unable to be line driven, therefore efficient operation is desirable. As mentioned in Chapter 4, the electronic converter is separated from the power supply due to its critical importance.

The power supply incorporated by the DVR involves active power factor correction due to the non-linear variable reactive load presented to the input supply; the topology used is boost conversion (Refer Appendix D.2 on page 233). The inclusion of power factor correction reduces the current being drawn from the supply for the same power output of the motor, and therefore line efficiency increases and motor output power increases, at the cost of increased resistive loss within the power supply of approximately 3%.

The power supply of the Teknatool DVR is required to provide the following rails:

- +360V for the direct current supply to the electronic converter circuit
- +15V for biasing the phase transistors in the electronic converter
- +5V for the control circuitry, current sensing, position sensing
- -5V for the current sensing
- +2.5V for the lower voltage devices in the control circuitry
- +5V Isolated for the user control panel
- 0V Isolated for the user control panel
- 0V circuit wide except isolated supplies

The rails supplied by the power supply are numerous and have differing requirements and methodologies for generation. It is important to note that the power supply does not utilise isolation between the motor and the control circuitry and this is an important point for discussion later in this thesis.

The incoming AC mains supply is full wave rectified before being boost converted by the power factor correction unit, regulation is provided by the presence of large capacitors. This provides the +360V rail to power the electronic converter circuit.

A transformer is situated downstream of the rectified mains signal, yet is connected before regulation. This ensures that a frequency is present to enable the transformer to operate. The transformer produces various outputs, +15V, -5V, +5V Isolated and 0V Isolated. The transformer contains no connection between the primary and secondary windings; however it is centre-tapped and this centre is connected to the return of the full wave bridge rectifier. This connection removes any isolation that would be present between the motor and the control circuitry.

The +15V rail is used to bias the driving transistors in the electronic converter, there is no regulation present on this supply, the +15V rail is used to bias a twin output voltage regulator which provides the +5V for the control circuitry, current sensing, and position sensing. It also provides the +2.5V rail for the control circuitry. The potential of these rails are all with respect to the ground of the motor.

The +5V isolated and 0v isolated rails are generated by the transformer. This is a completely separate winding in the transformer which contains no common point with the rest of the circuit. Regulation is provided by a linear 5V regulator. This rail is used to supply power for the user control panel, communication with the control panel requires opto-coupling due to the potential difference that results with the control circuitry as a result of the isolation.

At all times, the shape of the input waveform from the AC mains is being sampled for harmonic frequencies, and the phase difference is being measured between the voltage and current waveforms to correct for any disruption to power factor.

The power supply is a highly complex electrical circuit that operates from high voltages. The rectified mains supply makes direct measurements with instrumentation difficult unless isolated equipment is utilised. This is discussed in depth in Chapter 9, *Instrumentation and testing.*

6.4 Electronic Power Converter

The electronic power converter topology used by the Teknatool DVR product is the asymmetric half-bridge converter, which was discussed on page 70. This converter is the most expensive in terms of component cost, yet provides flexible control, high efficiency and reduced torque ripple due to phase overlap. The DVR is of three phase construction and the schematic of the full electronic converter is shown in Figure 6-5:

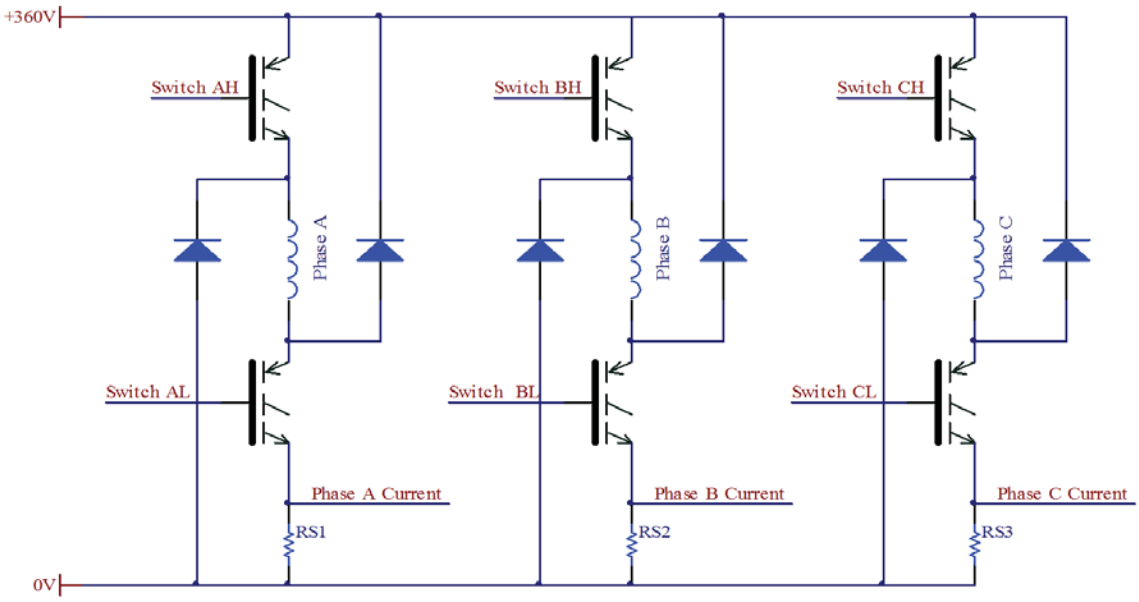

Figure 6-5: Teknatool DVR SRM Electronic Power Converter Schematic

This electronic converter allows the use of current chopping, PWM, or dwell angle control. It also allows either uni-polar or bi-polar switching which allows a reduction in switching frequency yet allows rapid current decay to maximise commutation time before negative torque generation occurs.

The switching elements consist of IGBT's (Refer Appendix D.4 on page 247); these transistors are biased with a voltage signal at the gate and are capable of high voltage and current. The converter circuit also incorporates winding current sensing via a resistor. The voltage drop across the resistance provides a voltage signal to the microcontroller that is proportional to the current flow, and this information is used to control the torque output of the motor.

A woodworking lathe requires precise speed control with minimal torque ripple, therefore the use of the asymmetric half bridge converter is justified.

6.5 Control Topologies

The Teknatool DVR operates both above and beneath the base speed ω_b. It employs both low speed and high speed control, namely current hysteresis delta modulation control, and singular pulse control for low-speed and high speed operation respectively. The phase excitations are overlapped, and this is shown by the commutation transistor switching signals in Figure 6-6; this result aligns with the theoretical switching schema shown in Figure 2-4 of Chapter 2, *Operating Principles*, on page 13 of this document.

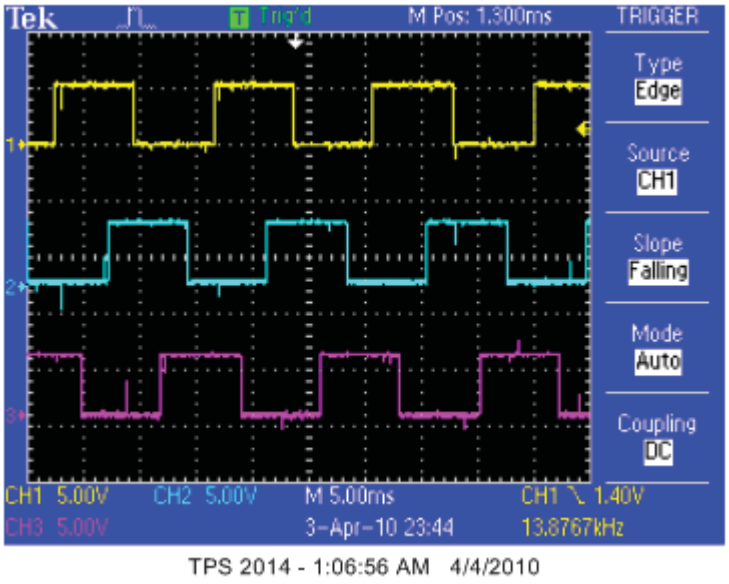

Figure 6-6: DVR Rotor Position Sensor Capture

To achieve this, there are three seperare position signals from the rotor; these signals provide the microcontroller with the instantaneous position of the rotor with significant resolution. This allows the calculation of the exact angle of rotation, the angular displacement from the phase poles and the current acceleration or deceleration rate of the rotor. There are also three current sensors, which measure the current flowing through each of the phase windings, this provides the controller with peak current, average current and rate of change of current.

Low speed operation is achieved through the use of a uni-polar current hysteresis delta modulation control scheme, shown in Figure 6-7:

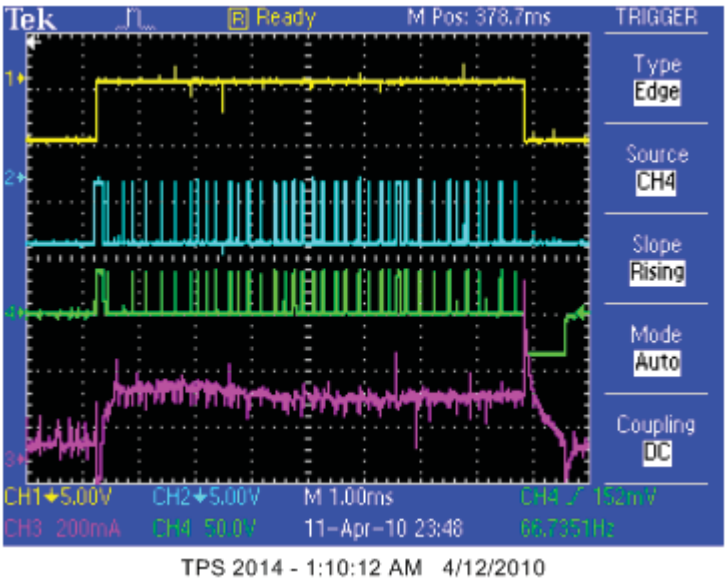

Figure 6-7: Low-Speed Control System Captures of DVR Motor

The chopping transistor in the asymmetric half bridge converter is switched synchronously with the dwell angle switching.

The top transister is switched at a fixed maximum frequency of approximately 6kHz, note that this does not match the frequency specified in Table A-4: DVR SRM Motor Parameters contained in Appendix A, *DVR Technical Information* on 188. which is the sampling frequency of the current waveform. The chopping transistor is frequently switched at much lower frequency as the current may not exceed the upper reference limit when the current waveform is observed; this allows control of average current, peak current and rate of change of current. This controls the average torque output, and thereby speed control with varying load is achieved within the Teknatool DVR controller.

High speed operation is achieved through singular pulse control, shown in Figure 6-8, as this is the only viable control algorithm for control of rotational speeds above the base speed. This is characterised by advancing the firing angle to a portion of the inductance ramp that allows current to build faster, as the inductance ramp builds the current is naturally constrained by the back-EMF. This approach maximises commutation time at high speed to reduce torque ripple, while providing control over average torque produced.

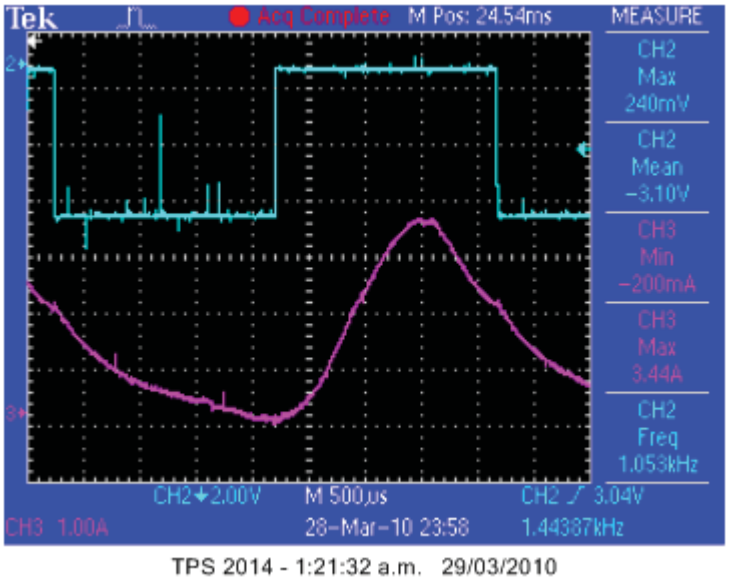

Figure 6-8: High-Speed Control System Captures of DVR Motor

This control setup allows appropriate torque control for low-speed and high-speed operation with minimal torque ripple. This is important for a woodworking lathe, as large ripple would impact on the ability of the motor to produce quality product.

6.6 Torque-Speed and Power-Speed Relationships

The Torque-Speed and Power-Speed relationships are shown in the following table of information contained in Table B-4: DVR Torque - Power - Speed Results in Appendix B, *Measurement* Data, on page 200. These results are graphed into the two respective relationships of Torque-Speed, and Power-Speed in Figure 6-9 and Figure 6-10 respectively. The results for these tables are obtained from the motor operating from a 115V AC power source.

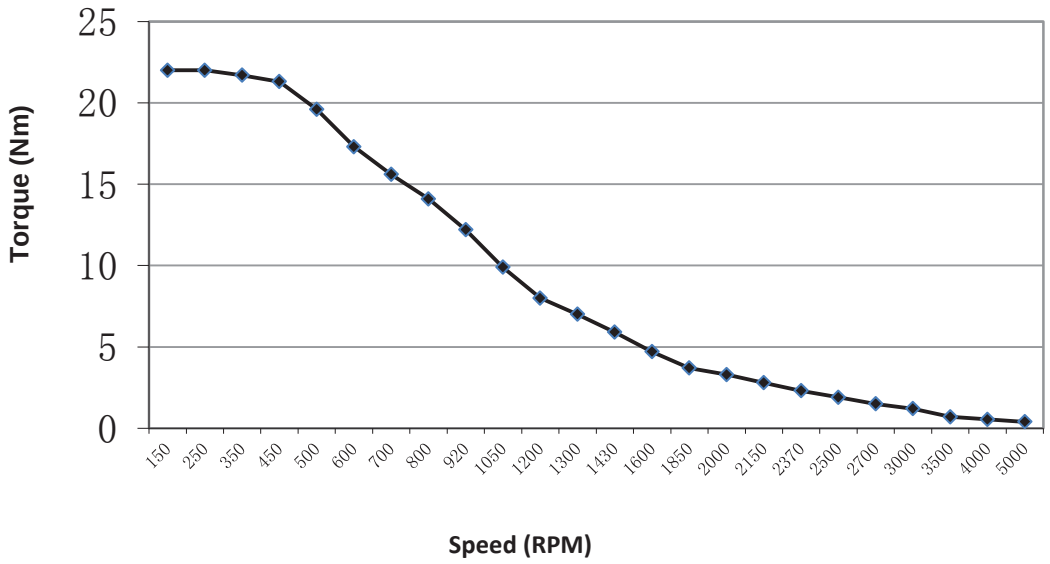

Figure 6-9: DVR Torque-Speed Plot

Comparing this torque-speed relationship to the idealised torque-speed relation presented in Figure 2-13 of Chapter 2, Operating *Principles*, on page 21, it can be observed that the two curves agree. The Power-Speed relationship can also be plotted as is shown in Figure 6-10 below:

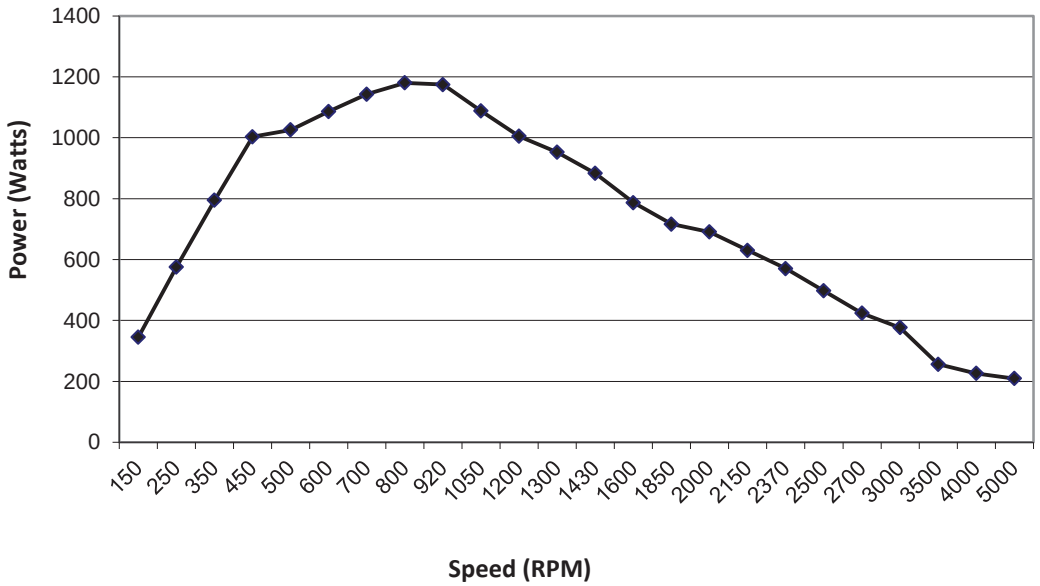

Figure 6-10: DVR Power-Speed Plot

As with the torque-speed relationship, the power-speed relationship is directly comparable to the idealised power-speed relationship presented in Figure 2-14, of Chapter 2, Operating *Principles*, on page 22 of this document.

It is apparent from these relationships that the constant torque region of operation extends to approximately 500rpm, and that the constant power region ranges from 500rpm to 1200rpm after which the motor operates in natural mode.

6.7 Acoustic Noise

The noise emitted from the Teknatool DVR motor is highlighted in Table below:

Speed (RPM)	Complete Band	63Hz	125Hz	250Hz	500Hz	1kHz	2kHz	4kHz	8kHz
1500	76dB	40dB	46dB	52dB	64dB	75dB	65dB	60dB	54dB
2500	74dB	45dB	53dB	54dB	62dB	71dB	70dB	66dB	53dB

Table 6-1: DVR Acoustic Noise Levels

The noise emitted by the DVR is not insignificant. However, the noise level is acceptable for use within a working environment.

6.8 Summary

This chapter reviews the Teknatool DVR implementation of an SRM. Namely, identifying the key component areas and the specific implementations; this allows discussion upon improvement or justification of the current topologies. Identification of the exact implementation is an important requirement to understanding the structure and specific implementation of the electronic drive to facilitate separation and reverse engineering.

The information of the Tekantool DVR implementation draws on and is related to the information presented in Chapters 2, 3, 4, and 5; highlighting a real world implementation of the theoretical topologies discussed.

Understanding of the information presented in this chapter is crucial to understanding the remaining chapters in this thesis as it forms the underpinning to the practical work that was undertaken as part of this research.

Chapter 7

Separation Process

"Success is neither magical nor mysterious. Success is the natural consequence of consistently applying the basic fundamentals"

- Jim Rohn

This chapter discusses the process of separating the electronic drive into separate circuit boards, including decisions, challenges, and solutions. The focus will be on the activities undertaken during separation; this provides an explanation of the separation as a whole and the difficulties encountered in achieving successful separation.

7.1 Familiarisation with DVR electronic drive

Familiarity with the topologies utilised in the motor construction, power supply, electronic converter, and the control circuitry is the first step in separating the power supply from the control board. The ability to identify the key topologies utilised, and connection points between the functional components will yield ideal separation points; these points being directly translatable to a drive component diagram.

Identifying the affinity of the major components of an SRM to either power supply or control architecture will highlight the connection points. A component diagram highlighting affinity is shown in Figure 7-1:

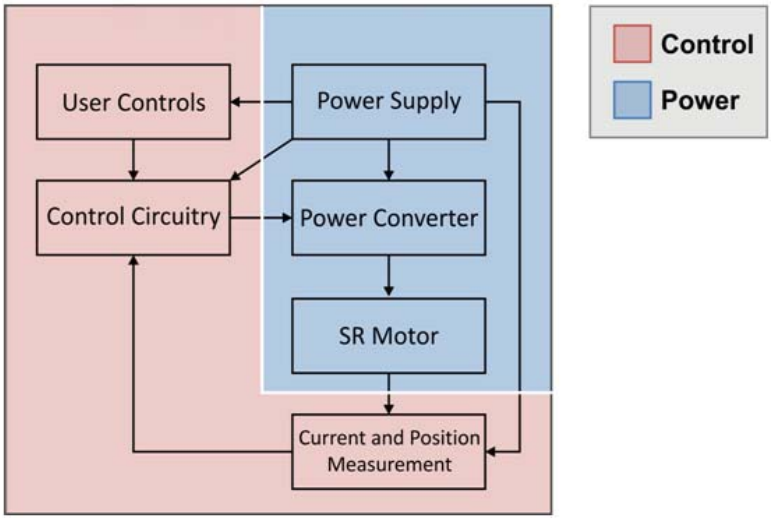

Figure 7-1: Drive Component Separation Diagram

The components are separated into control and power components on a simple basis; a component that is involved with adjusting the target speed, receiving feedback, or providing a variable output as to achieve constant speed operation is a control component. Therefore user controls, control circuitry, current and position measurement can be considered control components; they would benefit being separated from the power supply.

The power supply itself, the electronic converter, and the motor are all power components as they operate with *power signals*.

Identifying these major components on the drive schematic allows familiarisation with the design, their operation, and how they interconnect is possible due to the knowledge learned during the literature review. The drive schematic highlighting the functional components is shown in Figure C-1 in Appendix C.1 on page 204:

Identification of the major component areas simplifies the complex circuit schematic into smaller groups that are easily analysed and understood. Analysis of these groups resulted in the identification of the idealised separation points. These separation points can be considered the *theoretical separation points* where separation of the power supply and control circuits is plausible; these points are determined from a simplistic overview of the entire electronics and therefore are not the *actual separation points*. The reasons for the differences between the ideal and actual separation points are discussed in a later section.

7.2 Identification of ideal separation points

The ideal separation points can be found by locating the connection points between the major component groupings. As mentioned previously these component groupings can be assorted into power supply or control circuit affinity. Therefore, further simplification of the component grouping can be achieved.

By grouping the controller circuit, current measurement, position measurement, and user controls under the title of control circuitry, and the power supply, electronic converter, and motor windings under the title of power electronics, we can achieve the following groupings as shown in Figure C-2 in Appendix C.2 on page 205.

The ideal separation points are named in the following list:

1. Electronic converter IGBT gate drives (Phase A High Side, Phase A Low Side, Phase B High Side, Phase B Low Side, Phase C High Side, Phase C Low Side)
2. IGBT driver high side floating references (VS1, VS2, VS3)
3. Current sense resistors (RS1, RS2, RS3)
4. Bus Signals (FO, 1/0, UIN', IIN',SO)
5. Power Rails (+5V, -5V, OV_IZM, +5V_INT, 0V_INT, +15V, +360V)

While the above separation points are valid for the basic connection points between the two proposed circuit boards, they do however present safety problems as a result of high voltage and current signals.

These two factors alone make separation at these points implausible due to safety concerns, as well as the cabling requirements to connect the two circuit boards together. This highlights the inability to simply disconnect the power supply from the control circuitry due to the non-modularity of the SRM drive design and implementation. As mentioned earlier, it is common practice to combine the power supply and control circuit together.

This non-modularity typically arises from the presence of *grey-area components*. These components do not exhibit sole affinity to either the control circuit or the power supply; examples of such devices are the IGBT driver, and the current sense resistors.

Successful separation of the circuit boards is highly dependent on appropriate handling of the grey-area components. Fortunately these components typically exhibit a stronger affinity for one circuit, normally due to the presence of power signals.

The presence of power signals requires modification to the rules for deciding appropriate separation points. These modifications are:

- No high voltage signals are to be routed to the control circuit, unless unavoidable in the form of power signal feedback. If such a connection is required it must be made through significant resistance.
- No high current signals to be routed through the control circuit, no exceptions.

The results from the identification of the idealised separation points raised the need for deeper investigation into both the power supply and control circuits before a decision on the actual separation points could be made. The idealised separation points were not mapped onto the circuit board due to the implausibility of appropriate separation; the actual separation points form a line on the circuit board known as the *separation line.*

7.3 Detailed reverse engineering of electronic drive

The presence of grey-area components in the attempt to find the idealised separation points resulted in the original points being implausible for separation. Therefore, deeper analysis of the operation of the individual circuits was required to identify all grey-area components and tag them with the appropriate affinity. To help achieve this task a component listing was established. This listing gathered the following columns of information:

- Designator
- Type and Footprint
- Value
- Peak Voltage
- Proposed Location (affinity)
- Categorical Purpose
- Description of purpose

This point in the research timeline is considered to be the beginning of the reverse engineering process as both the design of the circuit and detailed information about the components is being collated. Not all the information could be collected during this stage of the project, namely footprint and value information.

The main purpose of this activity was to develop an intimate understanding of both the control and power supply circuits. This knowledge would later be used to identify more appropriate separation points and later plot the separation line on the circuit board.

During this activity it was noted that not only were grey-area components present, but also control components were nested within the power supply region of the schematic and vice versa for the power supply components. This observation reinforced the previously stated non-modularity of SRM electronic drive design.

It became apparent that the Teknatool DVR electronic drive could be described as a single circuit with two highly inter-dependent entities. This was in contradiction to an earlier assumption that the electronic drive was two related but independent circuits sharing a circuit board. This resulted in a change to the definition of the separation process of the electronic drive; separation was no longer attempting to find the points at which the two

circuits could be separated from each other. The separation process now focused upon unravelling the inter-dependent circuits into a coherent architecture.

It was also observed that the schematic did not exactly match the electronic drive. The schematic contained components which were not present on the drive, and vice versa. The schematic also contained typographical errors such as misrouted connections between components.

After deep analysis of the operation of the electronic drive, a bus and net listing was also added to the earlier component spreadsheet; this would prove an invaluable resource during testing.

The grey-area and missing components were noted on the schematic, and the control and power circuits were unravelled from each other. This resulted in the following changes to the schematic as shown in Figure C-3 in Appendix C.3 on page 206:

The schematic shows the power supply and control circuit components present on the electronic drive, it also shows the components which are not present on the circuit board. The components have been selected based not only on their behavioural role, but also the presence of power signals. If a component contains a power signal it is not considered to be part of the control circuit, unless its primary purpose is to add resistance to a power signal for feedback. The actual separation points are determined by the result of this activity and this is discussed in the next section.

7.4 Plausibility of proposed separation points

The change in rules that determine correct component location resulted in significant change to the possible separation points; this was due to the attempted removal of all power signals from the control board. The change in these rules resulted in the following separation points:

1. IGBT driver transistor control inputs (TO_HA, TO_HB, TO_HC, TO_LA, TO_LB, TO_LC)
2. Fault tolerance inputs for the IGBT driver(SD, F_CL, FLT_I, ITRP)
3. Negative voltage cap diode for IGBT driver input ITRP (Component VD31)
4. +5V Pull-up resistor for IGBT driver pin ITRP (Component R32)
5. IGBT driver ITRP current limiting resistor and Comparator D5:4 (Component R33)
6. +360V feedback voltage dividing resistor for Comparator D7:1 (Component R40)
7. Current sense resistors from motor phase windings (RS1,RS2,RS3)
8. Control bus signals (K_OVC, KOUT)
9. +360V feedback voltage dividing resistor for signal UD" (Component R12)
10. +360V feedback current limiting resistor (Missing Component R72)
11. Bridge rectifier return feedback resistor (Component R75)
12. Power factor correction bus signals (0/1, FO)
13. Power supply rails (+2.5V, +5V, -5V, 0V_PWR, OV_IZM, +5V_INT, 0V_INT)

These points are a plausible set of separation points when taken in context from the schematic diagram. In practice, there are significant differences between a schematic and the resulting printed circuit board. A key difference is that component placement may be very different to what is indicated by the circuit schematic. Attempting to plot a line through the separation points resulted in the following separation line for the electronic drive printed circuit board as shown in Figure C-4 in Appendix C.4 on page 207.

This separation line passes through several difficult areas. To ease separation, another rule was added to the separation point definition. This was to aid in finding the easiest separation points in terms of the physical separation line of the printed circuited board. The additional rule was to choose the easiest separation point providing that all previous rules regarding power signals and component behaviours were also met. These points would only be considered if sufficient justification for separation at the easier point could be provided.

Further investigation resulted in the finding of the final separation points which are discussed and justified in the following section.

7.5 Identification of final separation points

The attempt to plot an appropriate separation line on the printed circuit board led to the addition of a new rule in determining separation points which allowed for easier separation. This resulted in a small change to the boundaries of the control circuit and power supply and therefore shifted the separation line on the circuit board.

The resulting separation points are considered the final separation points and design of circuit boards incorporating these points could begin. The differing boundaries of the control and power supply circuits are shown in Figure C-5 in Appendix C.5 on page 208.

Therefore the final and justified separation points are as follows:

1. Transistor control inputs for the IGBT driver (TO_HA, TO_HB, TO_HC, TO_LA, TO_LB, and TO_LC). The IGBT driver is a grey-area component and therefore is shifted to the power supply to prevent the propagation of the high voltage DC supply to the control circuit. Separating at the low voltage high impedance switching inputs allows the IGBT driver to be shifted to the power supply circuit. There is concern here due to the increase in conductor length, this is somewhat negated due to the inputs to the IGBT being high impedance. The concern is with EMI causing spurious switching signals.
2. Fault tolerance inputs for the IGBT driver (SD, F_CL, FLT_I, and ITRP). As mentioned for the transistor control inputs, the IGBT driver is a grey-area power component and therefore must be placed on the power supply. Separation at the high impedance fault pins facilitates this movement. Signal integrity concerns are consistent with the transistor control inputs.
3. Negative voltage cap diode for IGBT driver input ITRP (Component VD31). This component should be placed as close as physically possible to the ITRP pin of the IGBT driver as possible, therefore this component is placed on the power supply circuit board.
4. +5V Pull-up resistor for IGBT driver pin ITRP (Component R32). This separation at this point was made for ease of separation, but also to keep the pull-up as close to

the comparator as possible, therefore this component is placed on the control circuit board.

5. Current limiting resistor for IGBT driver pin ITRP and Comparator D5:4 (Component R33). This point was chosen due to ease of separation and also to keep the component as close to the comparator as possible.
6. +360V feedback voltage dividing resistor for Comparator D7:1 (Component R40). The separation was made at this point to eliminate +360V from the control circuit board. The +360V supply is sourced through two resistors.
7. Current sense resistors from motor phase windings (R67, R68, and R69). The separation was made here to prevent high current flowing through the control circuit board and inter-board connections and prevent the ability to directly connect to the electronic converter circuit. It also facilities ease of separation and circuit board design. The current signal that is present by the voltage drop across the sense resistors may be sensitive to the increased conductor length and EMI
8. Control bus signals (K_OVC, KOUT). Separation made at these points for ease of separation. Both signals are generated by components that are not present on the circuit board.
9. +360V feedback voltage dividing resistor for signal UD" (Component R12). Separation was made here to eliminate +360V from the control circuit board.
10. +360V feedback current limiting resistor (Missing Component R72). Separated this point to prevent propagation of the +360V signal to the control circuit board.
11. Bridge rectifier return feedback resistor (Component R75). Separaton was made here to add resistance between the control circuit board and the return side of the bridge rectifier to increase safety of the control circuit board.
12. Power factor correction ON/OFF switch resistance (Component R86). This point was chosen to ease separation between the circuits.
13. Power factor correction fault output (Component C80). This point was chosen to ease separation between the two circuits.
14. Twin-rail switching voltage regulator output SO (Component R118). This point was chosen to ease separation the two circuits.
15. Twin-rail switching voltage regulator output +5V (Component C67). This separation was chosen because the control circuit contains the only components to operate from the +5V rail; however the regulator itself is a power supply component. Capacitor C67 is the output smoothing capacitor for the switching waveform and therefore this needs to remain close to the regulator as it forms an integral part of

its operation. The other capacitors present across this rail are decoupling capacitors and these must be kept close to their respective devices.

16. -5V Rail output (Component VD18). This point was chosen to ease separation of the two circuits.
17. Power supply rails (+2.5V, +5V, -5V, 0V_PWR, OV_IZM, +5V_INT, 0V_INT). These supply rails are integral to the operation of the control circuit and therefore must be carried over to the control circuit board.

These justified separation points can be considered final in the process of investigating the circuit schematic and printed circuit board for the appropriate separation points. Any revision to these points will come from difficulties in the manufacture of the circuit boards or in testing the circuit boards. When these separation points are plotted onto the circuit board, the following separation line is shown in Figure C-6 in Appendix C.6 on page 209.

This separation line follows a path which is less difficult to separate. It helps to avoid areas dense with tracks or other components; this helps to minimise the level of reworking required to achieve the separation. This is achieved because the separation line crosses significantly less unrelated connections than the previous attempt.

It should be noted that the circuit board cannot be physically cut and then bridged due to the aforementioned reasons; this requires two new circuit boards to be designed. The design of the new power supply and control circuit boards is discussed in Chapter 8, *Prototype design and manufacture.*

7.6 Summary

This chapter investigates the plausibility of separating the electronic drive utilised within the Teknatool DVR commercial system. It highlights the choice of points for separation based on theory presented in earlier chapters, and discusses the challenges of separating the electronic drive at these points.

This chapter highlights an iterative process of learning by continuously increasing the depth of analysis upon each-pass until reverse engineering the design became the focus; the migration of the separation points is detailed as the intimate knowledge of the electronic drive design was created. This facilitated the identification of plausible points of separation and provided appropriate justification for these points.

Understanding the information presented in this chapter is crucial to understanding the design, development, and testing of the prototype circuit boards, which is covered in Chapter 8, *Prototype design and manufacture*, and Chapter 9, *Instrumentation and Testing* respectively.

Chapter 8

Prototype design and manufacture

"Different is not necessarily better. But better is necessarily different"

- Georg C. Lichtenberg

This chapter discusses the process of designing the new prototype circuit boards, based upon the proposed separation line from Chapter 7, *Separation Process*. The discussions for this chapter include the criteria for the design of the new circuit boards, the viability of the proposed separation line, the specific challenges to overcome, and testing. Testing of the design forms an important discussion for the design process, as it resulted in further migration of the separation points and meeting the criteria in the least number of iterations.

8.1 Criteria for prototype circuit boards

Due to the inability to physically cut the existing electronic drive, it was necessary to design two new circuit boards to achieve separation. The two circuit boards would prove the viability of separation along the proposed separation line.

The design process also provides the ability to manufacture the electronic drive with separated power supply and control circuits; this is the direct result of the manufacturing information generated as a result of the design process.

To ensure the quality of the prototype circuit boards was of sufficient standard to be viable for manufacturing, some early decisions were made:

1. The prototype circuit boards would be designed and assembled to production quality.
2. The design of the circuit board would retain standard component placement as much as possible. This was to ensure familiarity between the original circuit board and the separated circuit boards. Significant change to the placement and layout would reduce the quality aspects of maintainability and repair.
3. The circuit boards would be designed to be dual-sided and utilise plated through holes. The reason for this was the ability to run a large ground plane and prevent the use of jumpers. This decision is in line with the design of the original circuit board.
4. Due to the high voltage nature of the circuit board, a high quality substrate would be utilised, of sufficient thickness to prevent blow-through arcing.
5. The circuit boards would utilise solder masking. While solder masking increases the difficulty of modifying prototype circuit boards, it will ease assembly significantly. This improves safety by reducing the chance of accidental electrocution, and short-circuits by foreign material on the board.
6. Component designators would be used where possible to aid in identifying incorrect component placement during assembly. This reduces the number of errors to be rectified during testing.
7. Maintaining the basic layout and shape of the power supply circuit board is important to allow the circuit board to be attached to the standard heat-sink. Preventing redesign to the heat-sink reduces the level of reworking required to manufacture the newly developed circuit boards.

8. The control circuit board is to be designed to fit behind the control panel of the DVR Lathe headstock. This placement is logical and reduces the presence of EMI due to the casing of the motor consisting entirely of metal.
9. There should be significant room left on the circuit boards at the end of the design process. This allows ease of modification to the existing circuits for improved quality or functionality. It also allows amalgamation with the smaller circuits such as the EMI filter.
10. The connections between the new circuit boards are to be separated into two separate connectors. These connectors being for input/output signals and power signals. These connectors are to be labelled IX1 and IX2 respectively; IX stands for inter-board connection

The circuit boards were designed with the establishment of these rules. The early design process involved measuring and identifying the footprints of all components on both sides of the separation line. This was a significant process and resulted in a large number of footprints that were not available in the footprint library of the circuit board design program. These missing footprints were created and added before design of the circuit boards could begin.

The initial design of the circuit boards themselves was to measure the power supply, the standard heat-sink, and the space available behind the control panel. The space behind the control panel became limited due to the tapering nature of the housing. The tapered housing is made from plastic and appears to be moulded; the angle of the taper could be reduced, or removed completely, to facilitate the height requirements of the control circuit board to fit. This possible rework for manufacture was noted and blank circuit boards were created to the dimensions measured. The large copper planes were then measured for their corner co-ordinates, and these co-ordinates were then mapped onto the blank circuit boards.

The next step was to mimic the standard placement and layout on both the power supply circuit board and control circuit for components not related to the separation line. The tracks between component pads and planes were placed during this stage. It should be noted that any flaws noticed during the design of the circuit board, poor track spacing, sharp track bends, and undersized tracks, were noted and corrected.

Design of the circuit boards around the separation point was very difficult. This was an iterative process beginning with placement of the component. The tracks for connection of the components were placed, then checked against the schematic and existing electronic drive, and modified if necessary. This process was iterated until no difference in the schematics between the separated circuit boards and the original circuit board could be identified.

The next step was organising the separation points into two connectors, the position of these connectors on the circuit board would be determined by ease of connection by track with the respective signals. The table of signals for the connectors is shown in Table C-11: Additional Connector Signals, in Appendix C, *Research Outputs* , on page 226.

The last step was to select and place an appropriate connector. The connectors had to have a flat profile as to fit comfortably in the space available for the control board, but have sufficient specification for voltage, current, temperature and connection cycles. The chosen connectors are shown in Table C-10: Additional Connector Information, also in Appendix C, on page 226. The datasheets for these connectors are available in Appendices D.10 and D.11 starting on page 278.

Based upon the physical location for the generation of the power supply rails, and the input/output signals, the location for the power signal connector was decided to be placed beside the twin-rail regulator on the bottom right of the power supply board, and beneath the motor phases on the top right of the power supply board for the input/output signal connector. These were placed in corresponding positions on the control circuit board, with the input/output signal connector placed at the top near the current signal processing components; the reason for this was to reduce the length of the conductor between the generation of the waveform and the operational amplifiers to reduce EMI concerns.

The power supply connector was placed as close to the necessary components as allowable to ease routing of the tracks.

The resulting circuit board designs can be seen in Appendix C, *Research Outputs*.

8.2 Manufacture and assembly of circuit boards

As mentioned in the previous section, the circuit boards were to be manufactured to production specification. Therefore manufacture of the base printed circuit boards was outsourced to a professional company; Advanced Circuits Ltd. This would allow the necessary manufacturing techniques to take place and the quality of the board would be very high.

The specifications for the manufactured printed circuit boards are:

1. High quality substrate of sufficient thickness, 2.0mm, to prevent blow-through arcing of the circuit boards.
2. Sufficient weight copper sheet to minimise track and plane resistance, 4oz was chosen for this purpose.
3. As the circuit boards are square, there is no need for routing operations and the circuit boards can be guillotined.
4. Green solder mask. This reduces the chance of electrocution, shorting by foreign material on circuit board, and eases assembly.
5. White component designators. This ensures component placement errors are highly visible when assembling the circuit boards. This is not a large concern for automated manufacturing, but was of significant concern to prototyping the separated electronic drive circuit boards by hand.
6. The use of high quality plated through holes to improve electrical contact and prevent the use of jumpers.
7. Pre-drilled for through-hole components.

The first step in the assembling process, upon arrival of the prototype printed circuit boards, was to drill out the necessary mounting holes to allow the boards to be mounted in their respective positions within the DVR motor housing. Assembly of the circuit board components could begin once correct mounting of the circuit boards was achieved

Before the components could be soldered onto the new circuit boards, they were required to be removed from the existing circuit board; this was due to the non-availability of new components. This presented a significant challenge to overcome to successfully assemble the circuit boards, it can be a difficult task to remove a component and re-solder it successfully without damaging it. Removal of the components allowed measurement of the

corresponding electrical values, which aided the reverse engineering process by allowing completion of the tabulated component data.

The most challenging components to remove were the microcontroller, the IGBT driver, and the **C**omplex **P**rogrammable **L**ogic **D**evice (CPLD); this was due to their flat package designs; the quad packages of the microcontroller and the CPLD proved exceedingly difficult.

This difficulty was due to the inability to access the appropriate equipment to facilitate the removal of surface mount quad flat packages. To remove these components required significant heating to the rear of the original circuit board and a piece of machined aluminium to soak up spillage of heat. The drawback to this approach was the permanent damage of the existing circuit board; however the components were removed without damage.

During the assembly process, numerous errors in the design and prototype circuit boards were found; these errors were as follows:

1. The pads in the footprint for the large power supply capacitors (Components C52 and C53) were spaced too far apart and required drilling
2. The large black capacitors (Components C52 and C53) are situated too close to the current feedback resistors (Components RS1,RS2 and RS3)
3. The pads in the footprint for the feedback resistor (Component R39) from the 360V rail are too close together
4. The plated through-hole from the +5.0V rail smoothing capacitor (Component C67) to the ground plane on the reverse of the board was not physically connected to the capacitor footprint pad with a track
5. The back-EMF protection diodes (Components VD2, VD3, VD4, VD5, and VD6) on the reverse of the board all have the correct spacing except for the protection diode (Component VD1) closest to the power factor correction unit, which has larger pad spacing and therefore was difficult to fit
6. The thyristor (Component VS1) footprint has uneven pad spacing and sizes and this made installation difficult
7. The very small capacitor (Component C81) at the top left hand side of the board has a footprint which is too large for it, installation was possible but difficult
8. The twin-rail voltage regulator (Component D15) does not have the pads underneath to allow a good thermal connection to its heat-sink

9. The capacitor (Component C86) closest to the voltage transformer has a pad which is spaced correctly but the pads are very long and could be shortened
10. The position sensor feedback connector is positioned too close to the surrounding components and needs to be moved to allow ease of connection
11. The crystal (Component ZQ1) is not spaced sufficiently from the components surrounding it
12. Some components were damaged during the de-soldering and re-soldering process and were required to be replaced

These changes were noted and corrected as a later revision; these changes will be compiled with any changes evident as a result of testing the new circuit boards. With the prototype circuit boards completely assembled they were ready to be tested; the results of testing are discussed in the next section.

8.3 Assembly testing of circuit boards

To ensure safe and eventual correct operation of the circuit boards, a plan for incremental testing of the circuit boards was decided upon and implemented. The steps in the testing plan can be grouped into the following steps:

1. Visual inspection of all components under a microscope to ensure quality soldering, prevention of bridging, and components are mounted flat with no broken legs.
2. Continuity test of all power rails on the power supply circuit board to ensure the lack of short circuits within the power rails, including the input to the power supply from the mains supply.
3. The circuit boards are mains powered, and are required to be tested by a registered electrician to ensure suitability for operating from the mains supply. The prototype circuit boards will therefore be tested by a registered electrician.
4. First switch-on to be undertaken with a registered and practicing electrician present.
5. Thorough testing of all power rails until satisfaction that the power supply is operating correctly.
6. Gradual connection of the control circuit board to ease fault finding.

Visually inspecting the circuit boards resulted in numerous dry solders being found; this was the direct result of poor quality flux. High quality flux was utilised and all joins reheated until the solder became molten. Both circuit boards were alcohol bathed in an ultrasonic cleaner to remove any surface impurities that could carry charge. The solder joints were then re-examined under a microscope; this process was iterated until all solder joints were of an excellent standard.

Further testing of the assembled power supply circuit board involved a thorough inspection of all components to ensure they were making a strong electrical connection after being re-soldered. Visually inspecting the board in this manner highlighted components which had been damaged during the assembly process; this also ensured that no components were installed in reverse polarity or in the wrong location.

Continuity testing of the power supply rails was then able to completed; this highlighted that the +5.0V rail contained a dead short condition. Extensive inspection with the microscope revealed that the microcontroller contained a damaged leg and was bridging the supply rail to the 0V_PWR rail; the microcontroller was de-soldered and replaced, It was found that the short condition was resolved upon retesting for the short condition following the repair.

The next step in the testing plan was to have the boards inspected by a registered electrician. The electrician was satisfied with the quality of the workmanship, the design of the circuit boards, and the prior testing. Upon his recommendation, live testing was to be made utilising a **R**esidual **C**urrent **D**evice (RCD) and an inline fuse to ensure safety for both electrocution and over-current respectively.

The power supply circuit board was connected to the mains supply with the registered electrician present, using the RCD and the inline fuse recommended. The power supply circuit board tripped neither device and did not exhibit any areas of unexpected heat generation. This successful first switch-on enabled progression to the next phase of testing.

The power supply has two main functions, to supply a stable and phase corrected voltage to the motor itself, and to supply a range of stable outputs to the control circuitry. In order to test that the power delivery to the motor is working effectively requires the control circuitry to operate; however, testing that the power rail for the motor is in operating condition and that all power rails to the control circuit operate is an acceptable

compromise in determining appropriate operation of the power supply as a whole. Further testing of the power supply rails can be undertaken once the control circuitry is operating.

The power supply outputs seven different rails and all but two of these were providing the correct voltage; these rails being the -5V measuring -13.6V peak while oscillating, and +5V_INT measuring 0.24V stable. Deeper investigation highlighted an oversight in the separation process with three of the components comprising the -5V power rail being placed on the new control circuit board; this was noted so that these components can be moved onto the power supply circuit board in the next revision. Testing of the +5V_INT rail resulted in the discovery of a damaged regulator and this was replaced.

The next step in the testing plan was to gradually connect and test the functionality of the control circuit board. The first connections made were all the power rails, these being +2.5V, +5V, -5V, 0V_PWR, +5V_INT and 0V_INT. At this point the board was quickly powered. The -5V rail was tested and found to be the correct voltage, all other rails were also functioning correctly.

The user control panel is powered by +5V_INT and +0V_INT and complained of a lack of connection to the main control unit; displaying the error “Not Connected” on the LCD. This was found to be the lack of tracks on the control circuit board responsible for providing power to the opto-couplers; this was noted to be changed in the next revision. The opto-couplers were powered by the use of jumpers and on next power cycle the user control panel and control circuit booted together successfully.

The next challenge to overcome in connecting the control circuit board was another error being reported by the LCD. The error displayed was “PFC Fault” this code is the result of the power factor correction FO signal remaining high. Therefore the next connections to make were the two PFC bus signals FO and ON/OFF. Upon the next power cycle the LCD displayed the error “Low Voltage” indicating the lack of feedback from the +360V supply; the feedback from the +360V rail was then connected.

The last error message displayed on the LCD was “Hardware Fault” which indicated a problem with the IGBT driver. Upon examination under a microscope it was found that there was a dry solder, that was missed under visual inspection testing, on one of the switching input pins; this was repaired with fresh flux and re-heating the solder joint.

At this point all the remaining connections were made, and an attempt at operating the motor was made. The motor rotated easily, however it was not operating smoothly. There

was an audible miss as the motor rotated, reinforcing the idea that the acoustic sound of the motor is an effective indicator of control circuit performance, and the motor refused to start from all operating positions. It was immediately apparent that one of the phases was not operating.

In depth testing revealed that the microcontroller was providing a switching signal for all transistors, both high side and low side driving. However the switching signal for the Phase C high side driver was not present at the input of the IGBT driver. It was noted at this point that the switching signals from the microcontroller pass through the CPLD, and the signal was not present after the CPLD.

Tracing all connections into the CPLD highlighted that the current feedback signal from Phase C was routed to pin 35, while the correct pin, 36, was left floating; this was resolved by cutting the offending track and connecting pin 36 to the current feedback signal for Phase C.

At this point the motor rotated smoothly, started from all rest angle positions and operated without detectable flaw; this indicated initial successful separation of the power and control circuit boards. Comparative performance testing would highlight any performance differences between the original solution and the new separated circuit boards. The results of this comparative testing are discussed in Chapter 9, *Comparative Evaluation Testing*.

8.4 Revision of circuit board design

The first revision of the circuit boards proved the successful separation of the power supply and control circuitry of the Teknatool DVR electronic drive; however various observations were made to improve the design of the circuit board. These observations ranged from footprint dimension errors to incorrect diagnosis of placement location for two components.

The necessary corrections to the circuit board design were:

1. Correction to the footprints for power supply capacitors (Components C52 and C53).
2. Moving the capacitors (Components C52 and C53) upwards to remove fouling on current sense resistors (Components RS1, RS2 and RS3).

3. Correction to the footprint for the +360V feedback resistor (Component R39).
4. Addition of the track to connect smoothing capacitor (Component C67) in the +5.0V rail to the plated through-hole connected to 0V_PWR.
5. Correct spacing for the footprint used in back-EMF protection diode (Component VD1).
6. Correction to the footprint for thyristor (Component VS1).
7. Correction to the footprint for a small power supply capacitor (Component C81).
8. Correction to the footprint of the twin-rail voltage regulator (Component D15).
9. Correction to the footprint for power supply capacitor (Component C86)
10. Shifting the position sensor feedback connector downwards to increase room for fitment.
11. Shifting of components surrounding the timing crystal (Component ZQ1) to allow ease of fitment.
12. Movement of the smoothing capacitor (Component C66) for the -5V rail to the power supply circuit board.
13. Movement of the reverse current protection diode (VD19) for the -5V rail to the power supply circuit board.

The movement of the two components comprising the -5V rail did not affect the separation points, as they were in parallel with each other and connected directly to the original separation point; It did however make a small change to the separation line. The resulting schematic highlighting the change is shown in Figure C-7 in Appendix C.7 on page 210.

This change in the boundaries between the two circuits results in a change which is shown in the separation line drawn on the circuit board in Figure C-8 in Appendix C.8 on page 211.

The individual printed circuit board designs for the power supply and control circuit can be found in Appendix C, *Research Outputs*.

8.5 Delivery Of Solution

The final manufacturable solution consists of the following information:

1. Printed circuit board design files
2. Printed circuit board gerber files
3. Printed circuit board machine drilling files
4. Electrical schematics of both separated circuits
5. Component listing, including all values, footprints, identifiers, component location
6. Additional information to assist with servicing, further design and improvement

This information is available in Appendix C, *Research Outputs,* starting on page 203.

A photo of the completed prototype separated circuit boards is shown in Figure 8-1.

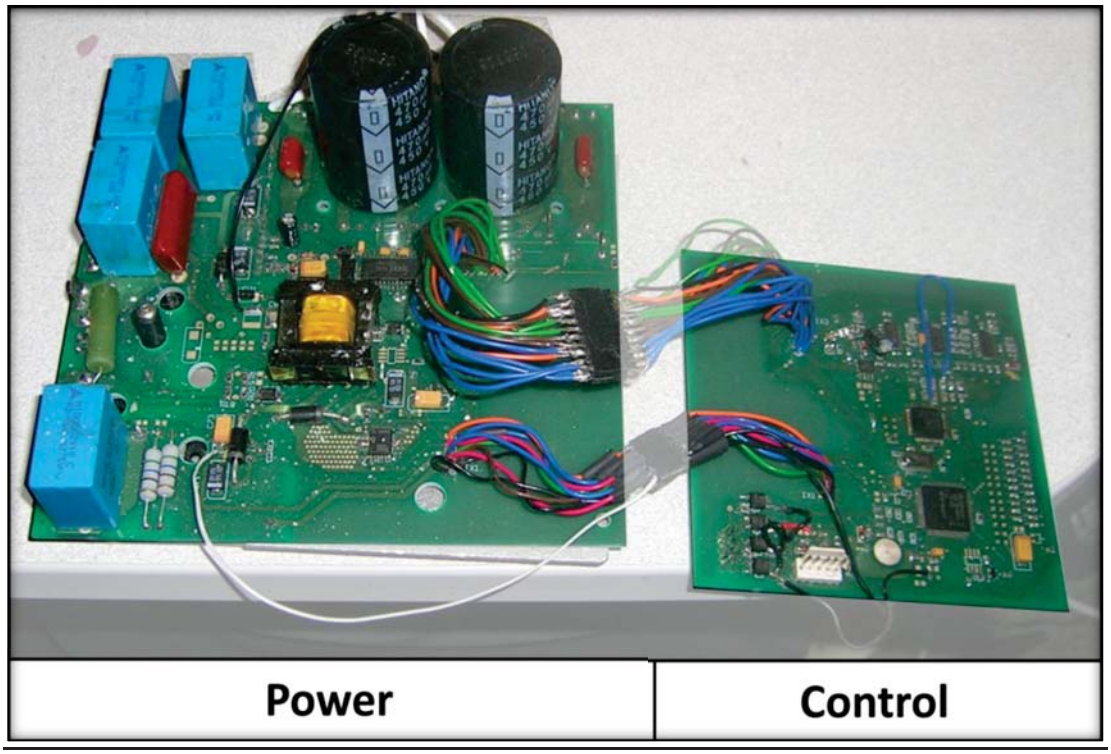

Figure 8-1: Photo Of Prototype Separated Electronic Drive

8.6 Summary

This chapter investigates the design process of the prototype separated circuit boards. It highlights the differences between working at a schematic level and a real world circuit.

This chapter continued the iterative process from Chapter 7: *Separation Process,* by attempting to design the circuit boards using the separation points discovered; this proves to be a failure and a revision of these points takes place to allow the circuit board to be developed.

This chapter also highlights the difficulty in producing the working prototype, and the need for iterative testing as the circuit is designed and then assembled. Finally, it highlights the vast amount of information gained from the reverse engineering process to design and build a successful prototype.

This chapter brings the reverse engineering and design process to conclusion, and leads the discussion to the comparison between the original and prototype solutions in Chapter 9, *Instrumentation and Testing*.

Chapter 9

Instrumentation and Testing

"The test is to recognize the mistake, admit it and correct it. To have tried to do something and failed is vastly better than to have tried to do nothing and succeeded"

- Dale E Turner

This chapter discusses the difficulty involved with obtaining waveform captures from the Teknatool DVR electronics; this difficulty was primarily due to the lack of appropriate instrumentation. Namely the lack of isolation between the earth of the mains supply and the negatives of the measurement channels present on the oscilloscope.

This chapter details the design and production of an interface board which provided isolated single sided signals to allow waveform capture utilising non-isolated instrumentation.

Finally, this chapter discusses the comparative evaluation testing undertaken to confirm that the performance of the electronic drive is maintained while operating the DVR SRM from the new prototype solution. The basis of this evaluation is a side by side analysis of key waveforms captured from both implementations of the electronic drive.

9.1 The need for isolated instrumentation

A key objective of this thesis is to compare the performance of the original solution against the prototype solution. This evaluation ensures the correct operation of the power supply and control electronics of the prototype solution.

The need for the isolated instrumentation is due to the rectification of the AC input voltage. Isolated instrumentation refers to all devices which operate from a separate power supply and allow differential measurement of system quantities regardless of negative reference rail potential; this is achieved through floating.

With non-isolated instrumentation, all measurements are taken with respect to the negative reference of the instrumentation itself. This prevents differential measurement of any system variable as short-circuiting of components present in the electronic drive or the instrumentation is a serious risk. For example, the original oscilloscope was not isolated from the mains ground, nor between individual channels; therefore direct usage of this oscilloscope on the Teknatool DVR electronics would result in a short of the rectifier bridge. This is illustrated in Figure 9-1:

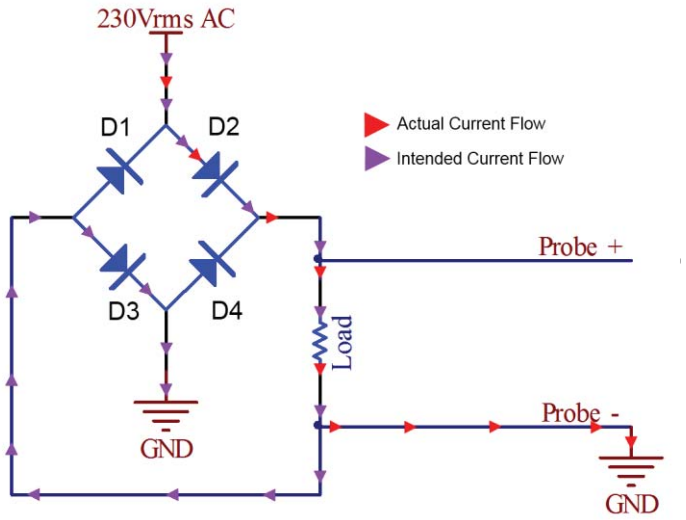

Figure 9-1: Short Circuit Current For Differential Measurements

Diode D3 in the bridge rectifier is shorted out by the negative of the probe pair as it is connected directly to mains earth, and to the negative of all probes connected to the oscilloscope. It is also not possible to measure directly across ground to the high side of the

load; this is because the output of the bridge rectifier is floating with significant potential difference between the positive and negative half cycles of the input waveform.

To take measurements in such a manner would be dangerous and result in erroneous waveforms. To remove the connection of the oscilloscope to mains earth by removing the pin in the **I**nternational **E**lectrotechnical **C**ommission (IEC) power connector would allow such measurements to be taken, however should more than one waveform be captured at once, the waveforms must be from the same reference potential due to the lack of isolation between channels.

To allow measurements to be taken from the electronic drive without isolated instrumentation requires the design and construction of an isolation and measurement circuit; this circuit can be designed to provide isolation from both mains and differing reference potentials. This allows measurement of waveforms referenced to the low side of the bridge rectifier, as well as concurrent measurement of signals across differing reference potentials with a non-isolated oscilloscope.

The original measurement equipment utilised was non-isolated and therefore the design of, and assembly of an isolation and measurement circuit was a critical requirement for the progress of the project. The need for this equipment later became superfluous due to the procurement of isolated measurement equipment.

9.2 Waveforms of significant interest

Due to the cost of isolation components, only the most significant waveforms need to be captured. It was determined that the most important waveforms to capture were the voltage and current waveforms of each phase as they would provide sufficient information to discuss the performance of the prototype solution.

Performance of the electronic drive can be estimated from the current and voltage waveforms of the motor windings for a given load and rotational speed. Average torque production can be observed from the current waveform, while the voltage waveform highlights the control and switching methodology being utilised for the current rotational speed and loading of the motor.

The ability to capture waveforms concurrently shows the overlap between phases and therefore the torque ripple can be investigated by the envelope of the overlapped current waveforms. The current waveforms can also highlight variability in the impedances of the phase circuits; this condition is known as *imbalance* and has significant negative impact on the generation of torque ripple.

The RMS and peak voltages of the +360V DC Bus can be investigated through the use of a digital voltmeter, or handheld single channel oscilloscope; these devices are capable of floating as they are powered by a battery. Both devices are rated for input voltages up to 600V and therefore require no conditioning of the input signals is required to reduce voltage.

Therefore the isolation circuit provided six outputs:

1. Phase A Voltage
2. Phase A Current
3. Phase B Voltage
4. Phase B Current
5. Phase C Voltage
6. Phase C Current

The mains supply was not included in this isolation and measurement circuit, as the negative reference is earth; this is the same negative reference as the oscilloscope. Therefore the mains supply waveform can be investigated by the non-isolated oscilloscope.

9.3 Voltage measurement

Measuring the voltage waveform present across the phase winding requires probing of the electronic converter. The electronic converter is a high voltage DC supply and therefore the potential of the measured voltage waveform must be divided to prevent damage to instrumentation and improve the safety of taking measurements.

The electronic converter is of asymmetric half bridge converter topology, therefore the peak voltages expected when the converter is operating in bi-polar switching is approximately +VDC and –VDC; +360V and -360V in the case of the Teknatool DVR drive.

Measurement of the voltage waveform can therefore not be made in reference to the 0V rail, and differential measurement must be used.

Differential measurement requires that both the top and bottom sides are measured and subtracted from each other. The difference in the input signals is known as the differential and represents the potential present across the winding; the polarity of the differential is equivalent to the polarity of the phase winding. The differential method for measurement of the phase voltage is shown in the schematic in Figure 9-2:

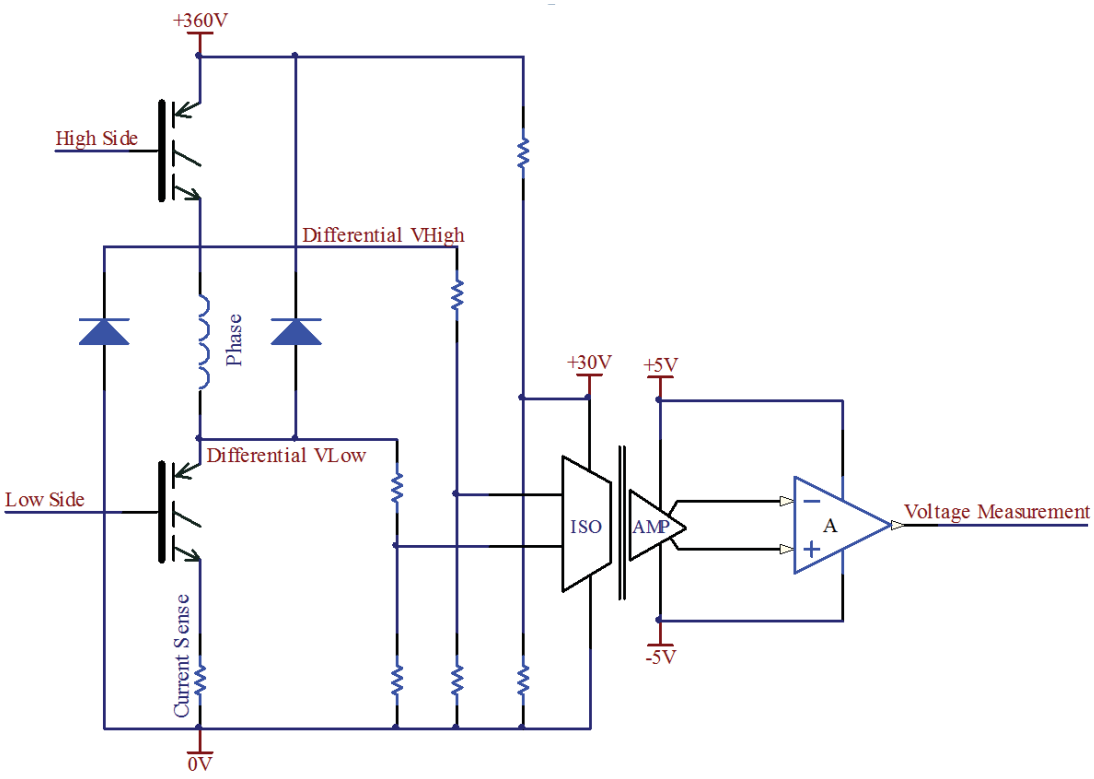

Figure 9-2: Differential Phase Voltage Isolated Measurement Circuit

The schematic shows the electronic converter circuit with the isolated and divided potential measurement of the phase winding voltage. It should be noted that the differential voltage across the phase winding was required to be of a much smaller potential to prevent damage to the isolation amplifier; this requires voltage dividers on both the high side and low differential measurements. The power supply for the isolation amplifier was also required to be divided as the isolation amplifier cannot operate from a +360V source.

The isolation amplifier takes the small differential voltage between the input pins and converts this to a fixed frequency variable duty cycle pulse to drive an LED; the isolation

barrier is therefore optically based. The pulsed light from the LED is received on the other side of the isolation barrier and the same potential differential voltage is created across the output pins; therefore the gain of this isolation amplifier is one (Refer Appendix D.12 on page 291).

To ensure that the isolation is complete, the lack of isolation between probes on the same oscilloscope needs to be taken into account, also the differential low output pin cannot be directly connected to ground; this requires the signal to be converted to single sided. An operation amplifier is used to achieve this, also with a gain of one. The operation amplifier will measure the differential across the input pins, and will bias the single sided output to be centred at the voltage in the middle of the differential inputs.

This results in a fully isolated voltage measurement, capable of being measured with a non-isolated oscilloscope or digital voltmeter.

9.4 Phase current measurement

Measurement of the current through the phase would require the addition of a component into the electronic phase converter. It is beneficial to place this component directly after the phase winding and before the lower switching element; this allows current measurement when the bottom transistor is open circuit and therefore the current decay rate can be measured. The original current sense resistor is not placed in a position to be able to measure the decaying current and therefore making use of this component is not an option. Placing another current sense resistor was discredited due to the need for differential voltage measurement techniques as it would experience reversal of the source voltage polarity when switching in bi-polar operation.

Measurement of the phase current was therefore provided by the means of a Hall Effect current sensor, operating on the principles of current transforming; this approach allows the current waveform to be fully isolated with the signal conditioning circuitry of the sensor operating on a different power supply to that of the Teknatool DVR drive. The schematic showing how the Hall-effect current sensor was connected in the electronic converter circuit is shown in Figure 9-3:

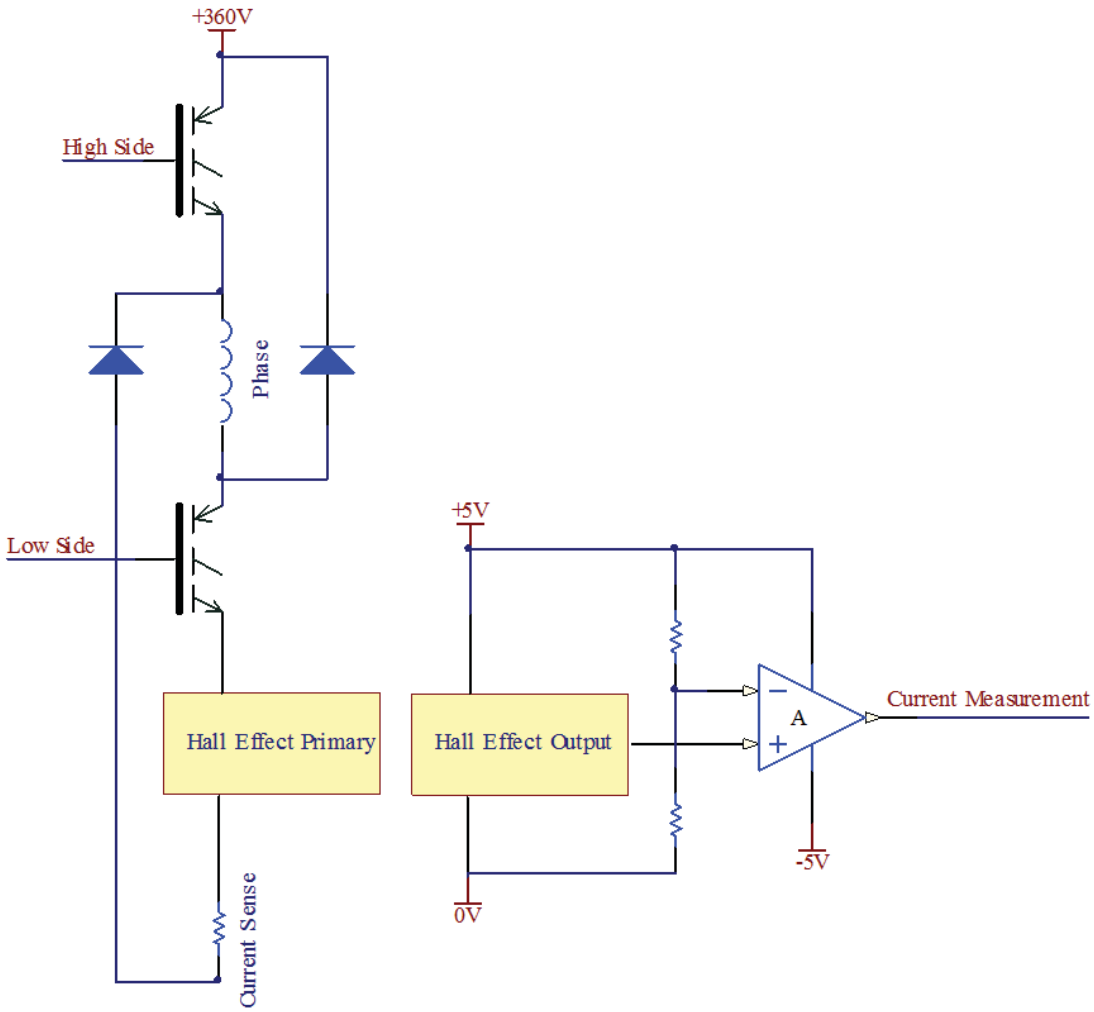

Figure 9-3: Phase Current Measurement Isolation Circuit

This schematic shows the electronic converter with the Hall Effect current sensor in series with the phase winding; the output of the Hall Effect current sensor is completely isolated and powered by a different supply. It should be noted that the current sensor utilised can measure both positive and negative current flow and outputs a 2.5V signal for no flowing current (Refer Appendix D.8 on page 272). This presented a problem for the oscilloscope which had no feature for adjusting DC offset voltage. The addition of a voltage subtraction circuit to remove the 2.5V bias was connected to the output of the current sensor to remedy this problem.

To ensure that complete isolation is achieved, the isolated supplies used here are also used for the voltage measurement circuitry; this allows measurement of a current and voltage waveform simultaneously without short-circuiting. The result of the circuit is complete isolation from the Teknatool DVR drive for the measurement of phase currents.

9.5 Electromagnetic Interference

Obtaining clear waveforms from the SRM was difficult due to the high generation of EMI presenting as white noise in captures. The most significant contributors, ordered in lowest to highest frequency, are:

- Radiation from Transformer T1
- Commutation Transistor Switching
- Chopping Transistor Switching
- +2.5/+5V Switching Regulator
- Power Factor Correction Switching

The result is the generation of white noise which interferes at frequencies of interest in the waveform captures; this is very difficult to filter. Fortunately, the amplitude of the EMI at frequencies of interest is small in comparison to the intended waveform which only results in a loss of fidelity in the information. The large amplitude noise is at frequencies much higher, therefore low pass filtering is an effective method.

The low pass filter schematic is shown in Figure 9-4:

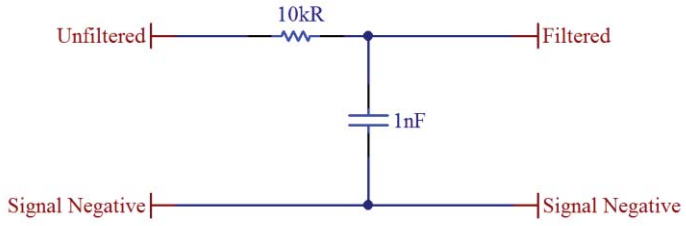

Figure 9-4: Low Pass EMI Filter Schematic

The frequency response of this filter is described by the following equation:

$$F_c = \frac{1}{2\pi RC} \tag{9.1}$$

Where R is the value of the resistance, and C is the value of the capacitance.

Therefore the cut frequency of this filter is 15915Hz.

9.6 Power Factor Comparison

Ensuring that the prototype circuit board performs PFC appropriately is of critical importance to realising the full power output of the motor. Power factor was compared by comparative evaluation, and the results are available in Appendix B; this result was extended to comparison of power factor with PFC disabled to ensure that the overall reactive load presented to the supply is identical between the two electronic drives.

The power factor results for the prototype electronic drive are listed in Table B-5: Power Factor Measurements (PFC On) and Table B-6: Power Factor Measurements (PFC Off), in Appendix B, *Measurement Data*, on page 201.

The power factor results for the original electronic drive are listed in Table B-7: Power Factor Measurement (PFC On) and Table B-8: Power Factor Measurement (PFC Off), in Appendix B, *Measurement Data*, on page 202.

The results of the power factor evaluation allows us to draw the conclusion that the load presented to the mains supply is overbalanced by the presence of capacitive reactance; this is because all the power factors are negative, implying that current leads the voltage waveform. This is further reinforced that by increased commutation angle, higher rotational speed and loading, of the motor windings results in an improved power factor even with power factor disabled.

Comparison of the results obtained with PFC enabled highlighted a significant performance difference between the prototype electronic drive and the original electronic drive; the prototype electronic drive displays significantly improved power factor. This is graphically represented for ease of observation in Figure 9-5:

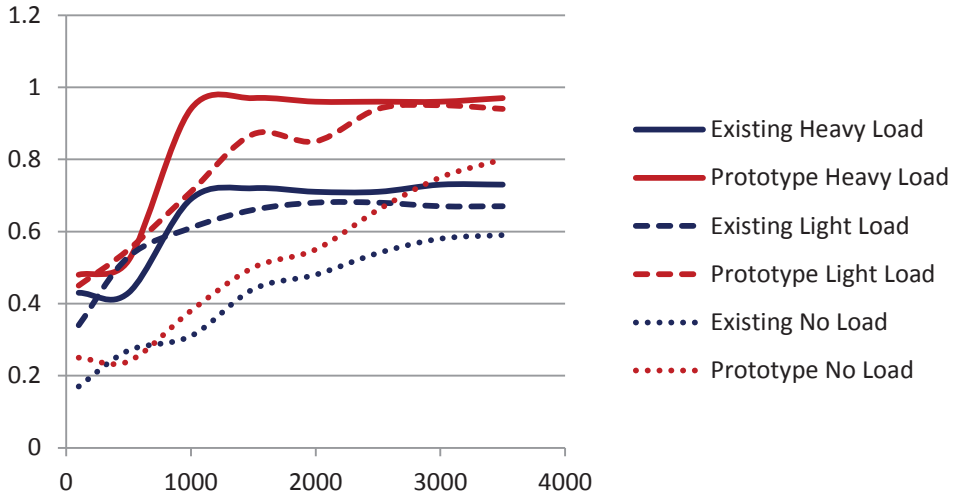

Figure 9-5: Power factor Correction Comparison

Capturing the voltage, current, and power waveforms from the AC mains supply will illustrate the current phase angle ϕ, and the harmonically distorted current waveform. These captures are shown in side-by-side comparison in Figure 9-6:

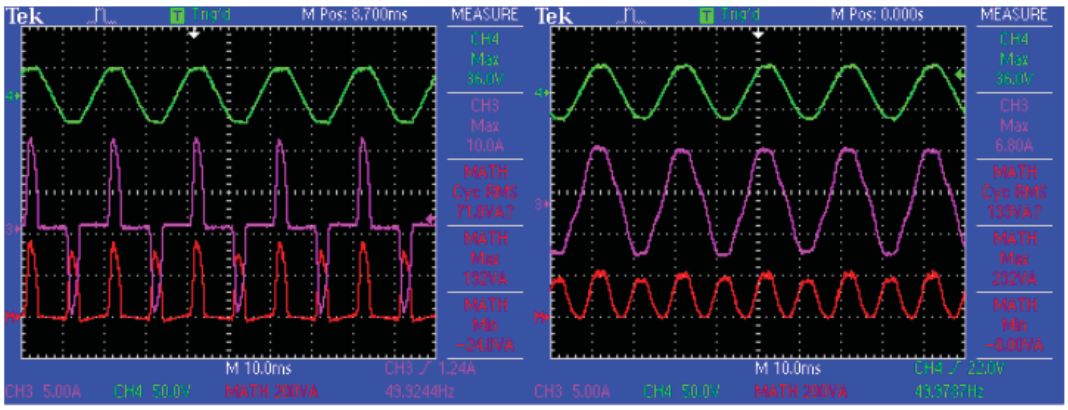

Figure 9-6: AC Supply Voltage, Current, And Power Waveform Comparison

The original electronic drive waveform is shown on the left, with the prototype electronic drive electronic shown on the right; the voltage waveform is shown in green and is a division of ten, the current waveform is shown in purple, and the power waveform is shown in red. It is immediately obvious that the original electronic drive shows significantly harmonically distorted current and power waveforms when compared to the prototype electronic drive; this is also present in increased vibration and noise from the motor while operating.

It can be seen that the power factor correction result of the prototype electronic drive is superior, at almost all rotational speeds and loading; this is an unexpected result as the aim of the research was to match the performance of the original electronic drive.

The PFC performance of the original electronic drive is disappointing, and it is unlikely that a commercial product would exhibit such an obvious flaw; therefore a hypothesis is formed that the PFC of the supplied original electronic drive has a fault preventing correct operation. To test this hypothesis, the results of the PFC enabled and disabled on the original electronic drive are compared graphically in Figure 9-7:

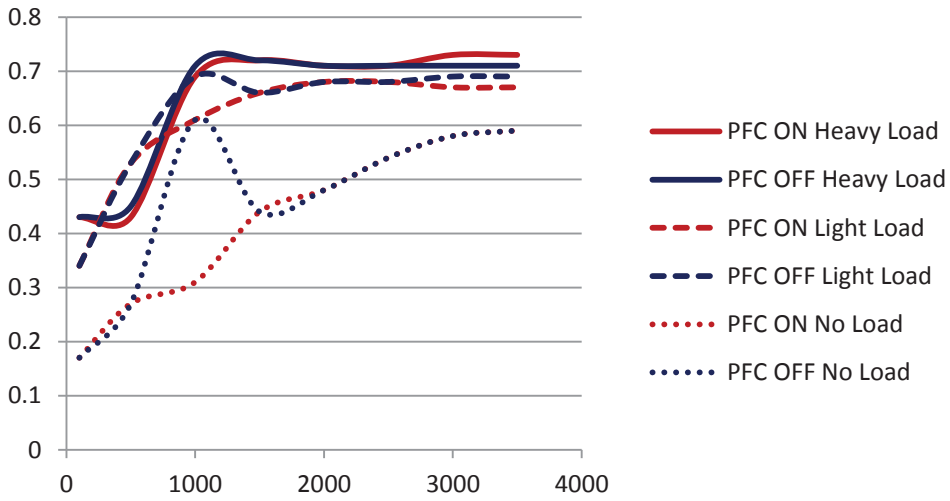

Figure 9-7: Power Factor Comparison of PFC Enabled And PFC Disabled

The observations from this graphical representation align with the hypothesis that the PFC is faulty. This conclusion is drawn because the power factor remains uncorrected for most combinations of speed and loading. There is a considerable increase in power factor at 1000rpm, which is seen at all loadings. This is important to note as it is contradictory to the hypothesis; investigation of the cause of this result are outside the scope of this thesis, and further investigation is not necessary to achieving the research objectives.

9.7 Power Supply Performance

The performance of the power supply can be determined by comparative analysis of the power rails it provides. The rails of interest are the +360V, +15V, +5V, +2.5V, -5V, and +5V_INT. The results of the comparisons are discussed in the following sections.

9.7.1 +360V Rail

The +360V rail is the output of the boost DC-DC converter of the APFC circuit which was noted in to be faulty in the original drive in 9.6, *Power* Factor Comparison*,* on page 137 of this document. A significant difference can be expected in the +360V rails between the two drives; the waveform captures of this rail are shown in Figure 9-8, these waveforms were captured with the motor operating at a rotational speed of 2500rpm with light loading.

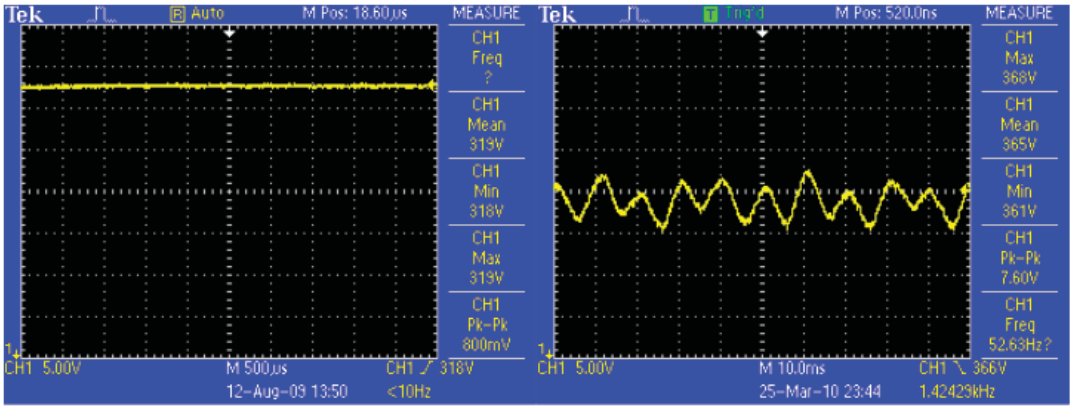

Figure 9-8: +360V Rail Waveform Comparison

The original electronic drive is shown on the left, while the prototype electronic drive is shown on the right; the waveforms of the two rails are significantly different; as expected from the results of the power factor comparison.

The original circuit board develops a peak voltage of 319V, which is close to the peak value expected of a 230Vrms supply if semi-conductor and resistive losses are considered. The prototype circuit board establishes a peak voltage of 368V, and can be seen to be constantly adjusting the DC bus voltage as expected of an active power factor correction supply; this is further evidence that the PFC of the original electronic drive supplied is faulty.

It can be concluded from this result that the +360V rail of the prototype electronic drive is superior to the original electronic drive it was compared against; this is only confirmed true for the original electronic drive supplied, and it is hypothesised that it is not representative of the original electronic drive design in general.

9.7.2 +15V Rail

The +15V charges the high-side IGBT driver capacitors for the electronic converter, and provides the input voltage to the +2.5V and +5V regulator; therefore appropriate performance is critical. The voltage waveforms of the +15V rail are shown in Figure 9-9, the motor was operating at 2000rpm and was lightly loaded:

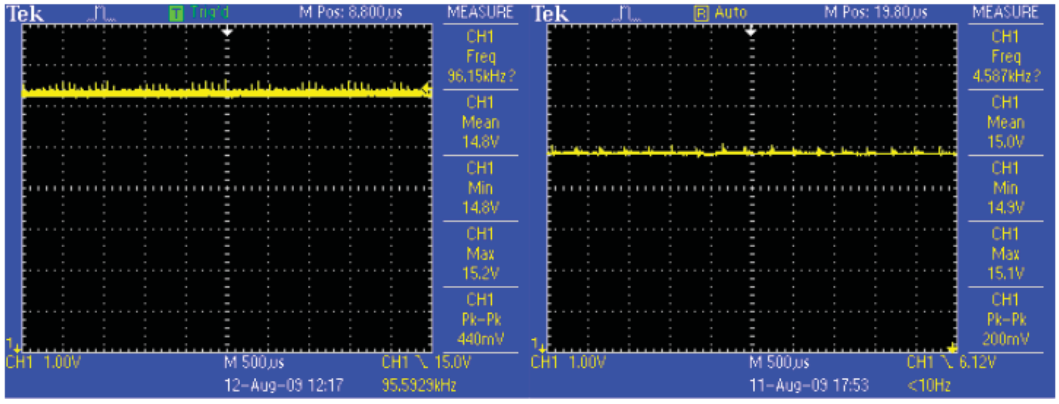

Figure 9-9: +15V Rail Waveform Comparison

Of note is the differing vertical positions within the trace; this is the DC offset of the oscilloscope and is not related to the +15V rail performance. The original electronic drive is shown on the left, while the prototype electronic drive is shown on the right.

The performance is almost identical; the +15V rail of the prototype drive exhibits less interference and less peak to peak variation; the mean voltage is exactly 15.0V. The increased interference and peak to peak swing in the original electronic drive is the possible result of harmonic current flow in the windings of Transformer T1 due to the lack of PFC. This is an untested hypothesis drawn from the results available. Both rails perform with acceptable performance. However, the prototype electronic drive has the favourable performance.

9.7.3 +5V Rail

The +5V rail is utilised to power the control circuitry, which is sensitive to poor rail regulation. The voltage waveforms of the +5V rail are shown Figure 9-10:

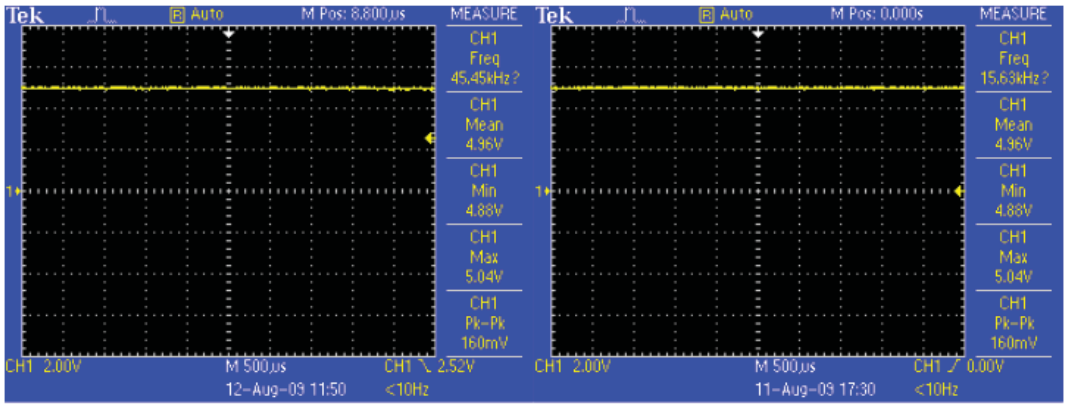

Figure 9-10: +5V Rail Waveform Comparison

The original electronic drive is shown on the left, while the prototype electronic drive is shown on the right. It can be seen that both drives show identical performance and therefore the +5V rail meets the research objective.

9.7.4 +2.5V Rail

The +2.5V rail also powers the control circuitry and is therefore appropriate regulation and performance is required. The voltage waveforms of the +2.5V rail from are shown in Figure 9-11:

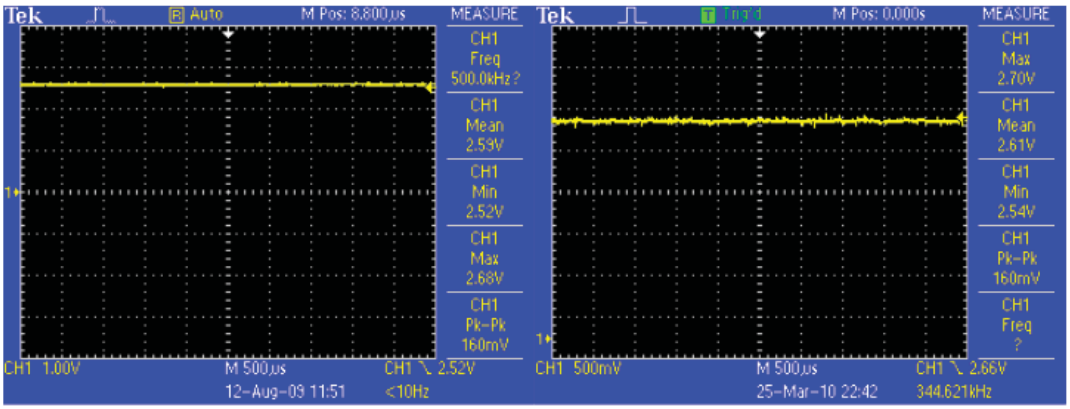

Figure 9-11: +2.5V Rail Waveform Comparison

The original electronic drive shown on the left, and the prototype electronic drive is shown on the right; there is a differing DC offset used to capture the two waveforms that is not related to the performance of the +2.5V rail.

The performance of the drives is almost identical, and the small difference can be explained by measurement error. The peak to peak variation is identical, and there is a small difference in the measured maximum potential, 2.59V against 2.61V, and the minimum voltage, 2.52V against 2.54V. The +2.5V rail of the prototype electronic drive meets the research objective requirements.

9.7.5 -5V Supply

The -5V power rail is utilised by the current sensor conditioning circuit. The voltage waveforms of the -5V rail are shown in Figure 9-12:

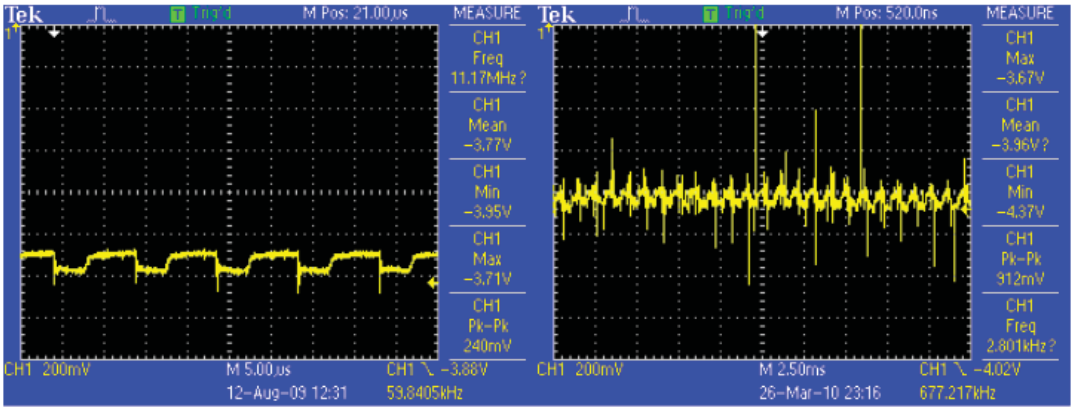

Figure 9-12: -5V Rail Waveform Compariosn

The -5V rail is shown to be working appropriately. The square step is present in both the original and prototype solutions. This square step forms the basis of a quality improvement and is discussed in Chapter 10, *Quality Improvement*. The excess noise present in the right capture was due to the capture being taken with a long wire connecting the probe to the negative of the supply rail. This capture was unable to be retaken due to the prototype boards being released to Teknatool.

9.7.6 +5V Isolated Rail

The +5V isolated rail provides power to the interface control panel; the components on this circuit board are sensitive to poor voltage regulation. The voltage waveforms are shown in Figure 9-13:

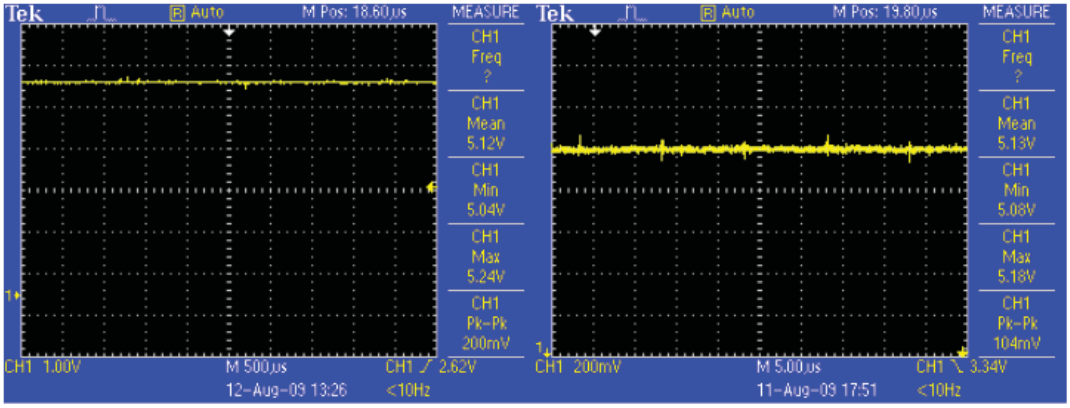

Figure 9-13: +5V_INT Isolated Rail Waveform Comparison

The original electronic drive is shown on the left, while the prototype electric drive is shown on the right. It can be seen that the two rails exhibit almost identical performance and are of acceptable performance. The prototype solution has lower peak to peak variation and therefore meets the requirements of the research objective.

9.8 Phase Winding Comparison

The chopping transistor control signal and resultant phase current waveforms indicate the performance of the motor. These waveforms can highlight speed control by the commutation period, and average torque control by the current waveform. The waveforms may not completely agree in comparative analysis due to the discontinuous nature of torque generation, resulting in variance between the sequential torque impulses of a given phase. This is illustrated in Figure 9-14:

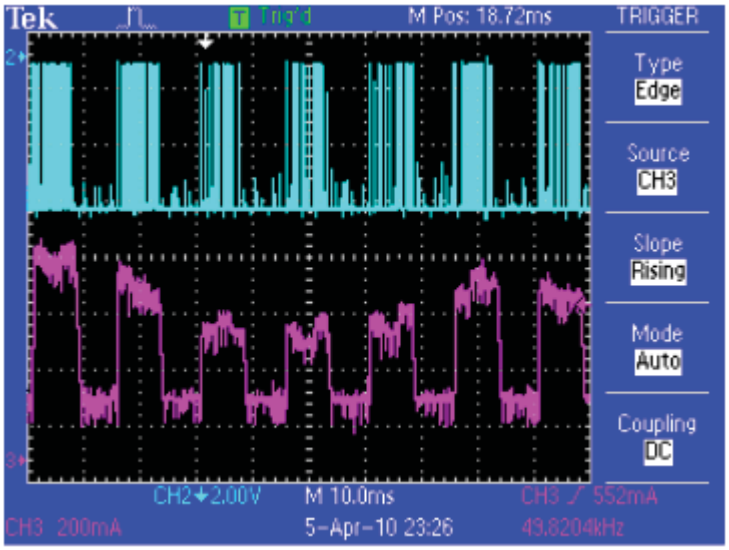

Figure 9-14: Current Waveform Variation At Constant Speed

The variation in average and peak phase current can be seen in sequential phase excitations. This behaviour is indicative of torque ripple present within an SRM, and illustrates the need to constantly adjust the torque contribution of any given phase to achieve steady state speed control.

The significant points to note are the appropriate control of the current waveform and the commutation period. These waveform captures are compared for motor speeds ranging from 500 to 3500rpm, and varying loads in the following sections.

9.8.1 100rpm

The chopping transistor control and phase current waveform captures for unloaded and light loading at 100rpm are shown in Figure 9-15, and Figure 9-16. Heavy loading was not possible due to insufficient motor power at this speed:

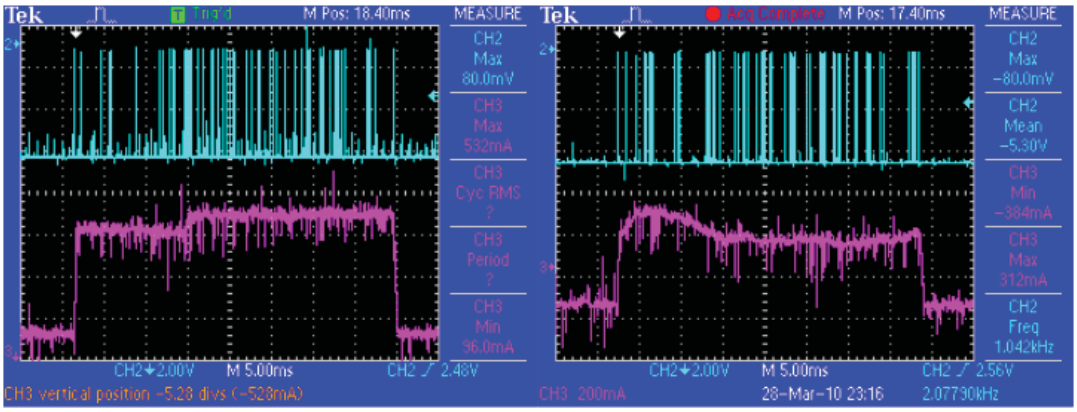

Figure 9-15: Chopping Signal And Phase Current At 100rpm Unloaded

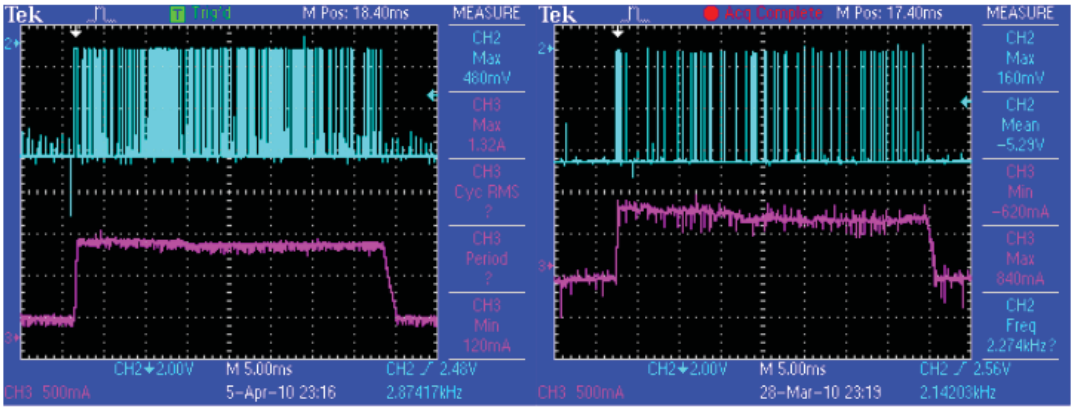

Figure 9-16: Chopping Signal And Phase Current At 100rpm Lightly Loaded

The original electronic drive waveforms are shown on the left, and the prototype drive waveforms are shown on the right; there is a DC offset difference between the waveforms, and this is not related to the performance of the electronic drives. There is some EMI inherent in the current waveforms; this was unable to be completely removed by filtering, as it would risk losing fidelity in the captures.

It can be seen from the captures that the commutation period and shape of the current waveform for both drives is similar but not identical; this shows the difficulty in obtaining identical waveform captures from an SRM due to the inherent variability of discontinuous torque generation. The performance of the prototype drive meets that of the original drive at 100rpm operation.

The waveform captures of the 100rpm results highlight the long commutation period available at low rotational speeds; approximately 37.5ms. The rise of the current waveform appears sharp but this due to the long time-base division of 5ms.

9.8.2 1000rpm

The chopping transistor control and phase current waveform captures for unloaded, light loading, and heavy loading at 1000rpm are shown in Figure 9-17, Figure 9-18, and Figure 9-19:

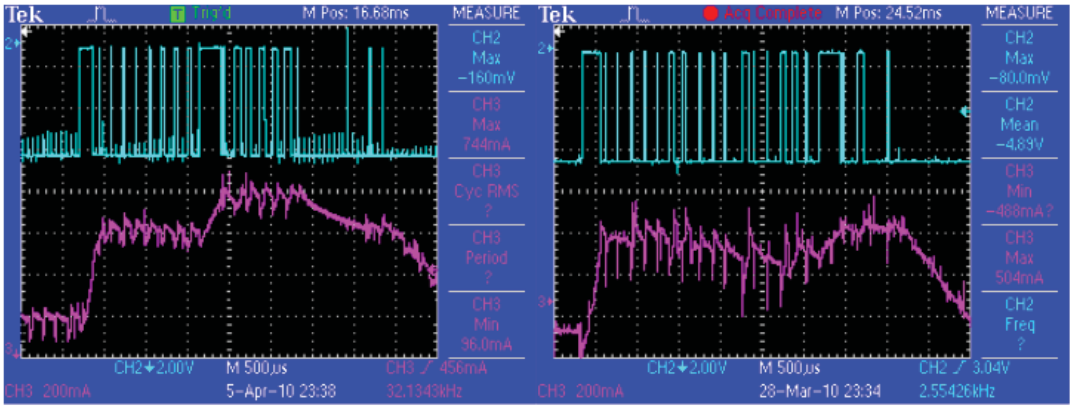

Figure 9-17: Chopping Signal And Phase Current At 1000rpm Unloaded

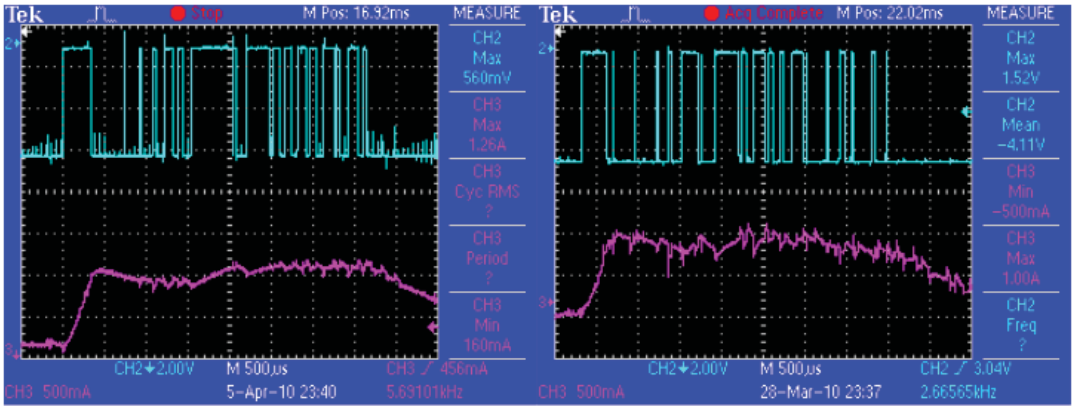

Figure 9-18: Chopping Signal And Phase Current At 1000rpm Lightly Loaded

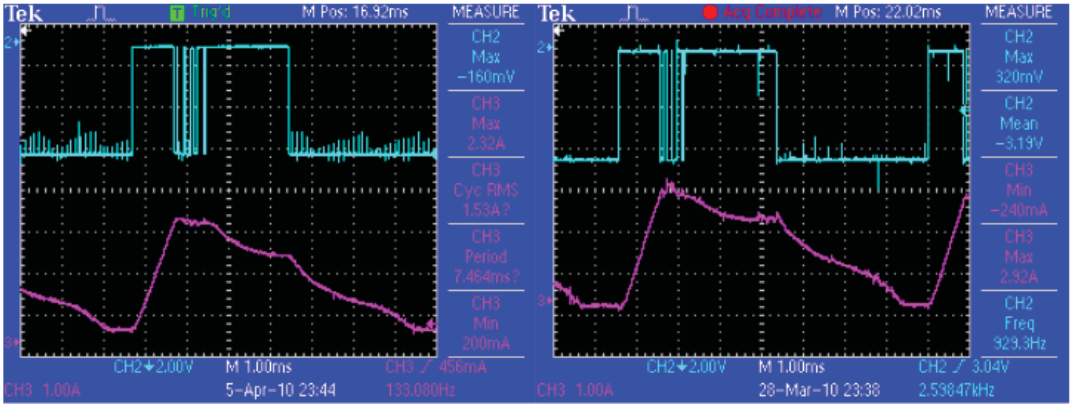

Figure 9-19: Chopping Signal And Phase Current At 1000rpm Heavily Loaded

The original electronic drive waveforms are shown on the left, and the prototype drive waveforms are shown on the right.

It can be seen from the results that the control algorithm moves towards singular pulse control as the loading increases; this indicates that the motor is operating at or near the base speed ω_b.

There is no significant difference between the waveform captures at any loading; therefore, the prototype drive meets the performance of the original drive while operating at 1000rpm.

The commutation can be seen to have noticeably decreased from approximately 37.5ms, at 100rpm, to approximately 3.75ms; this reduction is expected as the commutation period is inversely proportional to the rotational speed of the motor.

9.8.3 2000rpm

The chopping transistor control and phase current waveform captures for unloaded, light loading, and heavy loading at 2000rpm are shown in Figure 9-20, Figure 9-21, and Figure 9-22:

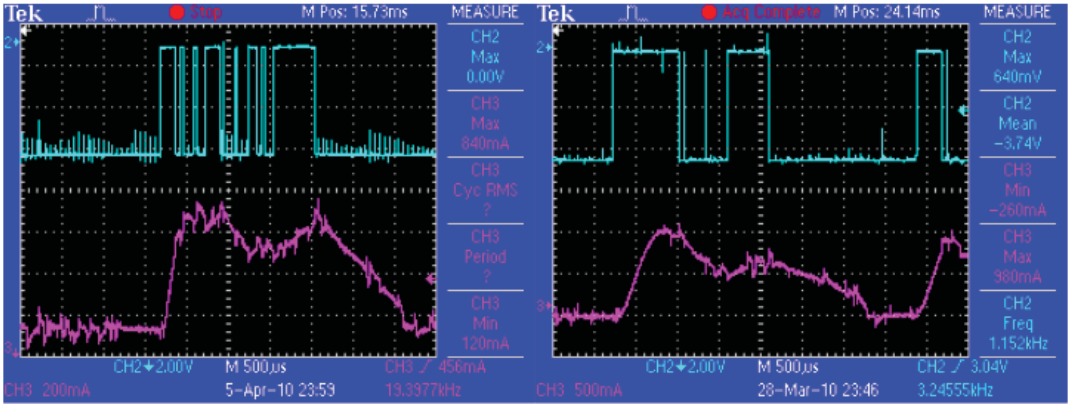

Figure 9-20: Chopping Signal And Phase Current At 2000rpm Unloaded

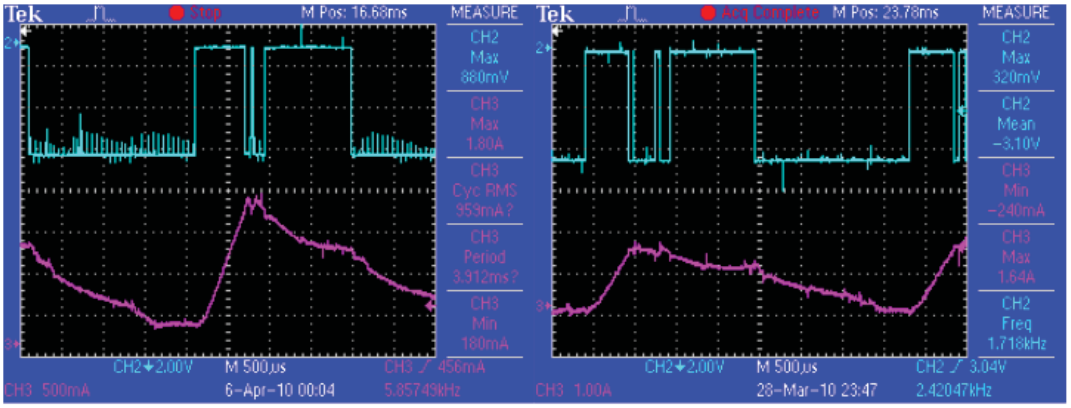

Figure 9-21: Chopping Signal And Phase Current At 2000rpm Lightly Loaded

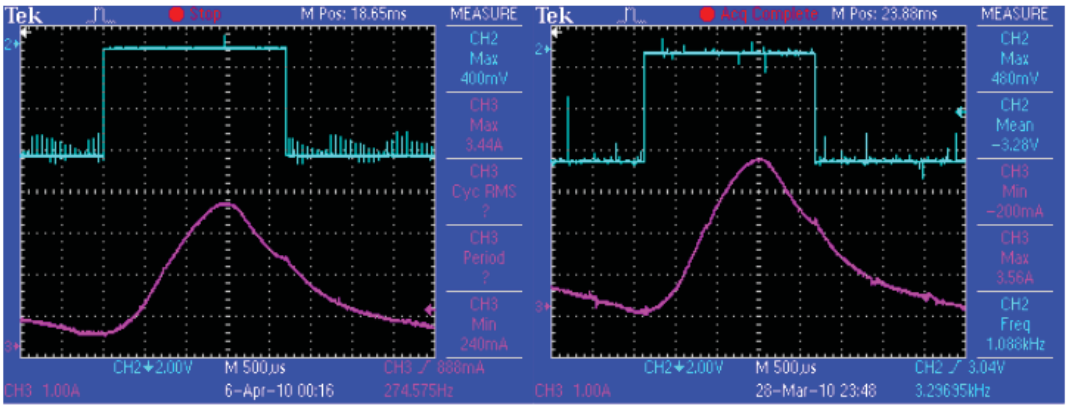

Figure 9-22: Chopping Signal And Phase Current at 2000rpm Heavily Loaded

The original electronic drive waveforms are shown on the left, and the prototype drive waveforms are shown on the right. Figure 9-20 uses a differing current-division scale of 200mA/division for the original drive, and 500mA/division for the prototype drive. Figure 9-21 also uses a differing current-division scale of 500mA/division for the original drive, and 1A/division for the prototype drive.

There is no significant difference between the waveform captures at any loading; therefore, the prototype drive meets the performance of the original drive while operating at 2000rpm.

It can be seen that the phase current is beginning to self-constrain and the dependence on phase voltage control is decreasing. This is apparent when the motor is running unloaded which is strong evidence that the motor is operating well above the base speed ω_b. Under heavy loading the control algorithm is operating in singular pulse control.

The commutation can be seen to have noticeably decreased from approximately 37.5ms, at 100rpm, to approximately 2ms.

9.8.4 3000rpm

The chopping transistor control and phase current waveform captures for unloaded, light loading, and heavy loading at 3000rpm are shown in Figure 9-23, Figure 9-24, and Figure 9-25:

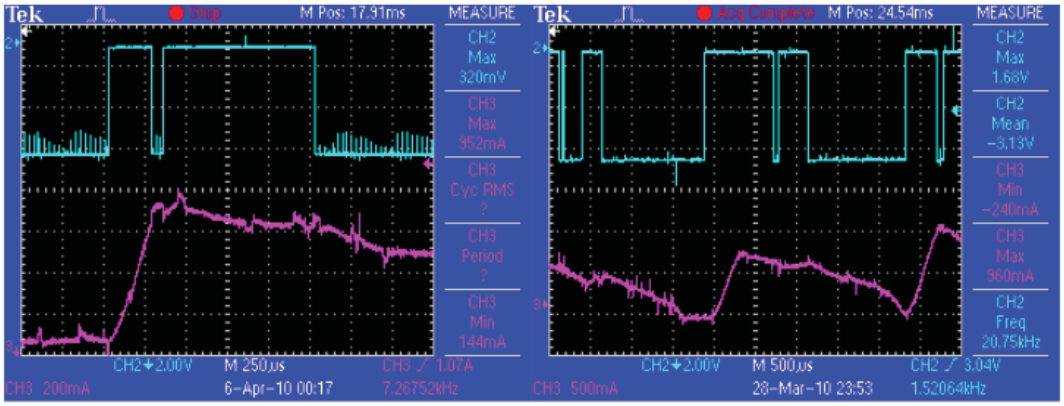

Figure 9-23: Chopping Signal And Phase Current At 3000rpm Unloaded

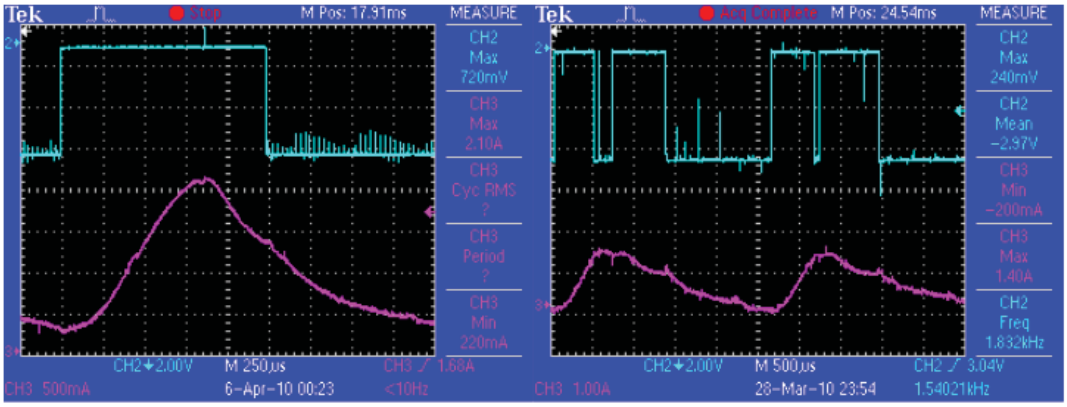

Figure 9-24: Chopping Signal And Phase Current At 3000rpm Lightly Loaded

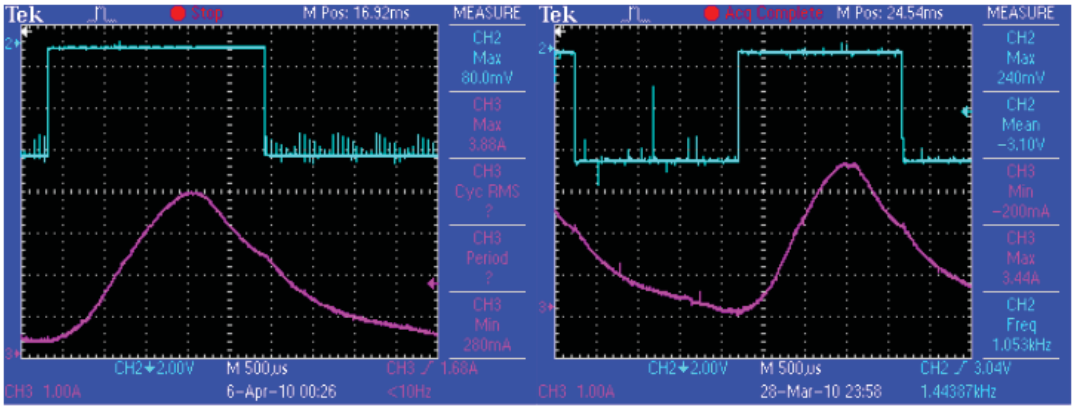

Figure 9-25: Chopping Signal And Phase Current At 3000rpm Heavily Loaded

The original electronic drive waveforms are shown on the left, and the prototype drive waveforms are shown on the right. Figure 9-23 uses a differing current-division scale of 200mA/division for the original drive, and 500mA/division for the prototype drive. Figure 9-23 also uses a differing time-base of 250µS/division for the original drive, and 500µS/division for the prototype drive. Figure 9-24 also uses a differing current-division scale of 500mA/division for the original drive, and 1A/division for the prototype drive. Figure 9-24 also uses differing time-base of 250µS/division for the original drive, and 500µS/division for the prototype drive.

There is no significant difference between the waveform captures at any loading; therefore, the prototype drive meets the performance of the original drive while operating at 3000rpm.

It can be seen that the phase current is more likely to self-constrain and the dependence on phase voltage control is further decreased over 2000rpm. Under heavy loading the control algorithm is operating in singular pulse control.

The commutation can be seen to have noticeably decreased from approximately 37.5ms, at 100rpm, to approximately 2ms.

9.8.5 Full-sweep acceleration

Acceleration of the motor from rest to maximum rotational speed, 3500rpm, with varying load illustrates the ability of the control algorithm to allow the production of positive torque with a continuously increasing shaft speed. This requires the peak of the phase current to be limited while allowing the generation of the highest average torque.

This also highlights the ability of the control algorithm to continuously adapt the frequency of switching the phases sequentially to prevent negative torque generation, and the ability to prevent overshoot of the target shaft speed. Therefore, it is important to show this behaviour in side-by-side comparative analysis between the original and prototype electronic drives. The current and chopping control signal waveform captures for unloaded, light loading, and heavy loading are shown for in Figure 9-26, Figure 9-27, and Figure 9-28:

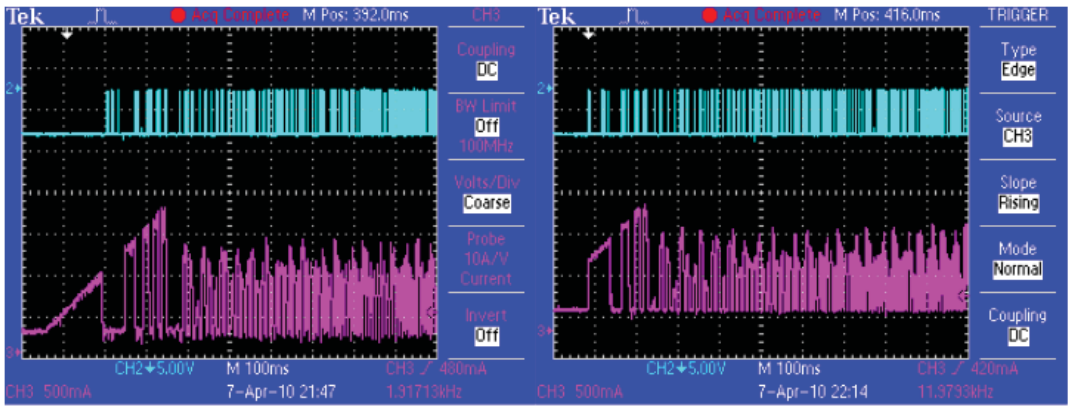

Figure 9-26: Full-sweep Acceleration Comparison Unloaded

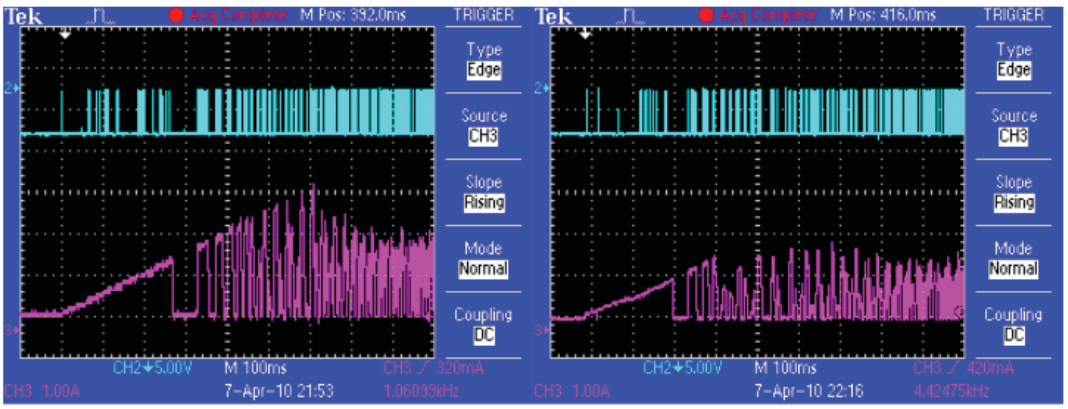

Figure 9-27: Full-sweep Acceleration Comparison Lightly Loaded

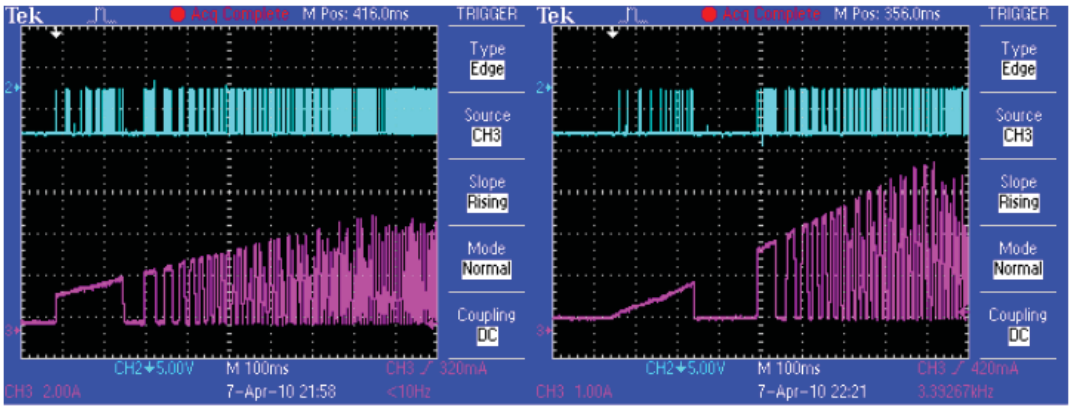

Figure 9-28: Full-sweep Acceleration Comparison Heavily Loaded

The original electronic drive waveforms are shown on the left, and the prototype drive waveforms are shown on the right. Figure 9-28 uses a differing current-division scale of 2A/division for the original drive, and 1A/division for the prototype drive. The control algorithm can be seen to regulate the speed of the motor following the acceleration in all of the captures above.

There is no significant difference present between any of the waveforms, the allowable current is high while the motor is accelerating, but is quickly constrained when the reference speed is reached. The average current then falls into a steady rhythmic pattern indicating the lack of overshoot. This confirms that the prototype electronic drive meets the performance of the original drive and therefore meets the requirements of the research objectives.

9.9 Summary

This chapter reviews the inability to take appropriate measurements from the electronic drive with conventional measurement equipment; specifically illustrating the need for isolation. A circuit is presented which allows measurement of key waveforms from the electronic drive without the need for an isolated oscilloscope. However, this circuit does not allow differential measurements to be taken.

This chapter also presents and discusses the results of a comparative evaluation between the original electronic drive and the prototyped separated electronic drive; this comparative analysis was carried out using an isolated oscilloscope.

The results of this evaluation prove that the prototype drive has no loss of performance when compared to the original solution. Conversely, the prototype displayed superior performance at correcting the power factor in both phase angle difference and purity factor; this may be the result of a faulty original drive and not the general case.

The information presented in this chapter highlights the achievement of a key objective of this research, this being the ability to demonstrate that there is no degradation in performance between the original drive and the prototype separated drive.

Chapter 10

Quality Improvement

"The ability of discerning high quality unavoidably implies the ability of identifying shortcomings“

- Edsger W. Dijkstra

This chapter introduces the various quality observations noted throughout the research. These quality observations are discussed in depth for their merits, and solutions are proposed to improve overall system quality. These observations form possible future development for the electronic drive, and this chapter will discuss the most appropriate combination of the proposed solutions to for improvement. These solutions are determined based upon the electronic drive's specific needs, manufacturing cost, development time, and implementation difficulty.

10.1 Appropriate Isolation of Control Circuitry

The electronic drive is required to achieve two major functional tasks, primarily to provide transformation and conversion of the input power signal to facilitate current flow through the windings of the motor without exceeding the capabilities of the components. Secondly, to continuously adjust that power delivery appropriately through a combination of feedback sensors, and actuators, to provide torque and speed control.

The power aspect of the electronic drive handles high voltage and high current signals; these signals are potentially lethal, and capable of generating large amounts of electrical noise. An example of this is the cyclic variation in the potential of the bridge rectifier return. This is due to the switched nature of the current flowing through the motor windings.

Conversely, the control circuit handles low voltage, and low current signals. The result being that the control circuit is more susceptible to EMI generated by the power supply circuitry.

There is also human interaction with the control circuitry, and it is common practice to isolate the control circuit from the power supply by allowing it to float**.** This floating allows high common mode signal rejection, improving the accuracy of the readings from sensors, and the presence of electrical isolation greatly reduces the chance of electrocution for the user. Therefore it is common industry practice to isolate the control circuit from the power supply.

A cursory glance at the schematic for the DVR SRM electronic drive gives the false impression that the control circuit and the power supply are isolated through the use of the isolated windings of transformer T1. It can also be noted that there are various electrical nets (e.g 0V, 0V_PWR, 0V_IZM) which allows the assumption that these are electrically separate; this is not the case as all negative nets are connected together.

It is important to note that the centre of the winding utilised to generate the control circuit power rails, +5V, +2.5V, is directly connected to 0V_PWR which removes any isolation that would be provided by the transformer T1. This removal of isolation by the transformer in this manner is shown in Figure 10-1, and is highlighted by the red circle:

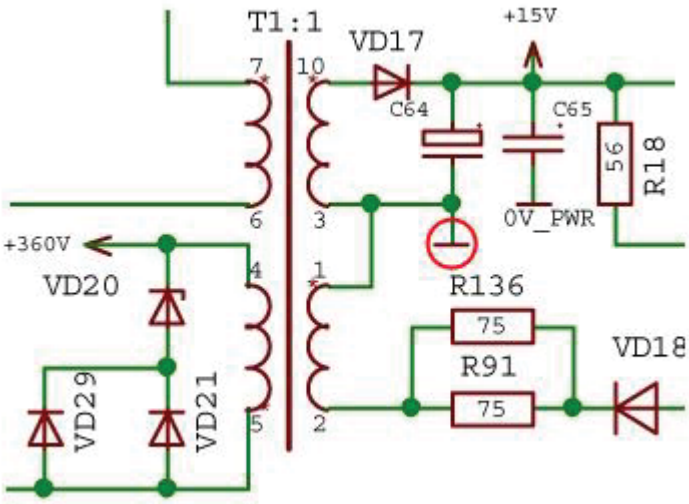

Figure 10-1: Transformer T1 Defeating Control Circuit Isolation

The schematic for the non-isolated control circuit supply rails is shown in Figure 10-2:

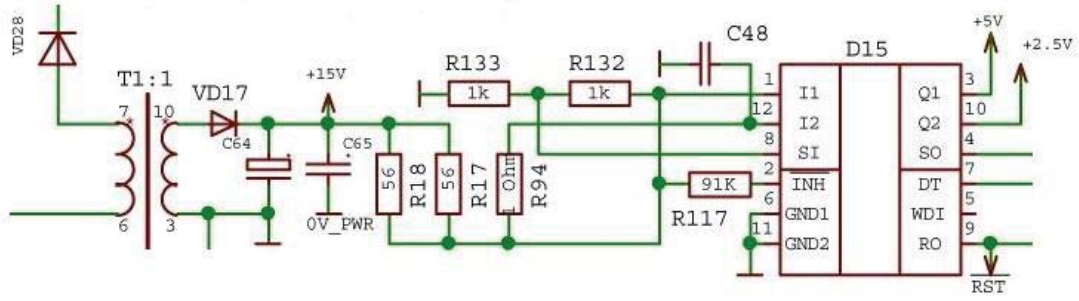

Figure 10-2: +2.5V/+5V Power Supply Schematic

The electronic drive does contain an isolated +5V supply, the nets for this supply being referred to as +5V_INT and +0V_INT respectively. This isolated supply provides power to the interface panel which ensures safe operation for the human user. The schematic for the isolated +5V_INT supply rail is shown in Figure 10-3:

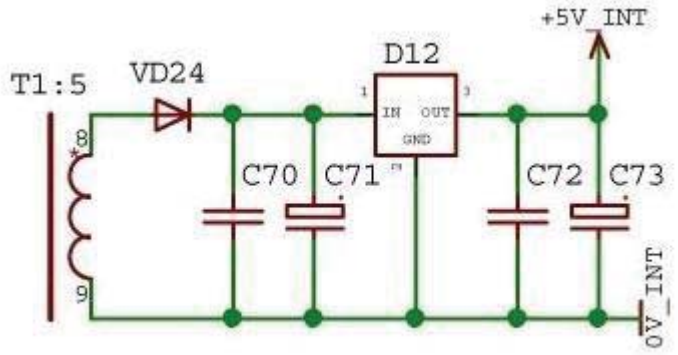

Figure 10-3: +5V_INT Isolated Power Supply Schematic

However, the combination of the non-isolated +5V and isolated +5V_INT causes communication difficulties between these two functionally related circuits, which requires opto-coupling to correct (Refer Appendix D.6 on page 263).

With the aim of providing complete separation between the control circuit and the power supply circuit, the line of isolation should be identical to the separation line. To achieve this, the secondary windings in transformer T1 should be allowed to float, and the duplicated +5V_INT isolated supply can be removed. The interface circuit board can operate from the same power supply rails as the rest of the control circuit. This requires the addition of opto-coupling to the digital communication inputs and outputs present between the power supply and the control circuit board, as well isolated operational amplifiers or hall-effect sensors for measurement of phase currents. The proposed changes to the control circuit board power supply rails schematic are shown in Figure 10-4, and are highlighted by the red circles:

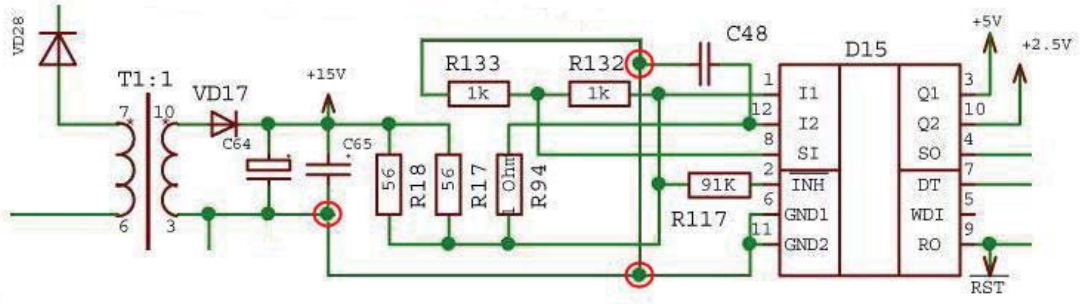

Figure 10-4: Proposed isolation Modification To +2.5V/+5V Power Supply

Achievement of this quality improvement is dependent upon modifying the extant current sensing, which is an implementation of resistive sensing. The required modifications to the phase current measurement are discussed in detail in the following section.

Implementation of this quality improvement allows the integration of the separate interface circuit board resulting in further reduction in complexity of the electronic drive, removal of a duplicated power rail, and removal of a surplus winding from the transformer; this translates into reduced cost and higher product quality.

10.2 Improved Current Sensing

An integral variable in the control of an SRM is the phase current; therefore accurate measurement of this current is of critical importance. The current waveform is beneficial to the control algorithm for several reasons, the primary reason being to detect an over-current condition in one, or many, of the motor phases. Operation of the motor is then ceased to prevent damage to the respective winding; this is also advantageous in displaying relevant error messages for machine diagnostics.

The measurement of current is also used to control the torque output of an SRM. As mentioned in Chapter 6, *Control Algorithms*, the current is continuously measured and the power switching devices are operated as to control the average torque produced by the motor, thereby achieving speed regulation. An accurate current measurement is crucial to extracting the greatest performance. An accurate current measurement can be used to estimate the rotational position of the rotor, thereby removing the need for additional position sensors [62].

There are various methods of measuring the phase current, these being the use of either a very small series resistance, known as *resistive sensing*, or coupling through the use of a hall-effect sensor, known as *inductive sensing*; the benefit of the hall-effect sensor is that it provides isolation by its nature of operation (Refer Appendix D.9 on page 274).

The present implementation of current sensing utilised by the DVR electronic drive is resistive sensing: the flow of current creates a measurable potential difference across the sensing resistance in series with the motor winding. The sensing resistor utilised is a wire hoop which is trimmed to length, and soldered through a plated through-hole on the circuit

board. This approach causes a large variance in the resistance of the sensing components, which skews the calibration of the current sensing between phases.

The schematic of the resistive sensing current approach utilised within the DVR electronic converter is shown in Figure 10-5:

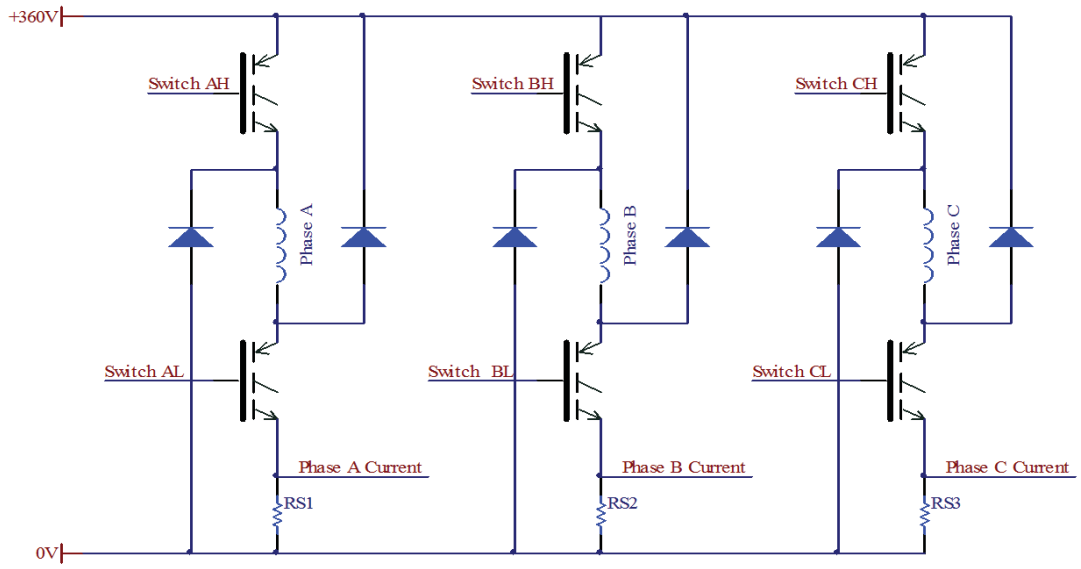

Figure 10-5: Converter Implementing Per-phase Resistive Current Sensing

An improvement to this approach would be the use of commercially available motor sense resistors (Refer Appendix D.7 on page 270). This would ensure accurate and consistent current measurement across all three phases. However, this approach lacks isolation. To allow isolation of the control circuit with this approach would require the use of isolation amplifiers (Refer Appendix D.12 on page 291). The isolation amplifier does not amplify the differential input as the gain is unity; it allows the same amplitude signal to be present relative to a different potential reference on the far side of the isolation barrier. This is the simplest approach to improving the accuracy of the current sensing, as well as providing signal isolation.

The use of a hall-effect sensor would provide extremely accurate and consistent current measurement that is isolated by the nature of the sensor, allowing appropriate isolation of the control circuit; the drawback to this approach is the individual cost of the sensors. A possible sensor is (Refer Appendix D.8 on page 272). A schematic for phase current measurement using inductive sensing is shown in Figure 10-6:

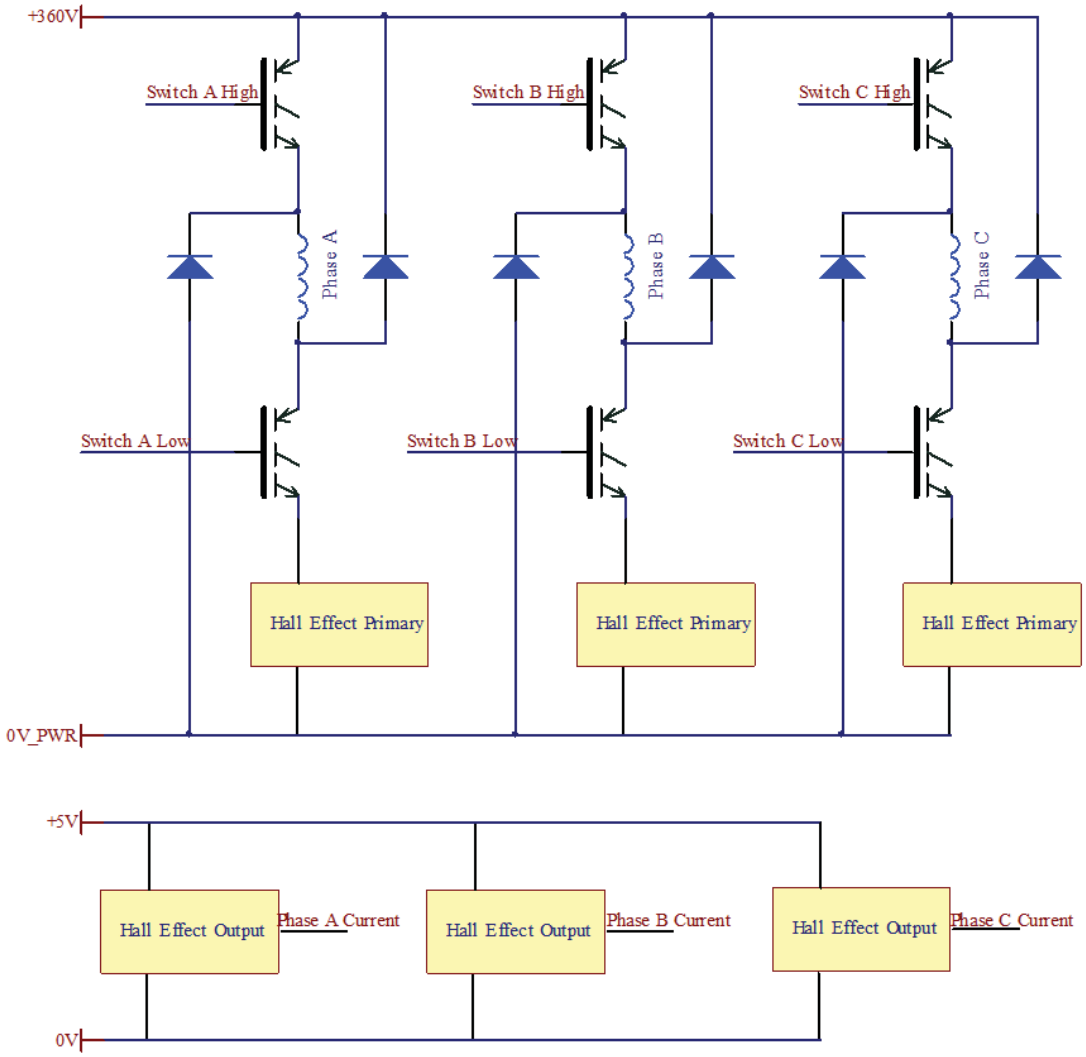

Figure 10-6: Converter Implementing Per-phase Inductive Current Sensing

In an effort to further reduce component count, the individual phase current sensors can be removed and replaced by a single DC Bus current sensor; this technique applies to both resistive sensing and inductive sensing.

Due to the near exclusivity of phase excitation, except for overlap between a phase becoming excited and a phase de-energising, it could be possible to use the envelope of the current waveform in combination with the rotor position sensors to provide an accurate current measurement for all phases. This technique may not scale to position sensor-less operation due to the inability to identify the respective phase for the measured current. This is a viable area for further investigation if position sensor-less operation is not desired. A schematic highlighting both resistive and inductive sensing techniques for a single DC bus current sensor is shown in Figure 10-7:

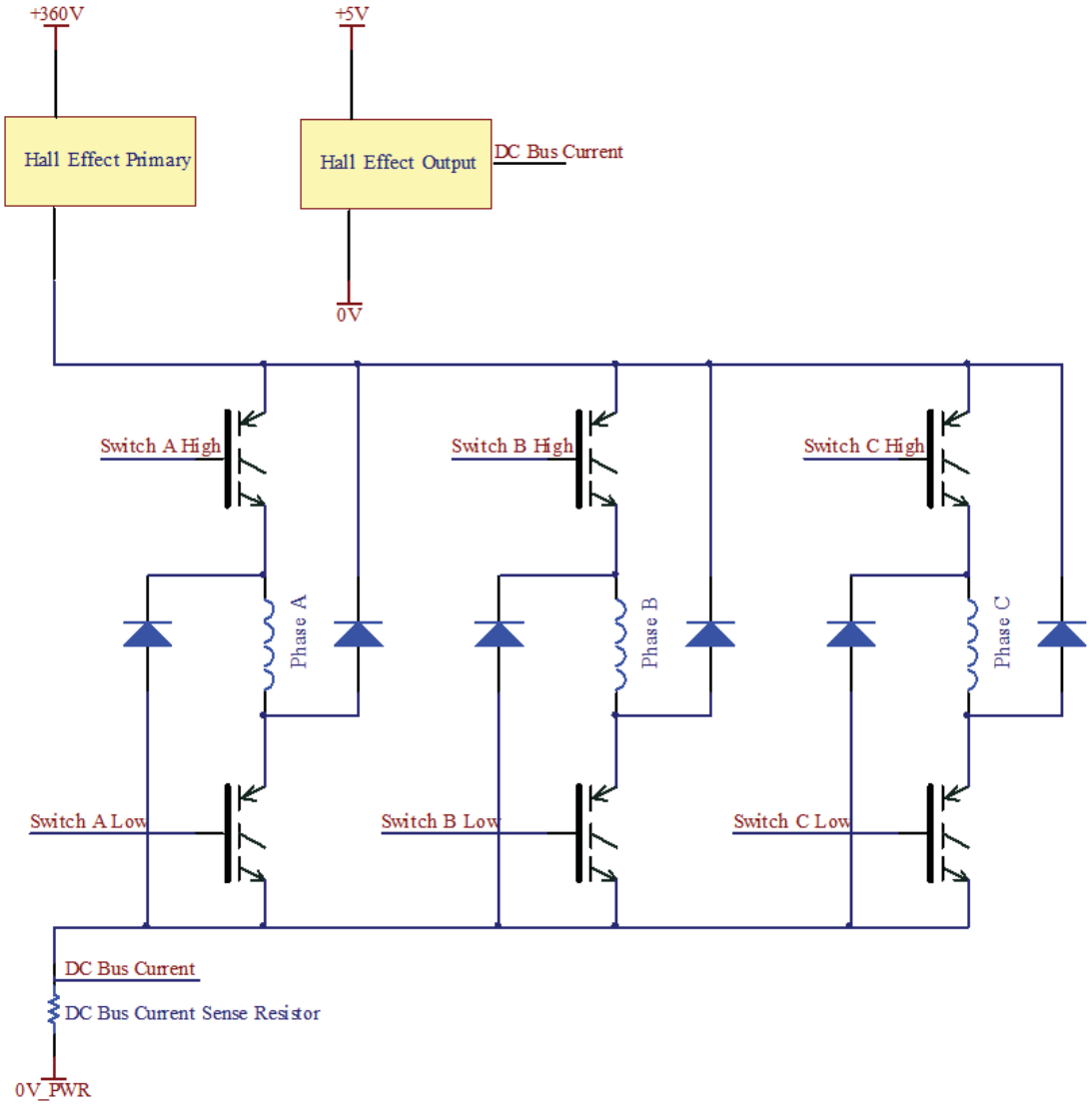

Figure 10-7: Converter Implementing DC bus Inductive And Resistive Current Sensing

This quality improvement promises to reduce the variability in the measurement of current flowing through the phase windings. This will result in a reduction in the variance of the torque produced by each phase and therefore a reduction in torque ripple. It also allows a higher peak torque output by allowing the motor to operate closer to the maximum allowable current flow of the windings.

10.3 -5V Rail Regulation

Capturing power rail waveforms for comparative analysis identified the -5V rail as an area for quality improvement. The power rail exhibited a cyclical square step present in the voltage waveform. The captured waveform is shown in Figure 10-8:

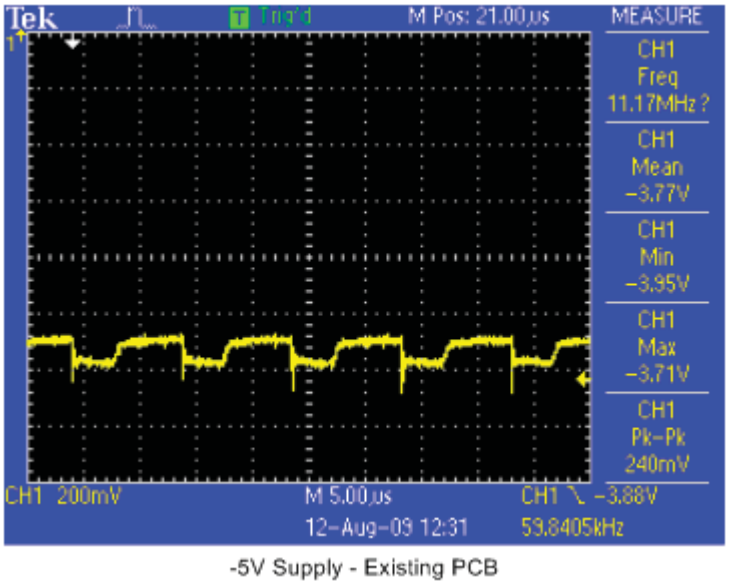

Figure 10-8: -5V Power Rail Capture Showing Cyclical Step

The current flowing through the primary winding of transformer T1 is coupled to the secondary winding and creates a path for the current to flow through. This current flows through capacitor C66 and creates a potential difference between 0V_IZM and the -5V rail; diode VD19 provides reverse polarity protection. The load presented to the -5V is related to the voltage regulation achieved. The schematic for the generation of the -5V rail is shown in Figure 10-9:

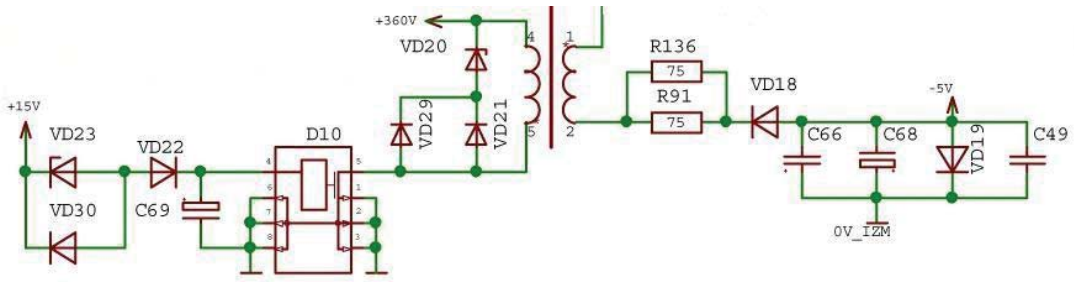

Figure 10-9: -5V Power Supply Schematic

The cyclical step as shown Figure 10-8 is caused by two factors. The first being that the +360V voltage present across the winding of transformer T1 is switched to earth through the TOPS switch D10; this results in a discontinuous voltage being applied to the winding and therefore a cyclical variation in the current. The second is the lack of a voltage regulator present on the output of the -5V rail.

The cyclical square step in the -5V rail could be completely eliminated with the use of a voltage regulator. A linear regulator would be the most appropriate choice due to the high frequency present in the -5V rail. A switching regulator could be utilised effectively if the rate of change of the voltage is reduced. A schematic for the proposed modification is shown in Figure 10-10, and is highlighted by the red square:

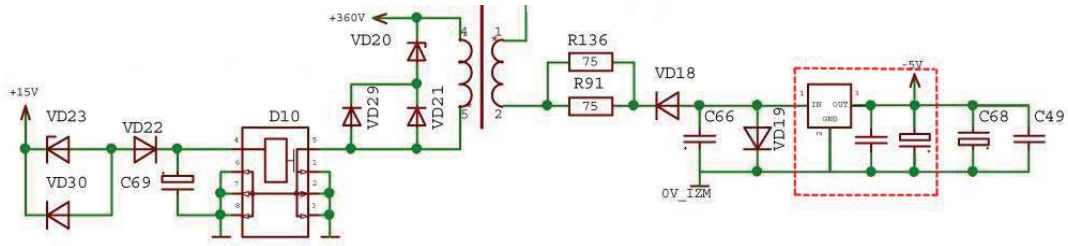

Figure 10-10: Proposed Regulator Modification To -5V Power Supply

This modification requires the inductance of the secondary winding to be increased to create a larger potential difference across the secondary winding; this will increase the magnitude of the negative potential, in reference to 0V_IZM, that capacitor C66 will charge to. The capacitance could also be increased to reduce the rate of voltage change, allowing the use of a switching regulator or reducing the losses of a linear regulator. The voltage stored in capacitor C66 should be of sufficient potential to exceed the sum of the dropout voltage and the rail potential of the voltage regulator. The output capacitors, in parallel with the voltage regulator, are present to improve the voltage regulation of transient voltage inputs such as the cyclical nature of the input to the voltage regulator.

This quality improvement promises to achieve a stable -5V supply rail, with significantly reduced ripple. The regulated output will provide a -5V supply regardless of load allowing changes to the circuit without the need to recalibrate the supply rail.

10.4 Phase Switching Components

The +360V DC Bus rail is switched by IGBT's to conduct current through the phases. They are used in both high and low side driving to allow a uni-polar switching scheme; the datasheet for the IGBT utilised can be found in Appendix D.4 on page 247. The schematic highlighting this arrangement can be seen in Figure 10.5:

The **B**i-polar **J**unction **T**ransistor (BJT) family has traditionally been the only plausible choice as a power transistor in high voltage, high current operation. However BJT transistors require a current signal for biasing, which increases the complexity of the control circuitry. BJT transistors also have a long current tail, and due to their negative temperature co-efficient are liable for thermal-runaway. The lowest on-state voltage drop attainable is voltage between the collector and the emitter while operating in saturation.

In comparison, the **M**etal **O**xide **S**trip **F**ield **E**ffect **T**ransistor (MOSFET) is biased by the voltage present at the gate which alleviates the complexity associated with current-controlled transistors. Thermal-runaway is prevented by the positive temperature co-efficient, and the current tail is very short. The on-state voltage drop is very minimal at low currents in comparison to the BJT transistor and this significantly reduces both the switching and on-state losses. Traditionally the MOSFET could not handle high voltage, and high current waveforms making it a poor choice as a power transistor.

The IGBT is a compromise between the BJT and MOSFET; it behaves as a BJT transistor, but is voltage controlled. The IGBT therefore carries over the inherent disadvantages in the design of the BJT transistor, such as long current tail, significant conductive voltage drop, thermal-runaway due to negative temperature co-efficient. The IGBT transistor was the power transistor of choice due to its exceptionally high current and voltage capabilities, while remaining a voltage-controlled device.

The MOSFET transistor has shown recent advances in the capabilities of high voltage and current handling, while maintaining the positive benefits over the IGBT transistor; particularly notable is the difference in cost. The two transistors can be utilised almost interchangeably with both devices available in the same packages, and being pin compatible. The same floating driving circuitry (Refer Appendix D.3 on page 238) can be utilised to switch either device as they are both voltage-controlled. The IGBT's utilised on

the Teknatool DVR electronic drive can be replaced for pin-compatible N-channel MOSFET's; the schematic showing this modification is shown in Figure 10-11:

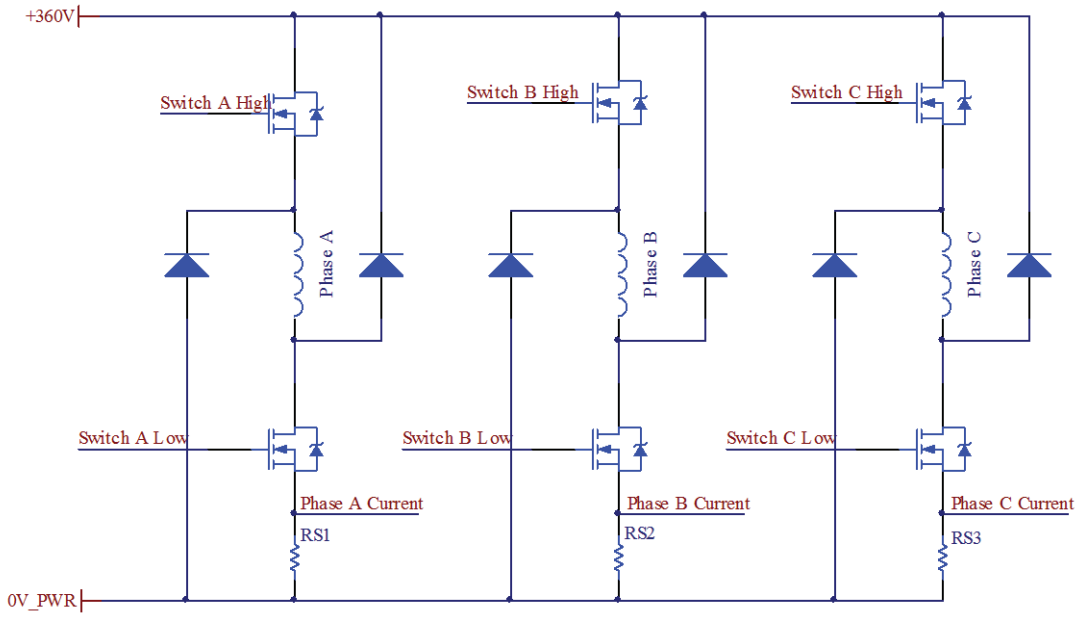

Figure 10-11: Asymmetric half-bridge Converter Implementing MOSFET Transistors

A suitable power N-channel Power MOSFET for this quality improvement is shown in Appendix D.5 on page 257.

This quality improvement promises the following benefits:

- Reduction in manufacturing cost
- Drop-in replacement, no modification to existing circuit board design
- Inclusion of body drain diode helps free-wheel limited currents
- Significant reduction in current tail on switch-off
- Prevention of thermal-runaway due to positive temperature co-efficient
- Improvement in overall circuit efficiency
- Reduction in heat generation of electronic drive
- Increase in life of phase switching transistors

10.5 Integration of circuit boards

This research focused on the electronic drive circuit board and separation of the power and control aspects onto respective individual circuit boards. An extension to this project would be to utilise the free space now available on each of the boards respectively, see Appendix C, Research *Outputs*, to amalgamate the remaining circuit boards.

In Chapter 4, *Power Supply Architecture*, Figure 4.1 shows the functional diagram of a typical SRM power supply. An important aspect of this diagram is the EMI filtering. In the present version of the electronic drive, the EMI filter is present on a separate circuit board. This circuit board can be amalgamated into the newly separated power supply circuit board to physically group all similar function components together.

Similarly, the main control circuit board, and the interface panel are also currently placed on separate circuit boards. These circuit boards can also be amalgamated together to further reduce electronic drive complexity. This amalgamation is logical following the introduction of appropriate isolation as discussed in section 10.1 of this chapter.

This quality improvement improves ease of manufacturing and reduces the number of connections between circuit boards, thereby reducing connectors and cabling.

10.6 Active Braking for Emergency Stop

A quality observation that was noticed initially was the run-down period of the motor following switch-off of the input power. Investigating this run-down period resulted in two major findings. The first being that the energy stored in the +360V DC Bus is not dumped on power switch-off, and the rotational momentum of the spinning rotor is not counteracted upon switch-off.

An initial proposal, to monitor the state of the +360V bus and switch in a dump resistance to bleed the energy from the capacitors, was decided against as this only provides a solution for the torque generation after switch-off, and required the addition of components to the power supply circuit.

An elegant solution is to implement *active braking* to utilise the energy stored in the capacitors to counteract the rotational momentum of the spinning rotor. To achieve this, the phases are excited after the salient rotor pole has passed the position of minimum reluctance; thereby operating in the negative torque generation region. This negative torque opposes the positive torque provided by the rotational momentum; to achieve the most rapid deceleration of the rotor requires the maximum allowable current to flow through the windings.

This quality improvement will result in the motor stopping rapidly upon power switch-off, in the attempt of reducing personal injury as the result of the motor continuing to generate torque after switch-off. There are no extra components required for this improvement as the state of the input power is already sensed.

This improvement does require an addition to the programming of the control algorithm to detect when the motor is rotating and the input power is not present.

10.7 Sensor-less Operation

Sensor-less operation is an area of extensive research in the field of SRMs [63], it proves to reduce manufacturing cost and improve system reliability by eliminating the need for position sensors. This is achieved by calculation of the rotor position from the current waveforms of each phase. Therefore, the term sensor-less operation is somewhat of a misnomer, as there is a heavier dependence upon an accurate current waveform; a more appropriate name would be position sensor-less operation.

Sensor-less operation is technically not a currently viable quality improvement for the Teknatool DVR electronic drive, as this is an area that is currently being researched. However, it does present itself as a possible long-term goal for quality improvement within the electronic drive.

Sensor-less operation allows a significant reduction in the manufacturing cost, and complexity of the electronic drive. This is because all of position sensors, and supporting hardware, can be removed; thereby removing a point of failure from the system. The position sensors have been a common failure within the Tekantool DVR electronic drive,

and removing the dependence of the control algorithm from them would result in a significant increase in product quality.

10.8 Recommendations for improvement

The previous sections of this chapter have discussed the various aspects of the circuit board where quality can be improved, and provided an appropriate solution for the respective observation. For some observations, many solutions were discussed. The focus of this section is to bring these improvements together into a coherent improvement plan that identifies the most appropriate solutions, in the correct order, to facilitate quality improvement of the Teknatool DVR electronic drive.

An ideal starting point for the quality improvement process is to replace the IGBT switching transistors with N-MOSFET equivalents. This is a relatively simple task, as the current IGBT driver circuitry will also operate FET devices with no modifications to the circuit board, and both transistors utilise the same package and are pin-compatible.

Improving the -5V power supply rail by the addition of regulation is another simple task. This requires the additional components, a voltage regulator and capacitors, for the power supply. My recommendation would be to increase the capacitance value of capacitor C66 to facilitate the use of a switching regulator for the highest efficiency. This will provide a stable -5V rail.

At this point, Isolation of the circuit boards is possible, and required to proceed with quality improvement. This task is simplified since the electronic drive has been separated into two circuit boards, therefore diminishing the task of identifying shorts between the two negative references significantly. Isolation can be achieved by removing the connection between 0V_PWR net and the centre tap of transformer T1, and correction of the negative references utilised during the generation of the control circuit power supply rails (+5V,+2.5).

Isolation also requires isolation of the analogue current sensor signals, and the digital communication lines between the power supply and control circuits. Therefore I propose not to remove the existing +5V_INT regulator and transformer winding, but to tie one end of the winding to 0V_PWR and replace the linear regulator with a switching regulator. This

will form the power supply for the isolation barrier components such as the isolation amplifiers, and opto-couplers, which require a reference to both negative nets.

Integration of the EMI filter into the power supply, and integration of the interface panel into the control circuit is now possible. There is sufficient space remaining on each board to facilitate the movement of these components. This will reduce manufacturing cost and group like function components together.

The recommendations so far have not required any modification to the control algorithm. However, the remaining quality improvements require this. Throughout the duration of the research I did not have access to the high-level microcontroller programming, therefore the next logical step in quality improvement is to obtain, or rewrite, the control algorithm. Completion of this allows further modification to the control algorithm and continued quality development.

The ability to modify the microcontroller programming facilitates the integration of the two microprocessors. The interface circuit board operates from a second microcontroller and therefore there is component overhead. Amalgamation of the two microcontrollers together reduces both cost and component count.

Upgrading the current sensing is an important step that requires the ability to adjust the calibration of the current sensor in the control algorithm. My recommendation for the current sensing is to utilise commercially available motor sense resistors for a number of reasons. The first being that the topology is a direct replacement for the current sensing already utilised, as it is also resistive sensing. The second reason is that it requires no modifications to the hardware of the electronic drive to facilitate, only correction in the control algorithm software. The last reason is the increase in phase impedance balance due to the very low variance, component value tolerance, in the motor sense resistors; this minimises torque ripple due to variations in the calibration of the current sensing. I do not recommend utilising a single DC bus current sensor at this time, as it is currently an area of active research, and there is some current waveform information loss when the phase currents overlap and the freewheeling current of the phases is also visible to the sensor.

Modification to the control algorithm allows the implementation of Active Braking by adjusting the firing angle of the phase excitations to the negative torque generation region; this allows the motor to stop rapidly. Implementation of Active Braking is a small addition to the programming of the control algorithm.

As mentioned in Chapter 10.7, Sensor-less operation is a long-term goal, but if successfully implemented would allow further reductions in cost, component overhead, and complexity, while improving system reliability. Therefore it has been placed as the final milestone in the quality improvement of the Teknatool DVR electronic drive.

10.9 Summary

This chapter investigated the quality improvement observations noted throughout the undertaking of this research. Namely concentrating on the ability to improve reliability, performance, and safety while reducing component count and manufacturing cost. The observations covered were:

- Isolation
- Current Sensing
- Regulation
- Switching Components
- Integration for manufacturing
- Active Braking
- Sensor-less position detection

Solutions for improving quality in all of these areas were presented, discussed and assembled into a roadmap for continuous quality development of the electronic drive.

Chapter 11

Conclusion

"If I have seen farther than others, it is because I was standing on the shoulders of giants."

- Sir Isaac Newton

This chapter considers the outcome of the research, and draws conclusions about the success of the research based upon achievement of the key research objectives, and appropriately addressing the problem domain. Finally, the possibilities of future work extending from this research are proposed.

11.1 Research Objectives

Successful completion of this research was attributed to the achievement of seven key objectives outlined in Chapter 1.6, *Research Objectives*. Therefore each of these objectives must be considered for achievement, with supporting justification, before the research can be concluded as a success.

The first objective states the requirement to "Provide intimate knowledge about the specific machine configuration, including motor and electronic topologies". Achievement of this objective can be shown by the detailed information presented in Chapter 6, Teknatool DVR SRM Implementation; this chapter builds upon knowledge presented in Chapter 2, *Operating principles*, Chapter 3, *Motor construction*, Chapter 4, *Power supply and electronic converter*, and Chapter 5, *Control algorithms*; these chapters contain the background information required for the specific implementations to be identified.

The second objective states the requirement of providing "The ability to take measurements of major signals present on the electronic drive". Achievement of this objective is presented in Chapter 9, *Instrumentation and testing,* which highlights the difficulties in obtaining measurements from the electronic drive. The outcome of this objective is the design of an instrumentation circuit that can be connected between the electronic drive and the motor; this circuit provides the ability to capture waveforms using non-isolated measurement equipment.

The third objective states the requirement for the identification of "Justified separation points between functional components of the electronic drive. These points must present the best possible separation based upon safety, circuit operation, and ease of future quality improvement". Achievement of this objective is presented in Chapter 7, *Separation process*, and Chapter 8*, Prototype design and manufacture*; these chapters discuss the process of identifying the separation points in an iterative process, and justifications for the decision of the final points.

The fourth objective states the requirement of "Development of a separated prototype electronic drive that can be demonstrated to operate the specific SRM correctly. The circuit boards will be of manufacturable standard, and be able to directly replace the existing electronics". Achievement of this objective is discussed in Chapter 8, Prototype design and

manufacture, which highlights the design process of the separated prototype electronic drive, and basic assembly testing to ensure operation of the SRM.

The fifth objective states the requirement to "Demonstrate that there is no degradation of performance between the prototype and the original electronic drive; comparative evaluation will be undertaken to achieve this". Achievement of this objective is shown in Chapter 9, *Instrumentation and testing*, which illustrates the validity of the prototype electronic drive performance by comparative analysis with the original electronic drive. The performance of the prototype electronic drive is shown to at meet, at minimum, the performance the supplied original electronic drive. In the case of power factor correction, the prototype electronic drive exhibited superior performance.

The sixth objective states the requirement of "Identification of areas for investigation of quality improvement. The inclusion of these areas will be discussed and justified". Achievement of this objective can be seen in Chapter 10, *Quality improvement*, which lists, prioritises, and discusses in depth, the quality observations recorded throughout the research. Plausible solution(s) are illustrated in response to each quality observation, and justified recommendations collated into a roadmap for improving the quality of the electronic drive design.

The seventh and last objective states the requirement to "Completed documentation of the electronic drive, including complete component and signal listing, connector information, and revised schematics. This thesis is evidence of the achievement of this objective as it provides SRM knowledge from general background through to specific implementations of component topologies present in the DVR SRM. The specific information pertaining to the electronic drive design is illustrated specifically in Chapter 7, *Separation process*, and Chapter 8, *Prototype design and manufacture*; the outcomes of achieving this objective can be found in Appendix C, *Research Outputs*, starting on page 203.

11.2 Research outcome

To consider this research successful, achievement of the research objectives must be met, and appropriate addressing of the problem domain; achievement of the research objectives is shown in Chapter 11.1, *Research objectives*.

The problem domain expressed in Chapter 1.3, *Description of Problem Domain*, states “The problem domain can be expressed as the inability to identify the cause(s) responsible for the lack of quality within the electronic drive. This inability arises from the complexity of the electronic drive architecture; this complexity must be reduced to allow the cause(s) for the lack of quality to be discovered and corrected”.

This can be expressed as two major constituents to be considered: the inability to identify the cause of insufficient quality, the complexity of the electronic drive must be reduced. These considerations need to be addressed before the research can be considered successful.

The complexity of the electronic drive has been reduced by separation into power and control functional components; these components are present on separate circuit boards. This has reduced the complexity of investigating each circuit in detail, and for isolating the cause of failures within each circuit. This has also standardised the necessary connections required between the power and control components should one of the circuits be redesigned.

The inability to identify the cause of insufficient quality was related to the lack of intimate product design knowledge, and the complexity of the electronic drive; both of these complications have been resolved. This thesis provides the intimate product design knowledge, including areas of potential quality improvement, and the design of the separated prototype electronic drive.

These deliverables address the problem domain and bring successful conclusion to this research.

11.3 Future work

The successful result of this research has resulted in the generation of intimate product design knowledge, a quality improvement roadmap, and a separated prototype electronic drive that is proven to operate with at least the same performance of the original electronic drive.

This facilitates into three major projects for future consideration: Manufacturing of the prototype separated electronic drive, detailed quality analysis, and implementation of the quality improvement roadmap. The prospects of these projects will be briefly considered.

Manufacturing of the prototype separated electronic drive is a project which will carry the current prototype solution through to a mass manufacturable solution, and is manufacturing engineering focused; the outcome of this project is the cost-effective manufacture and inclusion of the separated prototype electronic drive in the commercial product.

Detailed quality analysis involves using the intimate system knowledge gained here to find the root cause(s) of the common mode failures shown in Appendix A, *DVR Technical Information*, on page 186, and implementing the necessary solutions to reduce the frequency of electronic drive failure; this project is electronic engineering focused.

Implementation of the quality improvement roadmap involves utilising the quality observations recorded in this thesis and implementing the proposed changes to improve efficiency, performance, and reliability of the DVR SRM as a whole. This project is also electronic engineering focused.

11.4 Concluding remarks

Undertaking this research has been a great experience; the lessons learnt from this project will become an invaluable resource to me in my future career. I have enjoyed the challenge of improving my skills, and knowledge, to the proficiency that a Master's degree demands.

References

[1] L. Byeong-Seok, *et al.*, "Design of a linear switched reluctance machine," *Industry Applications, IEEE Transactions on,* vol. 36, issue. 6, pp. 1571-1580, 2000.

[2] U. S. Deshpande, *et al.*, "High-force density linear switched reluctance machine," *Industry Applications, IEEE Transactions on,* vol. 31, issue. 2, pp. 345-352, 1995.

[3] B. Han-Kyung, *et al.*, "A linear switched reluctance motor: converter and control," in *Industry Applications Conference, 1999. Thirty-Fourth IAS Annual Meeting. Conference Record of the 1999 IEEE*, 1999, pp. 547-554 vol.1.

[4] N. S. Lobo, *et al.*, "Comparison of Linear Switched Reluctance Machines for Vertical Propulsion Application: Analysis, Design, and Experimental Correlation," *Industry Applications, IEEE Transactions on,* vol. 44, issue. 4, pp. 1134-1142, 2008.

[5] M. Ayaz and A. B. Yildiz, "An equivalent circuit model for switched reluctance motor," in *Electrotechnical Conference, 2006. MELECON 2006. IEEE Mediterranean*, 2006, pp. 1182-1185.

[6] N. Vattikuti, *et al.*, "A novel high torque and low weight segmented switched reluctance motor," in *Power Electronics Specialists Conference, 2008. PESC 2008. IEEE*, 2008, pp. 1223-1228.

[7] T. J. E. Miller, *Electronic control of switched reluctance machines*: Oxford, Boston, 2001.

[8] I. Boldea and S. A. Nasar, *Electric Drives*: CRC Press LLC, 1999.

[9] A. Emadi, Ed., *Energy-Efficient Electric Drives* (Electrical And Computer Engineering. New York: Marcel Dekker, 2005, p.^pp. Pages.

[10] A. d. Almeida, *et al.*, *Energy Efficiency Improvements in Electric Motors and Drives*: Springer, 1997.

[11] B. Drury, Ed., *The Control Techniques Drives and Controls Handbook* (Power and Energy Series 57). London: The Institute of Engineering and Technology, 2009, p.^pp. Pages.

[12] J. Reinert and S. Schroder, "Power-factor correction for switched reluctance drives," *Industrial Electronics, IEEE Transactions on,* vol. 49, issue. 1, pp. 54-57, 2002.

[13] J. Reinert, *et al.*, "Optimizing performance in switched reluctance drives," in *Applied Power Electronics Conference and Exposition, 1998. APEC '98. Conference Proceedings 1998., Thirteenth Annual*, 1998, pp. 765-770 vol.2.

[14] L. Xu, *et al.*, "Analysis of a new variable-speed singly salient reluctance motor utilizing only two transistor switches," *Industry Applications, IEEE Transactions on,* vol. 26, issue. 2, pp. 229-236, 1990.

[15] H. C. Lovatt, *et al.*, "Comparative performance of singly salient reluctance, switched reluctance, and induction motors," in *Electrical Machines and Drives, 1997 Eighth International Conference on (Conf. Publ. No. 444)*, 1997, pp. 361-365.

[16] K. Vijayakumar, *et al.*, "Dynamic analysis of Switched Reluctance Motor using Soft Magnetic Composite material," in *Power Electronics, Drives and Energy Systems (PEDES) & 2010 Power India, 2010 Joint International Conference on*, 2010, pp. 1-6.

[17] C. Jae-Hak, *et al.*, "The effectiveness of anisotropic iron-core material on a switched reluctance motor," *Magnetics, IEEE Transactions on,* vol. 39, issue. 5, pp. 3352-3354, 2003.

[18] F. J. Bartos. (1999, 4th April 2009). *'Forward To The Past' with SR Technology* [Article]. Available: www.controleng.com

[19] W. Chi-Yao and C. Pollock, "Analysis and reduction of vibration and acoustic noise in the switched reluctance drive," *Industry Applications, IEEE Transactions on,* vol. 31, issue. 1, pp. 91-98, 1995.

[20] B. K. Bose, *Microcomputer Control of Power Electronics and Drives*: IEEE Press, 1987.
[21] M. Jae-Won*, et al.*, "Reduction of vibration and acoustic noise of SRM with hybrid excitation method," in *Industrial Electronics, 2001. Proceedings. ISIE 2001. IEEE International Symposium on*, 2001, pp. 1407-1412 vol.2.
[22] M. Besbes*, et al.*, "Influence of stator geometry upon vibratory behaviour and electromagnetic performances of switched reluctance motors," *Electric Power Applications, IEE Proceedings -,* vol. 145, issue. 5, pp. 462-468, 1998.
[23] M. Balaji*, et al.*, "Torque ripple minimization in switched reluctance motor drives," in *Power Electronics, Machines and Drives, 2004. (PEMD 2004). Second International Conference on (Conf. Publ. No. 498)*, 2004, pp. 104-107 Vol.1.
[24] S. Jebarani Evangeline and S. Suresh Kumar, "Torque Ripple Minimization of switched reluctance drives - A survey," in *Power Electronics, Machines and Drives (PEMD 2010), 5th IET International Conference on*, 2010, pp. 1-6.
[25] S. A. Long*, et al.*, "Effectiveness of active noise and vibration cancellation for switched reluctance machines operating under alternative control strategies," *Energy Conversion, IEEE Transactions on,* vol. 20, issue. 4, pp. 792-801, 2005.
[26] F. Sahin*, et al.*, "Optimum geometry for torque ripple minimization of switched reluctance motors," *Energy Conversion, IEEE Transactions on,* vol. 15, issue. 1, pp. 30-39, 2000.
[27] M. Sanada*, et al.*, "Novel rotor pole design of switched reluctance motors to reduce the acoustic noise," in *Industry Applications Conference, 2000. Conference Record of the 2000 IEEE*, 2000, pp. 107-113 vol.1.
[28] S. Stansfeld*, et al.*, "Noise and Health in the Urban Environment," *Reviews on Environmental Health,* vol. 15, issue. 1-2, pp. 43-82, 2000/01/01 2000.
[29] M. J. Reilly*, et al.*, "Occupational Noise-Induced Hearing Loss Surveillance in Michigan," *Journal of Occupational and Environmental Medicine,* vol. 40, issue. 8, pp. 667-674, 1998.
[30] H. Hayashi*, et al.*, "Efficiency Comparison of Switched Reluctance Motors with Low Loss Materials," in *Power Engineering Society General Meeting, 2007. IEEE*, 2007, pp. 1-6.
[31] A. Chiba*, et al.*, "Torque Density and Efficiency Improvements of a Switched Reluctance Motor without Rare Earth Material for Hybrid Vehicles," *Industry Applications, IEEE Transactions on,* vol. PP, issue. 99, pp. 1-1, 2011.
[32] F. Sixdenier*, et al.*, "Introducing dynamic behavior of magnetic materials into a model of a switched reluctance motor drive," *Magnetics, IEEE Transactions on,* vol. 42, issue. 3, pp. 398-404, 2006.
[33] T. Zhangjun*, et al.*, "Effects of material properties on switched reluctance motor vibration determination," in *Industry Applications Conference, 2003. 38th IAS Annual Meeting. Conference Record of the*, 2003, pp. 235-241 vol.1.
[34] S. Won*, et al.*, "Novel Rotor Shape of Switched Reluctance Motor for Windage Loss Reduction," in *Magnetics Conference, 2006. INTERMAG 2006. IEEE International*, 2006, pp. 193-193.
[35] L. Jong-Han and L. Eun-Woong, "Comparison of Single Phase SRM Characteristics Considering of the Rotor Type," in *Electric Machines & Drives Conference, 2007. IEMDC '07. IEEE International*, 2007, pp. 1610-1615.
[36] R. Hamdy*, et al.*, "Bidirectional starting of a symmetrical two-phase switched reluctance machine," *Energy Conversion, IEEE Transactions on,* vol. 15, issue. 2, pp. 211-217, 2000.
[37] P. C. Desai*, et al.*, "Novel Switched Reluctance Machine Configuration With Higher Number of Rotor Poles Than Stator Poles: Concept to Implementation," *Industrial Electronics, IEEE Transactions on,* vol. 57, issue. 2, pp. 649-659, 2010.

[38] H. Chen and S. Lu, "Comparison of three-phase 12/8 structure switched reluctance machine and four-phase 16/12 structure switched reluctance machine," in *Power Electronics and Motion Control Conference, 2004. IPEMC 2004. The 4th International*, 2004, pp. 1005-1008 Vol.2.

[39] P. C. Desai*, et al.*, "Switched Reluctance Machines with higher rotor poles than stator poles for improved output torque characteristics," in *Industrial Electronics, 2009. IECON '09. 35th Annual Conference of IEEE*, 2009, pp. 1338-1343.

[40] L. Jian*, et al.*, "Comparison of 12/8 and 6/4 Switched Reluctance Motor: Noise and Vibration Aspects," *Magnetics, IEEE Transactions on,* vol. 44, issue. 11, pp. 4131-4134, 2008.

[41] A. V. Radun, "Design considerations for the switched reluctance motor," *Industry Applications, IEEE Transactions on,* vol. 31, issue. 5, pp. 1079-1087, 1995.

[42] J. M. Jacob, *Advanced AC Electronics: Principles and Applications*. New York: Thomson Delmar Learning, 2004.

[43] T. Wildi, *Electrical Machines, Drives, And Power Systems*, Sixth ed. Upper Saddle River: Pearson Education, 2006.

[44] NJATC, *AC Theory*, Second ed. New York: Delmar Cengage Learning, 2009.

[45] A. R. Hambley, *Electrical Engineering: Principles and Applications*, Fifth ed. Upper Saddle River: Pearson Education, 2011.

[46] S. BASU, "Single Phase Active Power Factor Correction Converters, Methods for Optimizing EMI, Performance and Costs," Doctor of Philosophy PhD, Department of Energy and Environment, Division of Electric Power Engineering, CHALMERS UNIVERSITY OF TECHNOLOGY, Göteborg, 2006.

[47] "Power factor: How it works and what it means for your business," C. Energy, Ed., ed, 2009, p. 2.

[48] M. H. Rashid, *Power Electronics Handbook*, Third ed.: Butterworth-Heinemann, 2011.

[49] C. Yang*, et al.*, "An improved two-switch Buck-boost converter with reduced reverse-recovery losses," in *Energy Conversion Congress and Exposition (ECCE), 2010 IEEE*, 2010, pp. 1959-1964.

[50] Z. Fei*, et al.*, "Single-phase two-switch PCCM buck-boost PFC converter with fast dynamic response for universal input voltage," in *Power Electronics and ECCE Asia (ICPE & ECCE), 2011 IEEE 8th International Conference on*, 2011, pp. 205-209.

[51] J. Liang*, et al.*, "Direct instantaneous torque control of switched reluctance machines using 4-level converters," *Electric Power Applications, IET,* vol. 3, issue. 4, pp. 313-323, 2009.

[52] N. H. Fuengwarodsakul*, et al.*, "Analysis of Torque Dynamics for Switched Reluctance Drives with Instantaneous Torque Control," in *Industry Applications Conference, 2006. 41st IAS Annual Meeting. Conference Record of the 2006 IEEE*, 2006, pp. 2012-2019.

[53] M. Ehsani and B. Fahimi, "Elimination of position sensors in switched reluctance motor drives: state of the art and future trends," *Industrial Electronics, IEEE Transactions on,* vol. 49, issue. 1, pp. 40-47, 2002.

[54] J. J. Gribble*, et al.*, "Optimal commutation in average torque control of switched reluctance motors," *Electric Power Applications, IEE Proceedings -,* vol. 146, issue. 1, pp. 2-10, 1999.

[55] T. Koblara*, et al.*, "A low voltage sensorless Switched Reluctance Motor drive using flux linkage method," in *Optimization of Electrical and Electronic Equipment (OPTIM), 2010 12th International Conference on*, 2010, pp. 665-672.

[56] I. H. Al-Bahadly, "Magnetically based sensorless switched reluctance drive for general purpose applications," *Journal of Applied Physics,* vol. 87, issue. 9, pp. 5956-5958, 2000.

[57] G. Gallegos-Lopez*, et al.*, "A new sensorless method for switched reluctance motor drives," in *Industry Applications Conference, 1997. Thirty-Second IAS Annual Meeting, IAS '97., Conference Record of the 1997 IEEE*, 1997, pp. 564-570 vol.1.

[58] M. Bin-Yen*, et al.*, "Design and implementation of a sensorless switched reluctance drive system," *Aerospace and Electronic Systems, IEEE Transactions on,* vol. 34, issue. 4, pp. 1193-1207, 1998.

[59] N. Radimov*, et al.*, "Inductance measurements in switched reluctance machines," *Magnetics, IEEE Transactions on,* vol. 41, issue. 4, pp. 1296-1299, 2005.

[60] R. Saxena*, et al.*, "Measurement of Flux Linkage and Inductance Profile of SRM," *International Journal of Computer and Electrical Engineering,* vol. 2, issue. 2, pp. 389-393, 2010.

[61] B. Parreira*, et al.*, "Obtaining the magnetic characteristics of an 8/6 switched reluctance machine: from FEM analysis to the experimental tests," *Industrial Electronics, IEEE Transactions on,* vol. 52, issue. 6, pp. 1635-1643, 2005.

[62] B. Fahimi*, et al.*, "Review of sensorless control methods in switched reluctance motor drives," in *Industry Applications Conference, 2000. Conference Record of the 2000 IEEE*, 2000, pp. 1850-1857 vol.3.

[63] I. H. Al-Bahadly, "Examination of a Sensorless Rotor-Position-Measurement Method for Switched Reluctance Drive," *Industrial Electronics, IEEE Transactions on,* vol. 55, issue. 1, pp. 288-295, 2008.

Appendix A

DVR Technical Information

A.1 Fault Information

No.	Serial	Fault Mode	Repairs
1	(94)6967	N/A	OK
2	(94)6969	N/A	Re-soldered
3	(94)6970	N/A	New capacitors, LM2901, Transformer
4	(94)6972	N/A	OK
5	(94)6973	N/A	OK
6	(94)6974	N/A	Re-soldered
7	(94)6975	F1	New P6KE200A
8	(94)6977	N/A	New capacitors, TOP221, Transformer
9	(94)6979	C1	New capacitors, Transformer, Resistor
10	(94)6980	P1	OK
11	(94)6981	F1	New P6KE200A
12	(94)6982	N/A	New Processor
13	(94)6983	P1	New processor, Capacitors
14	(94)6984	P2	OK
15	(94)6985	C2	New Processor, PLM, Capacitors
16	(94)6986	N/A	New transformer
17	(94)6988	N/A	OK
18	(94)6990	F2	New P6KE200A
19	(94)6994	F3	New P6KE200A
20	(94)6995	N/A	New Capacitors
21	(94)6996	F1	New P6KE200A
22	(94)6997	C2	New Processor, PLM, Capacitors
23	(94)6998	F3	OK
24	(94)6999	C2	New Processor, PLM, Capacitors
25	(94)7012	N/A	OK
26	(94)7013	F4	OK
27	(94)7016	C2	New Capacitors, Transformer, Resistor, Thyristor

No.	Serial	Fault Mode	Repairs
28	(94)7071	C2	New Processor, Capacitors, PLM, Resonator
29	(94)7072	N/A	Re-soldered
30	(94)7074	F3	New P6KE200A
31	(94)7076	N/A	New P6KE200A
32	(94)7077	F1	New P6KE200A
33	(94)7078	N/A	New P6KE200A
34	(94)7079	F1	New P6KE200A
35	(94)6987	P1	Re-soldered
36	(94)6976	F5	Re-soldered
37	(94)6978	P2	OK
38	(94)6993	N/A	Re-soldered
39	(94)6971	N/A	New MCP100
40	(94)6963	F6	Film Capacitors was broken
41	(94)6964	F1	Transformer was broken
42	(94)6965	N/A	New Capacitors, TOP221
43	(94)6966	P2	N/A
44	(94)6968	F1	N/A
45	(94)6989	F1	N/A
46	(94)6991	N/A	N/A
47	(94)6992	P2	N/A
48	(94)7000	F7	New Transformer
49	(94)7001	C3	New Transformer
50	(94)7002	N/A	New Transformer
51	(94)7003	N/A	
52	(94)7004	C4	New Transformer
53	(94)7005	N/A	Replace PCB
54	(94)7006	X1	New Transformer
55	(94)7007	N/A	Replace PCB
56	(94)7008	P3	New Transformer
57	(94)7009	N/A	New Transformer

No.	Serial	Fault Mode	Repairs
58	(94)7010	N/A	N/A
59	(94)7011	N/A	New Capacitors
60	(94)7014	N/A	First board for testing
61	(94)7073	F1	N/A
62	(94)7075	P4	New Transformer

Table A-1: Fault Repair Information

Fault Mode	Fault Description	Count
C1	Broken Transformer	
C2	Tantalum Capacitor Burned	
C3	Circuit Board Burnt On Front Right	
C4	Mess 01 Bad Board	
F1	Pilot Lamp Flashing	
F2	Sometimes Goes To Reverse	
F3	Running On It's Own	
F4	Suddenly Slowed While Accelerating	
F5	RPS State Error	
F6	Flashing LCD	
F7	Motor Will Not Start	
P1	Lost Power	
P2	Overload Problem	
P3	No Power	
P4	Current Fault	
X1	Board Damaging In Shipping	

Table A-2: Fault Mode

A.2 Fault Messages

Fault Mode	Fault Description
Not connected	No Communication between Control and Interface PCBs
Unexpected Fault	Wrong error code was received by Interface PCB
SRM Not Rotate	Motor did not start successfully after five attempts
RPS State Error0	All Rotor Position Sensor Signals have the logical ”0” value
RPS State Error1	All Rotor Position Sensor Signals have the logical ”1” value
Low Voltage	DC Bus voltage is less than 300 VDC for two seconds
PFC fault	PFC Fault signal has the active for five seconds
Hardware fault	Hardware problems detected (See note below)
Unexpected Trap	Unexpected software trap

Table A-3: DVR Control LCD Board Fault Messages

Note: The hardware fault is detected in the following conditions:

1. The fault signal from the IGBT driver was detected
2. At least one motor phase current reached critical value (overcurrent protection)
3. Hardware fault in the driver/inverter circuit (i.e a damaged IGBT)
4. An overvoltage condition was detected on the DC bus capacitors

A.3 Motor Parameters

Parameter	Value
Motor Type	Switched Reluctance Motor (DVR)
Motor Phase Number	3
Rotor Pole Number	8
Stator Pole Number	12
Output Power	1.25kW
Power Supply Voltage	115V@60Hz, 230V@50Hz
Motor Speed Range	100 – 5500RPM
Power Factor	≥ 0.95
Temperature Range	0˚C - 70˚C
PWM Frequency	8kHz
PWM Protect Frequency	9kHz
Starting Torque	50% Maximum

Table A-4: DVR SRM Motor Parameters

A.4 Control Board Schematic

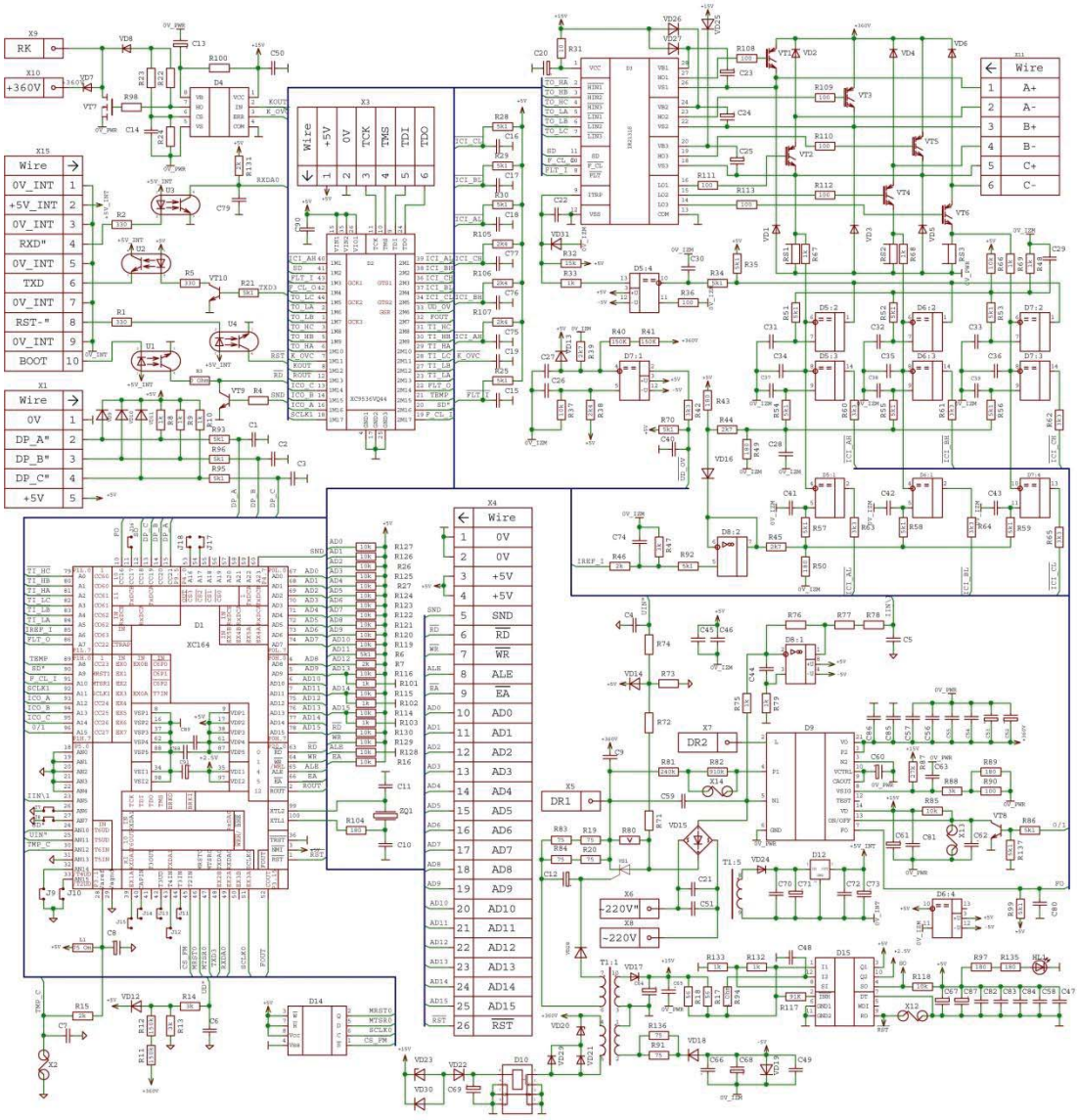

Figure A-1: DVR Control Board Schematic

A larger version of this schematic is available on the supplied CD

A.5 Interface Board Schematic

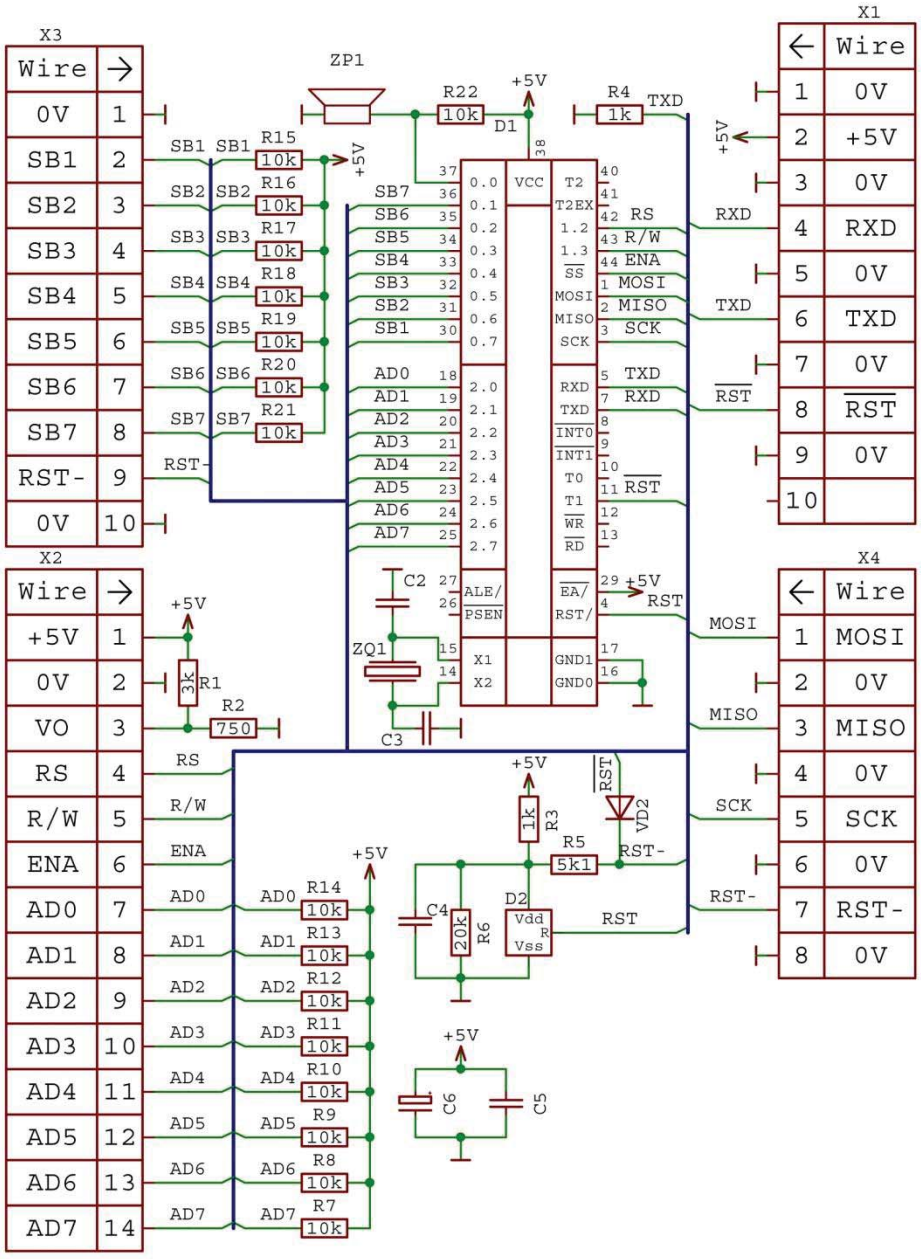

Figure A-2: Interface Board Circuit Schematic

A.6 Rotor Position Sensor Schematic

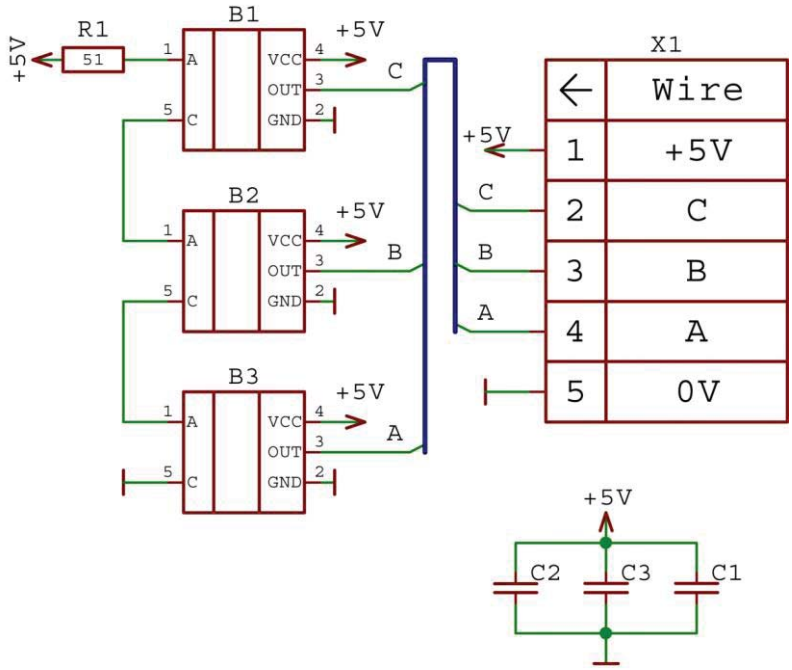

Figure A-3: Rotor Position Circuit Schematic

A.7 EMI Filter

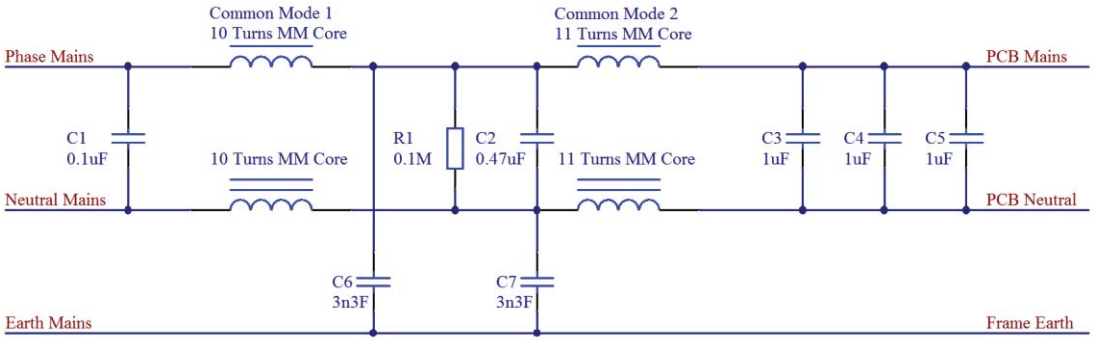

Figure A-4: Mains EMI Filter Schematic

A.8 Control Board Printed Circuit Boards

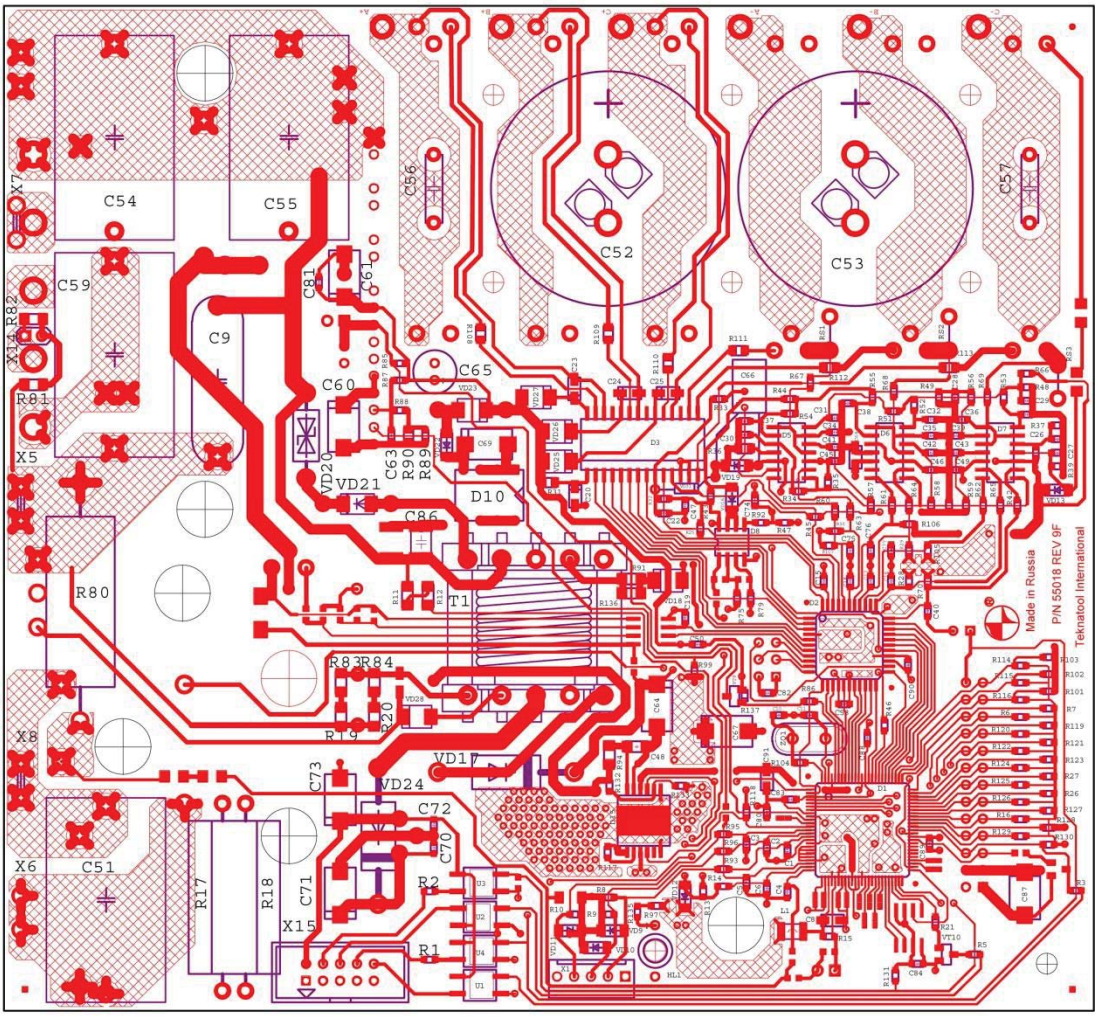

Figure A-5: DVR Control Circuit Board Top Layer

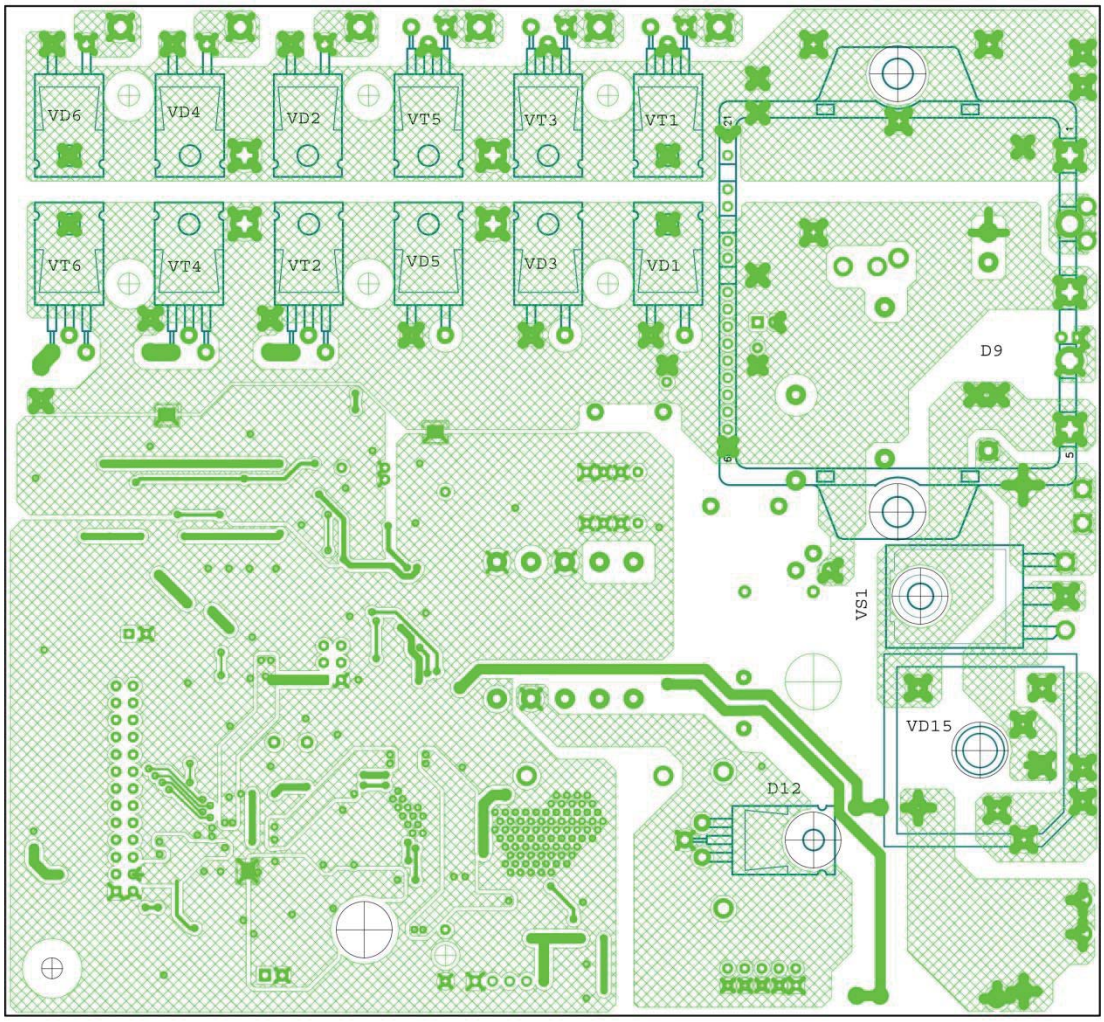

Figure A-6: DVR Control Circuit Board Bottom Layer

A.9 Interface Board PCB

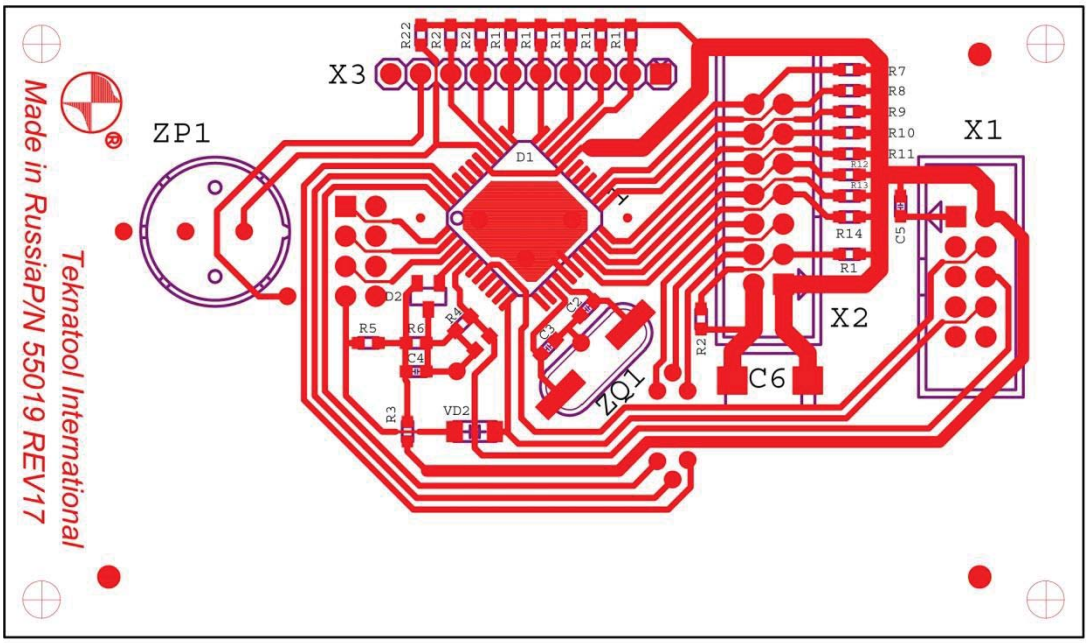

Figure A-7: Interface Panel Circuit Board Top Layer

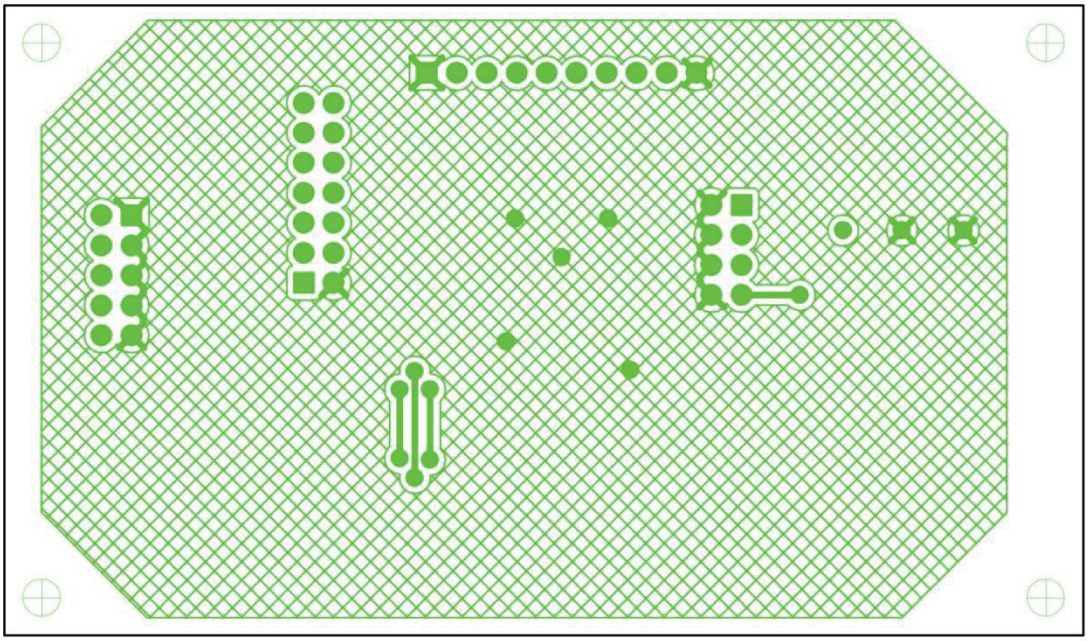

Figure A-8: Interface Panel Circuit Board Bottom Layer

A.10 Rotor Position Sensor PCB

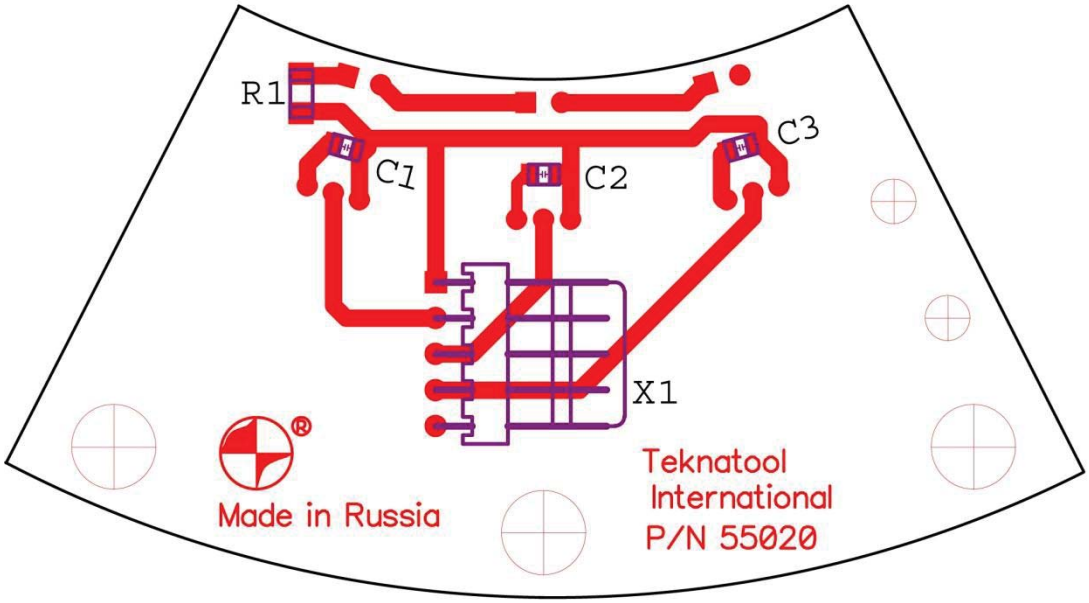

Figure A-9: Rotor Position Sensor Circuit Board Top Layer

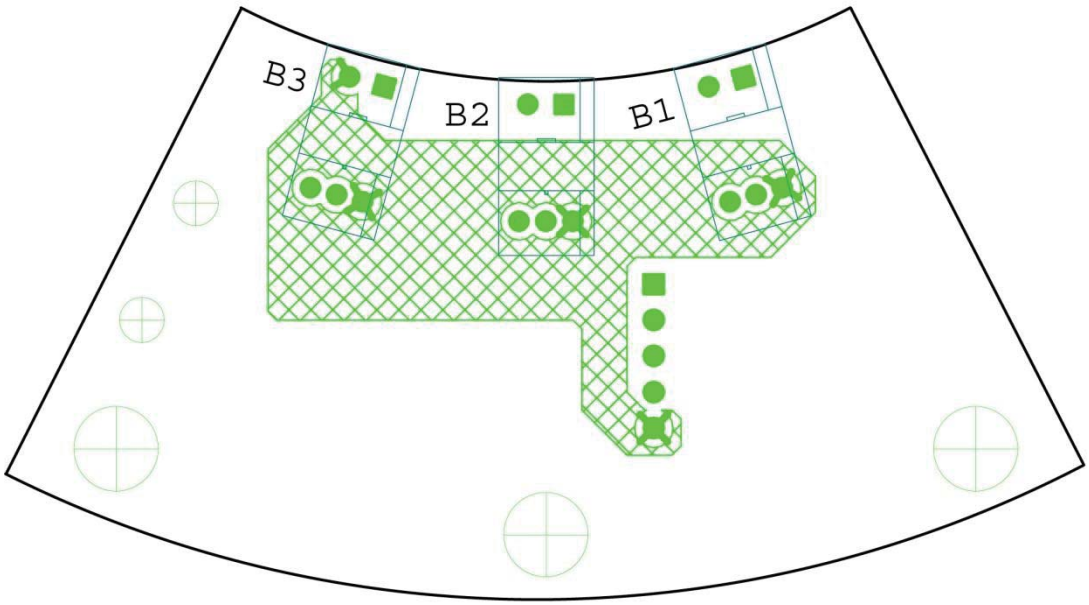

Figure A-10: Rotor Position Sensor Circuit Board Bottom Layer

Appendix B

Measurement Data

B.1 Motor Dimensions

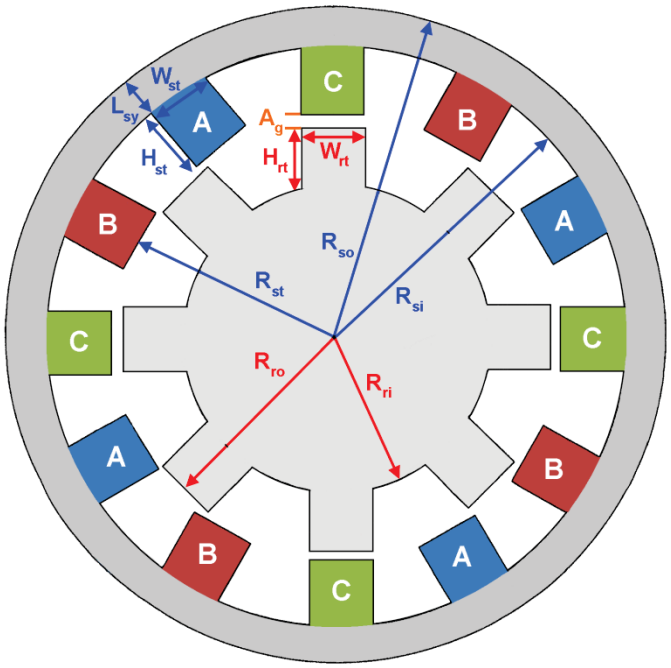

Figure B-1: Motor Dimensions

ID	Description	Dimension (mm)
Lsy	Stator yoke thickness	10
Wst	Stator teeth width	10
Hst	Stator teeth height	25
Rst	Stator teeth radius	40
Rsi	Yoke inner radius	65
Rso	Yoke outer radius	75
Wrt	Rotor teeth width	12.78-13.32 (trapezoidal)
Rri	Rotor inside radius	31.5
Rro	Rotor outer radius	39.65
Hrt	Rotor teeth height	8.2
Ag	Stator rotor air gap	0.35

Table B-1: Motor Dimensions

B.2 Flux-Linkage Characteristics

All values are in Volt-Seconds unless otherwise specified.

	Rotor Misalignment Angle (Degrees)									
Current (A)	**1**	**2.5**	**3.5**	**5.5**	**7**	**7.5**	**12**	**15**	**19.5**	**22.5**
0.48	0.06	0.07	0.08	0.09	0.17	0.17	0.21	0.29	0.34	0.06
1.04	0.11	0.14	0.15	0.15	0.32	0.34	0.36	0.52	0.58	0.15
1.52	0.17	0.21	0.23	0.23	0.48	0.50	0.52	0.77	0.83	0.23
2	0.21	0.28	0.30	0.31	0.62	0.65	0.66	0.98	1.03	0.29
2.48	0.27	0.35	0.38	0.40	0.77	0.79	0.81	1.17	1.20	0.37
3.04	0.34	0.45	0.47	0.48	0.91	0.93	0.95	1.27	1.30	0.46
3.52	0.41	0.53	0.54	0.56	1.00	1.02	1.04	1.31	1.34	0.54
4	0.47	0.60	0.62	0.63	1.06	1.09	1.12	1.34	1.36	0.60
4.48	0.54	0.67	0.69	0.71	1.13	1.15	1.18	1.37	1.40	0.68
5.04	0.60	0.76	0.78	0.78	1.20	1.22	1.23	1.40	1.41	0.79
5.52	0.66	0.83	0.85	0.86	1.26	1.28	1.29	1.41	1.42	0.86

Table B-2: Phase Flux-Linkage Characteristics

B.3 Inductance Characteristics

All values are in Henry's unless otherwise specified.

	Rotor Misalignment Angle (Degrees)					
Current (A)	**1**	**2.5**	**3.5**	**7.5**	**15**	**22.5**
0.48	0.13	0.15	0.17	0.36	0.61	0.71
1.04	0.10	0.13	0.15	0.33	0.50	0.56
1.52	0.11	0.14	0.15	0.33	0.51	0.55
2	0.10	0.14	0.15	0.32	0.49	0.51
2.48	0.11	0.14	0.15	0.32	0.47	0.48
3.04	0.11	0.15	0.16	0.31	0.42	0.43
3.52	0.12	0.15	0.15	0.29	0.37	0.38
4	0.12	0.15	0.15	0.27	0.33	0.34
4.48	0.12	0.15	0.15	0.26	0.31	0.31
5.04	0.12	0.15	0.15	0.24	0.28	0.28
5.52	0.12	0.15	0.15	0.23	0.25	0.26

Table B-3: Phase Inductance Characteristics

B.4 Torque-Power-Speed

Speed (RPM)	Loading	Voltage (V)	Power (W)
150	22.0	16.4	345.40
250	22.0	16.7	575.67
350	21.7	19.4	794.94
450	21.3	19.4	1003.23
500	19.6	19.6	1025.73
600	17.3	19.6	1086.44
700	15.6	19.5	1142.96
800	14.1	19.3	1180.64
920	12.2	17.8	1174.78
1050	9.9	15.7	1088.01
1200	8.0	13.6	1004.80
1300	7.0	12.5	952.47
1430	5.9	11.2	883.07
1600	4.7	10.0	787.09
1850	3.7	8.6	716.44
2000	3.3	8.1	690.80
2150	2.8	7.2	630.09
2370	2.3	6.7	570.53
2500	1.9	6.3	497.17
2700	1.5	5.9	423.90
3000	1.2	5.5	376.80
3500	0.70	-	256.43
4000	0.54	-	226.08
5000	0.40	-	209.33

Table B-4: DVR Torque - Power - Speed Results

B.5 Power Factor (Prototype)

Speed (RPM)	Loading	Voltage (V)	Current (A)	True Power (W)	Reactive Power (VAr)	Apparent Power (VA)	Power Factor
0	None	246	0.388	23.9	-j92.7	95.9	-j0.26
100	None	242	0.410	24.4	-j96.4	99.4	-j0.25
100	Light	242	0.523	56.8	-j113	126	-j0.45
100	Heavy	245	0.741	88	-j159	182	-j0.48
500	None	245	0.390	23.4	-j92.8	95.7	-j0.24
500	Light	245	1.260	169	-j257	308	-j0.55
500	Heavy	245	3.530	435	-j715	836	-j0.52
1000	None	245	0.484	44.7	-j110	119	-j0.38
1000	Light	244	1.120	194	-j192	273	-j0.71
1000	Heavy	235	3.280	724	-j265	771	-j0.94
1500	None	245	0.624	80.1	-j136	157	-j0.50
1500	Light	244	1.490	317	-j180	364	-j0.87
1500	Heavy	234	4.470	1010	-j261	1050	-j0.97
2000	None	245	0.709	96.2	-j145	174	-j0.55
2000	Light	244	1.440	300	-j184	352	-j0.85
2000	Heavy	234	4.510	1020	-j278	1050	-j0.96
2500	None	245	0.774	126	-j142	190	-j0.66
2500	Light	234	2.770	613	-j214	649	-j0.94
2500	Heavy	235	4.430	1000	-j279	1040	-j0.96
3000	None	245	0.903	165	-j146	221	-j0.75
3000	Light	234	2.570	569	-j197	602	-j0.95
3000	Heavy	235	5.090	1115	-j426	1190	-j0.96
3500	None	244	1.010	198	-j149	248	-j0.80
3500	Light	235	2.400	532	-j192	565	-j0.94
3500	Heavy	235	4.690	1070	-j265	1100	-j0.97

Table B-5: Power Factor Measurements (PFC On)

Speed (RPM)	Loading	Voltage (V)	Current (A)	True Power (W)	Reactive Power (VAr)	Apparent Power (VA)	Power Factor
0	None	247	0.388	23.9	-j92.7	95.9	-j0.26
100	None	247	0.410	24.4	-j96.4	99.4	-j0.25
100	Light	246	0.523	56.8	-j113	126	-j0.45
100	Heavy	236	0.741	88	-j159	182	-j0.48
500	None	247	0.390	23.4	-j92.8	95.7	-j0.24
500	Light	247	1.260	169	-j257	308	-j0.55
500	Heavy	239	3.530	435	-j715	836	-j0.52
1000	None	245	0.484	44.7	-j110	119	-j0.38
1000	Light	245	1.120	194	-j192	273	-j0.71
1000	Heavy	244	3.280	724	-j265	771	-j0.94
1500	None	245	0.624	80.1	-j136	157	-j0.50
1500	Light	236	1.490	317	-j180	364	-j0.87
1500	Heavy	234	4.470	1010	-j261	1050	-j0.97
2000	None	245	0.709	96.2	-j145	174	-j0.55
2000	Light	236	1.440	300	-j184	352	-j0.85
2000	Heavy	234	4.510	1020	-j278	1050	-j0.96
2500	None	245	0.774	126	-j142	190	-j0.66
2500	Light	236	2.770	613	-j214	649	-j0.94
2500	Heavy	234	4.430	1000	-j279	1040	-j0.96
3000	None	245	0.903	165	-j146	221	-j0.75
3000	Light	235	2.570	569	-j197	602	-j0.95
3000	Heavy	235	5.090	1115	-j426	1190	-j0.96
3500	None	245	1.010	198	-j149	248	-j0.80
3500	Light	235	2.400	532	-j192	565	-j0.94
3500	Heavy	234	2.400	532	-j192	565	-j0.94

Table B-6: Power Factor Measurements (PFC Off)

B.6 Power Factor (Original)

Speed (RPM)	Loading	Voltage (V)	Current (A)	True Power (W)	Reactive Power (VAr)	Apparent Power (VA)	Power Factor
0	None	244	0.334	14.0	-j80.2	81.5	-j0.15
100	None	244	0.375	15.5	-j90.0	91.3	-j0.17
100	Light	243	0.422	35.0	-j96.6	103	-j0.34
100	Heavy	239	0.613	64.7	-j134	149	-j0.43
500	None	245	0.361	23.8	-j85.1	88.4	-j0.27
500	Light	245	0.990	129	-j205	242	-j0.53
500	Heavy	237	4.50	471	-j985	1090	-j0.43
1000	None	246	0.435	32.9	-j101	106	-j0.31
1000	Light	244	1.42	213	-j274	347	-j0.61
1000	Heavy	243	4.20	701	-j737	1020	-j0.69
1500	None	246	5.01	54.1	-j111	123	-j0.44
1500	Light	244	2.65	429	-j483	646	-j0.66
1500	Heavy	243	6.03	1050	-j1020	1470	-j0.72
2000	None	246	0.591	73.4	-j136	156	-j0.48
2000	Light	244	3.66	605	-j654	891	-j0.68
2000	Heavy	243	5.98	1040	-j1020	1450	-j0.71
2500	None	244	0.771	101	-j159	188	-j0.54
2500	Light	242	3.22	527	-j574	779	-j0.68
2500	Heavy	241	5.72	978	-j968	1380	-j0.71
3000	None	244	1.01	142	-j200	245	-j0.58
3000	Light	243	3.05	500	-j547	741	-j0.67
3000	Heavy	241	6.70	1170	-j1110	1610	-j0.73
3500	None	244	1.09	157	-j217	267	-j0.59
3500	Light	243	3.21	526	-j576	780	-j0.67
3500	Heavy	240	6.49	1140	-j1070	1560	-j0.73

Table B-7: Power Factor Measurement (PFC On)

Speed (RPM)	Loading	Voltage (V)	Current (A)	True Power (W)	Reactive Power (VAr)	Apparent Power (VA)	Power Factor
0	None	238	0.342	13.6	-j80.2	81.5	-j0.15
100	None	237	0.385	15.5	-j90.0	91.3	-j0.17
100	Light	237	0.435	35.0	-j96.6	103	-j0.34
100	Heavy	236	0.631	64.7	-j134	149	-j0.43
500	None	237	0.373	23.8	-j85.1	88.4	-j0.27
500	Light	236	1.03	129	-j205	242	-j0.53
500	Heavy	235	5.94	632	-j1240	1390	-j0.45
1000	None	238	1.46	213	-j274	347	-j0.61
1000	Light	237	4.30	701	-j737	1020	-j0.69
1000	Heavy	236	6.13	1030	-j1010	1440	-j0.71
1500	None	238	0.517	54.1	-j111	123	-j0.44
1500	Light	236	2.16	337	-j383	510	-j0.66
1500	Heavy	234	6.11	1030	-j995	1430	-j0.72
2000	None	237	0.607	73.4	-j136	156	-j0.48
2000	Light	236	2.63	422	-j455	621	-j0.68
2000	Heavy	234	6.09	1020	-j1010	1430	-j0.71
2500	None	238	0.790	101	-j159	188	-j0.54
2500	Light	236	2.49	400	-j431	588	-j0.68
2500	Heavy	234	4.71	782	-j778	1100	-j0.71
3000	None	237	1.03	142	-j200	245	-j0.58
3000	Light	235	2.69	433	-j457	630	-j0.69
3000	Heavy	235	4.69	779	-j778	1100	-j0.71
3500	None	237	1.12	157	-j217	267	-j0.59
3500	Light	235	2.45	396	-j420	577	-j0.69
3500	Heavy	234	5.76	960	-j941	1340	-j0.71

Table B-8: Power Factor Measurement (PFC Off)

Appendix C

Research Outputs

C.1 Electronic Drive Functional Components

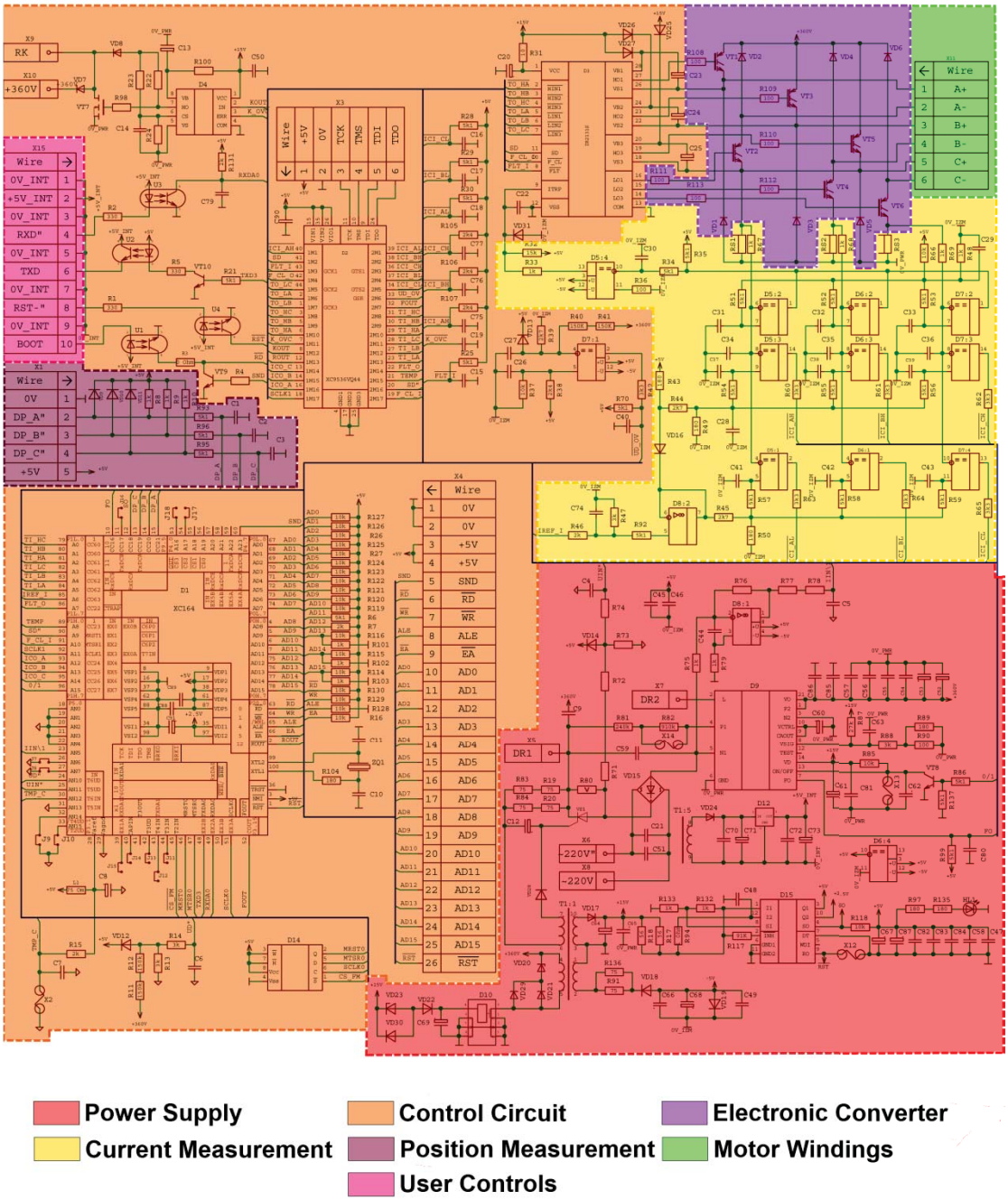

Figure C-1: Major Component Areas Within DVR Electronic Drive

C.2 Ideal Separation Points

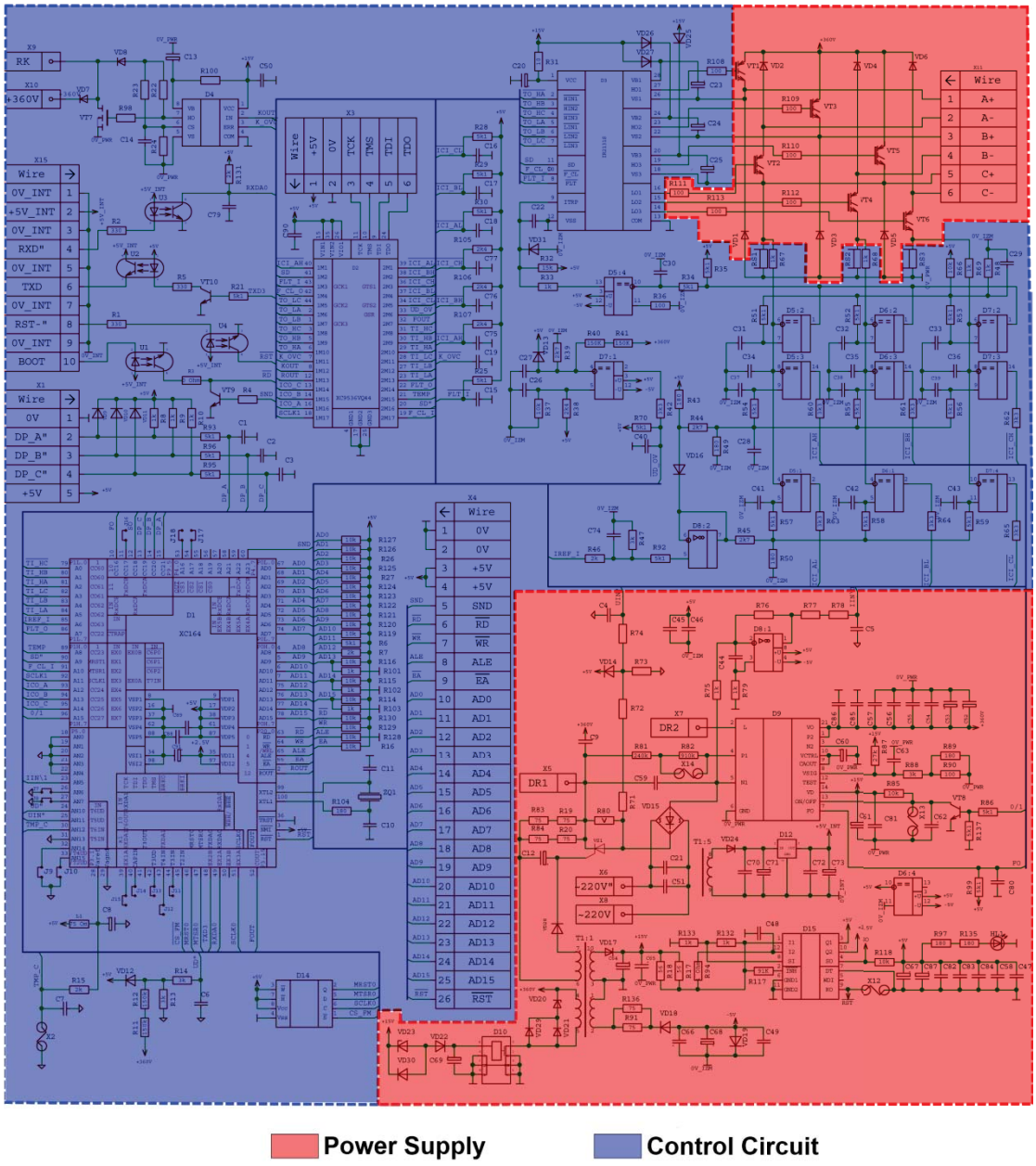

Figure C-2: Idealised Separation Points Within DVR Electronic Drive

C.3 Gray-Area Revised Separation Points

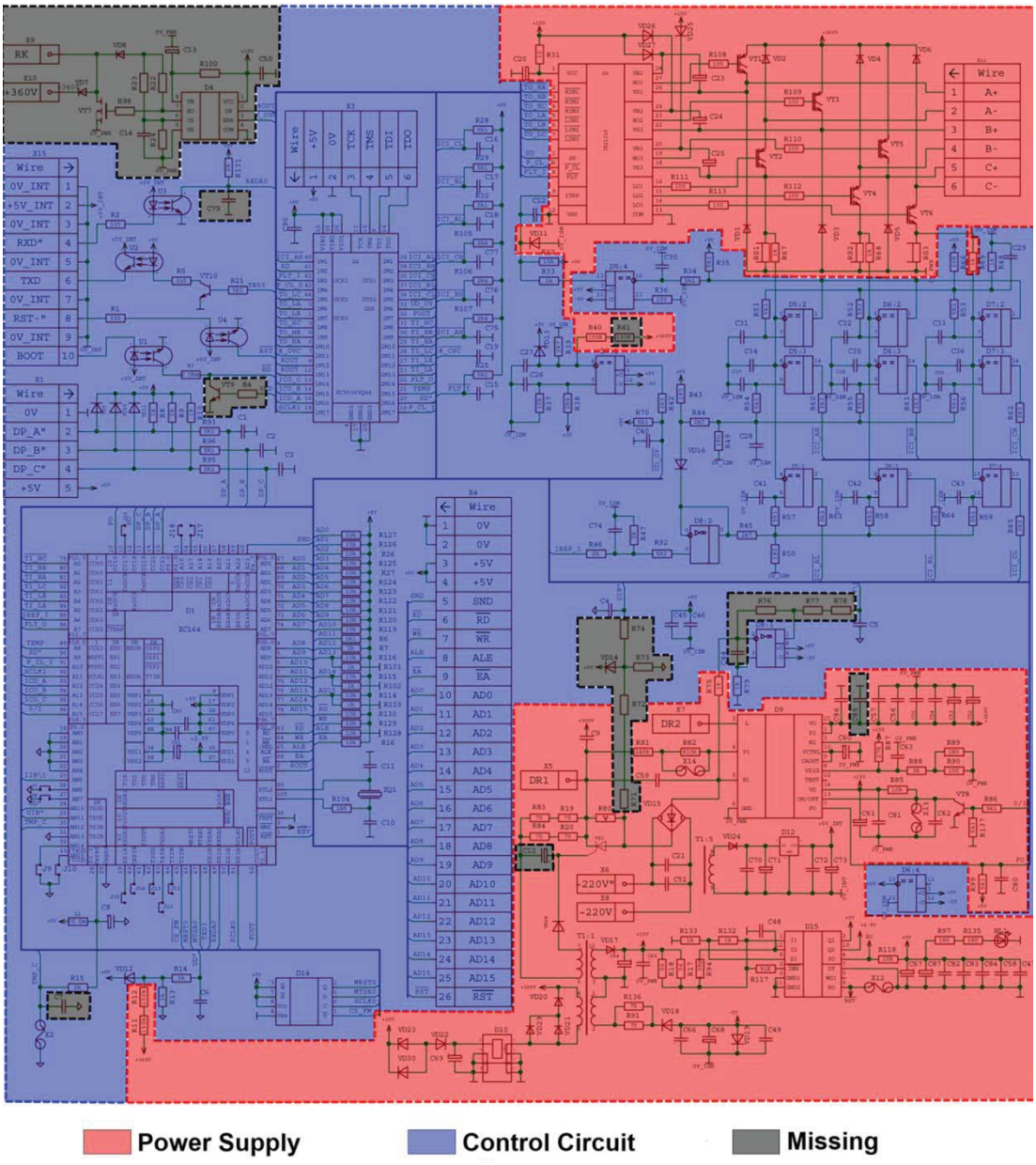

Figure C-3: Identification Of Groupings And Separation Points Following Deep Analysis

C.4 Initial Separation Line

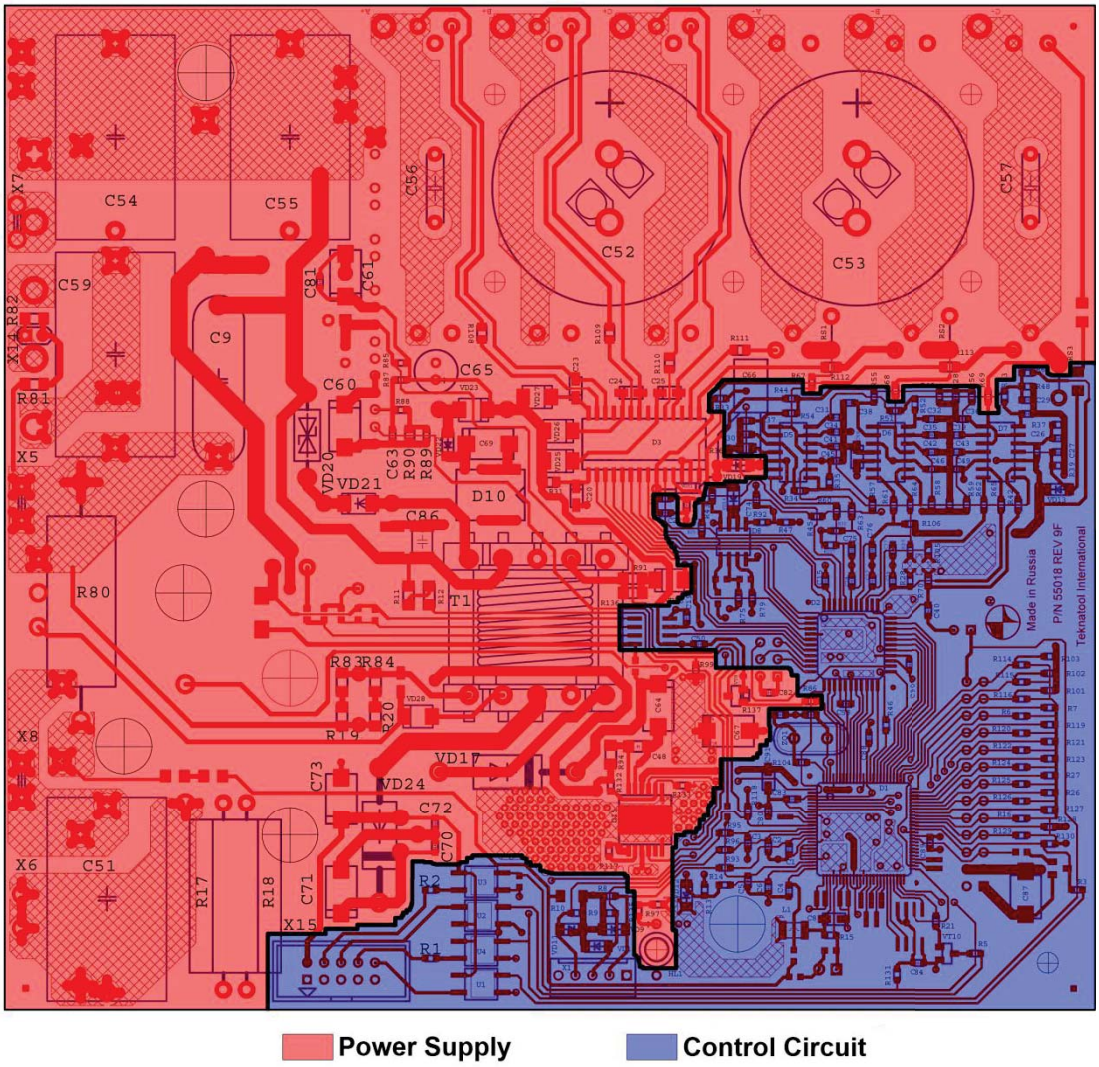

Figure C-4: Separation line Plotted From Proposed Separation Points

C.5 Proposed Separation Points

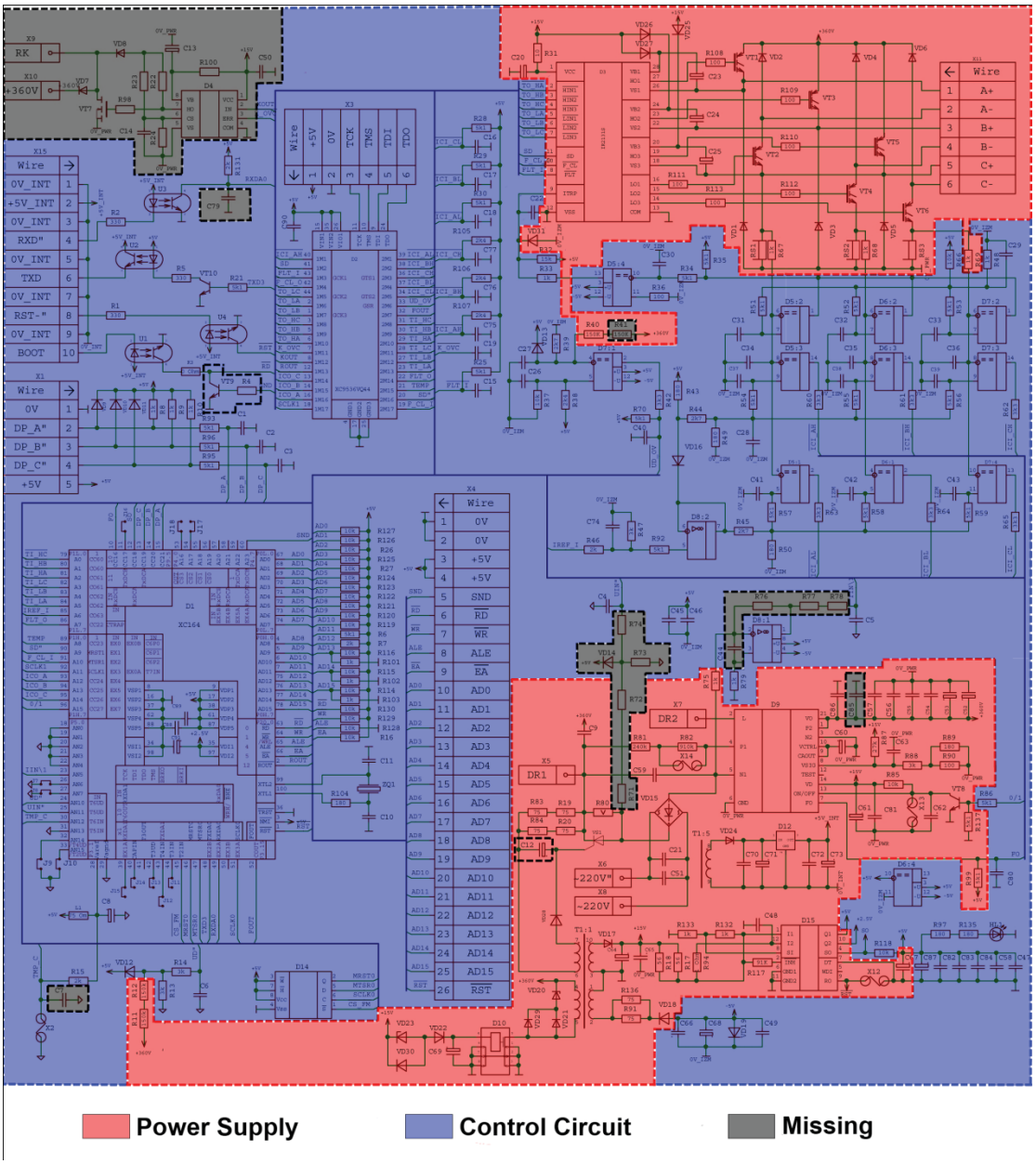

Figure C-5: Identification Of Proposed Separation Points Within DVR Electronic Drive

C.6 Proposed Separation Line

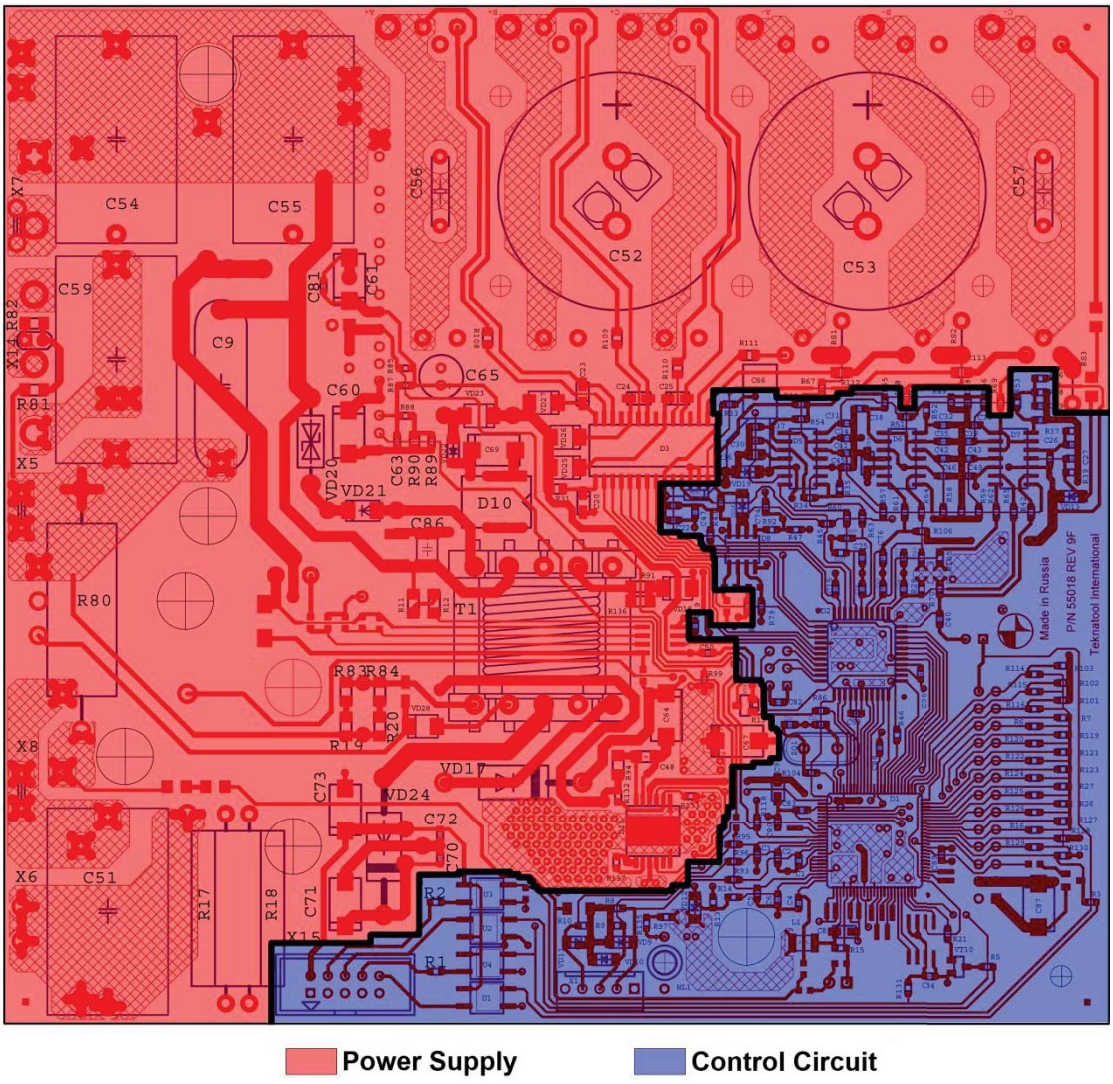

Figure C-6: Separation Line Plotted From Proposed Separation Points

C.7 Final Separation Points

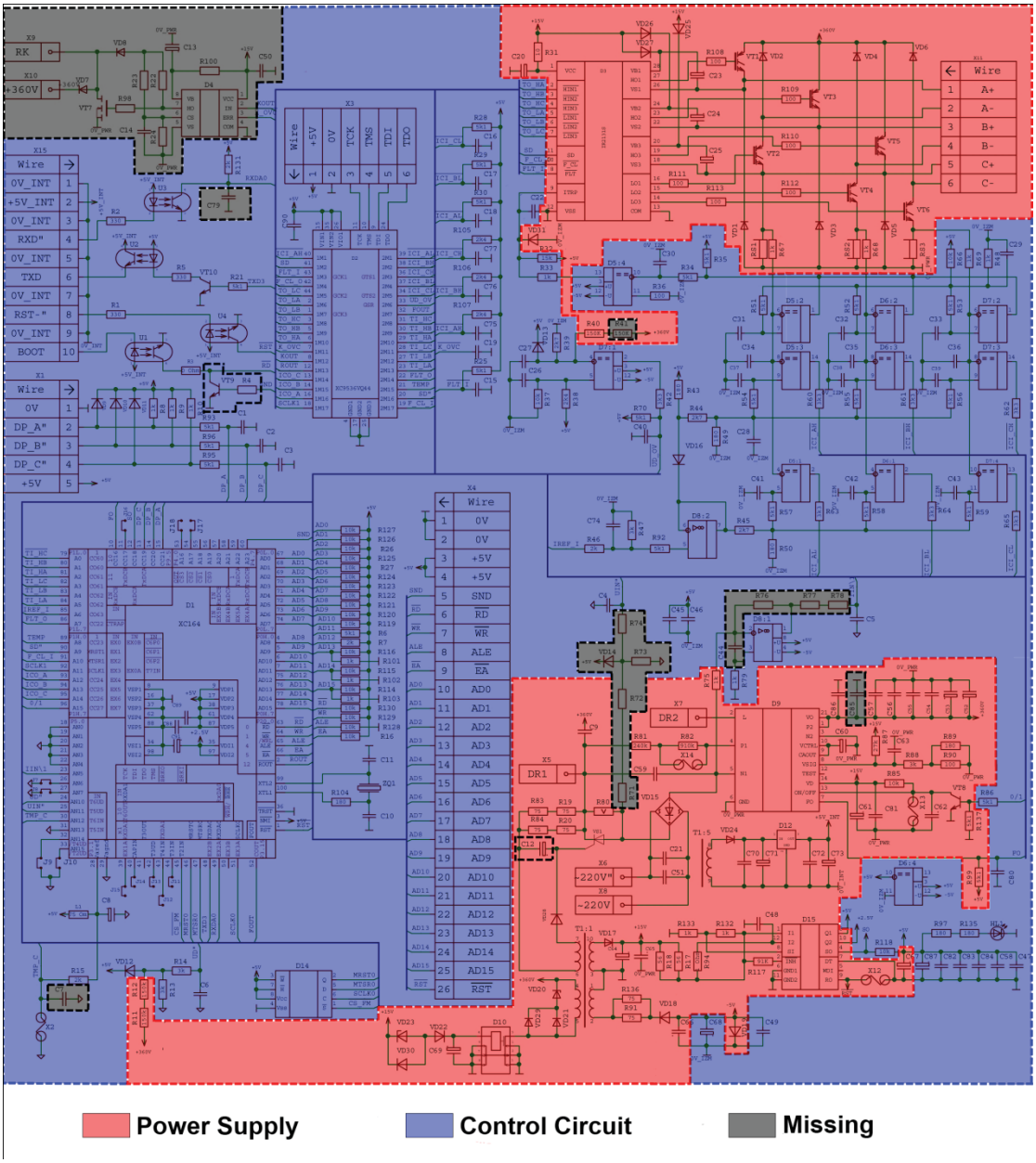

Figure C-7: Revised And Final Separation Points Within DVR Electronic Drive

C.8 Final Separation Line

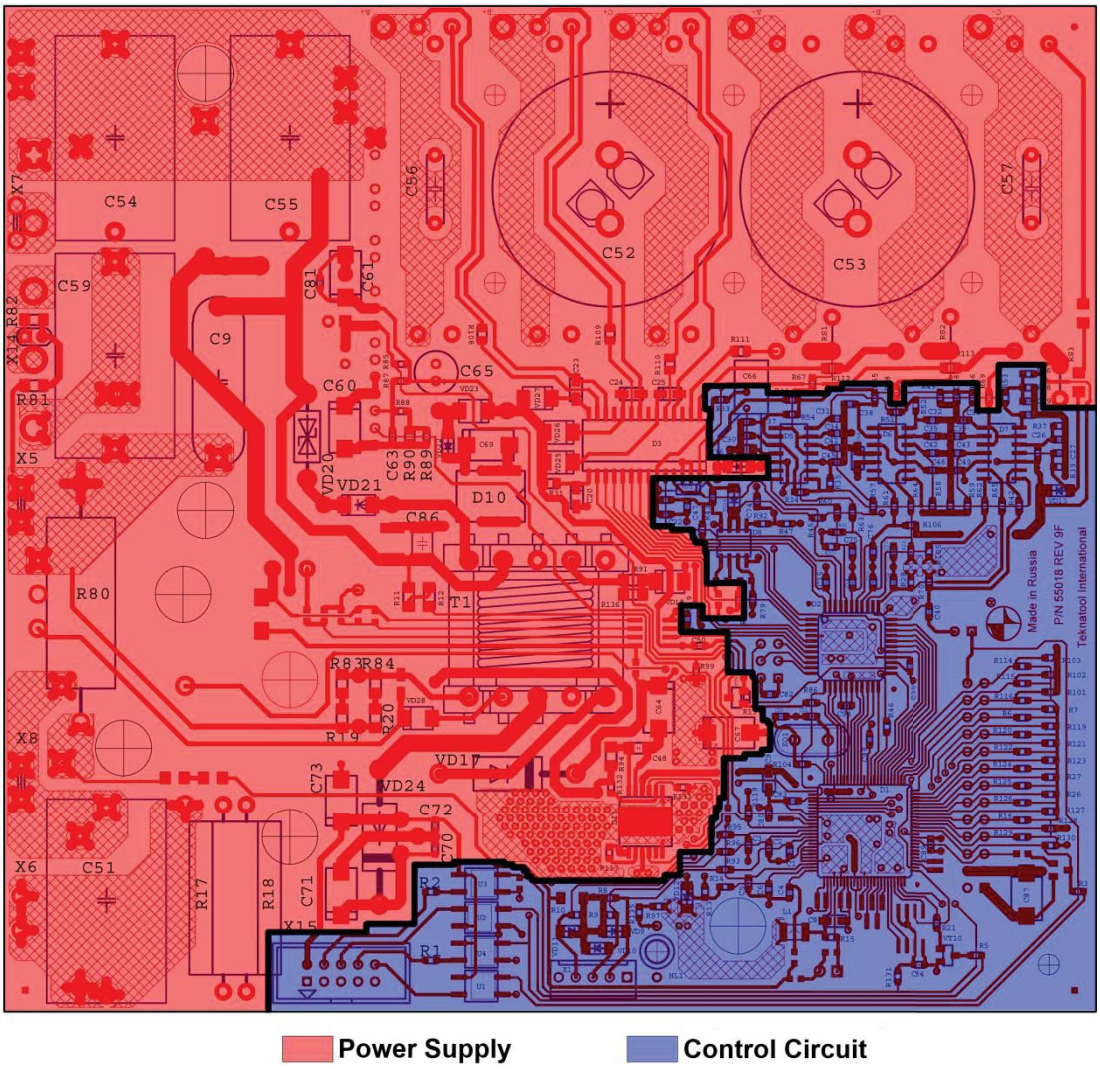

Figure C-8: Final Separation Line Plotted From Final Separation Points

C.9 Capacitive Components Listing

ID	Material	Present	Specification	Footprint	Use
C1	Ceramic	Yes	1nF, 25V	0805	Low Pass Filter
C2	Ceramic	Yes	1nF, 25V	0805	Low Pass Filter
C3	Ceramic	Yes	1nF, 25V	0805	Low Pass Filter
C4	Ceramic	Yes	270pF,25V	0805	Noise reduction
C5	Ceramic	Yes	270pF,25V	0805	Noise reduction
C6	Ceramic	Yes	820pF,25V	0805	Noise reduction
C7	N/A	No	N/A	N/A	N/A
C8	Tantalum	Yes	82uF, 16V	1206	Noise reduction
C9	Plastic	Yes	1.82uF, 630V,	Axial-0.9	Low Frequency Blocker
C10	Ceramic	Yes	180pF, 25V	0805	Timing Circuit
C11	Ceramic	Yes	550pF, 25V	0805	Timing Circuit
C12	N/A	No	N/A	N/A	N/A
C13	N/A	No	N/A	N/A	N/A
C14	N/A	No	N/A	N/A	N/A
C15	Ceramic	Yes	250pF, 25V	0805	Low Pass Filter
C16	Ceramic	Yes	820pF,25V	0805	Low Pass Filter
C17	Ceramic	Yes	360pF, 25V	0805	Low Pass Filter
C18	Ceramic	Yes	360pF, 25V	0805	Low Pass Filter
C19	Ceramic	Yes	470pF, 25V	0805	Noise reduction
C20	Tantalum	Yes	66uF, 25V	1206	Rail Regulation
C21	N/A	No	N/A	N/A	N/A
C22	Ceramic	Yes	590pF, 25V	0805	Noise reduction
C23	Tantalum	Yes	1.5uF. 25V	1206	Bootstrapping
C24	Tantalum	Yes	1.5uF, 25V	1206	High Voltage
C25	Tantalum	Yes	1.5uF, 25V	1206	High Voltage
C26	Ceramic	Yes	77nF, 25V	0805	Noise Reduction
C27	Ceramic	Yes	1uF, 25V	0805	Stable Reference
C28	Ceramic	Yes	750pF, 25V	0805	Stable Reference
C29	Ceramic	Yes	110pF, 25V	0805	Stable Reference
C30	Ceramic	Yes	420pF, 25V	0805	Low Pass Filter
C31	Ceramic	Yes	11.1nF, 25V	0805	Low Pass Filter
C32	Ceramic	Yes	11.1nF, 25V	0805	Low Pass Filter
C33	Ceramic	Yes	11.1nF, 25V	0805	Low Pass Filter
C34	Ceramic	Yes	91pF, 25V	0805	Low Pass Filter
C35	Ceramic	Yes	91pF, 25V	0805	Low Pass Filter
C36	Ceramic	Yes	140pF, 25V	0805	Low Pass Filter
C37	Ceramic	Yes	820pF, 25V	0805	Low Pass Filter
C38	Ceramic	Yes	820pF, 25V	0805	Low Pass Filter
C39	Ceramic	Yes	820pF, 25V	0805	Low Pass Filter
C40	Ceramic	Yes	350pF, 25V	0805	Noise reduction
C41	Ceramic	Yes	820pF, 25V	0805	Low Pass Filter
C42	Ceramic	Yes	820pF, 25V	0805	Low Pass Filter
C43	Ceramic	Yes	820pF, 25V	0805	Low Pass Filter
C44	N/A	No	N/A	N/A	N/A
C45	Ceramic	Yes	470nF, 25V	0805	Rail Regulation
C46	Ceramic	Yes	470nF, 25V	0805	Rail Regulation
C47	Ceramic	Yes	470nF, 25V	0805	Rail Regulation
C48	Ceramic	Yes	1.3uF, 25V	1206	Noise reduction
C49	Ceramic	Yes	470nF, 25V	0805	Rail Regulation
C50	Ceramic	Yes	470nF,25V	0805	Rail Regulation
C51	Electrolytic	Yes	2.2uF, 275VAC	CAPPA-46	EMI Suppression

ID	Material	Present	Specification	Footprint	Use
C52	Electrolytic	Yes	470uF, 450Vp	CAPPR-0.4	Rail Regulation
C53	Electrolytic	Yes	470uF, 450Vp	CAPPR-0.4	Rail Regulation
C54	Electrolytic	Yes	1.5uF, 630VDC	CAPPA-46	EMI Suppression
C55	Electrolytic	Yes	1.5uF, 630VDC	CAPPA-46	EMI Suppression
C56	Plastic	Yes	22nF, 630VDC	Axial-0.4	Rail Regulation
C57	Plastic	Yes	22nF, 630VDC	Axial-0.4	Rail Regulation
C58	Ceramic	Yes	470nF, 25V	0805	Rail Regulation
C59	Electrolytic	Yes	1.5uF	CAPPA-46	EMI Suppression
C60	Tantalum	Yes	22uF, 25V	2512-WAVE	Energy Storage
C61	Tantalum	Yes	15uF, 25V	2512-WAVE	Noise reduction
C62	N/A	No	N/A	N/A	N/A
C63	Ceramic	Yes	330nF, 25V	0805	Noise reduction
C64	Tantalum	Yes	95uF, 25V	2512-WAVE	Rail Regulation
C65	Electrolytic	Yes	47uF, 25V	CAPPR-0.1	Rail Regulation
C66	Electrolytic	Yes	47uF, 16V	CAPPR-0.1	Rail Regulation
C67	Tantalum	Yes	100uF, 16V	2512-WAVE	Rail Regulation
C68	Tantalum	Yes	47uF, 25V	1206	Rail Regulation
C69	Tantalum	Yes	47uF, 16V	2512-WAVE	Energy Storage
C70	Ceramic	Yes	240nF, 25V	0805	Energy Storage
C71	Tantalum	Yes	100uF, 25V	2512-WAVE	Energy Storage
C72	Ceramic	Yes	240nF, 25V	0805	Rail Regulation
C73	Tantalum	Yes	22uF, 16V	2512-WAVE	Rail Regulation
C74	Ceramic	Yes	74nF, 25V	0805	Duty Cycle -> Voltage
C75	Ceramic	Yes	170pF,25V	0805	Low Pass Filter
C76	Ceramic	Yes	170pF,25V	0805	Low Pass Filter
C77	Ceramic	Yes	170pF,25V	0805	Low Pass Filter
C79	N/A	No	N/A	N/A	N/A
C80	Ceramic	Yes	460nF,25V	0805	Noise reduction
C81	Ceramic	Yes	470nF.25V	0805	Noise reduction
C82	Ceramic	Yes	480nF, 25V	0805	Rail Regulation
C83	Ceramic	Yes	460nF, 25V	0805	Rail Regulation
C84	Ceramic	Yes	480nF, 25V	0805	Rail Regulation
C85	N/A	No	N/A	N/A	N/A
C86	Ceramic	Yes	47nF, 500V	2010-WAVE	Rail Regulation
C87	Tantalum	Yes	100uF, 16V	2512-WAVE	Rail Regulation
C88	Ceramic	Yes	460nF, 25V	0805	Rail Regulation
C89	Ceramic	Yes	460nF, 25V	0805	Rail Regulation
C90	Ceramic	Yes	460nF, 25V	0805	Rail Regulation
C91	Tantalum	Yes	20uF, 16V	1206	Rail Regulation

Table C-1: Capacitive Component Listing

C.10 Resistive Component Listing

ID	Present	Specification	Footprint	Use
L1	Yes	750Ω	1206	Pull Up Resistor
RS1	Yes	Wire-Link	Wire Hoop	Phase A Current Sensing
RS2	Yes	Wire-Link	Wire Hoop	Phase B Current Sensing
RS3	Yes	Wire-Link	Wire Hoop	Phase C Current Sensing
R1	Yes	330Ω	0805	Current Limiting
R2	Yes	330Ω	0805	Current Limiting
R3	Yes	Shorted-Link	0805	Jumper
R4	No	N/A	N/A	N/A
R5	Yes	330Ω	0805	Current Limiting
R6	Yes	5k1Ω	0805	Pullup Resistor
R7	Yes	2kΩ	0805	Pullup Resistor
R8	Yes	1kΩ	0805	Pullup Resistor
R9	Yes	1kΩ	0805	Pullup Resistor
R10	Yes	1kΩ	0805	Pullup Resistor
R11	Yes	150kΩ	1206	Voltage Divider
R12	Yes	150kΩ	1206	Voltage Divider
R13	Yes	3kΩ	0805	Voltage Divider
R14	Yes	3kΩ	0805	Low Pass Filter
R15	Yes	2kΩ	0805	Current Limiting
R16	Yes	10kΩ	0805	Pull Up Resistor
R17	Yes	56Ω	Axial-0.9	Current Limiting
R18	Yes	56Ω	Axial-0.9	Current Limiting
R19	Yes	75Ω	1206	Current Limiting
R20	Yes	75Ω	1206	Current Limiting
R21	Yes	5k1Ω	0805	Current Limiting
R22	No	N/A	N/A	N/A
R23	No	N/A	N/A	N/A
R24	No	N/A	N/A	N/A
R25	Yes	5k1Ω	0805	Pullup Resistor
R26	Yes	10kΩ	0805	Pullup Resistor
R27	Yes	10kR	0805	Pullup Resistor
R28	Yes	5k1Ω	0805	Pullup Resistor
R29	Yes	5k1Ω	0805	Pullup Resistor
R30	Yes	5k1Ω	0805	Pullup Resistor
R31	Yes	10Ω	0805	Low Pass Filter
R32	Yes	15kΩ	0805	Pull Up Resistor
R33	Yes	1kΩ	0805	Current Limiting
R34	Yes	5k1Ω	0805	Low Pass Filter
R35	Yes	5k1Ω	0805	Low Pass Filter
R36	Yes	100Ω	0805-WAVE	Current Limiting
R37	Yes	10kΩ	0805	Voltage Divider
R38	Yes	2k4Ω	0805	Voltage Divider
R39	Yes	2k7Ω	0805	Pull Up Resistor
R40	No	N/A	N/A	N/A
R41	No	N/A	N/A	N/A
R42	Yes	3k3Ω	0805	Current Limiting
R43	Yes	180Ω	0805	Voltage Divider
R44	Yes	2k7Ω	0805	Voltage Divider
R45	Yes	2k7Ω	0805	Current Limiting
R46	Yes	2kΩ	0805	Current Limiting
R47	Yes	3kΩ	0805	Capacitor Discharge

ID	Present	Specification	Footprint	Use
R48	Yes	1kΩ	0805	Voltage Divider
R49	Yes	180Ω	0805	Voltage Divider
R50	Yes	180Ω	0805	Voltage Divider
R51	Yes	5k1Ω	0805	Low Pass Filter
R52	Yes	5k1Ω	0805	Low Pass Filter
R53	Yes	5k1Ω	0805	Low Pass Filter
R54	Yes	5k1Ω	0805	Low Pass Filter
R55	Yes	5k1Ω	0805	Low Pass Filter
R56	Yes	5k1Ω	0805	Low Pass Filter
R57	Yes	5k1Ω	0805	Low Pass Filter
R58	Yes	5k1Ω	0805	Low Pass Filter
R59	Yes	5k1Ω	0805	Low Pass Filter
R60	Yes	3k3Ω	0805	Current Limiting
R61	Yes	3k3Ω	0805	Current Limiting
R62	Yes	3k3Ω	0805	Current Limiting
R63	Yes	3k3Ω	0805	Current Limiting
R64	Yes	3k3Ω	0805	Current Limiting
R65	Yes	3k3Ω	0805	Current Limiting
R66	Yes	10kΩ	0805	Voltage Divider
R67	Yes	1kΩ	0805	Current Limiting
R68	Yes	1kΩ	0805	Current Limiting
R69	Yes	1kΩ	0805	Current Limiting
R70	Yes	5k1Ω	0805	Pull Up Resistor
R71	No	N/A	N/A	N/A
R72	No	N/A	N/A	N/A
R73	No	N/A	N/A	N/A
R74	No	N/A	N/A	N/A
R75	Yes	1kΩ	0805	Current Limiting
R76	No	N/A	N/A	N/A
R77	No	N/A	N/A	N/A
R78	No	N/A	N/A	N/A
R79	Yes	1kΩ	0805	Pull Down Resistor
R80	Yes	10Ω, C5-37B	Axial -1.2	Inrush Current Limiting
R81	Yes	240kΩ	120	Current Limiting
R82	Yes	910kΩ	1206	Current Limiting
R83	Yes	75Ω	1206	Current Limiting
R84	Yes	75Ω	1206	Current Limiting
R85	Yes	10kΩ	1206	Discharge Resistor
R86	Yes	5k1Ω	0805	Current Limiting
R87	Yes	27kΩ	0805	Voltage Divider
R88	Yes	3kΩ	0805	Voltage Divider
R89	Yes	180Ω	0805	Voltage Divider
R90	Yes	100Ω	0805-WAVE	Voltage Divider
R91	Yes	75Ω	1206	Current Limiting
R92	Yes	5k1Ω	0805	Current Limiting
R93	Yes	5k1Ω	0805	Current Limiting
R94	Yes	1Ω	1206	Current Limiting
R95	Yes	5k1Ω	0805	Current Limiting
R96	Yes	5k1Ω	0805	Current Limiting
R97	Yes	180Ω	0805	Current Limiting
R98	No	N/A	N/A	N/A
R99	Yes	5k1Ω	0805	Low Pass Filter
R100	No	N/A	N/A	N/A
R101	Yes	1kΩ	0805	Voltage Divider
R102	Yes	1kΩ	0805	Voltage Divider

ID	Present	Specification	Footprint	Use
R103	Yes	1kΩ	0805	Voltage Divider
R104	Yes	180Ω	0805	Timing Circuit
R105	Yes	2k4Ω	0805	Pull Up Resistor
R106	Yes	2k4Ω	0805	Pull Up Resistor
R107	Yes	2k4Ω	0805	Pull Up Resistor
R108	Yes	100Ω	0805-WAVE	Current Limiting
R109	Yes	100Ω	0805-WAVE	Current Limiting
R110	Yes	100Ω	0805-WAVE	Current Limiting
R111	Yes	100Ω	0805-WAVE	Current Limiting
R112	Yes	100Ω	0805-WAVE	Current Limiting
R113	Yes	100Ω	0805-WAVE	Current Limiting
R114	Yes	10kΩ	0805	Voltage Divider
R115	Yes	10kΩ	0805	Voltage Divider
R116	Yes	10kΩ	0805	Voltage Divider
R117	Yes	91kΩ	0805	Current Limiting
R118	Yes	10kΩ	0805	Current Limiting
R119	Yes	10kΩ	0805	Pull Up Resistor
R120	Yes	10kΩ	0805	Pull Up Resistor
R121	Yes	10kΩ	0805	Pull Up Resistor
R122	Yes	10kΩ	0805	Pull Up Resistor
R123	Yes	10kΩ	0805	Pull Up Resistor
R124	Yes	10kΩ	0805	Pull Up Resistor
R125	Yes	10kΩ	0805	Pull Up Resistor
R126	Yes	10kΩ	0805	Pull Up Resistor
R127	Yes	10kΩ	0805	Pull Up Resistor
R128	Yes	10kΩ	0805	Pull Down Resistor
R129	Yes	10kΩ	0805	Pull Up Resistor
R130	Yes	10kΩ	0805	Pull Up Resistor
R131	Yes	2kΩ	0805	Pull Up Resistor
R132	Yes	1kΩ	0805	Voltage Divider
R133	Yes	1kΩ	0805	Voltage Divider
R135	Yes	180Ω	0805	Current Limiting
R136	Yes	75Ω	1206	Current Limiting
R137	Yes	5k1Ω	0805	Pull Down Resistor

Table C-2: Resistive Component Listing

C.11 Semi-Conductor and Inductive Component Listing

ID	Device	Present	Specification	Footprint	Use
D1	Microcontroller	Yes	XC164CS	P-TQFP-100-16	Control
D2	CPLD	Yes	XC9536-15VQ44	VQFP44	Control
D3	IGBT Driver	Yes	IR2131S	SOIC28	IGBT Control
D4	N/A	No	N/A	N/A	N/A
D5	Comparator	Yes	LM2901D	SO-14	Current Sensing
D6	Comparator	Yes	LM2901D	SO-14	Current Sensing
D7	Comparator	Yes	LM2901D	SO-14	Current Sensing
D8	Op Amplifier	Yes	LM2904D	SO-8	
D9	PF Controller	Yes	PM52AUBW060	Proprietary	PF Correction
D10	PWM Switch	Yes	TOP221P	DIP-8	Current control
D11	N/A	No	N/A	N/A	N/A
D12	Regulator	Yes	KA7805A	TO-220	+5V_INT Supply
D13	N/A	No	N/A	N/A	N/A
D14	N/A	No	N/A	N/A	N/A
D15	Regulator	Yes	TLE7469	PG-DSO12	+2.5,+5V Supply
U1	Opto-coupler	Yes	SFH690BT	SOP-4	Isolation
U2	Opto-coupler	Yes	SFH690BT	SOP-4	Isolation
U3	Opto-coupler	Yes	SFH690BT	SOP-4	Isolation
U4	Opto-coupler	Yes	SFH690BT	SOP-4	Isolation
VD1	Diode	Yes	HFA15TB60	TO-220	Back-EMF
VD2	Diode	Yes	HFA15TB60	TO-220	Back-EMF
VD3	Diode	Yes	HFA15TB60	TO-220	Back-EMF
VD4	Diode	Yes	HFA15TB60	TO-220	Back-EMF
VD5	Diode	Yes	HFA15TB60	TO-220	Back-EMF
VD6	Diode	Yes	HFA15TB60	TO-220	Back-EMF
VD7	Diode	No	N/A	N/A	N/A
VD8	Diode	No	N/A	N/A	N/A
VD9	Diode	Yes	LL4148-SMD	4148	Signal Conditioning
VD10	Diode	Yes	LL4148-SMD	4148	Signal Conditioning
VD11	Diode	Yes	LL4148-SMD	4148	Signal Conditioning
VD12	Diode	Yes	LL4148-SMD	4148	Voltage Constraint
VD13	Diode	Yes	LL4148-SMD	4148	Voltage Constraint
VD14	Diode	No	N/A	N/A	N/A
VD15	Bridge Rectifier	Yes	GBPC3506W	Proprietary	Rectification
VD16	Diode	Yes	LL4148-SMD	4148	Current Direction
VD17	Diode	Yes	SF54 MIC	Axial-0.8	Current Direction
VD18	Diode	Yes	SMD Diode	2010-WAVE	Current Direction
VD19	Diode	Yes	LL4148-SMD	4148	Polarity Protection
VD20	Diode	Yes	EIC 35 00A	Axial-0.5	Back EMF
VD21	Diode	Yes	UFC40 MIC	Axial-0.4	Back EMF
VD22	Diode	Yes	LL4148-SMD	4148	Current Direction
VD23	Zener Diode	Yes	BZX55C8V2-SMD	DO-35	TOPS Reference
VD24	Diode	Yes	SF54 MIC	Axial-0.8	Current Direction
VD25	Diode	Yes	SMD Diode	2010-WAVE	Bootstrapping
VD26	Diode	Yes	SMD Diode	2010-WAVE	Bootstrapping
VD27	Diode	Yes	SMD Diode	2010-WAVE	Bootstrapping
VD28	Diode	Yes	SMD Diode	2010-WAVE	Polarity Protection
VD29	Diode	No	N/A	N/A	N/A
VD30	Diode	No	N/A	N/A	N/A
VD31	Diode	Yes	Germanium	Diode Axial-0.35	Voltage Clamping
VS1	Thyristor (SCR)	Yes	40TPS08A	TO-247	Inrush Current

ID	Device	Present	Specification	Footprint	Use
VT1	IGBT Transistor	Yes	G4BC30F	TO-220	Phase Switching
VT2	IGBT Transistor	Yes	G4BC30F	TO-220	Phase Switching
VT3	IGBT Transistor	Yes	G4BC30F	TO-220	Phase Switching
VT4	IGBT Transistor	Yes	G4BC30F	TO-220	Phase Switching
VT5	IGBT Transistor	Yes	G4BC30F	TO-220	Phase Switching
VT6	IGBT Transistor	Yes	G4BC30F	TO-220	Phase Switching
VT7	FET Transistor	No	N/A	N/A	N/A
VT8	BJT Transistor	Yes	SMD BJT	SOT-23	Current Switch
VT9	BJT Transistor	No	N/A	N/A	N/A
VT10	BJT Transistor	Yes	SMD BJT	SOT-23	Current Switch
ZQ1	Crystal	Yes	18MHz	Axial-0.2	Clock Genereration
T1	Transformer	Yes	Custom	EP25	Voltage Conversion

Table C-3: Semi-Conductor and Inductive Component Listing

C.12 Connector Component Information

ID	Connection	Present	Specification	Footprint
X1	Rotor Position Sensors	Yes	Connector Terminal	N/A
X2	N/A	No	N/A	N/A
X3	CPLD Programming Header	Yes	2x3 Pin Header	3 x 2 @ 0.1
X4	Microcontroller Programming	Yes	2x13 Pin Header	13 x 2 @ 0.1
X5	Inductor to R80, DR1	Yes	Blade Terminal	N/A
X6	AC 230V Input, ~220V"	Yes	Blade Terminal	N/A
X7	Inductor to PFC, DR2	Yes	Blade Terminal	N/A
X8	AC 230V Input, ~220V	Yes	Blade Terminal	N/A
X9	N/A	No	N/A	N/A
X11	Power Supply to Motor	Yes	6-Pin Connector	N/A
X12	N/A	No	N/A	N/A
X13	N/A	No	N/A	N/A
X14	Input Voltage Select	Yes	2 Pin Header	1x2 @ 0.1
X15	Interface Board	Yes	2x5 Pin Header	2x5 @ 0.1

Table C-4: Connector Component Listing

C.13 Capacitive Component Location

ID	Voltage	Location	Details
C1	5V	Control	Used with R93 to low pass filter Position Sensor A output
C2	5V	Control	Used with R96 to low pass filter Position Sensor B output
C3	5V	Control	Used with R95 to low pass filter Position Sensor B output
C4	5V	Control	Removes white noise on the UIN signal line
C5	5V	Control	Removes white noise on the IIN\I signal line
C6	5V	Control	Removes white noise on the UD signal line
C7	N/A	N/A	N/A
C8	5V	Control	Provides energy storage on signal TMP_C to catch white noise.
C9	360V	Supply	Reduces amplitude of the DC component
C10	5V	Control	Used in clock signal generation for the Microcontroller
C11	5V	Control	Used in clock signal generation for the Microcontroller
C12	N/A	N/A	N.A
C13	N/A	N/A	N/A
C14	N/A	N/A	N/A
C15	5V	Control	Used in combination with R25 as a low pass filter for signal FLT_I
C16	5V	Control	Used in combination with R28 as a low pass filter for signal ICI_CL
C17	5V	Control	Used in combination with R29 as a low pass filter for signal ICI_BL
C18	5V	Control	Used in combination with R30 as a low pass filter for signal ICI_AL
C19	5V	Control	Provides energy storage to signal K_OVC to catch white noise

ID	Voltage	Location	Details
C20	15V	Supply	Used to provide a stable 15V rail for the IGBT driver D3
C21	N/A	N/A	N/A
C22	5V	Control	Used to provide energy storage to signal ITRP to catch white noise
C23	15V,360V	Supply	Provides 15V floating reference for switching high side IGBT VT1
C24	15V,360V	Supply	Provides 15V floating reference for switching high side IGBT VT3
C25	15V,360V	Supply	Provides 15V floating reference for switching high side IGBT VT5
C26	5V	Control	Catches white noise at input of Comparator D7:1
C27	5V	Control	Provides stable reference at the '-' input of D7:1
C28	5V	Control	Provides stable reference at the '+' inputs of D5:1, D6:1 and D7:4
C29	5V	Control	Provides stable reference at the '+' inputs of D5:2, D6:2 and D7:2
C30	5V	Control	Low pass filter with R34 for the '-' input of Comparator D5:4
C31	5V	Control	Low pass filter with R51 for the '+' input of Comparator D5:2
C32	5V	Control	Low pass filter with R51 for the '+' input of Comparator D6:2
C33	5V	Control	Low pass filter with R51 for the '+' input of Comparator D7:2
C34	5V	Control	Low pass filter with R67 for the '-' inputs of D5:1, D5:2, D5:3
C35	5V	Control	Low pass filter with R68 for the '-' inputs of D6:1, D6:2, D6:3
C36	5V	Control	Low pass filter with R69 for the '-' inputs of D7:2, D7:3, D7:4
C37	5V	Control	Low pass filter with R54 for the '+' input of Comparator D5:3
C38	5V	Control	Low pass filter with R55 for the '+' input of Comparator D6:3
C39	5V	Control	Low pass filter with R56 for the '+' input of Comparator D7:3
C40	5V	Control	Removes white noise from signal UD_OV
C41	5V	Control	Low pass filter with R57 for the '+' input of Comparator D5:1
C42	5V	Control	Low pass filter with R58 for the '+' input iof Comparator D6:1
C43	5V	Control	Low pass filter with R59 for the '+' input into Comparator D7:4
C44	N/A	N/A	N/A
C45	5V	Control	Decouples Comparator D5
C46	5V	Control	Decouples Comparator D6
C47	5V	Control	Decouples Operation Amplifier D8
C48	5V	Control	Removes white noise at input I2 on Regulator D15
C49	5V	Control	Decouples Comparator D7
C50	15V	Control	Decouples D4 which is not present on the circuit board
C51	230V AC	Supply	Used to suppress EMI induced onto the mains input rails
C52	360V	Supply	Provides energy storage on +360V Rail
C53	360V	Supply	Provides energy storage on +360V Rail
C54	360V	Supply	Provides low ESR energy storage on the +360V Rail
C55	360V	Supply	Provides low ESR energy storage on the +360V
C56	360V	Supply	Provides energy storage on the +360V Rail
C57	360V	Supply	Provides energy storage on the +360V Rail
C58	5V	Control	Decouples CPLD D2
C59	360V	Supply	Provides energy storage on the +360V Rail
C60	25V	Supply	Provides energy storage for pins CAOUT and VCTRL on PFC
C61	15V	Supply	Removes white noise at ON/OFF pin of PFC
C62	N/A	N/A	N/A
C63	15V	Supply	Removes white noise at VSIG pin of PFC
C64	15V	Supply	Stores energy from pulsed output of Transformer T1 for 15V Rail
C65	15V	Supply	Stores energy from pulsed output of Transformer T1 for 15V Rail
C66	-5V	Supply	Stores energy from pulsed output of Transformer T1 for -5V Rail
C67	5V	Supply	Used to smooth the output of the 5V output of Regulator D15 5V
C68	-5V	Control	Decouples Comparator D6
C69	15V	Supply	Provides energy storage for the input to the TOPS switch
C70	16V	Supply	Steadies input voltage for Regulator D12
C71	16V	Supply	Steadies input voltage for Regulator D12 D12
C72	5V DC	Supply	Reduces voltage ripple of the 5V switching regulator
C73	5V DC	Supply	Reduces voltage ripple of the 5V switching regulator
C74	5V	Control	Integrates digital signal from D1 to generate analog signal IREF_I

ID	Voltage	Location	Details
C75	5V	Control	Forms a low pass filter with R107 to filter the signal ICI_AH
C76	5V	Control	Forms a low pass filter with R106 to filter the signal ICI_BH
C77	5V	Control	Forms a low pass filter with R105 to filter the signal ICI_CH
C79	N/A	N/A	N/A
C80	5V	Control	Provides energy storage to signal FO to catch white noise
C81	25V	Supply	Removes white noise at ON/OFF pin of PFC
C82	5V	Control	Decouples the power pins on the CPLD programming connector
C83	5V	Control	Decouples Microcontroller D1
C84	5V	Control	Used to provide rail regulation to the 5V rail
C85	N/A	N/A	N/A
C86	360V	Supply	Catches white noise radiated from Transformer T1
C87	5V	Control	Provides rail regulation to the 5V rail
C88	2.5V	Control	Decouples +2.5V Input of Microcontroller D1
C89	2.5V	Control	Decouples +2.5V Input of Microcontroller D1
C90	5V	Control	Decouples CPLD D2
C91	2.5V	Control	Ensures smooth regulation of the 2.5V Rail

Table C-5: Capacitive Component Location

C.14 Resistive Component Location

ID	Voltage	Location	Details
L1	5V	Control	Strong pull up for signal TMP_C
RS1	360V	Supply	Measures current flowing through Phase A
RS2	360V	Supply	Measures current flowing through Phase B
RS3	360V	Supply	Measures current flowing through Phase C
R1	5V_INT	Control	Current limiting resistor LED in opto-coupler U4 input
R2	5V_INT	Control	Current limiting resistor LED in opto-coupler U4 input
R3	5V	Control	Provides a jumper across a track
R4	N/A	N/A	N/A
R5	5V_INT	Control	Current limiting resistor LED in opto-coupler U2 input
R6	5V	Control	Pull-up for Pin AD11 on Microcontroller
R7	5V	Control	Pull-up for Pin AD12 on Microcontroller
R8	5V	Control	Pull-up for DP_A Rotor position hall effect sensor
R9	5V	Control	Pull-up for DP_B Rotor position hall effect sensor
R10	5V	Control	Pull-up for DP_C Rotor position hall effect sensor
R11	360V	Supply	Voltage Divider for 360V in series with R12
R12	360V	Supply	Voltage Divider for 360V in series with R11
R13	5.7V	Control	Lower half of voltage divider with R11 & R12
R14	5.7V	Control	Low pass filter for noise reduction with C6
R15	5V	Control	Current limiting resistor for P3.1 on Microcontroller
R16	5V	Control	Pull up resistor for EA pin on Microcontroller
R17	15V	Supply	Current limiting resistor for the input to 5V and 2.5 regulator
R18	15V	Supply	Current limiting resistor for the input to 5V and 2.5 regulator
R19	360V	Supply	Limits the current from the 360V rail through the transformer
R20	360V	Supply	Limits the current from the 360V rail through the transformer
R21	5V	Control	Limits the current flowing into the base of the BJT Transistor VT10
R22	N/A	N/A	N/A
R23	N/A	N/A	N/A
R24	N/A	N/A	N/A
R25	5V	Control	Pull-up resistor for FLT_I signal
R26	5V	Control	Pull-up for Pin AD2 on Microcontroller
R27	5V	Control	Pull-up for Pin AD4 on Microcontroller
R28	5V	Control	Pull-up resistor for ICI_CL signal
R29	5V	Control	Pull-up resistor for ICI_BL signal
R30	5V	Control	Pull-up resistor for ICI_AL signal
R31	15V	Supply	Provides low pass filtering with C20 for Component D3
R32	5V	Control	Pull-up resistor for ITRP signal
R33	5V	Control	Current limiting for output of Comparator D5 into D3
R34	5V	Control	Low Pass filter with C30 for input into Comparator D5
R35	5V	Control	Low pass filter with C29 for input on Comparator D5
R36	0V_IZM	Control	Current limiting for input into Comparator D5
R37	5V	Control	Lower half of voltage divider with R38
R38	5V	Control	Upper half of voltage divider with R37
R39	5V	Control	Pull up resistor for input into Comparator D7
R40	N/A	N/A	N/A
R41	N/A	N/A	N/A
R42	5V	Control	Current limiting resistor for input into Comparator D7 pin 2
R43	5V	Control	Used with R44 and R49 to provide a reference voltage
R44	5V	Control	Used with R43 and R49 to provide a reference voltage
R45	5V	Control	Current limits and divides D8 output with R50
R46	5V	Control	Used to limit the current, slow charging rate, into Capacitor C74
R47	5V	Control	Provides a consistent draw on Capacitor C74 to cause discharge

ID	Voltage	Location	Details
R48	5V	Control	Sets voltage with R66 for input for Comparators D5,D6,D7
R49	5V	Control	Used with R43 and R44 to provide a reference voltage
R50	5V	Control	Reduces D8 by forming a voltage divider with R45
R51	5V	Control	Used in combination with C31 to low pass filter the input to D6
R52	5V	Control	Used in combination with C32 to low pass filter the input to D6
R53	5V	Control	Used in combination with C33 to low pass filter the input to D7
R54	5V	Control	Used in combination with C37 to low pass filter the input to D5
R55	5V	Control	Used in combination with C38 to low pass filter the input to D6
R56	5V	Control	Used in combination with C39 to low pass filter the input to D7
R57	5V	Control	Used in combination with C41 to low pass filter the input to D5
R58	5V	Control	Used in combination with C42 to low pass filter the input to D6
R59	5V	Control	Used in combination with C43 to low pass filter the input to D7
R60	5V	Control	Used to limit the current from the output of D5:3
R61	5V	Control	Used to limit the current from the output of D6:3
R62	5V	Control	Used to limit the current from the output of D7:3
R63	5V	Control	Used to limit the current from the output of D5:1
R64	5V	Control	Used to limit the current from the output of D6:1
R65	5V	Control	Used to limit the current from the output of D7:4
R66	5V	Control	Sets voltage with R48 as an input to Comparators D5,D6,D7
R67	5V	Control	Current limits all Phase A current inputs into Comparator D5
R68	5V	Control	Current limits all Phase B current inputs into Comparator D6
R69	5V	Control	Current limits Phase C current inputs into Comparator D7
R70	5V	Control	Used to pull signal UD_OV up to 5V
R71	N/A	N/A	N/A
R72	N/A	N/A	N/A
R73	N/A	N/A	N/A
R74	N/A	N/A	N/A
R75	360V	Supply	Used to limit the current into Operational Amplifier D8:1
R76	N/A	N/A	N/A
R77	N/A	N/A	N/A
R78	N/A	N/A	N/A
R79	5V	Control	Pulls the positive input to Operational Amplifier D8:1 down
R80	360V	Supply	Provides inrush current protection to the PFC
R81	360V	Supply	Limits the current flowing into the PFC voltage select pin
R82	360V	Supply	Limits the current flowing into the PFC voltage select pin
R83	360V	Supply	Limits the current from the 360V rail through the transformer
R84	360V	Supply	Limits the current from the 360V rail through the transformer
R85	15V	Supply	Used to provide a resistive discharge path for Capacitors, C61, C81
R86	5V	Control	Limits the current into the base of BJT Transistor VT8
R87	15V	Supply	Sets the voltage on VSIG pin on PFC
R88	15V	Supply	Sets the voltage on VSIG pin on PFC
R89	15V	Supply	Sets the voltage on VSIG pin on PFC
R90	15V	Supply	Sets the voltage on VSIG pin on PFC
R91	-18V	Supply	Limits the current able to be provided by the -5V rail
R92	5V	Control	Limits the current able to flow into Operational Amplifier D8:2
R93	5V	Control	Limits the current provided from Position Sensor A output
R94	15V	Supply	Limits the current provided to the input of Voltage regulator D15
R95	5V	Control	Limits the current provided from Position Sensor C output
R96	5V	Control	Limits the current provided from Position Sensor B output
R97	5V	Control	Limits the current flow through L.E.D HL1 with R135
R98	N/A	N/A	N/A
R99	5V	Supply	Used in combination with C80 to low pass FO signal
R100	N/A	N/A	N/A
R101	5V	Control	Divides voltage with R116 for input to D1:AD13
R102	5V	Control	Divides voltage with R115 for input to D1:AD14

ID	Voltage	Location	Details
R103	5V	Control	Divides voltage with R114 for input to D1:AD15
R104	5V	Control	Used in the clock generation timing circuit
R105	5V	Control	Used to pull signal ICI_CH up
R106	5V	Control	Used to pull signal ICI_BH up
R107	5V	Control	Used to pull signal ICI_AH up
R108	360V	Supply	Used to limit the current into the gate of IGBT VT1
R109	360V	Supply	Used to limit the current into the gate of IGBT VT3
R110	360V	Supply	Used to limit the current into the gate of IGBT VT5
R111	360V	Supply	Used to limit the current into the gate of IGBT VT2
R112	360V	Supply	Used to limit the current into the gate of IGBT VT4
R113	360V	Supply	Used to limit the current into the gate of IGBT VT6
R114	5V	Control	Divides voltage with R103 to provide an input to D1:AD15
R115	5V	Control	Divides voltage with R102 to provide an input to D1:AD14
R116	5V	Control	Divides voltage with R101 to provide an input to D1:AD13
R117	15V	Supply	Limits the current into INH pin of Voltage Regulator D15
R118	5V	Control	Limits the current that can flow from +5v into SO in Regulator D15
R119	5V	Control	Pulls up pin AD10 on the Microcontroller
R120	5V	Control	Pulls up pin AD9 on the Microcontroller
R121	5V	Control	Pulls up pin AD8 on the Microcontroller
R122	5V	Control	Pulls up pin AD7 on the Microcontroller
R123	5V	Control	Pulls up pin AD6 on the Microcontroller
R124	5V	Control	Pulls up pin AD5 on the Microcontroller
R125	5V	Control	Pulls up pin AD3 on the Microcontroller
R126	5V	Control	Pulls up pin AD1 on the Microcontroller
R127	5V	Control	Pulls up pin AD0 on the Microcontroller
R128	5V	Control	Pulls down pin ALE on the Microcontroller
R129	5V	Control	Pulls up pin WR on the Microcontroller
R130	5V	Control	Pulls up pin RD on the Microcontroller
R131	5V	Control	Pulls up RXDA0 bus signal
R132	15V	Supply	Divides voltage with R133 to provide a reference to pin SI on D15
R133	15V	Supply	Divides voltage with R132 to provide a reference to pin SI on D15
R135	5V	Control	Limits the current flow through L.E.D HL1 with R97
R136	-18V	Supply	Limits the current able to be provided by the -5V rail in with R91
R137	5V	Supply	Pulls down the base of the BJT Transistor VT8

Table C-6: Resistive Component Location

C.15 Semi-Conductor and Inductive Component Location

ID	Voltage	Location	Details
D1	5V	Control	Contains the programming and motor control algorithm
D2	5V	Control	Provides fail-safe logic for control signals
D3	360V	Supply	Provides floating driving for the IGBT Transistors
D4	N/A	N/A	N/A
D5	+5/-5V	Control	Provides over-current signal for Phase A
D6	+5V/-5V	Control	Provides over-current signal for Phase B
D7	+5/-5V	Control	Provides over-current signal for Phase C
D8	360V	Control	Provides AC Power On signal
D9	360V	Supply	Actively corrects the power factor of the circuit.
D10	360V	Supply	Controls current flow through transformer winding for -5V Rail
D11	N/A	N/A	N/A
D12	15V	Supply	Provides the +5_INT isolated supply rail
D13	N/A	N/A	N/A
D14	N/A	N/A	N/A
D15	15V	Supply	Used to provide 5.0V and 2.5V rails for use in the control circuit
U1	5V	Control	Allows signal to pass to isolated interface board
U2	5V	Control	Allows signal to pass to isolated interface board
U3	5V	Control	Allows signal to pass to isolated interface board
U4	5V	Control	Allows signal to pass to isolated interface board
VD1	360V	Supply	Back-electromotive force protection for IGBT VT1
VD2	360V	Supply	Back-electromotive force protection for IGBT VT2
VD3	360V	Supply	Back-electromotive force f protection for IGBT VT3
VD4	360V	Supply	Back-electromotive force protection for IGBT VT4
VD5	360V	Supply	Back-electromotive force protection for IGBT VT5
VD6	360V	Supply	Back-electromotive force protection for IGBT VT6
VD7	N/A	N/A	N/A
VD8	N/A	N/A	N/A
VD9	5V	Control	Used to condition the signal from Position Sensor A
VD10	5V	Control	Used to condition the signal from Position Sensor B
VD11	5V	Control	Used to condition the signal from Position Sensor C
VD12	5V	Control	Used to cap the voltage at R12,R13 to 5V
VD13	5V	Control	Used to cap the voltage at C27 to 5V
VD14	N/A	N/A	N/A
VD15	325VDC	Supply	Rectifies 230V Mains AC to 325V DC
VD16	5V	Control	Prevents negative feedback of Voltage affecting divider R43,R44
VD17	15V	Supply	Prevents discharge C64 of from pulse output of Transformer T1
VD18	-5V	Supply	Prevents discharge C64 of from pulse output of Transformer T1
VD19	-5V	Supply	Reverse polarity protection -5V Rail
VD20	360V	Supply	Voltage clamp at 1.4V for TOPS Switch D10
VD21	360V	Supply	Voltage clamp at 1.4V for TOPS Switch D10
VD22	15V	Supply	Allows current flow into the control pin of TOPS/ C69
VD23	15V	Supply	Provides input switching for TOPS to control current through T1
VD24	15V	Supply	Prevents discharge of C70,C71 from pulsed output of T1
VD25	360V	Supply	Prevents discharge of VT1 floating reference C25
VD26	360V	Supply	Prevents discharge of VT2 floating reference C24
VD27	360V	Supply	Prevents discharge of VT3 floating reference C23
VD28	360V	Supply	Used to prevent current flowing from the gate of Thyristor VS1
VD29	N/A	N/A	N/A
VD30	N/A	N/A	N/A

ID	Voltage	Location	Details
VD31	15V	Supply	Prevents voltage on D3 ITRP pin from exceeding -0.3V
VS1	360V	Supply	Prevents Inrush current by switching R80 at turn on
VT1	360V	Supply	Used to switch the current through Winding 1 (Phase A)
VT2	360V	Supply	Used to switch the current through Winding 1 (Phase A)
VT3	360V	Supply	Used to switch the current through Winding 2 (Phase B)
VT4	360V	Supply	Used to switch the current through Winding 2 (Phase B)
VT5	360V	Supply	Used to switch the current through Winding 3 (Phase C)
VT6	360V	Supply	Used to switch the current through Winding 3 (Phase C)
VT7	N/A	N/A	N/A
VT8	5V	Supply	Used to turn the PFC off when biased
VT9	N/A	N/A	N/A
VT10	5V	Control	Used to switch current through Optocoupler U2
ZQ1	5V	Control	Used to generate 18MHz clock signal for Microcontroller D1
T1	360V	Supply	Generates varies output voltages from a single input voltage

Table C-7: Semi-Conductor and Inductive Component Location

C.16 Connector Component Location

ID	Voltage	Present	Details
X1	5V	Control	Rotor Position Sensor Connectors
X2	N/A	N/A	N/A
X3	5V	Control	Programming the CPLD
X4	5V	Control	Programming/Additional I/O Microcontroller
X5	230V RMS	Supply	Connection to external inductor
X6	230V RMS	Supply	Mains input connection
X7	230V RMS	Supply	Connection to external inductor
X8	230V RMS	Supply	Mains input connection
X9	N/A	N/A	N/A
X11	N/A	N/A	N/A
X12	360V	Supply	Connects the motor to the power supply
X13	N/A	N/A	N/A
X14	N/A	N/A	N/A
X15	360V	Supply	For 230V or 115V PFC Select

Table C-8: Connector Component Location

C.17 Power NET Designators

NET	Connection	Regulated	Isolated
~220V"	230V RMS Phase	No	No
~220V	230V RMS Neutral	N/A	No
+360V	360V	Yes – Via PFC	No
+15V	15V	No	No
+5V_INT	5V Isolated	Yes	Yes
+5V	5V Internal	Yes – Via D15	No
-5V	-5V Internal	N/A	No
0V_IZM	Control Circuitry negative	N/A	No
0V_PWR	Power Negative	N/A	No
0V_INT	0V Isolated Negative	N/A	Yes
+2.5V	2.5V Internal	Yes – Via D15	No

Table C-9: Power NET Designators

C.18 Additional Connector Information

ID	Connection	Part Number
IX1	Power Supply -> Control Board (I/O)	DF11-20DP-2DSA/DF11-20DS-2C
IX2	Power Supply -> Control Board (Power)	Molex 90130-1210 2x5

Table C-10: Additional Connector Information

Signal	IX1 Connector (I/O Signal)	IX2 Connector Power Signal
TO_HA	Yes	No
TO_HB	Yes	No
TO_HC	Yes	No
TO_LA	Yes	No
TO_LB	Yes	No
TO_LC	Yes	No
SD	Yes	No
F_CL	Yes	No
FLT_I	Yes	No
ITRP	Yes	No
Resistor 67	Yes	No
Resistor 68	Yes	No
Resistor 69	Yes	No
K_OVC	Yes	No
K_OUT	Yes	No
Power Factor Correction ON/OFF R86	Yes	No
Power Factor Correction FO	Yes	No
Twin-rail Regulator Reset Line	Yes	No
Twin-rail Regulator SO	Yes	No
+2.5V Rail	No	Yes
+5.0V Rail	No	Yes
-5.0V Rail	No	Yes
Resistor 72	No	Yes
+5V_INT Isolated	No	Yes
0V_INT Isolated	No	Yes
Resistor 12	No	Yes
Resistor 75	No	Yes
Resistor 40	No	Yes
OV_PWR/OV_IZM	Yes	Yes

Table C-11: Additional Connector Signals

C.19 Prototype Power Supply Printed Circuit Board

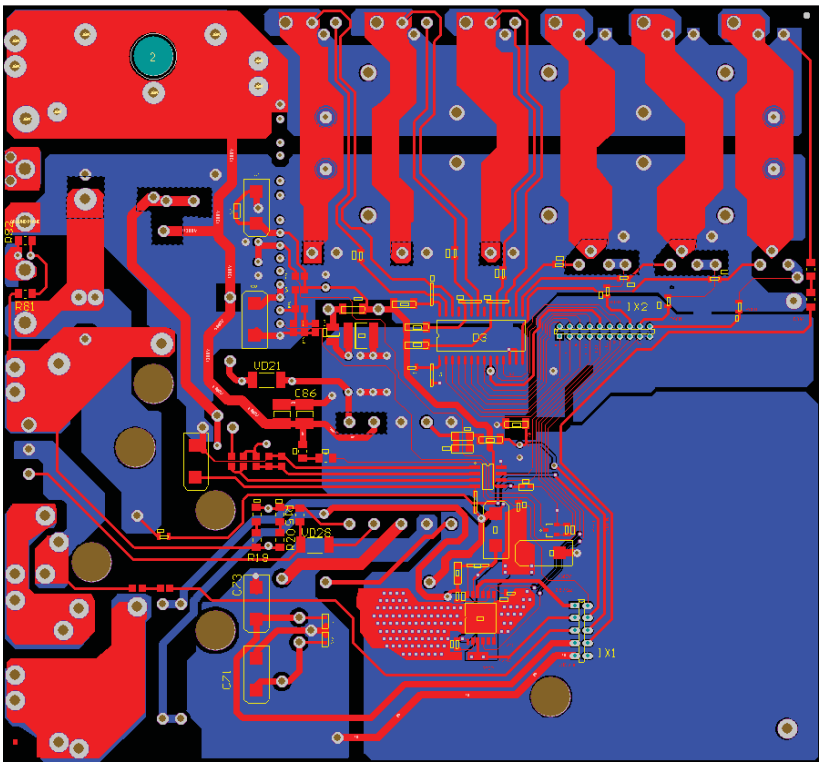

Figure C-9: Prototype Power Supply PCB Top Layer

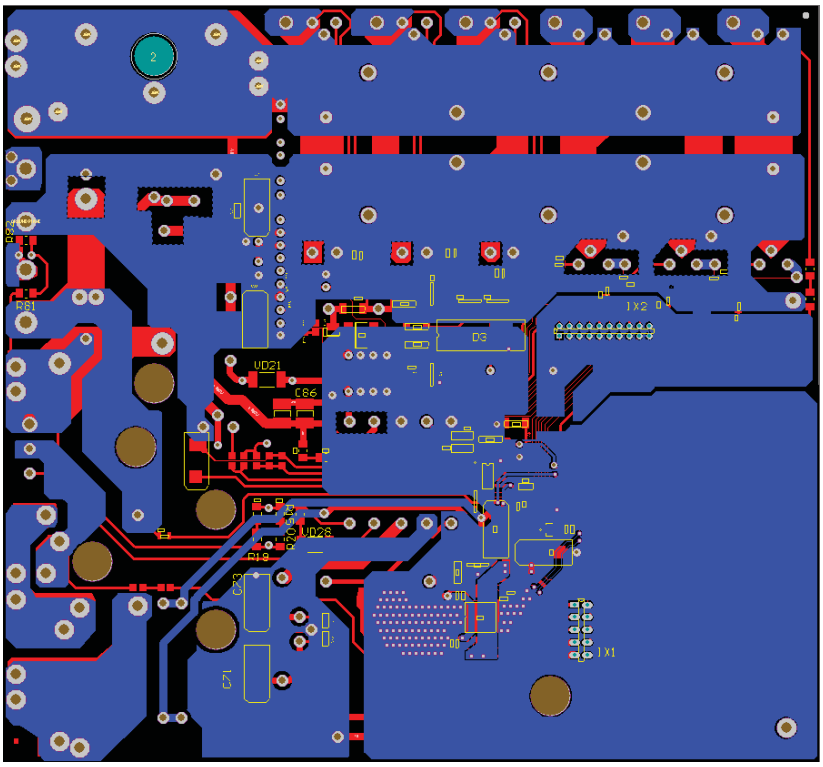

Figure C-10: Prototype Power Supply PCB Bottom Layer

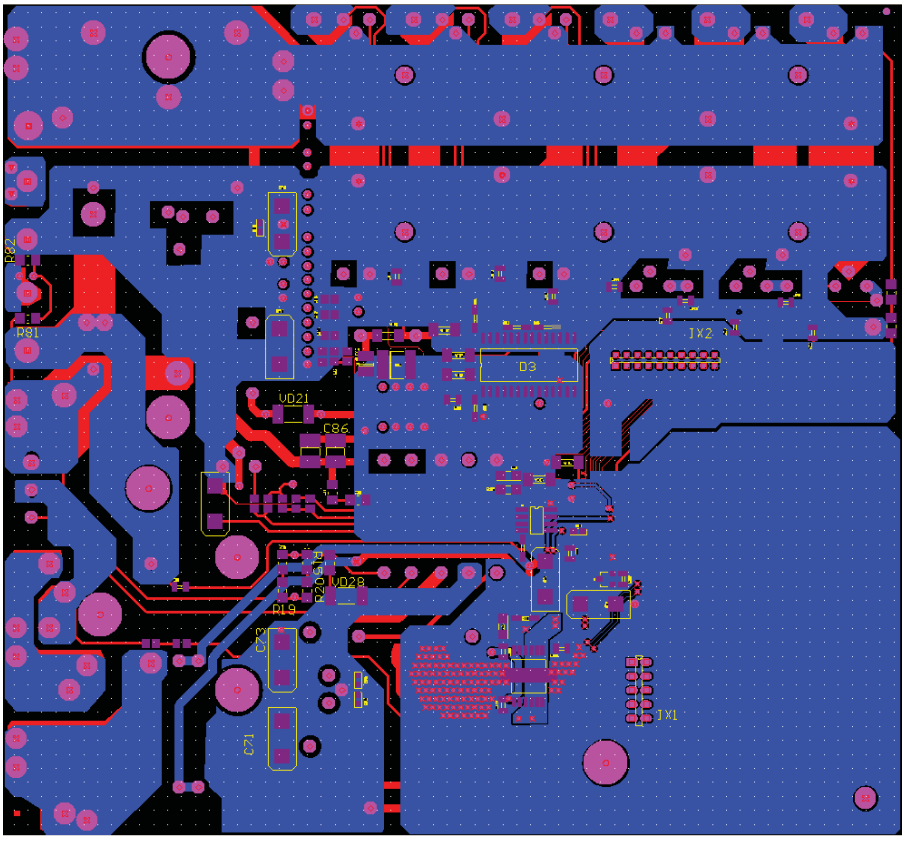

Figure C-11: Prototype Power Supply Gerber Data

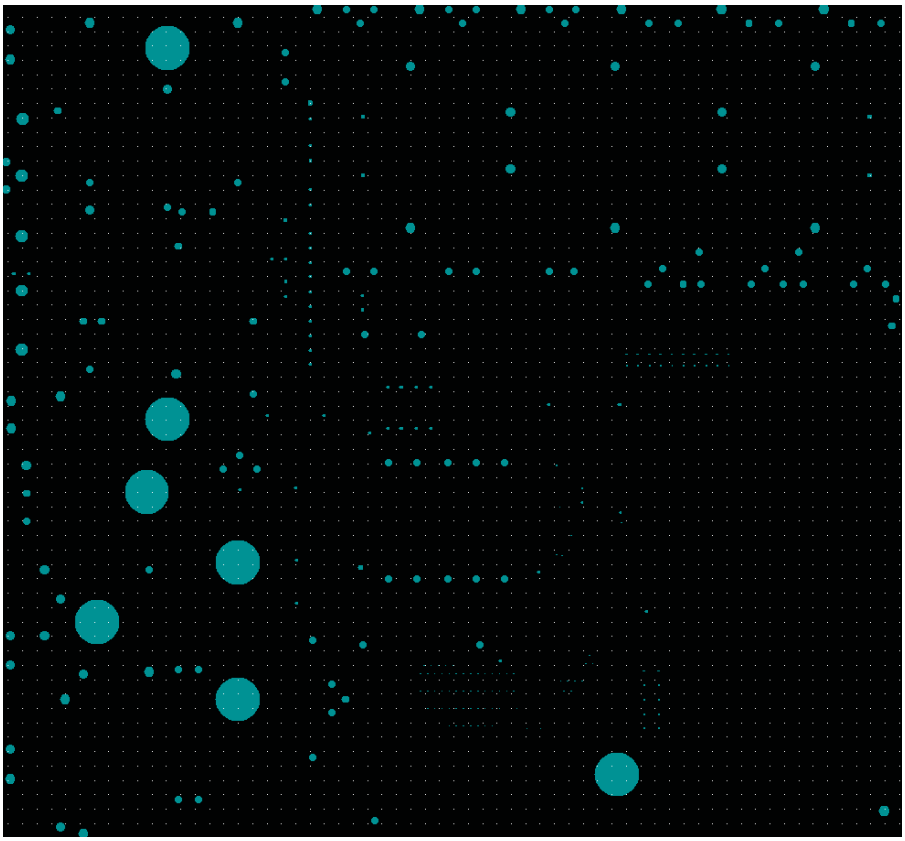

Figure C-12: Prototype Power Supply PCB NC Drill Data

C.20 Prototype Control Printed Circuit Board

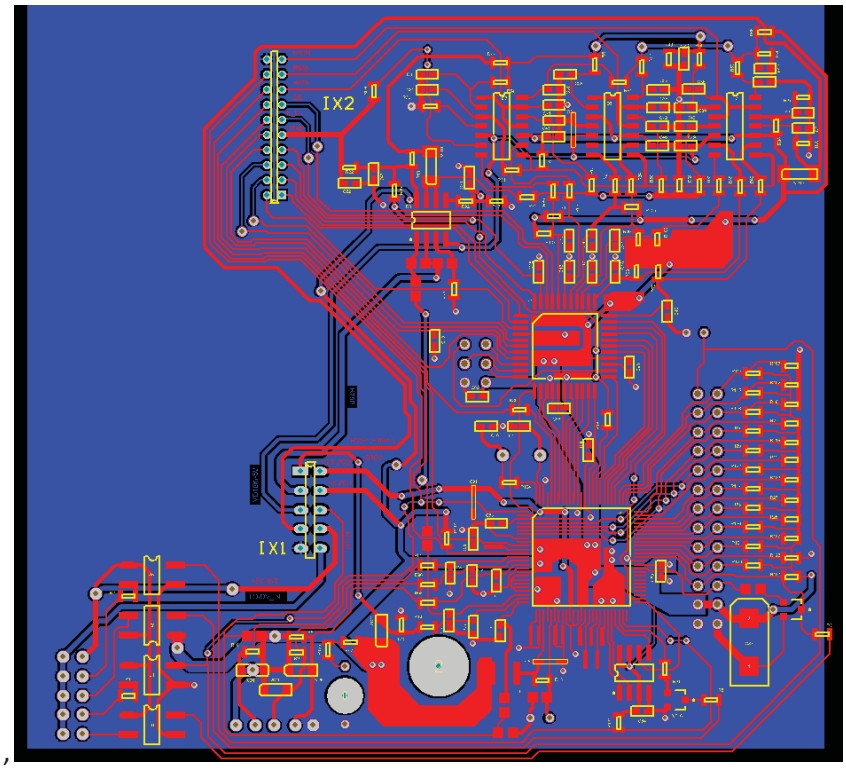

Figure C-13: Prototype Controller PCB Top Layer

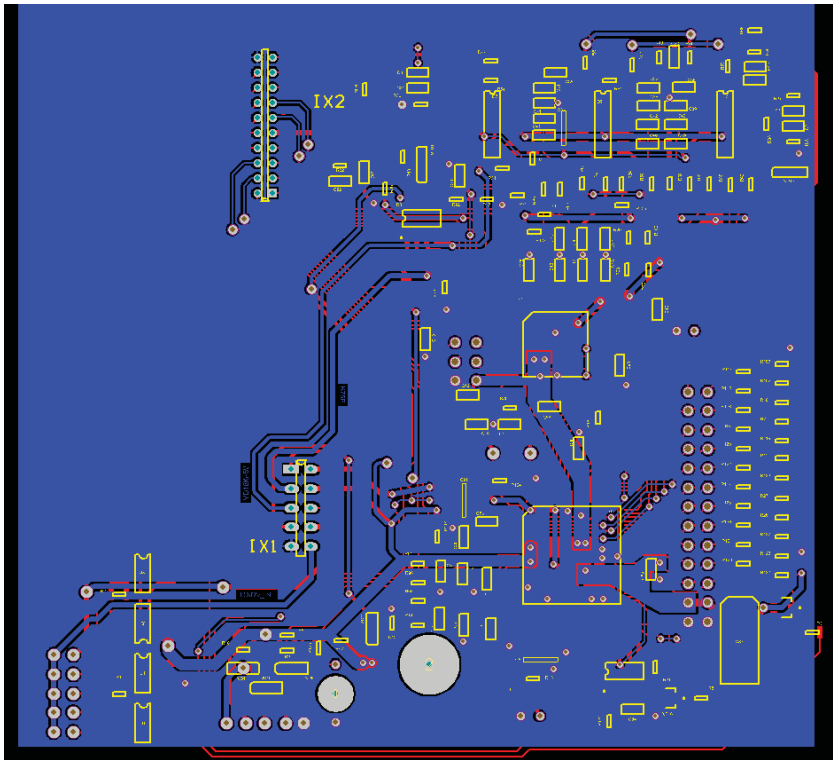

Figure C-14: Prototype Controller PCB Bottom Layer

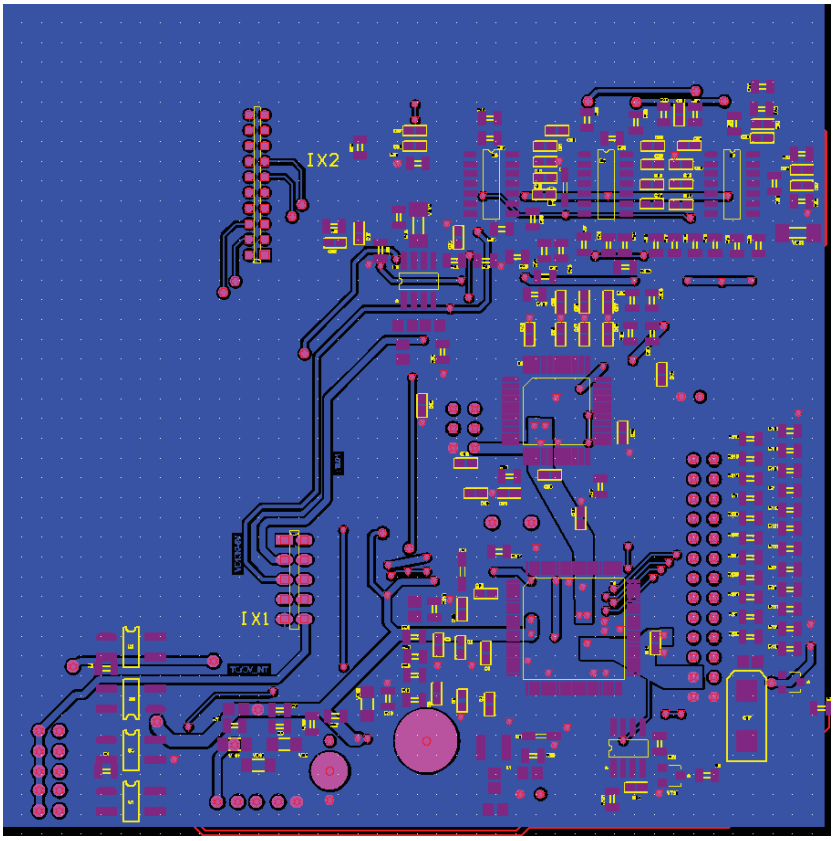

Figure C-15: Prototype Controller Gerber Data

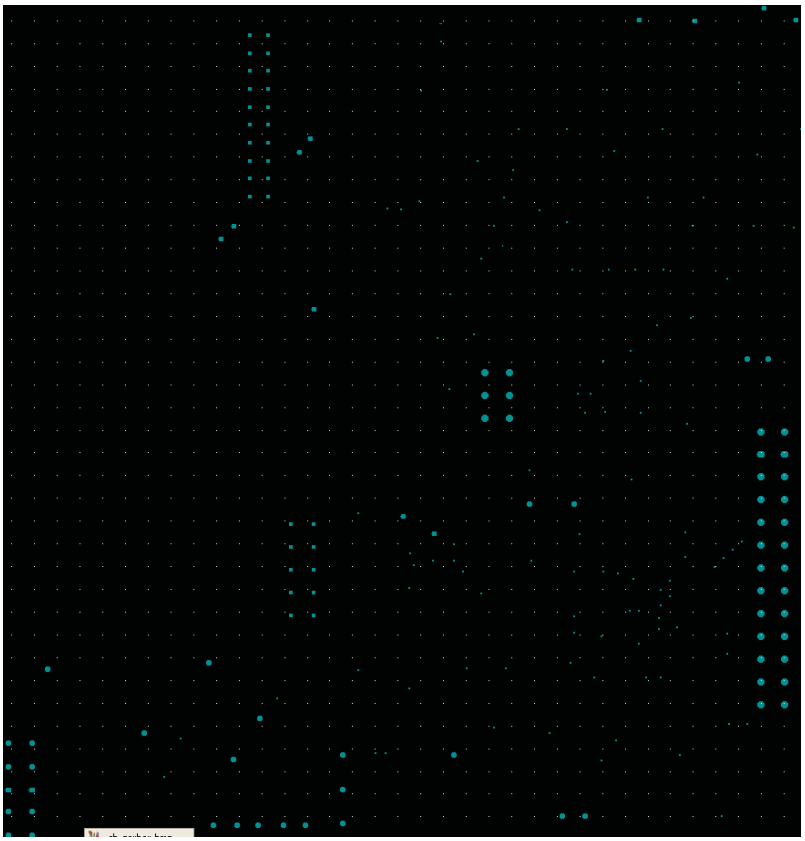

Figure C-16: Prototype Controller NC Drill Data

Appendix D

Component Datasheets

Appendix E

Photos

Experimental Setup of Teknatool DVR. Showing 72V Lead-Acid Battery Array, Tektronix Isolated Oscilloscope, Current Probe, DC Power Supply, And Function Generator

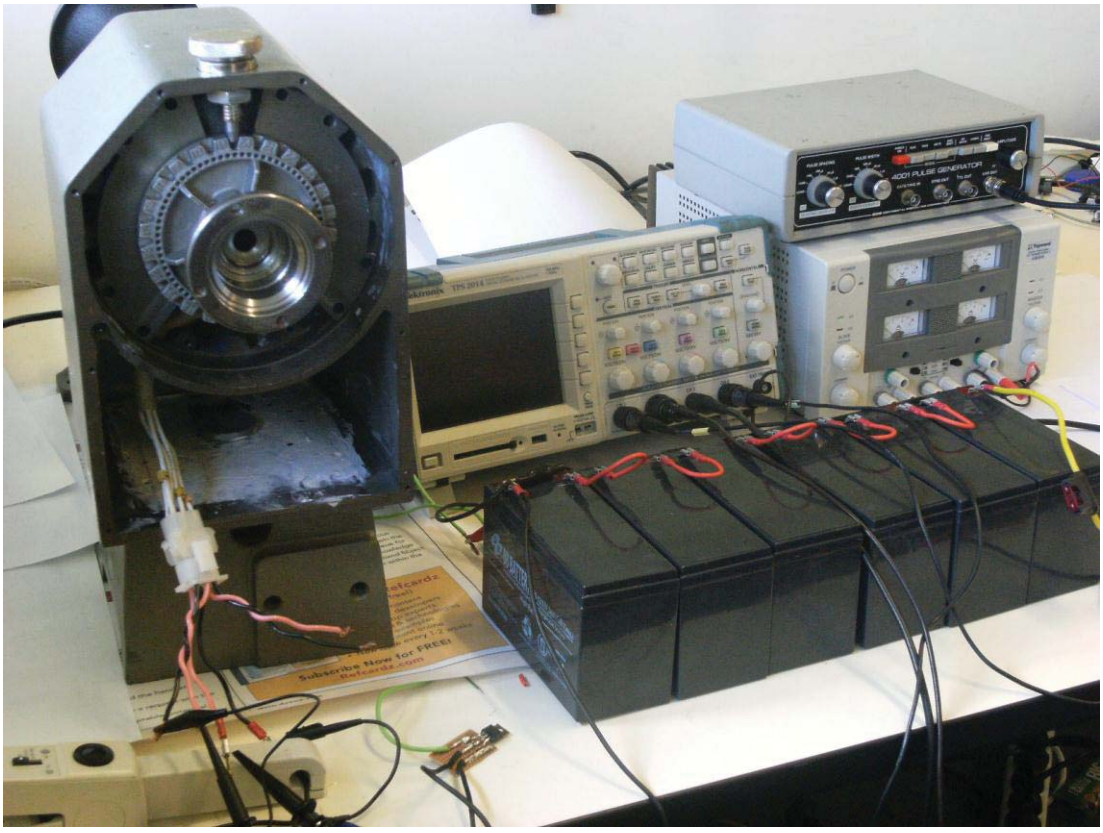

Experimental Setup Showing Rotor Locking Mechanism And Left Hand Brake

DVR SRM Rotor With Rear Shaft Bearing Housing. Note The Rotational Balance Drillings

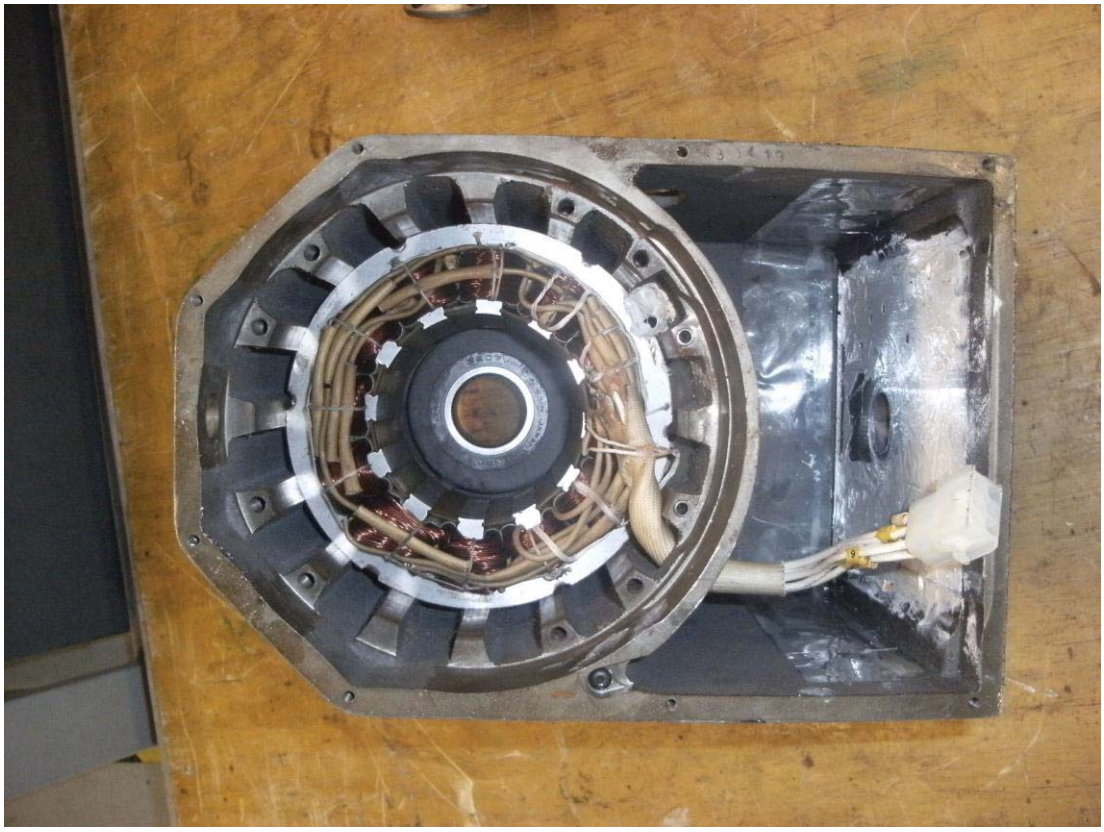

DVR SRM Iron Stator Housing Showing Windings And Electronics Cavity

DVR SRM Rotor Showing Laminates And Rotary Position Encoder Wheel

DVR SRM Rotor Showing 8 Trapezoidal Salient Poles

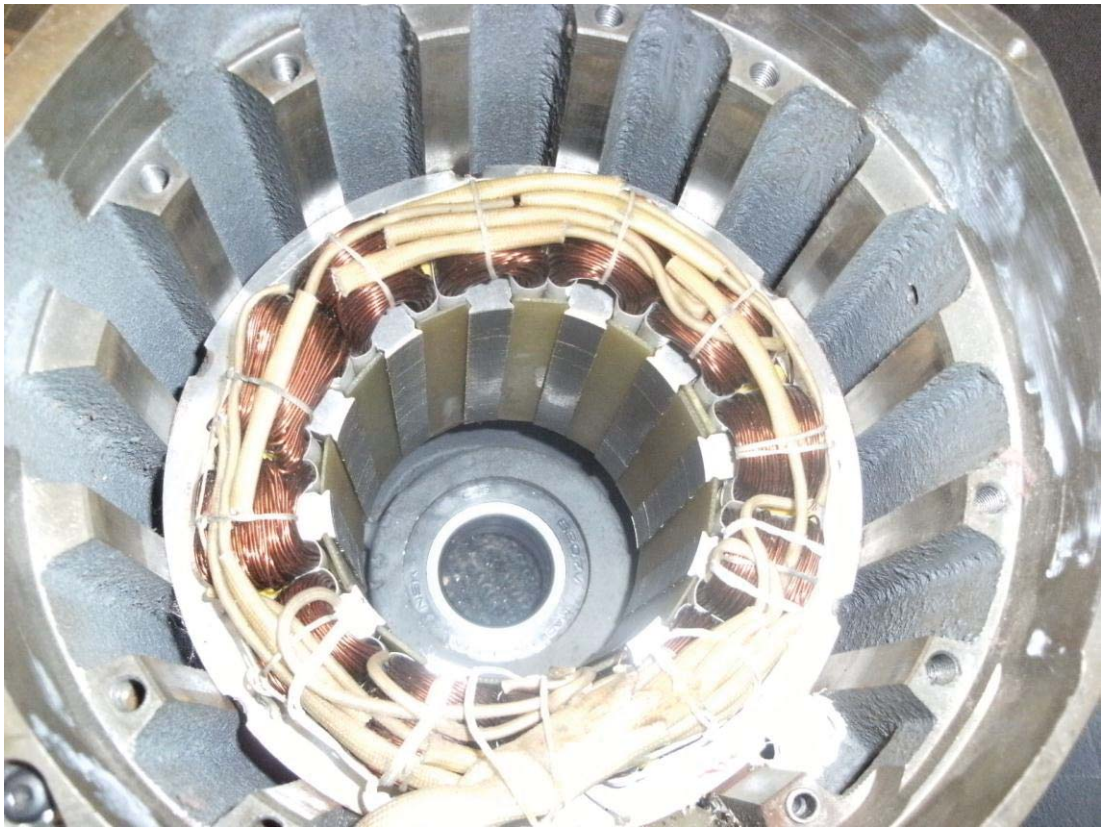

DVR SRM Stator Housing Showing Twelve Windings Grouped Into Three Phases

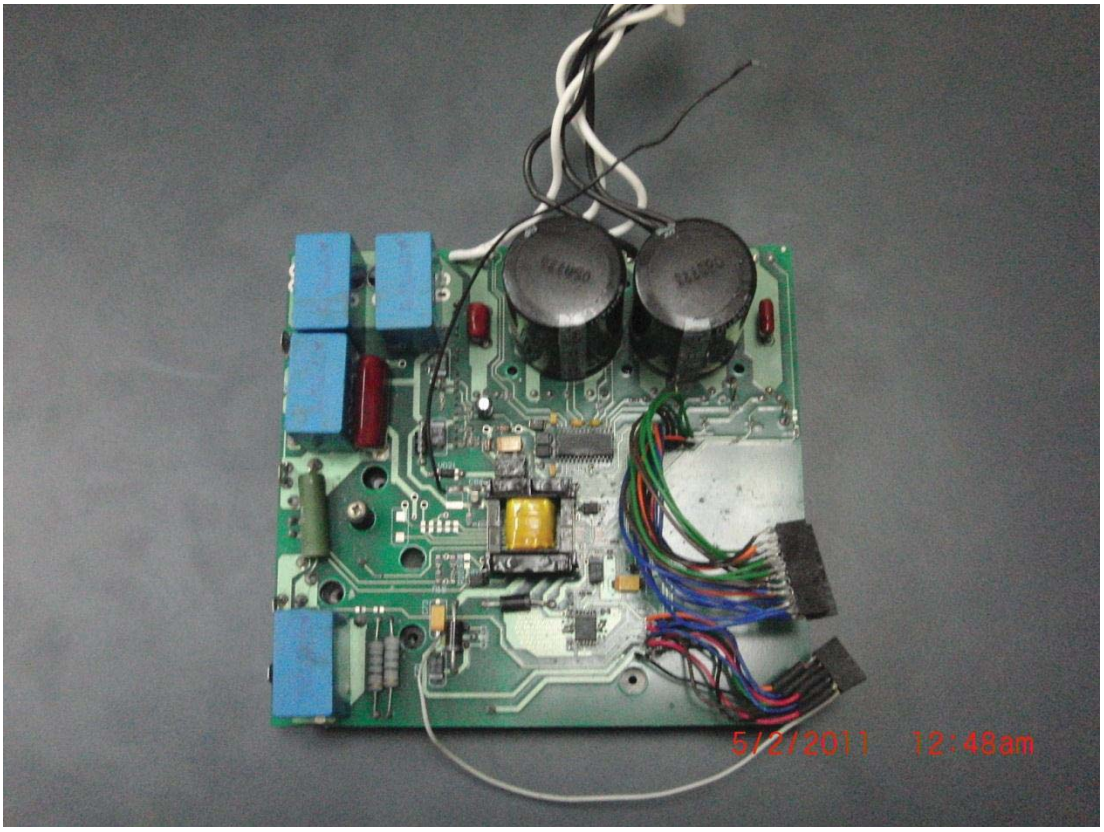

Prototype Power Supply Circuit Board Top Side

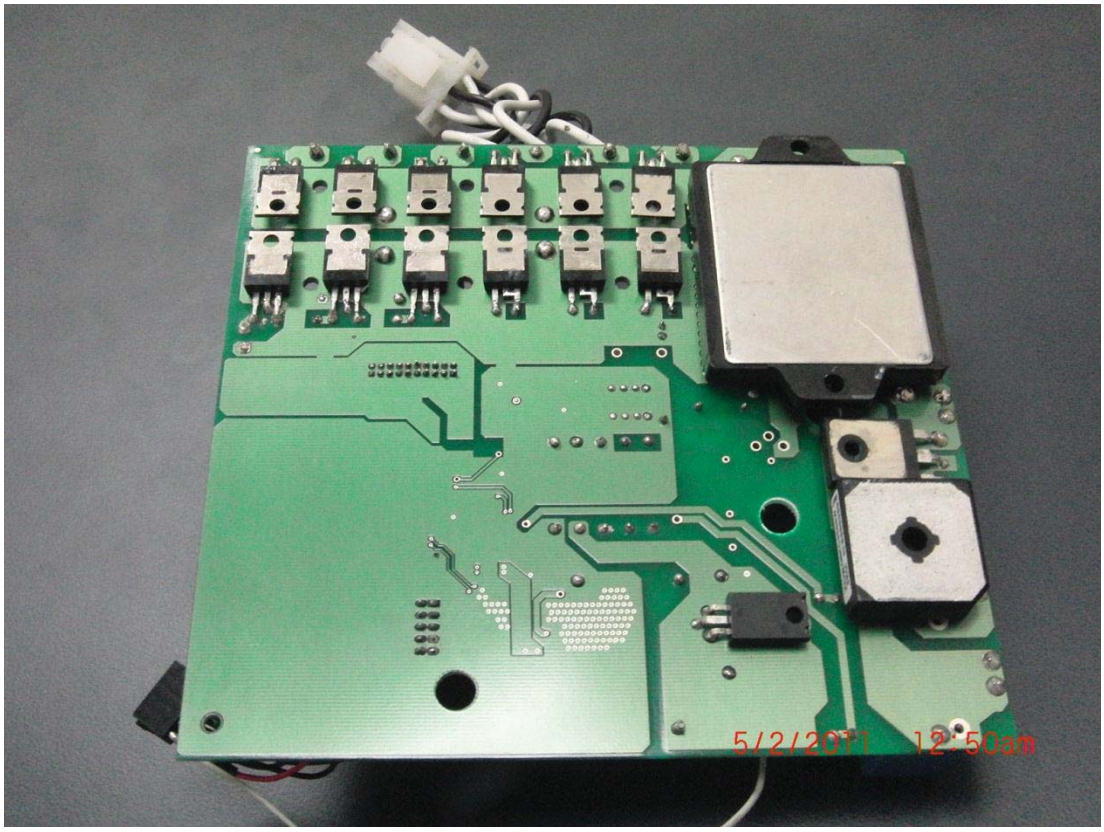

Prototype Power Supply Circuit Board Bottom Side

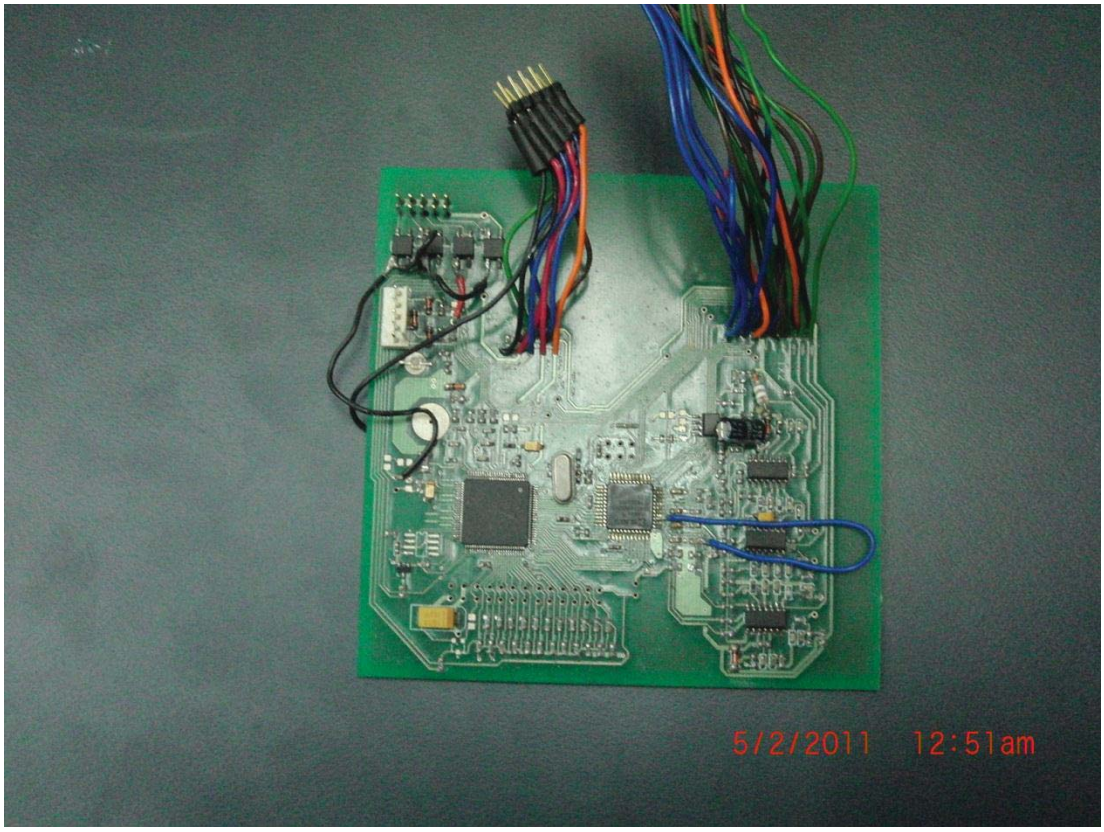

Prototype Control Circuit Board Top Side

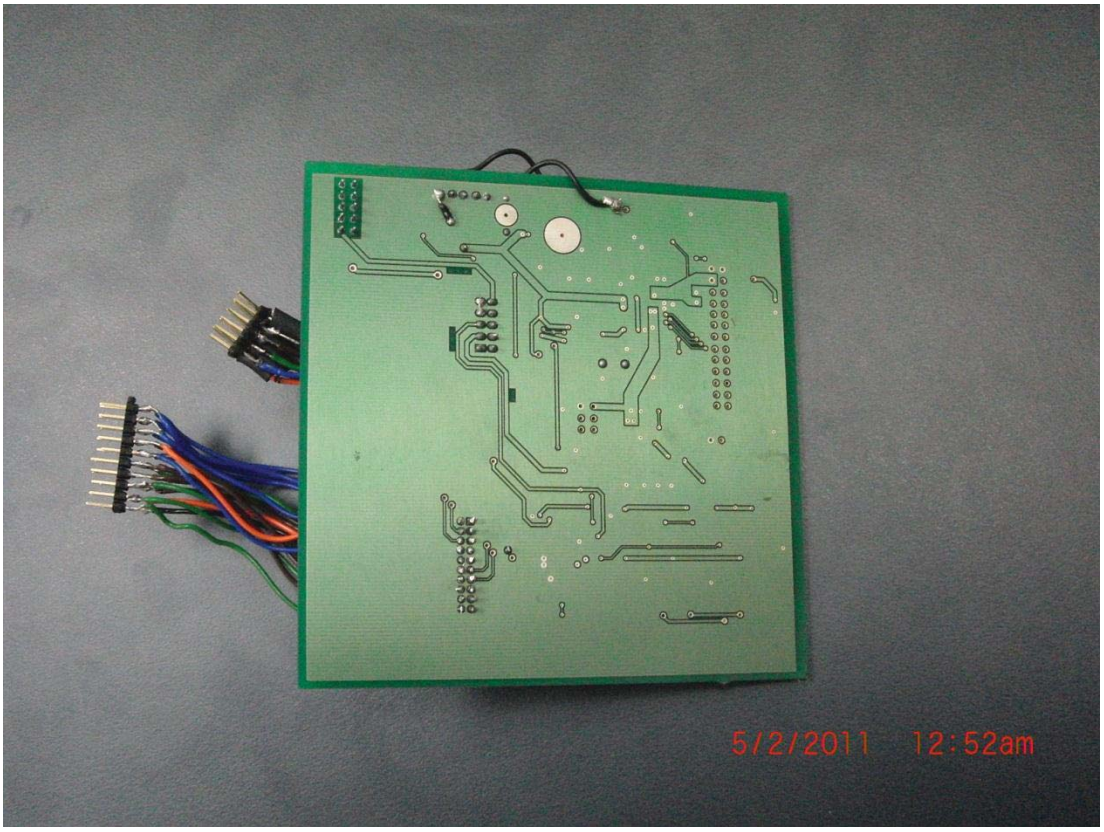

Prototype Control Circuit Board Bottom Side

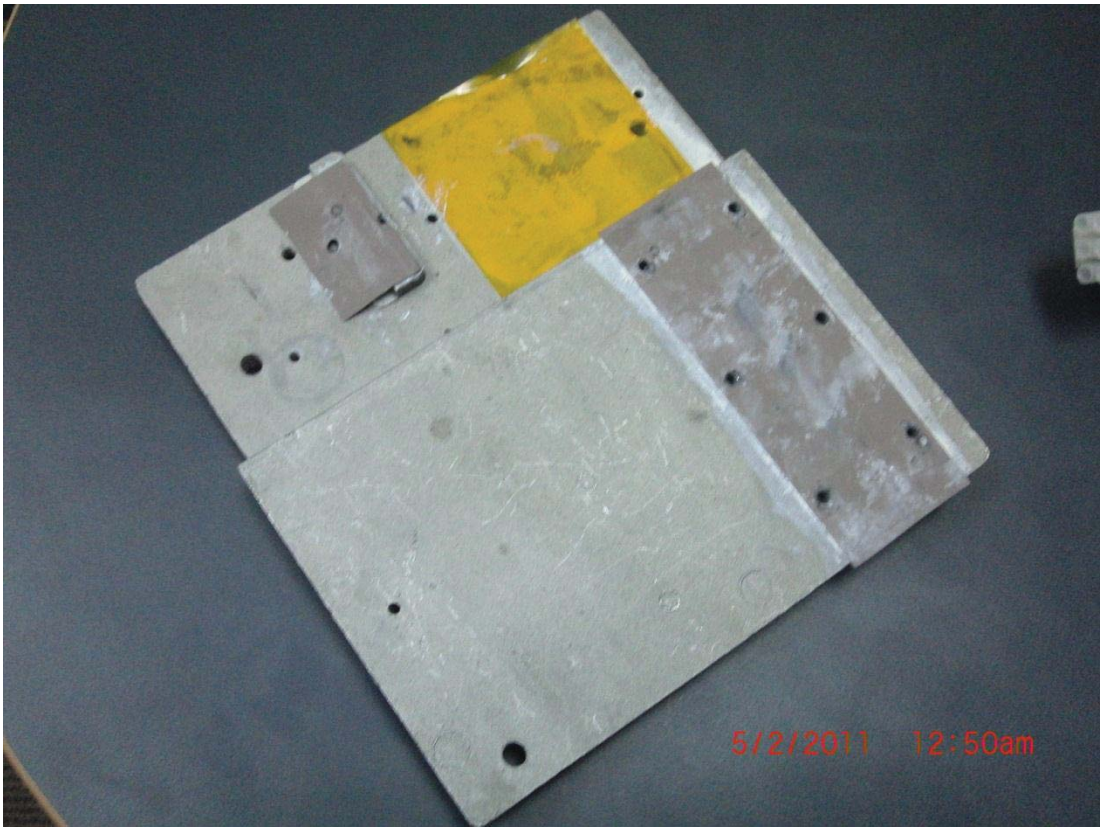

Power Supply Circuit Board Heatsink Top Side

Power Supply Circuit Board Heatsink Bottom Side